Interactions between the skeletal dihydropyridine receptor β subunit, the α_{1s} II-III loop and the ryanodine receptor

by

Yamuna Alles Karunasekara

A thesis submitted for the degree of Doctor of Philosophy of the Australian National University

The John Curtin School of Medical Research
Australian National University
Canberra
AUSTRALIA

THE AUSTRALIAN NATIONAL UNIVERSITY

THE JOHN CURTIN SCHOOL OF MEDICAL RESEARCH

June 2011

THE AUSTRALIAN
LIBRARY
NATIONAL UNIVERSITY

Statement

This thesis presents the results of research undertaken in the Biomolecular Structure Group, Department of Translational Biosciences, The John Curtin School of Medical Research, The Australian National University between February 2007 and June 2011. This study was supported by an Australian Postgraduate Award, an Australian National University Supplementary Scholarship and the Peter Gage Memorial Supplementary Scholarship in Membrane Physiology.

All experiments and data analyses presented in this thesis are my own original work, accomplished under the supervision of Dr. Marco G. Casarotto, Prof. Angela F. Dulhunty and Prof. Philip G. Board, except where otherwise acknowledged.

Yamuna Alles Karunasekara

Structural Biology Group
Department of Translational Biosciences
The John Curtin School of Medial Research
College of Medicine, Biology and Environment
The Australian National University

Acknowledgements

First of all I would like to thank my main PhD supervisor, Dr. Marco Casarotto for his excellent guidance and assistance during the course of this PhD. The brain storming sessions formed the basis for this project and it is much appreciated. I thank you for your immense patience, humor and understanding through the ups and downs of this project as well as my personal life. Without your advice and understanding, the completion of this PhD would not have been possible. Your ability to turn tears and frustration into laughter and optimism is admirable.

I would also like to express my gratitude to the other two members of my supervisory panel, Prof. Angela Dulhunty and Prof. Phil Board. Angela's extensive and in depth knowledge in the field of muscle EC coupling has been invaluable during the course of this project. I appreciate very much her efforts to introduce me to the international community in the field of EC coupling. Putting a face to names in scientific papers made a big difference to the way I approached this project. I would also like to thank Angela for all the help and input in the electrophysiology aspects of this PhD.

I would like to thank Prof. Phil Board for making me always welcome in his laboratory and for the use of resources in the Molecular Genetics group. He has been a wonderful mentor and his door was always open for any questions/problems at any time of the day. His numerous suggestions and input during this project is greatly appreciated.

I acknowledge the contribution to this project by Dr. Marco Casarotto (NMR), Dr. Yanfang Cui (NMR), Dr. Nicole Norris (ITC), Dr. Esther Gallant (Lipid bilayer experiments) and Ms. Robyn Rebbeck (Lipid bilayer experiments). A special thank you goes to Esther and Robyn for teaching me lipid bilayer techniques and single channel data analysis. I also acknowledge the contribution of Ms. Suzy Pace and Ms. Joan Stivala in producing RyR1 vesicles for lipid bilayer experiments carried out in this project. Thank you also to Dr. Dan Liu for proof-reading this thesis within a very short time frame.

My heartfelt gratitude goes out to members of three research groups – The Biomolecular Structure group, the Muscle Research group and the Molecular Genetics group. I greatly appreciate their help and support in various aspects of this project. I would specially like to mention Dr. Han Shen Tae who has been a wonderful friend and

colleague. His help and support contributed substantially to the completion of this project. I would also like to thank him for the companionship and laughter and for making the lab an enjoyable place to work in.

A very big thank you goes to my two daughters – Niluka and Nadeeka. I appreciate you putting up with a constantly "busy" Mummy for the last few years. I would like to specially mention and thank Niluka for her help during the thesis writing process. Your help was invaluable and it is much appreciated. Last but not least I would like to thank the person who made all this possible – my husband, Neil. Without his endless patience, understanding and support I could not have ventured on this journey. Thank you Neil, for being there and for everything you have done for me.

Abstract

Excitation-contraction (EC) coupling in skeletal muscle requires a physical coupling between the dihydropyridine receptor (DHPR) Ca^{2+} channel in the surface membrane and the ryanodine receptor (RyR1) Ca^{2+} release channel in the sarcoplasmic reticulum (SR) Ca^{2+} store. However, the exact molecular mechanism of this interaction remains unresolved. Both the α_{1s} and β_{1a} subunits of the DHPR are essential for the skeletal EC coupling process and a central critical region of the α_{1s} II-III loop has been shown to be important for this interaction. The β subunit plays an essential role in the targeting of the pore-forming α_1 subunit to the t-tubular membrane and in the modulation of the DHPR Ca^{2+} channel. In addition the skeletal isoform, β_{1a}, supports tetrad formation of the DHPRs opposite the ryanodine receptors. β_{1a} has a modular structure consisting of N, C termini and SH3/guanylate kinase (GK) domains separated by a Hook region. A high affinity interaction between the α_{1s} I-II loop and the β_{1a}-GK domain is responsible for the targeting function of the β subunit. However the functional significance of the SH3 domain remains unclear.

SH3 domains are protein interaction domains that typically bind to proline rich motifs in their interacting partners. The critical region of the α_{1s} II-III loop contains at least two such proline rich motifs. Therefore this study investigated the possibility of an interaction between the β_{1a}-SH3 domain and the α_{1s} II-III loop. The β_{1a} subunit and its SH3 domain bound to the critical region of the α_{1s} II-III loop with an affinity of ~ 2 μM. One of these interactions was narrowed down to the first proline-rich motif of the critical region which encompasses four skeletal specific residues (A739, F741, P742 and D744) that have been previously shown to be important for skeletal type EC-coupling *in-vivo*. Mutation of these residues to their cardiac counterparts showed residues P742 and D744 to be important for the binding of the β_{1a}-SH3 domain to the critical region of the α_{1s} II-III loop.

The C-terminus of the β_{1a} subunit binds to RyR1 *in vitro* and the end 35 residues of the β_{1a} C-terminus is important for skeletal type EC coupling. This study investigated the structure of a peptide corresponding to this region by NMR and identified a nascent helical region extending from residues L^{493} to G^{506}. Three hydrophobic residues (L^{496}, L^{500} and W^{503}) within this helical region form a hydrophobic surface which could be a

putative binding surface for the skeletal ryanodine receptor. Mutation of these residues to alanines partially disrupts the helical surface and decreases the ability of the mutant peptides to activate the ryanodine receptor.

In conclusion this study shows that the SH3 domain of the skeletal β subunit is able to bind to the critical region of the α_{1s} II-III loop *in-vitro*. This study also identifies a quasi-structured helical region in the C terminal tail of the β_{1a} subunit that affects its interaction with the skeletal ryanodine receptor. Based on these findings, a model is proposed where the β_{1a} subunit acts as a conduit in the transformation of the EC coupling signal from the skeletal DHPR to RyR1.

Publications

Papers

Karunasekara, Y., Dulhunty,A.F. & Casarotto, M.G. 2009. The voltage-gated calcium-channel beta subunit: more than just an accessory. *Eur Biophys J,* 39, 75-81.

Rebbeck, R.T., **Karunasekara, Y**., Gallant, E.M., Board, P.G., Beard, N. A., Casarotto, M.G.& Dulhunty, A.F. 2011. The [beta]1a Subunit of the Skeletal DHPR Binds to Skeletal RyR1 and Activates the Channel via Its 35-Residue C-Terminal Tail. Biophysi*cal Journal,* 100, 922-930.

Selected conference presentations

Yamuna Karunasekara, Esther Gallant, Angela Dulhunty, Phil Board, Marco Casarotto. Interactions of the DHPR β_{1a} subunit with the α_{1s} subunit and RyR1. 2011 Biophysical Society Meeting, Abstracts, Biophysical journal, 100, L266-Poster. March 5-9, 2011, Baltimore, MD, USA.

Yamuna Karunasekara, Esther Gallant, Angela Dulhunty, Phil Board, Marco Casarotto. Interactions between the skeletal DHPR β-subunit, the α_{1s} II-III loop and RyR1. Poster presentation, Gordon Research Conference on Muscle: Excitation / Contraction Coupling June 14-19, 2009, Waterville Valley Resort, Waterville Valley, NH, USA.

Yamuna Karunasekara, Esther Gallant, Angela Dulhunty, Phil Board, Marco Casarotto. Biophysical Interactions of the skeletal dihydropyridine receptor Ca^{2+} channel β-subunit. Poster presentation. Curtin conference on Ion Channels and Transporters in Honour of Prof. Peter Gage. 15 – 17 April 2009. Canberra, ACT, Australia.

Commonly used Abbreviations

AID	Alpha Interaction Domain
ATP	Adenosine triphosphate
C region	Critical region of the α_{1s} II-III loop (residues 720–765)
CD	Circular Dichroism spectroscopy
CDCL	Cardiac Dihydropyridine receptor Cytoplasmic Loop (α_{1c} II-III loop)
cDNA	Complementary deoxyribonucleic acid
CICR	Calcium Induced Calcium Release
CSQ	Calsequestrin
C-terminus	Carboxyl-terminus
DHPR	Dihydropyridine Receptor
EC-coupling	Excitation Contraction Coupling
FPLC	Fast Performance Liquid Chromatography
FRET	Fluorescence Resonance Energy Transfer
GK	Guanylate kinase
GST	Glutathione S-transferase
HVA	High voltage activated
IMAC	Immobilized metal affinity chromatography
ITC	Isothermal Calorimetry
jSR	Junctional Sarcoplasmic Reticulum
kDa	Kilo Dalton
LVA	Low voltage Activated
MAGUK	Membrane Associated Guanylate Kinase

NMR	Nuclear Magnetic Resonance
N-terminus	Amino-terminus
RNA	Ribonucleic acid
RyR	Ryanodine Receptor
SDCL	Skeletal Dihydropyridine receptor Cytoplasmic Loop (α_{1s} II-III loop)
SH3	Src Homology 3
SR	Sarcoplasmic Reticulum
T-tubule	Transverse Tubule
VDCC	Voltage Dependant Calcium Channel
VGCC	Voltage Gated Calcium Channel

Table of Contents

Chapter 1 Introduction and background 1

1.1 Muscle 1

1.1.1 Overview of muscle tissue 1

1.1.2 Developmental aspects of muscle 2

1.1.3 Macroscopic anatomy of skeletal muscle (Figure 1-1) 2

1.1.4 Microscopic anatomy of a skeletal muscle fibre (Figure 1-2) 5

1.2 Role of ionic calcium in muscle contraction 8

1.3 Sarcoplasamic Reticulum (SR) and T (Transverse) -tubules 9

1.4 Proteins of the triad junction 11

1.5 Excitation-Contraction Coupling 12

1.5.1 Overview 12

1.5.2 Mechanisms of EC coupling 15

1.6 Ryanodine receptor Ca^{2+} release channel (RyR) 18

1.6.1 Overview 18

1.6.2 History 18

1.6.3 RyR isoforms and distribution 18

1.6.4 RyR1 structure 19

1.6.5 Modulation by pharmacological agents 21

1.6.6 Modulation by endogenous effectors 22

1.6.7 Gene knockout studies 23

1.6.8 Functional interactions and accessory proteins 23

1.7 Dihydropyridine receptor (DHPR) L-type Ca^{2+} channel 25

1.7.1 Overview of voltage gated Ca^{2+} channels (VGCCs) 25

1.7.2 History and classification 25

1.8 Subunit structure of the skeletal DHPR Ca^{2+} channel 27

1.8.1 3D structure 30

1.8.2 The pore forming α_{1s} subunit 32

1.8.3 Auxiliary subunits 39

1.9 β subunit 42

1.9.1 History and nomenclature 42

1.9.2 Structural modularity of the β subunit 43

1.9.3 The SH3 Domain of the β subunit 46

1.9.4 Role in membrane expression and modulation of calcium channels 47

1.9.5 Gene knockout studies and disease 50

1.9.6 $Ca_v\beta$ subunit in skeletal muscle 50

1.9.7 The role of β_{1a} subunit in skeletal EC coupling? 53

1.10 This thesis 54

Chapter 2 General Materials and Methods 55

2.1 Materials 55

2.2 Methods 55

2.2.1 Peptide synthesis 55

2.2.2 Plasmid Construction 56

2.2.3 Polymerase Chain Reaction (PCR) 56

2.2.4 DNA extraction 58

2.2.5 Site directed mutagenesis 58

2.2.6 DNA sequencing 59

2.2.7 Plasmid Transformation 59

2.2.8 Protein expression 59

2.2.9 Protein purification by IMAC (Immobilized metal affinity chromatography) 60

2.2.10 Denaturing (SDS) Polyacrylamide Gel Electrophoresis (PAGE) 62

2.2.11 Protein Quantitation 63

2.2.12 Circular Dichroism (CD) spectroscopy 63

Chapter 3 Expression and Purification of the recombinant DHPR-β_{1a} subunit 65

3.1 Introduction 65

3.2 Aim 68

3.3 Materials and Methods 68

3.3.1 Plasmid Construction 68

3.3.2 Protein Expression 71

3.3.3 Purification 71

3.3.4 Western blotting 73

3.3.5 Circular Dichroism (CD) spectroscopy 74

3.3.6 Mass spectrometry 74

3.4 Results 74

3.4.1 Protein Expression 74

3.4.2 Purification 75

3.4.3 Western blotting 77

3.4.4 Mass spectrometry 77

3.4.5 Circular Dichroism (CD) spectroscopy 79

3.5 Discussion 81

Chapter 4 Interactions between the DHPR-β_{1a} subunit and the α_{1s} II-III loop 84

4.1 Introduction 84

4.2 Aim 87

4.3 Materials and Methods 89

4.3.1 Expression of proteins and synthesis of peptides 89

4.3.2 Tryptophan fluorescence quenching spectroscopy 93

4.4 Results 96

4.4.1 β_{1a} subunit 96

4.4.2 α_{1s} II-III loop 96

4.4.3 SH3 domain 96

4.4.4 Tryptophan fluorescence quenching spectroscopy 97

4.5 Discussion 111

Chapter 5 Structural analysis of the DHPR β_{1a} subunit C-terminal tail.....117

5.1 Introduction 117

5.2 Aim 118

5.3 Materials and Methods 118

5.3.1 Peptide synthesis 118

5.3.2 Solution State Nuclear Magnetic Resonance (NMR) Spectroscopy 118

5.3.3 Circular Dichroism (CD) spectroscopy 123

5.4 Results 123

5.4.1 NMR structural studies 123

5.4.2 Circular Dichroism (CD) spectroscopy 131

5.4.3 Structure of the β_{1a}-C35 peptide and design of mutant peptides 133

5.4.4 Comparison of the H_N-H_N region of the β_{1a}-C35 mutant peptides 134

5.5 Discussion 134

Chapter 6 Functional interactions between the DHPR-β_{1a} C-terminal tail and the skeletal ryanodine receptor.....141

6.1 Introduction 141

6.2 Aim 142

6.3 Materials and Methods 142

6.3.1 Expression and purification of full length recombinant β_{1a} subunit 142

6.3.2 Peptide synthesis 142

6.3.3 Peptide and protein quantitation 143

6.3.4 Planar bilayer recordings of ryanodine receptor channels 143

6.4 Results 149

6.4.1 The effect of full length β_{1a} subunit on RyR1 channel activity 149

6.4.2 The effect of the 35-residue C terminal tail of β_{1a} (β_{1a}-C35) on RyR1 channel activity 151

6.4.3 The effect of the β_{1a}-C35 mutant peptides on RyR1 channel activity 157

6.5 Discussion 168

Chapter 7 Discussion 170

7.1 Recombinant β_{1a} subunit 171

7.2 Interaction between β_{1a}-SH3 domain and the α_{1s} II-III loop 171

7.3 Structure and function of the 35-residue C terminal tail of the β_{1a} subunit ... 173

7.4 Role of the β_{1a} SH3 domain and the β_{1a} C terminus in skeletal EC coupling? 175

7.5 Conclusion 176

7.6 Future directions 178

References.....174

Appendix.....196

A.1 Buffers and Solutions.....196

A.2 Reagents.....198

Chapter 1 Introduction and background

1.1 Muscle

1.1.1 Overview of muscle tissue

Movement is essential to life, and takes many forms, from cytoplasmic streaming and the growth of neurons at the cellular level, to the flight of a bird or the explosive performance of a sprinter. Muscle is an organ specializing in the transformation of chemical energy into movement.

Muscle is made up of muscle tissue which in turn consists of muscle fibers. The most distinguishing functional characteristic of muscle fibers is their ability to transform chemical energy (ATP) into directed mechanical energy. In doing so, they become capable of exerting force. As a result muscle fibers are able to change the dimensions or shape of anatomical structures or cause movement of body parts with respect to each other.

There are three types of muscle tissue:

Skeletal muscle tissue is packaged into the skeletal muscles, organs that attach to and cover the bony skeleton. Skeletal muscle fibers are syncytia formed by the fusion of muscle cells. They have obvious stripes called striations and can be controlled voluntarily. Although it is often activated by reflexes, skeletal muscle is called voluntary muscle because it is the only type subject to conscious control. Skeletal muscle is responsible for overall body mobility. It can contract rapidly, but it tires easily and must rest after short periods of activity. Nevertheless, it can exert tremendous power.

Cardiac muscle tissue occurs only in the heart, where it constitutes the bulk of the heart walls. Like skeletal muscle fibers, cardiac muscle cells are striated, but cardiac muscle is not voluntary. Cardiac muscle usually contracts at a fairly steady rate set by the heart's pacemaker, but neural controls allow the heart rate to vary for brief periods.

Smooth muscle tissue is found in the walls of hollow visceral organs, such as the stomach, urinary bladder, and respiratory passages. Its role is to force fluids and other

substances through internal body channels. It has no striations, and like cardiac muscle, it is not subject to voluntary control. Contractions of smooth muscle fibers are slow and sustained.

The types of muscle are summarized in **Table 1-1**

1.1.2 Developmental aspects of muscle

With rare exceptions, all muscle tissues develop from embryonic mesoderm cells called myoblasts. Multinucleate skeletal muscle fibers form by the fusion of several myoblasts to form multinuclear myotubes, a process guided by the integrins (cell adhesion proteins) forming part of the myoblast membranes. Functional sarcomeres are present, and skeletal muscle fibers are contracting by week 7 when the human embryo is only about 1 inch long. Myoblasts producing cardiac and smooth muscle cells do not fuse. However, both develop gap junctions at a very early embryonic stage.

1.1.3 Macroscopic anatomy of skeletal muscle (Figure 1-1)

Each skeletal muscle is a discrete organ. In an intact muscle, the individual muscle fibers are wrapped and held together by several different connective tissue sheaths. Together these connective tissue sheaths support each cell and reinforce the muscle as a whole, preventing the bulging muscles from bursting during exceptionally strong contractions. The endomysium is the fine sheath of connective tissue that surrounds each individual muscle fiber. Within each skeletal muscle, the endomysium-wrapped muscle fibers are grouped into fascicles that resemble bundles of sticks. Surrounding each fascicle is a layer of fibrous connective tissue called perimysium. Bundles of fascicles are in turn covered by an "overcoat" of dense irregular connective tissue called the epimysium that surrounds the whole muscle (Marieb, Human Anatomy and Physiology, 7 ed.).

Table 1-1 Comparison of muscle types

Cell Type	Structure	Contractile properties	Function
Skeletal muscle	Long syncytial, Multinucleated cells; orderly arrangement of myosin and actin filaments gives striated appearance, each fiber is directly innervated by a motor neuron.	Rapid, powerful contractions; can shorten to 60-80% of resting length; contraction is initiated by the central nervous system under voluntary control.	Movement of the bones across joints.
Cardiac muscle	Similar to skeletal muscle but extrinsic innervation is only at the specialized nodal pacemakers; the action potential is conducted from cell to cell via gap junctions (nexuses).	Similar to skeletal muscle but contraction is initiated by automatic firing of pacemaker cells; contraction is slower and more prolonged than in skeletal muscle.	Movement of blood by repetitive rhythmic contraction; beats about 3 billion times during a normal lifetime.
Smooth muscle	Elongated, tapering cells; mononuclear; no striations; occurs singly, in small clusters, or in sheets enclosing organs; innervated by local plexuses and extrinsically by autonomic nerves.	Slow contractions under involuntary control; can shorten to 25% of resting length.	Control of shape and size of hollow organs such as the digestive, respiratory,genital, and urinary tracts and the vascular system.

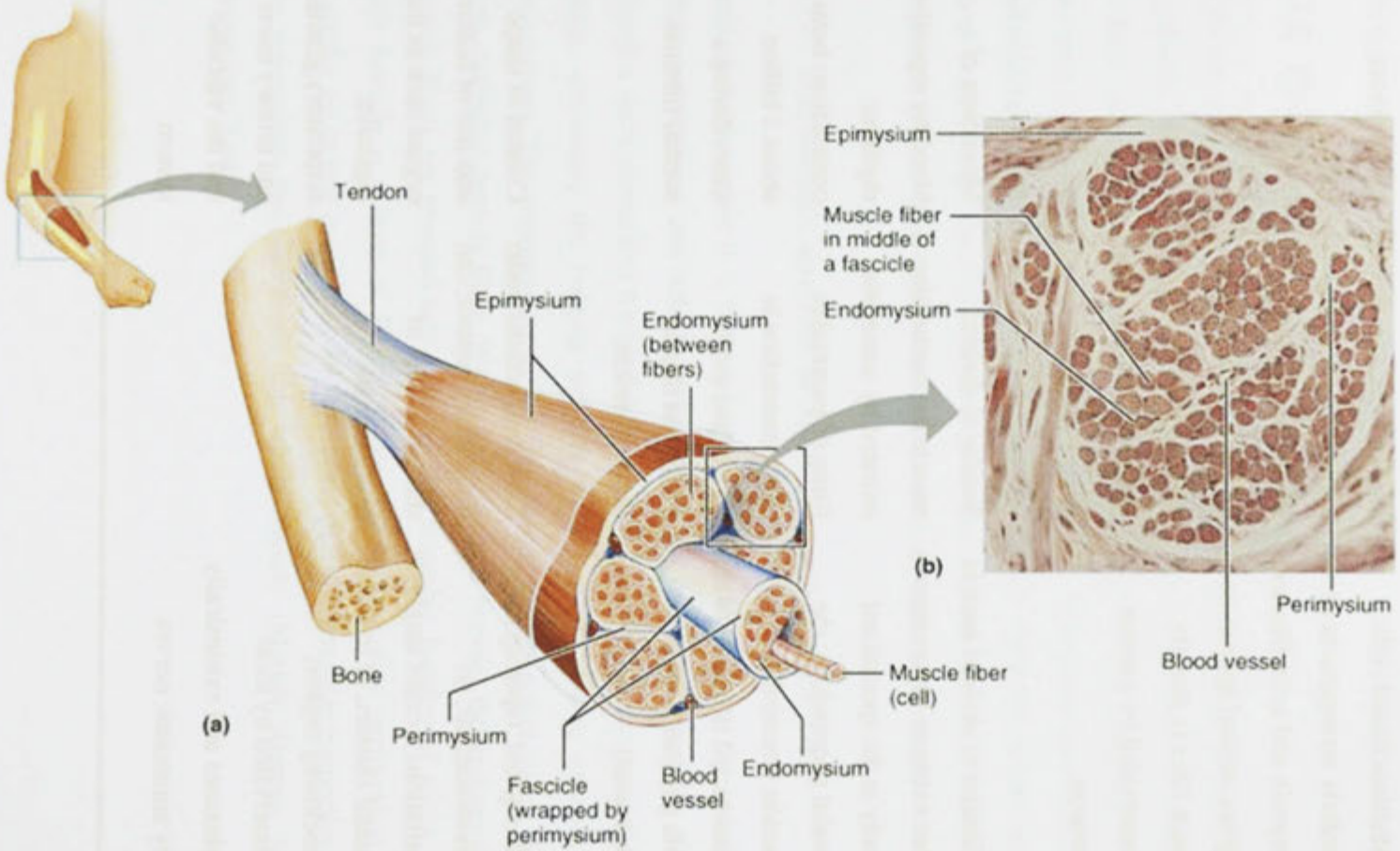

Figure 1-1 Macroscopic anatomy skeletal muscle (Marieb, Human Anatomy and Physiology, 7 ed.).

1.1.4 Microscopic anatomy of a skeletal muscle fibre (Figure 1-2)

Each skeletal muscle fiber is a long cylindrical structure with multiple oval nuclei arranged just beneath its sarcolemma, or plasma membrane. Their diameter typically ranges from 10 to 100 μm.

The sarcoplasm of a muscle fiber is similar to the cytoplasm of other cells, but contains large amounts of glycosomes (granules of stored glycogen) and myoglobin, a pigment that stores oxygen. Muscle cells also contain many mitochondria which are often present as reticulum-like structures extending longitudinally in the fiber near the sarcolemma.

Each muscle fiber contains many rod-like myofibrils that run parallel to its length. The myofibrils, each 1–2 μm in diameter are densely packed and account for about 80% of cellular volume. The myofibrils contain the contractile elements of skeletal muscle cells.

In skeletal and cardiac muscle, striations, a repeating series of dark A bands and light I bands, are evident along the length of each myofibril. In an intact muscle fiber, the A and I bands are nearly perfectly aligned with one another, giving the cell as a whole its striped (striated) appearance.

Each A band has a lighter stripe in its midsection called the H zone. Each H zone is bisected vertically by a dark line called the M line. The I bands also have a midline interruption, a darker area called the Z disc (or Z line). A sarcomere is the region of a myofibril between two successive Z discs, that is, it contains an A band flanked by half an I band at each end. Averaging 2 μm long, the **sarcomere** is the contractile unit of a muscle fiber.

The banding pattern of a myofibril arises from an orderly arrangement of two types of structures, called myofilaments within the sarcomeres. The central thick filaments extend the entire length of the A band. The more lateral thin filaments extend across the I band and partway into the A band. The Z disc, a coin-shaped sheet composed largely of the protein alpha actinin, anchors the thin filaments. Intermediate (desmin) filaments extending from the Z disc connect each myofibril to the next throughout the width of the muscle cell. The H zone of the A band appears less dense because the thin filaments

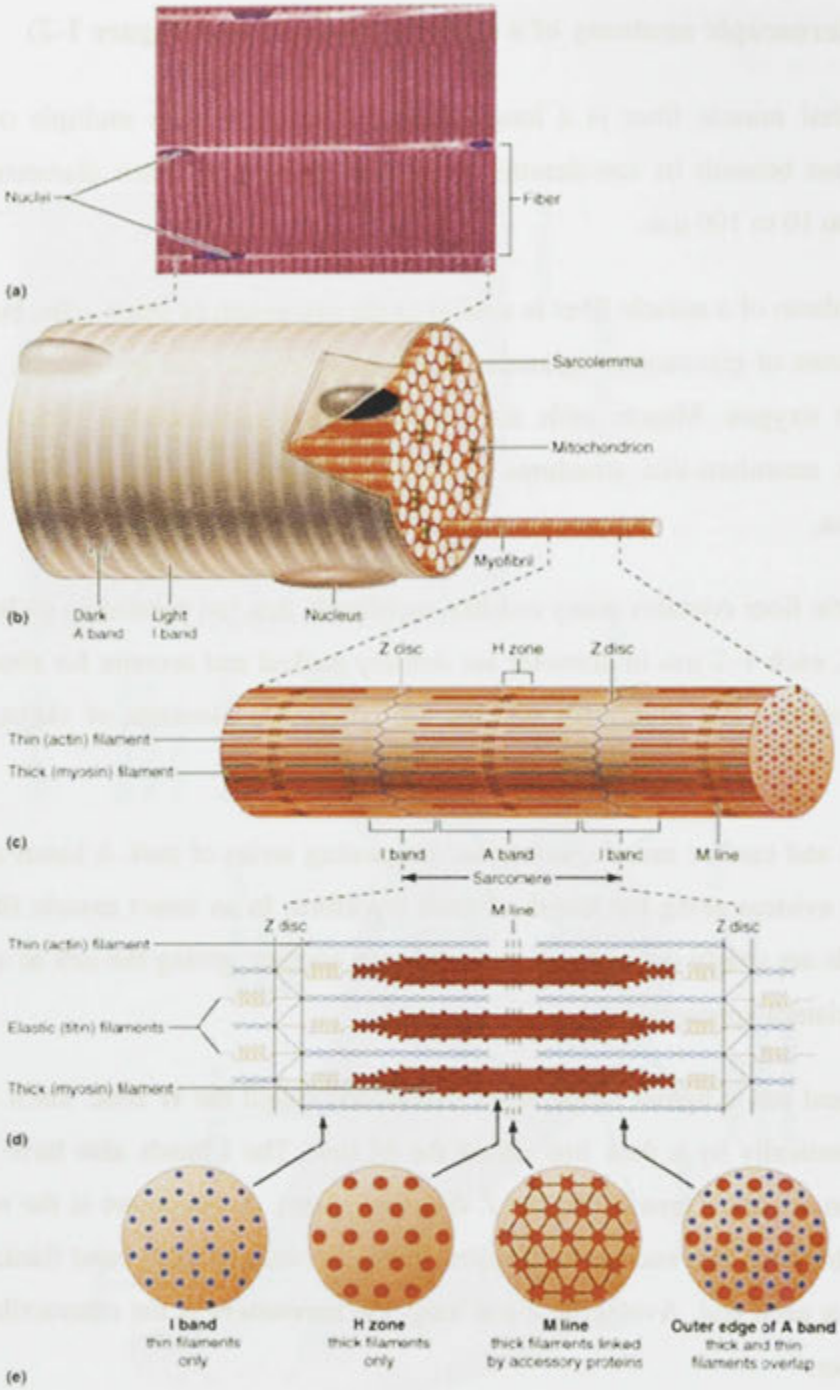

Figure 1-2 Microscopic anatomy of a skeletal muscle fiber. (a) Photomicrograph of portions of two isolated muscle fibers (700×). (b)Diagram of part of a muscle fiber showing the myofibrils. One myofibril extends from the cut end of the fiber. (c) A small portion of one myofibril enlarged to show the myofilaments responsible for the striation pattern. Each sarcomere extends from one Z disc to the next. (d) Enlargement of one sarcomere (sectioned lengthwise). (e) Cross-sectional view of a sarcomere cut through in different areas. (Marieb, Human Anatomy and Physiology, 7 ed.)

do not extend into this region. The M line in the center of the H zone is slightly darker because of the presence there of fine protein strands that hold adjacent thick filaments together. The myofilaments are connected to the sarcolemma at the Z discs and the M lines. In areas where thick and thin filaments overlap, each thick filament is surrounded by a hexagonal arrangement of six thin filaments, and each thin filament is enclosed by three thick filaments.

Thick filaments (about 16 nm in diameter) are composed primarily of the protein myosin. Each myosin molecule has a rod-like tail and two globular heads that link the thick and thin filaments together (form cross bridges). The thin filaments (7–8 nm thick) are composed chiefly of the protein actin. Several regulatory proteins are also present in the thin filament. Two strands of tropomyosin, a rod-shaped protein, spiral about the actin core and help stiffen it. The other major protein in the thin filament, troponin is a three-polypeptide complex. One of these polypeptides (TnI) is an inhibitory subunit that binds to actin; another (TnT) binds to tropomyosin and helps position it on actin. The third (TnC) binds calcium ions. Both troponin and tropomyosin help control the myosin-actin interactions involved in contraction.

During the past decade or so other filament types also have been discovered. The elastic filament is composed of the giant protein titin, which extends from the Z disc to the thick filament, and then runs within the latter to attach to the M line. It holds the thick filaments in place and assists the muscle cell to spring back into shape after being stretched or shortening. Another important structural protein is dystrophin, which links the thin filaments to the integral proteins of the sarcolemma. A genetic defect in the dystrophin gene leads to Duchenne muscular dystrophy, a severe x-linked form of muscle dystrophy. Other proteins that act to bind filaments or sarcomeres together include nebulin, myomesin, and vimentin.

The **sliding filament theory of contraction** states that during contraction the thin filaments slide past the thick ones so that the actin and myosin filaments overlap to a greater degree. In a relaxed muscle fiber, the thick and thin filaments overlap only at the ends of the A band. But when muscle fibers are stimulated by the nervous system, and in the presence of Ca^{2+}, the myosin heads latch on to myosin binding sites on actin in the thin filaments, and the sliding begins. These cross bridge attachments are formed and broken several times during a contraction, acting like tiny ratchets to generate

tension and propel the thin filaments toward the center of the sarcomere. As this event occurs simultaneously in sarcomeres throughout the fiber, the muscle fiber shortens.

Skeletal muscle fibers also contain two important sets of intracellular tubules that participate in the initiation of muscle contraction: the **sarcoplasmic reticulum (SR) and the T (Transverse) tubules**. The major role of the SR is to store Ca^{2+} and regulate intracellular levels of ionic calcium. It stores calcium and releases it on demand when the muscle fiber is stimulated to contract. The T-tubules provide the conduit for the action potential to reach the fiber interior, and brings the outer membranes into close proximity with the internal sarcoplasmic reticulum (SR) (Marieb, Human Anatomy and Physiology, 7 ed.).

1.2 Role of ionic calcium in muscle contraction

In a resting muscle fiber, the SR actively maintains cytosolic Ca^{2+} concentration at sub-micromolar levels, typically 0.1 μM, by active transport mediated by Ca^{2+}-ATPase molecules present at high density along its length and circumference. Upon receiving a stimulus from the T-tubule the SR rapidly releases Ca^{2+} into the cytosol at rates approaching 100 μM/ms to raise cytosolic Ca^{2+} concentration to micro molar levels (typically 1-10 μM). Released Ca^{2+} ions diffuse and bind to troponin-C (TnC), the regulatory subunit of troponin, thereby removing troponin's inhibitory effect on the contractile proteins, actin and myosin, which shorten to generate force. Upon repolarization, Ca^{2+} release terminates and multiple mechanisms act in concert to return cytosolic Ca^{2+} to resting levels. High-density Ca^{2+}-ATPase pumps on the SR membrane rapidly pump Ca^{2+} back in to the SR where it is largely bound to the Ca^{2+} binding protein calsequestrin. Cytosolic Ca^{2+}-binding proteins with rapid kinetics buffer Ca^{2+} transiently while the slower SR pumps return it to the SR. Force terminates when cytosolic Ca^{2+} returns to resting levels. Thus, cytosolic Ca^{2+} is the central link between membrane excitation and activation of the contractile proteins. Contraction is inhibited at low resting Ca^{2+} levels and proceeds when Ca^{2+} is elevated transiently in response to membrane excitation (Cell Physiology Sourcebook: A Molecular Approach, third edition).

1.3 Sarcoplasamic Reticulum (SR) and T (Transverse) -tubules

Synchronous activation of skeletal muscle depends on effective, rapid communication between the specialized extracellular membranes of the sarcolemma/T-tubules and the intracellular SR. To achieve this, the membranes of skeletal muscle are highly organized to bring into close physical proximity the proteins involved in each of the key events: membrane excitation, Ca^{2+} release, and force generation.

The sarcolemma and T-tubule membranes are organized to conduct the action potential rapidly to all parts of the fiber. The T-tubules compose the majority of the sarcolemma membrane, representing 50-80% of the total sarcolemma area. They invaginate from the sarcolemma in a transverse plane approximately twice every 1-2 μM (at two planes per sarcomere in mammalian muscle). Within this plane they branch extensively to form a network that covers the entire cross-sectional area of the muscle cell (**Figure 1-3**)

The sarcoplasmic reticulum (SR) is an elaborate smooth endoplasmic reticulum. Its interconnecting tubules surround each myofibril. Most of these tubules run longitudinally along the myofibril. Others form larger, transverse cross channels at the A band–I band junctions. These channels are called terminal cisternae ("end sacs") and they always occur in pairs.

As each T tubule protrudes deep into the cell, it runs between the paired terminal cisternae of the SR to form successive groupings of the three membranous structures called triads (**Figure 1-4**). Up to 80% of the tubular membrane is associated with the SR at triad junctions (Dulhunty, 1984). Given this membrane architecture, no part of the sarcolemma is more than a few tenths of a micrometer from the Ca^{2+} release channels of the SR.

Variations on this architecture theme for the intracellular junctions occur in different species (Burighel et al., 1977). These include dyads, in which a junctional region of terminal cisterna is apposed to a single short segment of T-tubule, and peripheral couplings, in which a junctional region of terminal cisterna is apposed to an approximately circular junctional domain of the surface membrane. Triads, dyads, and peripheral couplings are structurally and functionally equivalent. Each is the intracellular site at which the

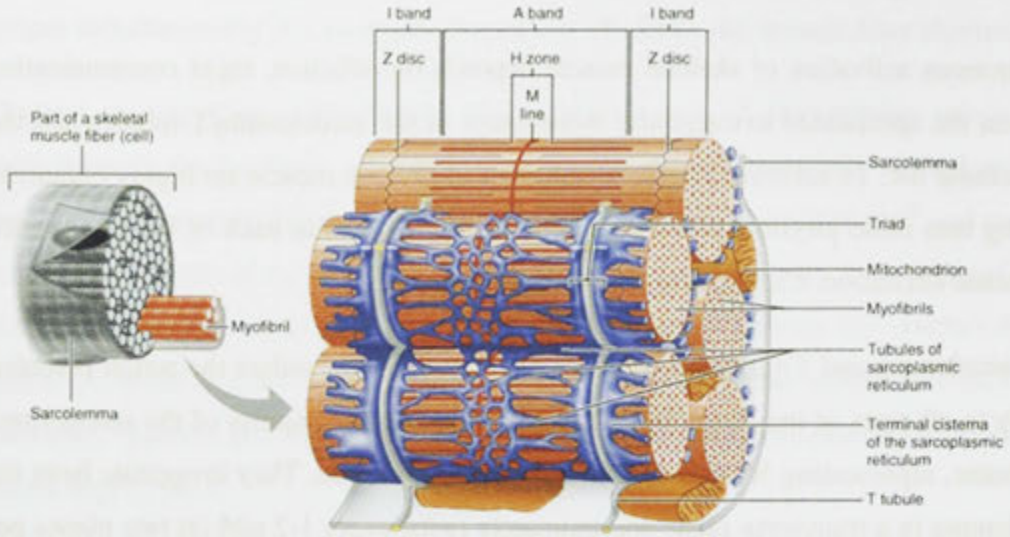

Figure 1-3 Sarcoplasmic reticulum and T-tubular network of skeletal muscle (Marieb, Human Anatomy and Physiology, 7 ed.)

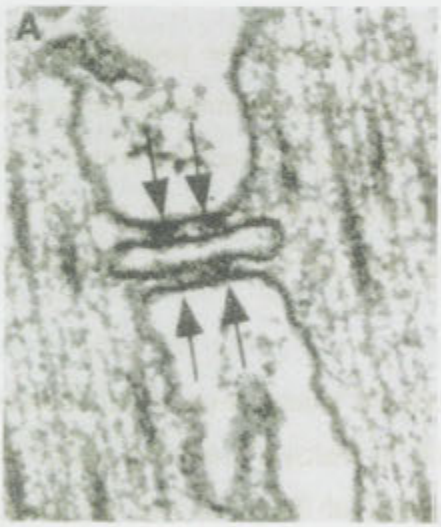

Figure 1-4 An electron micrograph of a section through a triad junction of a frog tonic fibre, showing a central t-tubular element flanked on either side by a terminal cisternae element of the sarcoplasmic reticulum. The arrows point to electron-dense junctional feet spanning the junctional gap on either side of the t-tubule between the t-tubule and terminal cisternae. (From Franzini-Armstrong et al. Ann N Y Acad Sci. 1998 Sep 16;853:20)

interaction between electrical excitation of the outer membrane is linked to the intracellular Ca^{2+} release. Collectively, these intracellular junctions are called calcium release units (CRUs) (Franzini-Armstrong et al., 1999).

1.4 Proteins of the triad junction

At the triad junctions, voltage-dependent Ca^{2+} channels in the T-tubular membrane (also known as voltage sensors because they respond to the action potential depolarization, or dihydropyridine receptors (DHPRs) because of their sensitivity to the dihydropyridine class of Ca^{2+} channel blocking drugs) detect the depolarization and transduce it into a signal for opening Ca^{2+} release channels (also called the ryanodine receptors (RyRs) because they bind this plant alkaloid with high affinity) on the closely opposed SR membrane (Leong and MacLennan, 1998).

The two key proteins of the calcium release units (CRU), the DHPRs and the RyRs, associate at the triad junctions to form a functional signal transduction complex (Flucher et al., 1996). At the junctions, the T-tubule and SR membranes flatten and face each other across a narrow gap of about 10 nm. The junctional surface of the terminal cisternae of the SR (jSR) contains two rows of proteins corresponding to the Ca^{2+} release channels/RyRs (Franzini-Armstrong, 1970). The RyRs are packed in highly ordered arrays, in a skewed pattern with a center-to-center spacing of about 30 nm. The RyRs are also termed foot proteins because of their unique appearance as dense, bridging structures in electron micrographs of transverse section of the triad (**Figure 1-4**). Each RyR/ Ca^{2+} release channel is composed of four identical subunits. Each subunit has a membrane-spanning domain and a large cytosolic domain that extends across the junctional gap and comes to within 1 nm of the T-tubule membrane. In a top view, the large cytosolic domains of the tetramer roughly resemble four spheres assembled in a four-leaf clover or quatrefoil pattern. The large cytoplasmic domain is identified with the foot structure observed in electron micrographs of the triad junction (Inui et al., 1987). In a side view, the tetramer assumes a mushroom shape with a smaller central region composed of four equal lobes that presumably insert into the jSR membrane to form the ion-conducting pore of the molecule (Wagenknecht et al., 1989). In skeletal muscle the junctional T-tubule membranes also contain a high density of proteins that are aligned with a regular periodicity in parallel rows of four-particle

arrays, termed junctional tetrads (Block et al., 1988). The tetrads have been identified as groups of four voltage sensors/DHPRs and are arranged in a pattern approximately corresponding to the outer coners of the cytosolic spheres of the RyR tetramer (Takekura et al., 1994). Tetrads are associated with RyRs in an alternate disposition such that one tetrad is associated with every other RyR (**Figure 1-5**, **Figure 1-6**).

In cardiac muscles, DHPRs are also clustered in close proximity to RyRs but they do not form tetrads and are not disposed in a detectable ordered arrangement (**Figure 1-6**). The T-tubules in cardiac muscle have a much larger diameter than in skeletal muscle, and the most common junctions are in the form of dyads formed by the close apposition of a flat SR cisterna, which contacts the T-tubule over a wide area (Franzini-Armstrong et al., 1998).

1.5 Excitation-Contraction Coupling

1.5.1 Overview

Excitation-contraction (EC) coupling is a term used to describe the events that link plasma membrane depolarization to the release of Ca^{2+} from the SR, which in turn triggers muscle contraction. Central to this process is the functional interaction between the ryanodine receptor and the surface voltage-activated L-type Ca^{2+} channel, the dihydropyridine receptor (DHPR).

Activation begins when an action potential from a motor neuron arrives at the neuromuscular junction, resulting in the release of the neurotransmitter acetylcholine (ACh) into the synaptic clefts. Binding of ACh to ACh receptors on the adjacent end plate locally depolarizes the postsynaptic membrane to threshold and elicits an action potential on the muscle sarcolemma. The action potential rapidly propagates the depolarization to the entire sarcolemma and into the fiber interior via the T-tubular network. At the triad junctions, the dihydropyridine receptors detect the depolarization and transduce it into a signal for opening the ryanodine receptor Ca^{2+} release channels on the closely opposed SR membrane. This leads to a rapid Ca^{2+} release from the SR into the cytosol. The released Ca^{2+} binds to troponin-C and leads to the cascade of events that result in muscle contraction (**Figure 1-7**).

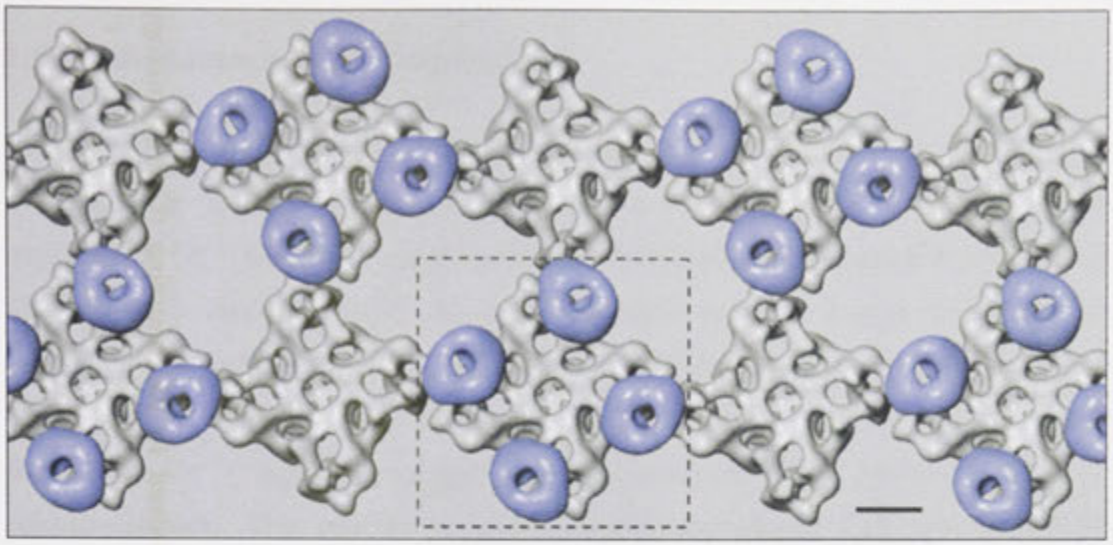

Figure 1-5 Arrangement of RyR1 and DHPR in skeletal muscle. Model based on freeze-fracture studies and 3D reconstructions of the two Ca^{2+} channels, generated by electron cryomicroscopy and single particle reconstruction. Two arrays of RyRs are overlaid by arrays of DHPRs grouped into tetrads. Scale bar represents 100 Å (Serysheva et al., 2002).

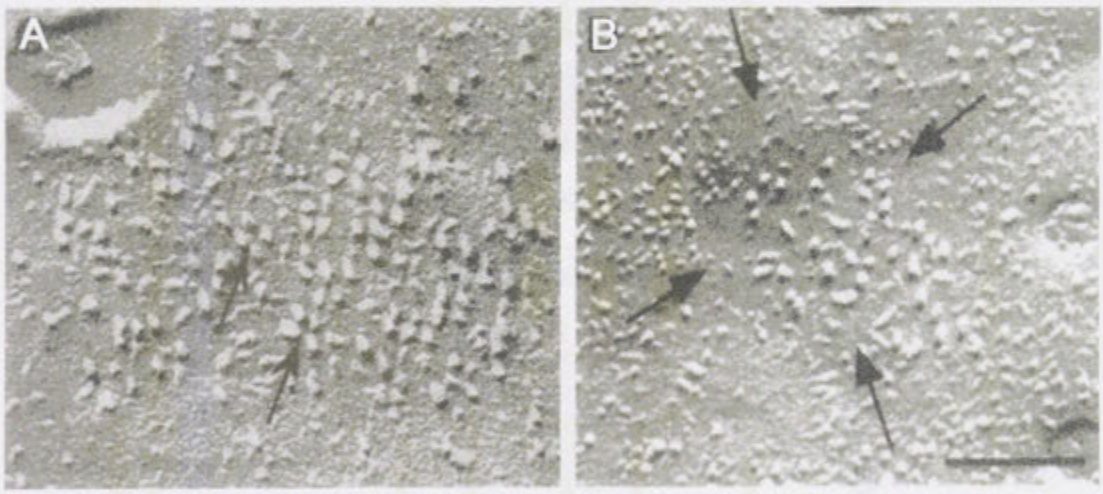

Figure 1-6 Freeze-fracture electron micrographs of the surface membrane of developing mouse skeletal and cardiac muscle. DHPRs are clustered in both cardiac and skeletal muscle but in a different manner. A. In skeletal muscle DHPRs form an array of tetrads (arrows point to individual tetrads) B. In cardiac muscle DHPRs are randomly disposed. Scale bar = 0.1 μm (from Franzini-Armstrong et al. Ann N Y Acad Sci. 1998 Sep 16;853:20-30)

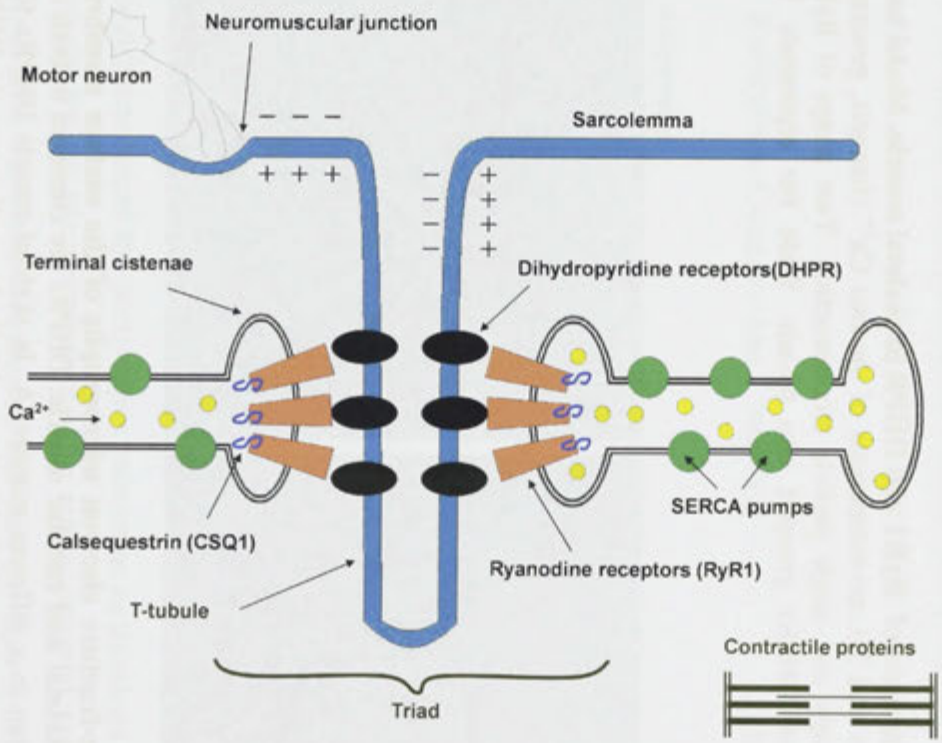

Figure 1-7 Schematic representation of a triad junction illustrating the major components involved in EC coupling (Cell Physiology Sourcebook: A Molecular Approach, third edition).

1.5.2 Mechanisms of EC coupling

Different EC coupling mechanisms exist in skeletal and cardiac muscles. A distinguishing feature is that EC coupling in cardiac muscle is dependent on extracellular Ca^{2+}, whereas skeletal muscle EC coupling is not (**Figure 1-8**) (Nabauer et al., 1989). In cardiac muscle, the dihydropyridine-sensitive, L-type Ca^{2+} channels located in the surface membrane and T-tubule mediate the influx of Ca^{2+} during an action potential by functioning as voltage-dependent Ca^{2+} channels. The resulting rise in intracellular Ca^{2+} concentration triggers the massive release of Ca^{2+} by opening SR Ca^{2+} release channels. This process is known as calcium-induced Ca^{2+} release (CICR) (Tanabe et al., 1990).

In vertebrate skeletal muscle, a different mechanism of EC coupling is present. A unique mechanism, referred to as the mechanical coupling mechanism, has been formulated and suggests that the SR Ca^{2+} release channel is opened via a direct physical interaction with a voltage-sensing molecule in the T-tubule. In a classic experiment, Armstrong and colleagues (1972) demonstrated that a frog skeletal muscle fiber continues to twitch in the absence of extracellular Ca^{2+} when stimulated with action potentials. Similarly, voltage-clamp experiments demonstrated that a skeletal muscle fiber can develop tension provided only that the membrane is depolarized to a minimum potential and duration, termed the mechanical threshold. Subsequently, Schneider and Chandler (1973) discovered the presence in skeletal muscle membranes of mobile intramembrane charges whose movement could be detected electrically as a voltage-dependent dielectric current, termed charge movement. Based on the similarity of the kinetics and voltage dependence of charge movement to mechanical activation, they proposed that it reflected the movement of charged intra-membrane domains of a molecule in the T-tubules that functioned as the essential voltage sensor for EC coupling. They further suggested that the voltage sensor might interact directly with a hypothetical Ca^{2+}-conducting protein on the SR to cause its opening. It was not until the late 1980s that this hypothetical protein on the SR was identified as the ryanodine receptor (RyR1).

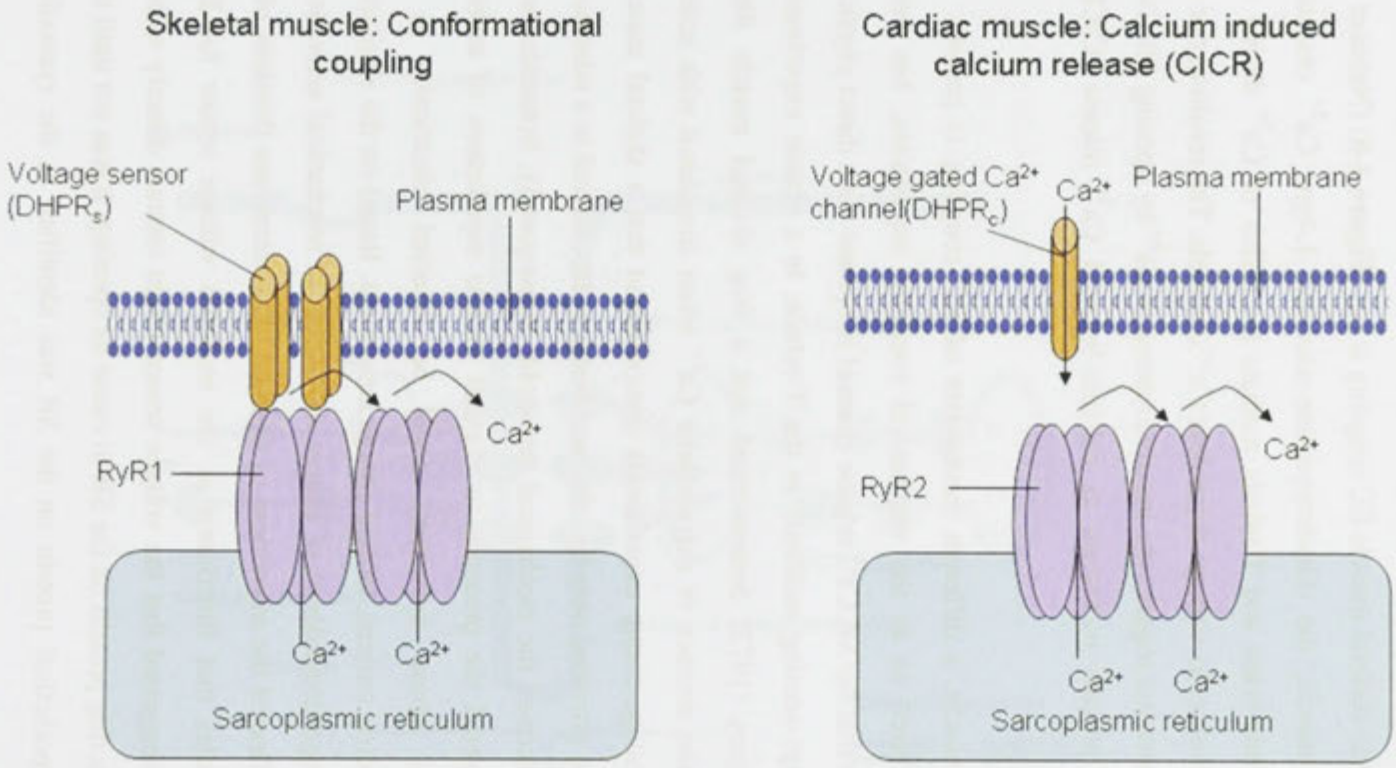

Figure 1-8 Models of skeletal and cardiac muscle EC coupling. EC coupling in cardiac muscle is dependent on extracellular Ca^{2+}, whereas skeletal muscle EC coupling is not.

Biophysical and pharmacological evidence, as well as molecular expression studies, suggest that the T-tubule DHPR is the voltage sensor for EC coupling in vertebrate skeletal muscle (Rios et al., 1987, Rios and Pizarro, 1991). The mechanical or allosteric hypothesis of EC coupling (electromechanical coupling) proposes that movement of charged voltage-sensing domains of the skeletal DHPR allosterically alters an activation domain of RyR1. This early allosteric model of EC coupling, formulated before the identity of the proteins of the triad junction, has formed the framework for subsequent investigations into the nature of the molecular interactions at the skeletal triad junction complex. *However, the exact molecular relationship between the dihydropyridine receptor and the ryanodine receptor in skeletal muscle remains ill-defined* (Dirksen,R.T.,2009, Beam and Bannister,2010). *Whether there is a direct interaction between these proteins or whether this interaction requires accessory proteins as part of a larger complex remains to be established.*

Further studies also found that the proper targeting of DHPRs into tetrads (groups of 4) that are aligned with RyRs is essential for skeletal type EC coupling. The discovery of bidirectional signalling between the DHPR and RyR allowed a distinction between misalignment(defective targeting) and interruption of EC coupling (Nakai et al., 1996). One arm of the bidirectional coupling is the **'orthograde'** EC coupling process (signalling from the DHPR to RyR1). The second arm is a **'retrograde'** signal in which the coupling between the DHPR and the RyR markedly increases the size of the L-type Ca^{2+} current. Thus, a large L-type Ca^{2+} current recorded at the same time as a small external Ca^{2+}-independent Ca^{2+} release implies correct targeting of the DHPR and RyR, but defective EC coupling (Dirksen,R.T., 2002, Dulhunty, 2006).

The existence of two populations of skeletal muscle RyRs, one coupled to tetrads and one not, as evidenced by the spacing of the DHPR tetrads (Takekura et al., 1994), raises the question of how unlinked RyRs are activated. One suggestion is that Ca^{2+} released by DHPR-linked RyRs activates DHPR-unlinked RyRs in skeletal muscle by a Ca^{2+}-induced mechanism resembling that in cardiac muscle (Rios and Pizarro, 1991). An alternative mechanism is that neighboring skeletal muscle RyRs are physically linked, leading to simultaneous channel opening and closing, termed coupled gating (Marx et al., 1998)

1.6 Ryanodine receptor Ca^{2+} release channel (RyR)

1.6.1 Overview

The RyR Ca^{2+} release channel belongs to a superfamily of ligand-gated ion channels (Franzini-Armstrong and Protasi, 1997). RyRs share significant sequence and structural homology with the inositol 1,4,5- trisphosphate (IP 3) receptors that release Ca^{2+} from internal stores in other cell types (Berridge 1993). RyRs are larger molecules with a significantly greater Ca^{2+} conductance than IP 3 receptors and are found in cells such as muscle that generate large, fast changes in intracellular Ca^{2+} concentration (Mackrill et al., 1997).

1.6.2 History

RyRs were initially observed in skeletal muscle in the early 1970s, where they were visualized in electron micrographs as large electron-dense masses situated along the face of the sarcoplasmic reticulum (SR), spanning the junctional gap between SR and the plasma membrane, and they were therefore termed junctional foot proteins (Saito et al., 1984, Franzini-Armstrong, 1999). But at the time the molecular identity of this structure was not known. The RyR was identified as the foot protein and gained its present name in the late 1980s after it was found by Fleischer et al to be the protein that binds ryanodine, a plant alkaloid that enabled purification and molecular characterization of the protein (Fleischer et al., 1985, Inui et al., 1987).

1.6.3 RyR isoforms and distribution

Mammalian tissues express three types of RyRs that are encoded by three different genes. The three RyR isoforms are also known as the skeletal muscle (RyR1), cardiac muscle (RyR2), and brain (RyR3) RyR because they were first identified and isolated from skeletal muscle (Takeshima et al., 1989, Zorzato et al., 1990), cardiac muscle (Otsu et al., 1990, Nakai et al., 1990), and brain (Hakamata et al., 1992), respectively. Hence, the currently accepted terminology is based on the abundance and timing of purification of the RyRs from various tissues. RyR1 and RyR2 are the predominant isoforms in skeletal muscle and cardiac muscle, respectively; however, both isoforms are also expressed in brain and other tissues at low levels. In turn, the brain RyR is expressed as a minor component in skeletal and cardiac muscles. All three share a

high-affinity binding site for [^{3}H] ryanodine and a high-conductance pathway for Ca^{2+} and monovalent cations, but display isoform- and species-dependent differences in their *in vitro* regulation by Ca^{2+} and other effector molecules.

1.6.4 RyR1 structure

The skeletal muscle RyR is composed of four polypeptides as evidenced by (a) the four-leaf clover-like (quatrefoil) appearance of negatively stained samples (**Figure 1-9**) (b) a high apparent sedimentation coefficient of 30S, and (c) cross-linking studies (Lai et al., 1989). Each of the large RyR polypeptides in RyR1, RyR2, and RyR3 is comprised of ~5000 amino acids with a predicted molecular mass of ~560 kDa and amino acid sequence identity of 65-70% between the isoforms.

Three dimensional reconstructions of RyR1 based on cryo-electron microscopy show a four-fold symmetry and a characteristic mushroom shape, which comprises of two square-shaped regions interconnected by four column densities. A large square-shaped region with overall dimensions of 270 x 270 x 120 Å represents a bulky cytoplasmic region exposed to the gap between the SR membrane and the t-tubule membrane. The cytoplasmic (CY) assembly has numerous distinctive structural domains and intervening cavities that appear suitable for interaction with channel-specific ligands. The clamp-shaped regions, located at the corners of the CY assembly are interconnected by "handle" domains and form a continuous network with the central rim and the column domains of the CY region via several bridging densities. The small square-shaped structure with dimensions of 120 x 120 x 60 Å is rotated by ~40° with respect to the CY assembly and represents the region which spans the SR membrane (Serysheva, 2004) (**Figure 1-10**).

The proposed assignment of two major morphological regions within the 3D reconstruction of RyR is consistent with the topological arrangement that is predicted based on hydropathy analysis of the channel protein sequence (Takeshima et al., 1989, Zorzato et al., 1990). Sequence analysis indicates a large hydrophilic N-terminal region thought to constitute the cytoplasmic or foot domain and a smaller mostly hydrophobic C-terminal region predicted to form the intra-membrane channel. The foot region contains four repeat motifs that occur in two tandem pairs. Studies with site-directed

antibodies suggest that the N and C-termini of RyR1 are cytoplasmically localized, with the C-terminus being important for the expression of a functional RyR1 complex

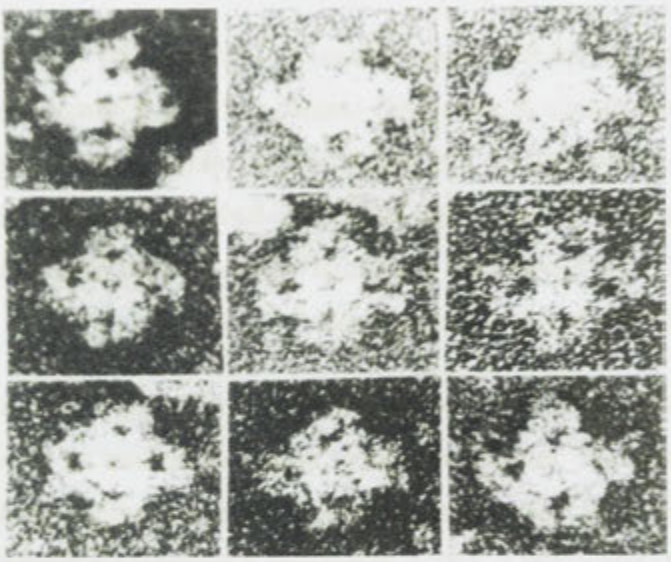

Figure 1-9 Negative-stain electron micrograph of the purified rabbit skeletal muscle RyR. A selected panel of particles displaying the characteristic four-leaf clover (quatrefoil) structure of the 30S RyR complex. Dimensions of the quatrefoils are 34 nm from the tip of one leaf to the tip of the opposite one, with each leaf 14 nm wide. The central electron-dense region has a diameter of 14 nm with the central hole of a diameter of 1-2 nm (from Lai et al., Nature 331, 315-319, 1988)

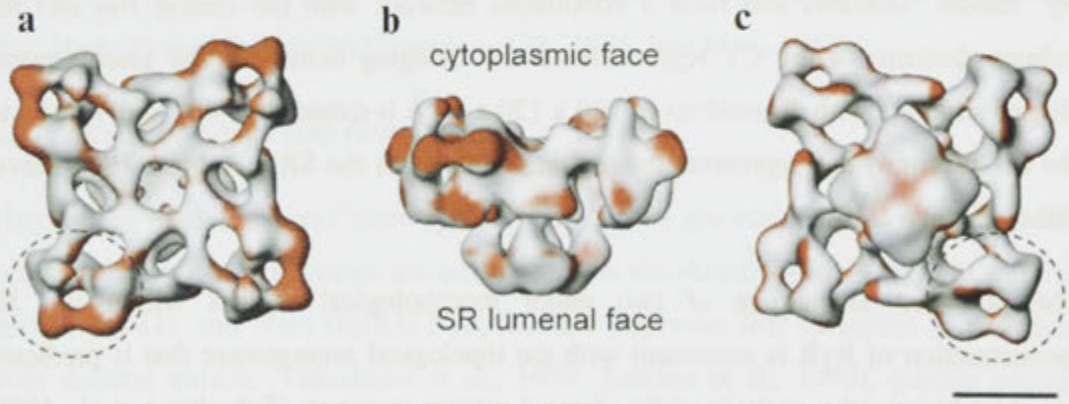

Figure 1-10 3D Reconstruction of the RyR1 based on cryoelectron microscopy. Regions of significant differences between open and closed state of the channel are shown in red. (a) view from the cytoplasm, (b) side view (c) view from the SR lumen. The clamp shaped domains are indicated with dashed circles. The scale bar represents 100 A^0 (Serysheva, 2004)

(Gao et al., 1997). The membrane-spanning region is highly conserved and has strong similarity with the same region of the IP 3 receptor. The number of trans-membrane helices in the C-terminal region has not been established, but is proposed to be between 4 and 12 (**Figure 1-11**) Experimental data obtained by Du et al indicate 8 trans-membrane helices (Du et al., 2002).

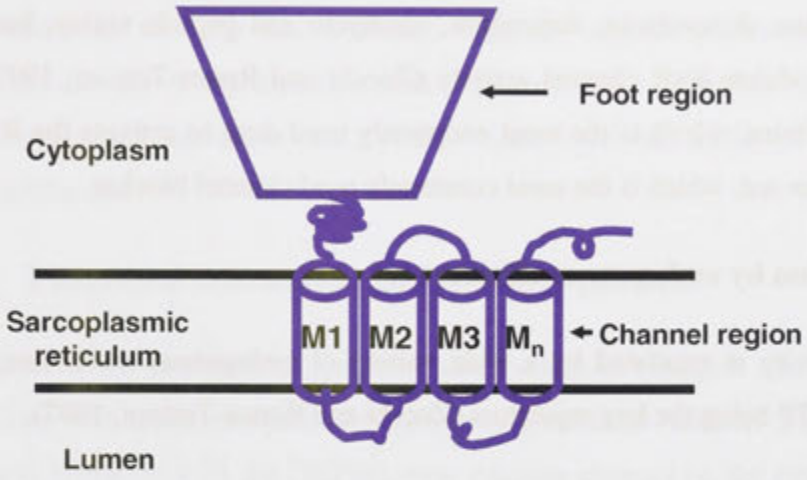

Figure 1-11 Schematic Diagram of the Ryanodine receptor showing the secondary membrane topology. M 1, 2 etc. denotes the transmembrane domains which are proposed to be between 4 and 12 (Adapted from Gao et al., 1997)

The structure of RyR has also been analysed under conditions that drive the channel population predominantly to its "open" (conducting) and "closed" (non-conducting) states. These studies of the RyR in different functional states suggest that channel activation is associated with significant mass rearrangements in the channel complex, implying a highly allosteric regulation of channel gating (Orlova et al., 1996, Serysheva et al., 1999, Samso et al., 2009).

1.6.5 Modulation by pharmacological agents

The isolation and structural determination of the SR Ca^{2+} release channel has been greatly facilitated by the identification of ryanodine as a channel-specific ligand. Ryanodine is a neutral plant alkaloid that is obtained from the stems of the South American shrub, *Ryania speciosa*, and is composed of two major compounds: ryanodine and 9,21- didehydroryanodine. Ryanodine binds to the RyR with high affinity and specificity, preferably in its open conformation, and thus, ryanodine binding is used as

an index of channel activation. Ryanodine activates the channel at low (nanomolar) concentrations, but inhibits the channel at high (micromolar) concentrations. Activation is associated with prolonged channel opening to a reduced conductance level (Ehrlich et al., 1994).

A plethora of exogenous compounds, including volatile and local anaesthetics, 4-chloro-m-cresol, polylysine, doxorubicin, dantrolene, neomycin and peptide toxins, has also been shown to modulate RyR channel activity (Zucchi and Ronca-Testoni, 1997). Of special note is caffeine, which is the most commonly used drug to activate the RyR *in vitro* and ruthenium red, which is the most commonly used channel blocker.

1.6.6 Modulation by endogenous effectors

RyR channel activity is regulated by a wide variety of endogenous molecules, with Ca^{2+}, Mg^{2+} and ATP being the key regulators (Zucchi and Ronca-Testoni, 1997).

SR Ca^{2+} flux measurements, single channel recordings and ryanodine-binding assays have demonstrated that cytosolic Ca^{2+} has a biphasic effect on skeletal muscle RyR channel activity (Meissner et al., 1997, Meissner et al., 1986). The threshold for channel activation is approximately 100 nM with a maximum in the range of 10–100 μM, whereas millimolar Ca^{2+} strongly inhibits the channel.

Mg^{2+} is a potent RyR channel inhibitor. SR Ca^{2+} flux measurements, single channel recordings and ryanodine-binding assays have demonstrated that Mg^{2+} inhibits RyR1 in a dose-dependent manner, with millimolar concentrations resulting in complete inactivation (Laver et al., 1997, Meissner et al., 1986). This Mg^{2+} inhibition must be relieved during EC coupling for Ca^{2+} release (channel opening) to proceed (Laver et al., 2004)

The adenine nucleotides ATP, ADP, AMP and cyclic-AMP, as well as adenine, activate RyR channel activity (Meissner et al., 1986). SR Ca^{2+} flux measurements, single channel recordings and ryanodine-binding assays have demonstrated that ATP at millimolar levels is a potent agonist of skeletal muscle RyR (Laver et al., 2001, Meissner et al., 1986, Smith et al., 1986). RyR1 is stimulated by ATP even at very low nanomolar Ca^{2+} concentrations, whereas the combination of micromolar Ca^{2+} and millimolar ATP elicits persistent channel activation.

1.6.7 Gene knockout studies

The physiological role of the RyR has been addressed by gene knock-out studies. Mutant mice lacking RyR1 (dyspedic mice) died perinatally and the skeletal muscle fibers failed to show a contractile response to electrical stimulation under physiological conditions (Takeshima et al., 1994). RyR3 knockout mice showed an impairment of contraction in neonatal but not adult skeletal muscle (Sonnleitner et al., 1998, Takeshima et al., 1996). Deletion of RyR2 resulted in embryonic lethality and altered cardiomyocytes (Takeshima et al., 1998). Hence RyR1 and RyR2 are essential proteins, but RyR3 is not.

1.6.8 Functional interactions and accessory proteins

The RyR is the centre of a dynamic macromolecular complex interacting directly or indirectly with numerous proteins that affect its channel function (**Figure 1-12**). RyR1 interacts primarily with the DHPR/L-type calcium channel on the cytoplasmic side and with the calcium binding protein calsequestrin (Beard et al., 2004) on the luminal side of the jSR through the anchoring proteins, Triadin and Junctin. It uses the DHPR as a 'voltage sensor' to detect the surface membrane action potential and calsequestrin to detect the environment within the sarcoplasmic reticulum. Consequently, the RyR is able to respond to surface depolarization in a manner that depends on the Ca^{2+} load within the calcium store.

In addition, the RyR also interacts with other components of the jSR including triadin, junctin, FKBP12 protein (FK506 binding protein) and a 90-kDa jSR protein that may associate with RyR1 in fast-twitch skeletal muscle (Froemming et al., 1999). Junctin and triadin both bind to CSQ and RyRs (Goonasekera et al., 2007, Jones et al., 1995) and are thought to anchor CSQ close to the RyR. Junctin plays a distinct and important role in Ca^{2+} homeostasis (Dulhunty et al., 2009) although the potential impact of the triadin association with RyR1 in skeletal muscle EC coupling remains elusive (Allen, 2009, Marty et al., 2009). FKBP12 protein is stably bound to the corners of the cytosolic domain of the RyR in a 1:1 ratio and may mediate a subunit

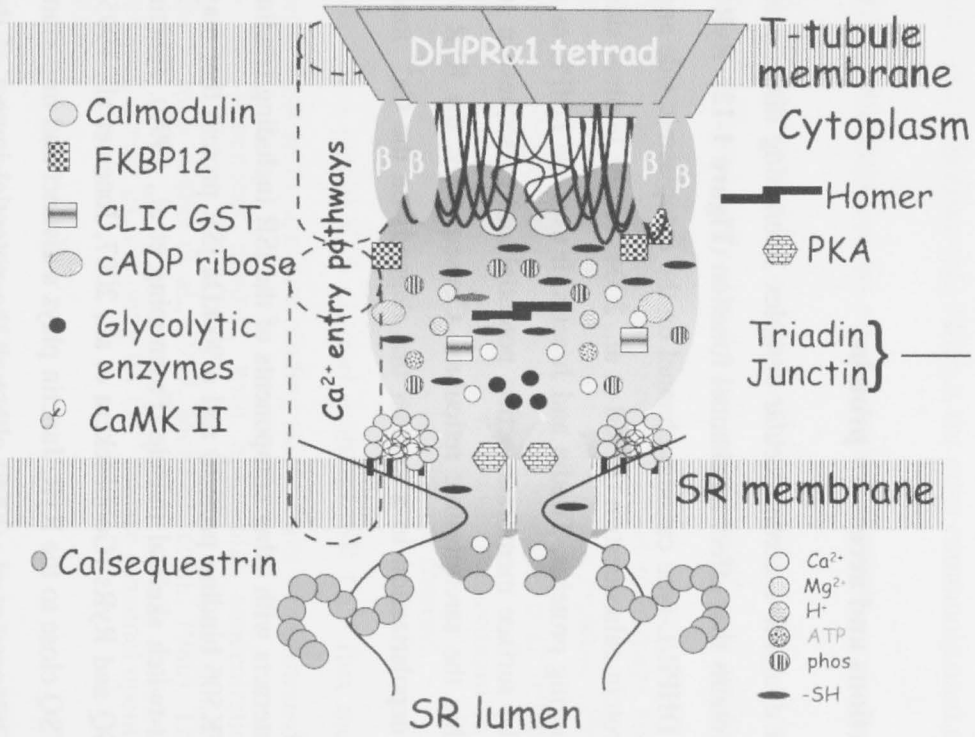

Figure 1-12 Model illustrating the many protein–protein interactions that contribute to the macromolecular complex that forms the calcium release unit of skeletal muscle sarcoplasmic reticulum (SR). The core of the complex is the dihydropyridine receptor (DHPR)/ryanodine receptor (RyR)/triadin/junctin/ calsequestrin (CSQ) interaction that provides continuity from the extracellular space (lumen of the t-tubule) to the lumen of the SR. Interactions with other cytoplasmic components that also alter EC coupling are shown, including protein kinase A (PKA), FK506 binding protein 12 (FKBP12), chloride intracellular channel (CLIC), glutathione S-transferase (GST), calmodulin kinase II (CaMK II), Ca2+ binding sites, Mg2+ binding sites, protonation sites, ATP binding sites, phosphorylation and oxidation sites. phos, phosphorylation (Dulhunty 2006)

to subunit interaction stabilizing a closed state of the channel (Avila et al., 2003, Chelu et al., 2004, Cornea et al., 2010).

The skeletal RYR1 is capable of dual modes of activation, both allosteric and ligand gated. It can be allosterically opened by an associated skeletal DHPR or opened by direct Ca^{2+} binding when not associated with a skeletal DHPR. When isolated and purified in the absence of triad junctions or DHPRs, the skeletal RYR1 behaves as a ligand-gated ion channel with a high single-channel ion flux. Studies in which DHPRs have been inserted into dysgenic myotubes that congenitally lack DHPRs have demonstrated that RyR1 can be activated by Ca^{2+} entering through DHPRs when the inserted DHPR contains key cardiac-specific sequences. On the other hand, RyR1 can be opened allosterically and mediate a skeletal-type EC coupling (independent of extracellular Ca^{2+}) only when associated with a skeletal-type DHPR. Thus, the complete skeletal DHPR-RyR1 complex is required to initiate Ca^{2+} release by the physiologically relevant mode in fast-twitch skeletal muscle.

1.7 Dihydropyridine receptor (DHPR) L-type Ca^{2+} channel

1.7.1 Overview of voltage gated Ca^{2+} channels (VGCCs)

The skeletal muscle dihydropyridine receptor is a slowly-activating (L-type) voltage gated calcium channel that requires large depolarisations for activation and functions as the voltage sensor in excitation-contraction coupling.

Voltage-gated Ca^{2+} channels or VGCCs (also known as voltage-dependant calcium channels or VDCCs) are activated in response to membrane depolarization and are essential in cytoplasmic Ca^{2+} signaling processes in a variety of cells. VGCCs regulate a number of cellular processes including muscle contraction, secretion, neurotransmitter release, gene regulation and neuronal migration.

1.7.2 History and classification

Voltage-gated calcium channels were first identified by Fatt and Katz in 1953 (Fatt and Katz, 1953). Later it was discovered that there were different channel subtypes in excitable cells and, consequently, voltage-gated calcium channels were classified and named according to various schemes (Lacinova, 2005).

In the 1980's, the calcium channel protein was purified and shown to consist of several subunits (Borsotto et al., 1985, Flockerzi et al., 1986, Takahashi et al., 1987, Leung et al., 1988). The principal subunit of the voltage-gated calcium channel (VGCC) was named α_1, and auxiliary subunits were named β, α_2, δ, and γ. Cloning of the genes encoding individual subunits followed soon after. So far, ten genes for α_1 subunits, four for β subunits, four for the α_2-δ complex and eight for γ subunits have been identified.

The very first channel classification was based on basic electrophysiological and pharmacological properties. An observation was made that some calcium channels need only a small depolarization to be activated, while others require a relatively high step in membrane voltage to open (Hagiwara et al., 1975, Llinas and Yarom, 1981). According to this criterion, calcium channels were divided into low-voltage activated (LVA) and high-voltage-activated (HVA). LVA calcium channels activate at a membrane voltage positive to –70 mV. Because of the small amplitude of single channel conductance and its fast decay, these channels were also called T-type calcium channels (T for tiny or transient). HVA channels have an activation threshold at membrane voltages positive to –20 mV. Because of its large-single channel conductance amplitude and slow kinetics of current decay, it was named L-type calcium channel (L for large or long-lasting) in contrast to the T-type. A pharmacological hallmark of all L-type channels is their sensitivity to 1,4-dihydropyridines (DHPs) – which include a wide class of drugs with either inhibitory (nifedipine, felodipine, amlodipine) or activatory (Bay K 8644) action on the channel.

In the 1980's, experiments with neuronal cells revealed novel calcium channels, insensitive to DHPs and with single-channel conductances between those of T-type and L-type channels (Nowycky et al., 1985, Fox et al., 1987). These channels were named N-type calcium channels (N for neuronal). Later, it was shown that neuronal non-L-type channels could be further classified into subtypes according to their sensitivity to peptide toxins isolated from cone snails and spiders. The channel sensitive to ω-conotoxin, kept the name N-type channel, while the channels sensitive to ω-Agatoxin was named P/Q-type calcium channel (P for Purkinje cells, where this channel was characterized) (Llinas et al., 1989). The channels resistant to these toxins were named R-type calcium channel (R for resistant).

The second classification of voltage-gated calcium channels was developed in the 1980's and was based on cloning of cDNAs encoding individual channel types. Since the α_1 subunit is responsible for basic electrophysiological and pharmacological properties, it formed the basis of early channel classifications. Investigators tried to establish links between the newly cloned subunits and channel complexes identified earlier by traditional electrophysiological experiments in native tissues.

The first α_1 subunit was purified from rabbit skeletal muscle (Curtis and Catterall, 1984). It was cloned, sequenced and named α_{1s} (Tanabe et al., 1987). Due to its structural and sequence similarities to the voltage-dependent sodium channel it was suggested that in the transverse tubule membrane of skeletal muscle the dihydropyridine receptor may act both as voltage sensor in excitation-contraction coupling and as a calcium channel. In 1988 Tanabe and colleagues demonstrated that Ca^{2+} currents and EC coupling could be restored in DHPR α-subunit null (dysgenic) muscle fibers transfected with cDNA for the α-subunit, confirming the essential role of the DHPR as the voltage sensor in signal transduction to the SR (Tanabe et al., 1988).

As the number of cloned calcium channel α_1 subunits increased, a need arose for a systemic nomenclature. It was agreed that individual α_1 subunits will be named according to the Ca_vx.y scheme (Ertel et al., 2000), where Ca_v stands for voltage-gated calcium channel (VGCC), x is a number designating the channel subfamily (i.e., L-type, neuronal, and T-type in the initial classification), and y is a number designating individual members of subfamilies. An overview of VGCC classification is given in **Table 1-2**.

1.8 Subunit structure of the skeletal DHPR Ca^{2+} channel

VGCCs are multi-subunit membrane complexes which are composed of a pore-forming α_1 subunit together with associated auxiliary subunits, α_2-δ, β and in skeletal muscle, γ subunit (**Figure 1-13**).

Table 1-2 Voltage gated Ca2+ Channel types based on their electrophysiological and pharmacological properties

Electrophysiological nomenclature		α1 subunit nomenclature		Gene name	Specific blockers	Primary locations
		Old	New			
HVA	L	α_{1S}	Ca_V 1.1	CACNA1S	Dihydropyridines	Skeletal muscle
		α_{1C}	Ca_V 1.2	CACNA1C	Dihydropyridines	Cardiac muscle, smooth muscle, Endocrine cells, Neurons
		α_{1D}	Ca_V 1.3	CACNA1D	Dihydropyridines	Endocrine cells, Neurons
		α_{1F}	Ca_V 1.4	CACNA1F	Dihydropyridines	Retina
	P/Q	α_{1A}	Ca_V 2.1	CACNA1A	ω – Agatoxin	Nerve Terminals, Dendrites
	N	α_{1B}	Ca_V 2.2	CACNA1B	ω – Conotoxin	Nerve terminals, Dendrites
	R	α_{1E}	Ca_V 2.3	CACNA1E	None	Nerve terminals, Dendrites
LVA	T	α_{1G}	Ca_V 3.1	CACNA1G	None	Cardiac muscle, smooth muscle, Neurons
		α_{1H}	Ca_V 3.2	CACNA1H	None	Cardiac muscle, Neurons
		α_{1I}	Ca_V 3.3	CACNA1I	None	Neurons

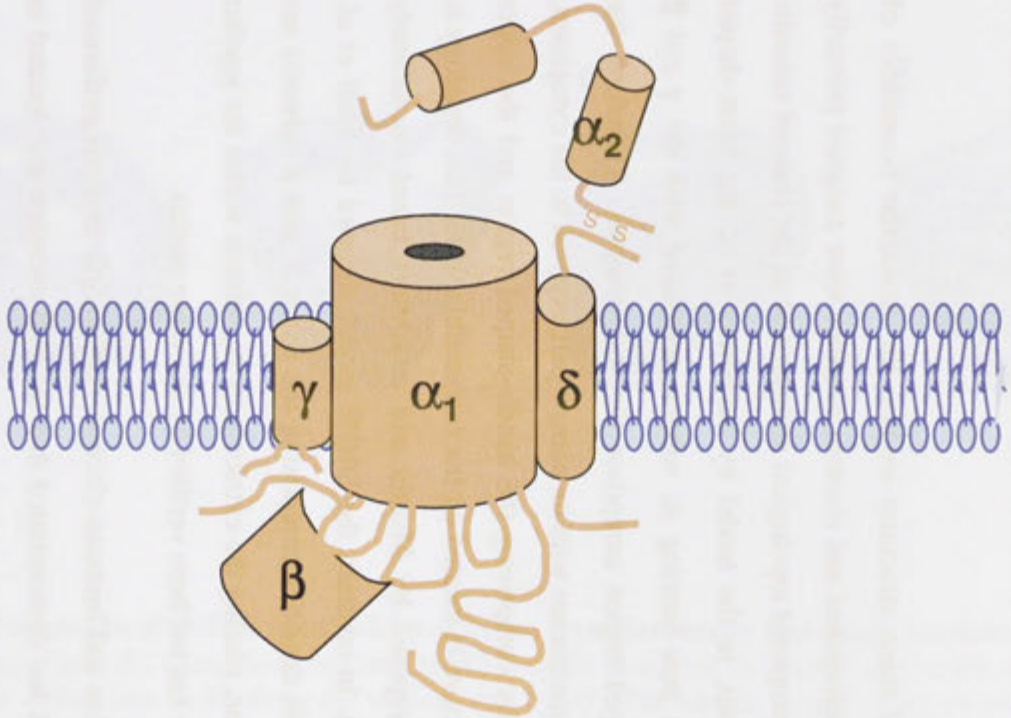

Figure 1-13 A schematic structure of VGCC. The principal α_1 subunit is a transmembrane protein containin a conducting pore. The α_1 subunit is further regulated by auxiliary subunits; intracellular β subunit, transmembrane γ subunit and a complex of extracellular α_2 subunit and transmembrane δ subunit, connected by a disulfide bridge.

1.8.1 3D structure

Structural studies of DHPR have been hampered by difficulties in isolation, purification, and expression of this large channel protein complex. However a number of groups have been pursuing structural studies of the DHPR by various types of electron microscopy. A 30 Å resolution 3D structure of the skeletal muscle DHPR determined by Serysheva *et al.* show an asymmetrical channel structure measuring about 130x115x120 Å (Serysheva et al., 2002). This structure consists of two major regions: a heart-shaped region connected at its widest end with a handle-shaped region (**Figure 1-14**)

Due to the low resolution of these structural studies, the molecular boundaries of individual subunits were not determined and electron densities were assigned primarily based on molecular mass and proposed topological arrangement of the channel subunits in the t-tubule membrane. Thus, in the model by Serysheva *et al.* the heart-shaped region accounts for the main pore-forming α_1 subunit associated with the γ and β subunits, and the handle-shaped region comprises the $\alpha_2\delta$ complex. Therefore, the heart-shaped region spans the membrane with its narrow part exposed to the cytoplasm, while the major protein density comprising the handle-shaped region and the upper lobes of the heart-shaped structure is located on the extracellular side. This topology is consistent with the model proposed by Murata and coworkers based on antibody labeling (Murata et al., 2001). In contrast, the DHPR model reported by Wolf *et al.* suggests that the major protein densities comprising the α_1, γ, δ, and β subunits are embedded within the membrane, placing the extracellular α_2 subunit within the smaller "leg" region. But this topology has not been verified by any other studies.

A more recent 3D reconstruction and immuno-electron microscopic analysis performed on the purified skeletal DHPR has demonstrated that the α_1-β complex was located in the large globular portion of the DHPR, and the N-terminal region of the β subunit was extended to the leg-shaped protrusion of the DHPR, which includes the $\alpha_2\delta$ subunits (Murata et al., 2010).

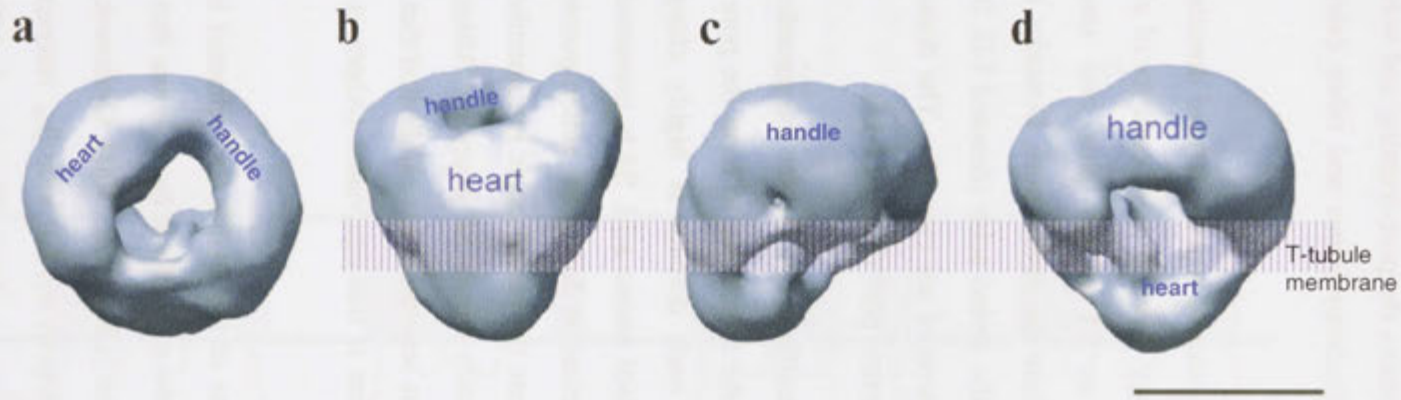

Figure 1-14 30 Å resolution 3D structure of DHPR obtained by electron cryomicroscopy and single particle reconstruction. The structure is shown in four different views: (a) top view; (b) front view obtained by 90° rotation along the horizontal axis of the top view in (a); (c) and (d) are views obtained by stepwise rotation of the view in (b) along the vertical axis by 90°. The handle-shaped structure and the upper lobes of the heart-shaped region were proposed to account for the extracellular channel region and to include the α_2-δ subunit. Thus, the heart-shaped region includes the voltage-sensitive transmembrane region of the L-type Ca^{2+} channel and the cytoplasmically located β subunit. The scale bar represents 100 Å (Serysheva et al., 2002).

1.8.2 The pore forming α_{1s} subunit

The primary α_{1s} subunit contains the major functional domain of the ion channel. It is a large integral membrane protein of 212 kDa that contains the pore-forming and voltage sensing regions as well as the binding site for dihydropyridines and other calcium channel blockers.

The alpha subunit is composed of four hydrophobic internal repeats, termed domains I, II, III, and IV, that share a high degree of homology. Each domain consists of eight transmembrane alpha-helical segments denoted as S1 to S6 plus two shorter intramembrane helices that fold into the bilayer to form the central pore. Domains I-IV are connected by longer segments of more hydrophilic amino acids (denoted I-II, II-III and III-IV loops). The loops as well as N- and C-termini are cytosolic. The domains assemble to form a trans-membrane protein with a central pore (**Figure 1-15**).

The major functional domains on α_{1s} have been identified. The shorter intramembrane helices (P-linker helices) of each domain fold into the membrane to form the pore for ion flux. The S4 trans-membrane helix within each domain is highly charged, containing a positively charged residue on every third amino acid. S4 is presumed to form the voltage sensor that responds to the depolarization during the action potential. Movement of the S4 segments is presumed to generate the macroscopic intramembrane charge movement currents that are detected electrically during EC coupling. Although further studies expressing the I-II and III-IV domains separately have indicated that the contribution of each domain to the charge movement is non-equivalent (Ahern et al., 2001a)

Contributions of the individual cytoplasmic domains of the DHPR Ca^{2+} channel have also been extensively studied. Crystal structures of the α_{1c} isoform have shown that the I-II loop interacts with the β_{2a} and β_3 auxiliary subunit (Chen et al., 2004, Opatowsky et al., 2004, Van Petegem et al., 2004). And the analogous α_{1s} I-II loop-β_{1a} interaction has been shown to be critical for triad targeting of the pore subunit (Gregg et al., 1996).

The α_{1s} III–IV loop (residues 1066–1118) contains the lone locus for DHPR mutations linked to malignant hyperthermia. (R1086H and R1086C (Monnier et al., 1997)).

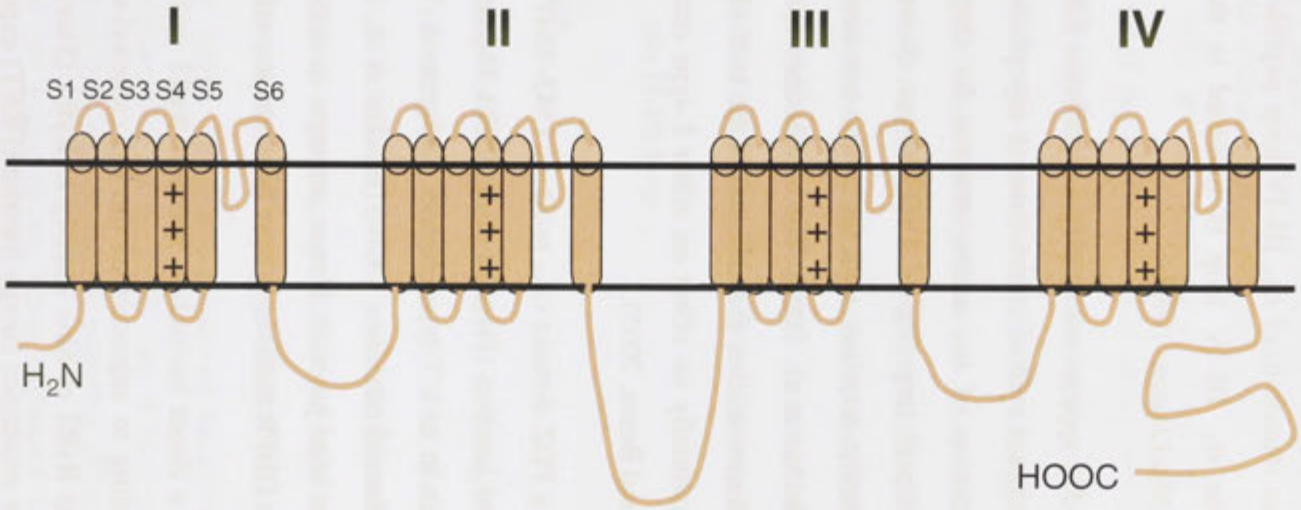

Figure 1-15 Schematic representation of the DHPR α_{1s} subunit. It consists of four homologous domains I –IV, each containing six transmembrane segments S1-S6 and a pore region between segments S5 and S6. Putative α-helices are shown as cylinders. The fourth trans-membrane segment S4 in each domain bears a net positive charge.

Myoplasmic Ca^{2+} release in dysgenic myotubes expressing DHPRs carrying the R1086H mutation was found to be somewhat more sensitive to both pharmacological (caffeine) and physiological (membrane depolarization) stimuli, suggestive of a negative allosteric contribution of the α_{1s} III–IV loop in coupling with RyR1 (Weiss et al., 2004). The observation that a peptide encompassing RyR1 residues 922–1112 bound specifically to a column with an immobilized α_{1s} III–IV loop peptide is also consistent with the possibility that the α_{1s} III–IV loop is involved in the basic mechanism of EC coupling (Leong and MacLennan, 1998b).

The amino-terminus of α_{1s} (residues 1–51) appears not to play a significant role in EC coupling. The ability of the DHPR to support evoked contractions or myoplasmic Ca^{2+} transients was not hindered by substitution of α_{1c} amino-terminus for that of α_{1s} (Tanabe et al., 1990). Likewise, junctional targeting of DHPRs was shown to be unaffected by replacement of the α_{1s} amino-terminus with the amino-terminus of the less-conserved neuronal α_{1a} subunit (Flucher et al., 2000). The conclusions from these studies have been strengthened by the demonstration that deletion of the bulk of the α_{1s} amino-terminus (residues 2–37) has essentially no effect on either L-type currents or myoplasmic Ca^{2+} transients (Bannister and Beam, 2005).

The carboxyl terminus of α_{1s} contains a PDZ domain (α_{1s} residues 1543–1647) that is essential for targeting of α_{1s} to the triad junction (Proenza et al., 2000, Flucher et al., 2000). But incorporation of this domain in to a T-type channel background (Wilkens and Beam, 2003) or an α_{1s} I– II hemichannel (residues 1–670) (Flucher et al., 2002) is insufficient to deliver the chimera to the triad junction. Hence, attempts to demonstrate the singular importance of this region in DHPR trafficking have been unsuccessful.

Many *in vitro* studies have identified a direct interaction between RyR1 and the α_{1s} carboxyl-terminus. Peptides corresponding to segments of the α_{1s} carboxyl-terminus inhibit the binding of [^{3}H] ryanodine to RyR1 or bind directly to RyR1 (Slavik et al., 1997, Sencer et al., 2001). Fluorescence resonance energy transfer (FRET) experiments have also shown that the α_{1s} carboxyl-terminus and RyR1 may make such a liaison further supporting the idea that EC coupling may be influenced by a functional interaction between the C-terminus of α_{1s} and RyR1 (Lorenzon et al., 2004, Papadopoulos et al., 2004).

The relatively long and variable carboxyl-terminus of α_{1s} contains many other motifs that may facilitate interactions with various signaling and scaffolding proteins. For example, Ca^{2+}-calmodulin (CaM) has been shown to interact with a synthetic peptide identical to α_{1s} residues 1522–1542 (the conserved IQ domain; (Pate et al., 2000) and a recombinant peptide corresponding to α_{1s} residues 1393–1527 (Sencer et al., 2001). JP-45 is a junctional protein that interacts with calsequestrin within the lumen of the SR while the amino-terminus extends across the myoplasm to make contacts of variable affinity with the α_{1s} carboxyl-terminus, the α_{1s} I–II loop and/or the β_{1a} subunit (Anderson et al., 2006). The scaffolding protein AKAP15 interacts with α_{1s} residues 1774–1821 via a modified leucine-zipper motif (Hulme et al., 2002) that lies in the region of the α_{1s} carboxyl-terminus that is protoelytically cleaved. It is speculated that the cleaved α_{1s} carboxyl-terminus may function as a regulator of excitation–transcription coupling, in a similar manner as has been shown for the α_{1c} carboxyl-terminus in neurons (Gomez-Ospina et al., 2006). Splice variants of another scaffolding protein, Homer H1 have also been postulated to interact with α_{1s} via an EVH1 motif present within the carboxyl-terminus (Feng et al., 2002).

1.8.2.1 α1s II-III loop

Overview

Conformational coupling with RyR1 is a unique property of the skeletal muscle DHPR (Tanabe et al., 1990, Garcia et al., 1994, Nakai et al., 1998b, Grabner et al., 1999, Kasielke et al., 2003). Tanabe and colleagues (Tanabe et al., 1990) first identified the α_{1s} II–III loop as a major contributor to skeletal-type EC coupling by examining the functional properties of chimeric DHPRs consisting of the individual α_{1s} cytoplasmic domains within the highly-conserved background of the cardiac α_{1c} subunit. The chimera containing the α_{1s} II–III loop (CSk3) was the only chimera with a single loop substitution that was capable of restoring EC coupling to a comparable degree to that observed for wild-type α_{1s} when expressed in dysgenic (α_{1s} null) myotubes. In a subsequent study, a direct interaction between the full α_{1s} II–III loop and RyR1 was detected by Lu et al. (Lu et al., 1994), who showed that a peptide corresponding to the α_{1s} II–III loop activated purified RyR1 in planar lipid bilayers and enhanced [H^3] ryanodine binding in isolated skeletal SR vesicles. Structural studies of the α_{1s} II-III

loop by nuclear magnetic resonance (NMR) have shown it to be an intrinsically unstructured protein (IUP) with a short helical region towards the N-terminus (Cui et al., 2009, Casarotto et al., 2004). As such it belongs to a burgeoning structural class of functionally important proteins. The unstructured nature of the II–III loop may allow it to rapidly change its conformation in response to a signal from the voltage sensor.

A region of the II-III loop

Although there has been general agreement among investigators that the II-III loop of the α_{1s} subunit plays a key role in transmitting the EC coupling signal to RYR1, the precise portion of the loop that is involved in this process has been a topic of contention due to differing results obtained in *in vitro* and *in vivo* studies (Dulhunty, 2006, Beam and Bannister, 2010, Bannister, 2007). In 1995 El-Hayek et al, synthesized several peptides (A, B, C, C1, C2 and D) corresponding to different regions of the α_{1s} II-III loop (**Figure 1-16**). In these experiments a peptide corresponding to residues 671–690 in the α-helical peptide A region was shown to activate RyR1 in reconstituted lipid bilayers and to increase [H^3] ryanodine binding in SR vesicles (el-Hayek et al., 1995). However, the physiological implications of this interaction are unclear because several studies have shown that EC coupling can be restored in dysgenic myotubes expressing α_{1s} constructs in which the peptide A domain has been disrupted or even deleted (Ahern et al., 2001a, Ahern et al., 2001b, Bannister et al., 2009, Wilkens et al., 2001).

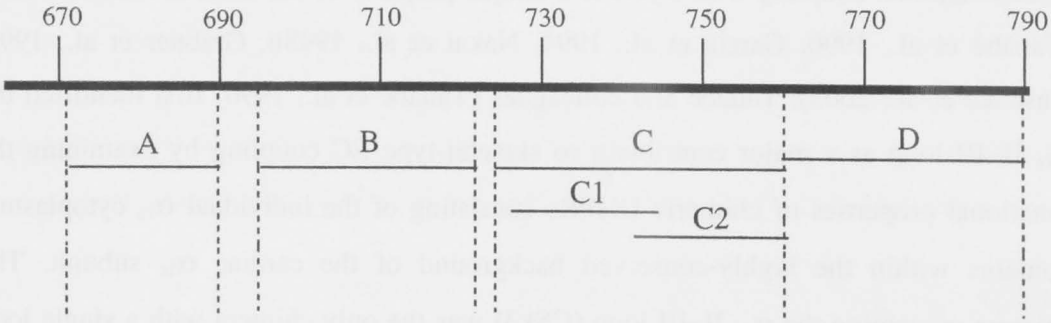

A : ^{671}TSAQKAKAEERKRRKMSRGL^{690}
B : ^{694}REEEKSVMAKKLEQKPKGEGIPTTAKLKV^{722}
C : ^{724}EFESNVNEVKDPYPSADFPGDDEEDEPEIPVSPRPRP^{760}
C1: ^{725}FESNVNEVKDPYPSADFPG^{743}
C2: ^{740}DFPGDDEEDEPEIPVSPRPRP^{760}
D : ^{760}PLAELQLKEKAVPIPEASSFFIFSPTNKVRV^{790}

Figure 1-16 Different regions of the II-III loop of the α subunit of the rabbit skeletal muscle dihydropyridine receptor as depicted by El-Hayek *et al.* (El-Hayek R et al. J. Biol. Chem. 1995;270:22116-22118).

Critical region (C region) of the II-III loop

Following on from the A region, chimeric studies in dysgenic (α_{1s} null) myotubes identified a 46 amino acid sequence within the α_{1s} II–III loop (α_{1s} residues 720–765) that was necessary to produce myoplasmic Ca^{2+} release in response to membrane depolarization in intact cells (''orthograde coupling;'' (Nakai et al., 1998b)). Likewise, the integrity of this region was also found to be necessary for the RyR1-dependent potentiation of L-type Ca^{2+} current (''retrograde coupling;'' (Nakai et al., 1996, Nakai et al., 1998a, Avila and Dirksen, 2000) as retrograde coupling cannot be supported by a chimera in which the cardiac α_{1c} II– III loop was substituted for the corresponding region of α_{1s} (chimera SkLC; (Grabner et al., 1999). However, retrograde coupling was restored by re-introduction of α_{1s} residues 720–765 into the cardiac α_{1c} II–III loop of this construct (chimera SkLCS46; (Grabner et al., 1999)). The necessity of this domain for both orthograde and retrograde coupling between RyR1 and the DHPR precipitated the term ''critical domain''.

Critical residues of the C region of the II-III loop

Within this critical region, four skeletal-specific residues (A739, F741, P742 and D744) have been shown to be important for skeletal type EC coupling (Kugler et al., 2004) (**Figure 1-17**). In this study it was proposed that α_{1s} residues 744–751 within the critical domain adopt a random coil conformation that enables α_{1s} to interact with other junctional proteins (e.g., RyR1), whereas the corresponding region of α_{1c} forms a putative α-helix that inhibits any such interactions. The four residues unique to α_{1s} were postulated to deter formation of the α-helix. However, substituting the skeletal residues (A739, F741, P742) to the equivalent cardiac counterparts did not significantly alter the NMR-based secondary structure of the α_{1s} II-III loop or the skeletal C region (Dulhunty et al., 2005). This study also showed that residue A739 is critical for the functional consequences of interactions between the skeletal DHPR and RyR1 (Dulhunty et al., 2005).

```
α1S 734- DPYPSADFPGDDEEDEPEIPVSPRPRPLAEL -764
         ***   ·   *··*·*** ** ****** **
α1C 865- SPYPNPETTGEEDEEEPEMPVGPRPRPLSEL -895
```

Figure 1-17 The critical residues shown to be essential for skeletal type EC coupling are highlighted and compared with their cardiac counterparts. (Adapted from Kugler G et al. J. Biol. Chem. 2004;279:4721-4728).

Critical region not alone ?

Examinations of modified α_{1s} subunits expressed in dysgenic myotubes have indicated that the critical domain is not necessary to produce a component of skeletal-type EC coupling. A construct that lacked both the C and the A region (Ahern et al., 2001b) regained about 15% of the orthograde signal compared with 0% after the deletion of only the critical region. It was also observed that a component of voltage-dependent Ca^{2+} release was lost in a chimera composed of the skeletal α_{1s} II–III loop in the context of a cardiac α_{1c} backbone in comparison to an α_{1s}/α_{1c} chimera that contained all five intracellular domains of α_{1s} (Carbonneau et al., 2005).

The presence of the critical domain is also not absolutely required for tetrad formation because the SkLM chimera, which is composed of the fairly divergent (~ 75 % dissimilarity) Musca domesticus II–III loop in an α_{1s} background, is able to support tetrad formation (Takekura et al., 2004, Beam and Bannister, 2010). This chimera is the one notable exception to the tetrad-EC coupling correlate because SkLM is the only engineered α_{1s}-based II–III loop chimera that forms tetrads but is incapable of supporting skeletal-type EC coupling (Wilkens et al., 2001, Kugler et al., 2004).

Simultaneous substitution of the critical domain and the putative triad targeting region of the α_{1s} carboxyl-terminus (residues 1543–1620; (Proenza et al., 2000, Flucher et al., 2000) for the corresponding regions of α_{1H} , a relatively non-conserved T-type Ca^{2+} channel, proved to be insufficient to support triad targeting and to reconstitute EC coupling when this chimera was expressed in dysgenic myotubes (Wilkens and Beam, 2003).

These results indicate that the presence of the critical domain alone is insufficient to support skeletal-type EC coupling in the absence of other elements conserved amongst L-type Ca^{2+} channels.

In addition to the A and C regions, a recent study has indicated that the conserved C-terminal portion of the α_{1s} II-III loop, downstream of the critical domain, plays an important role in bidirectional coupling either by conveying conformational changes to the critical domain from other regions of the DHPR or by serving as a site of interaction with other junctional proteins such as RyR1 (Bannister et al., 2009).

Binding studies

Biochemical binding assays have been employed to investigate a direct interaction between the α_{1s} II–III loop and RyR1. Leong and MacLennan (Leong and MacLennan, 1998a) found that the α_{1s} II–III loop binds residues 922–1112 of RyR1. This interaction of the α_{1s} II– III loop with the RyR1 fragment was dependent on positively- charged residues (K677, K682) within the α_{1s} II–III loop A-region. An alternative study of a segment of α_{1s} II–III loop encompassing the critical domain (residues 719–767) was found to interact weakly with the R16 region (residues 1837–2168) of RyR1 in a yeast two-hybrid assay, whilst no interaction with a portion of the amino-terminal region of the α_{1s} II–III loop (residues 666–709) was detected (Proenza et al., 2002).

A recent *in-vitro* study has also showed binding between the peptide A region of the α_{1s} II-III loop and a SPRY domain of RYR1 (Cui et al., 2009).

1.8.3 Auxiliary subunits

Although the α_{1s} subunit is shown to carry the characteristic pharmacological and functional properties for voltage sensing, Ca^{2+} ion permeability, and drug binding, complete receptor function (including targeting and modulation) requires the presence of all the subunits (Suh-Kim et al., 1996). An auxiliary (accessory) subunit is a protein that meets the following criteria : (1) existence in purified channel complexes (2) direct interaction with the α_1 pore forming subunit (3) capability to directly modulate the biophysical properties and/or trafficking of the α_1 subunits and (4) stable association with the α_1 subunit (Arikkath and Campbell, 2003).

1.8.3.1 α2δ subunit

The $\alpha_2\delta$ subunit is a product of a single gene that is post-translationally cleaved into α_2 and δ peptides, and is associated via disulfide bonds (De Jongh et al., 1990, Jay et al., 1991, Bauer et al.). A total of four genes (CACN$\alpha_2\delta$1 –4) code for $\alpha_2\delta$ subunits ($\alpha_2\delta$-1 to $\alpha_2\delta$-4), which display distinct tissue distributions (Ellis et al., 1988, Gao et al., 2000, Hanke et al., 2001, Qin et al., 2002). $\alpha_2\delta$-1 and $\alpha_2\delta$-2 are targets of gabapentin and pregabalin, two anti-epileptic drugs that are also used in the therapy of neuropathic pain (Dworkin et al., 2007).

The α_2 subunit is a highly glycosylated extracellular protein that interacts with the α_1 subunit (Gurnett et al., 1997). Topological analysis of the $\alpha_2\delta$ subunit supports a model for the protein in which α_2 is entirely extracellular and δ has a single transmembrane region with a very short intracellular portion, which serves to anchor the protein in the plasma membrane (Gurnett et al., 1996). Recent biochemical, immunohistochemical and electrophysiological studies have shown that $\alpha_2\delta$ subunits are glycosylphosphatidylinositol (GPI)-anchored (Davies et al., 2010).

The 125 kD, DHPR $\alpha_2\delta$-1 subunit is the major $\alpha_2\delta$ isoform of skeletal muscle. But it has a wide tissue distribution and is also part of calcium channels in the cardiovascular and nervous systems. Therefore, unlike the skeletal muscle α_{1s} and β_{1a} null mutants which develop fairly normally up to birth, attempts to generate knock-outs of the DHPR $\alpha_2\delta$-1 subunit have been problematic, indicating that this auxiliary channel subunit serves vital functions in tissues other than skeletal muscle (Obermair et al., 2008a). A viable $\alpha_2\delta$-1 knockout has recently been published, with a cardiac phenotype, showing reduced cardiac calcium currents and decreased myocardial contractility (Fuller-Bicer et al., 2009).

Coexpression of α_{1s} subunits with $\alpha_2\delta$ in various heterologous cell systems increased membrane expression of the channels and altered their L-type Ca^{2+} current properties (Shistik et al., 1995, Felix et al., 1997, Sipos et al., 2000, Canti et al., 2005). In dysgenic ($Ca_V1.1$-null) skeletal myotubes $\alpha_2\delta$-1 is expressed diffusely throughout the plasma membrane in the absence of α_{1s} (Flucher et al., 1991, Obermair et al., 2005). Reconstitution of dysgenic myotubes with GFP-tagged $Ca_V1.1$ and also $Ca_V1.2$ caused a redistribution of $\alpha_2\delta$-1 together with the α_1 subunit into triads (Obermair et al., 2005, Tuluc et al., 2007). Conversely, short hairpin RNA (shRNA) knockdown of $\alpha_2\delta$-1 did not affect the correct triad targeting and membrane expression of $Ca_V1.1$. Hence, in skeletal muscle, membrane trafficking of $\alpha_2\delta$-1 and α_1 subunits occur independently of each other and both subunits can exist in the plasma membrane separately. Moreover, correct triad targeting of α_{1s} is independent of $\alpha_2\delta$-1. However, the $\alpha_2\delta$-1 needs the interaction with α_{1s} for its own targeting into the triad (Obermair et al., 2005).

Whereas knockdown of $\alpha_2\delta$-1 in the dysgenic muscle expression system had no effect on functional membrane expression, it significantly accelerated activation and

inactivation kinetics of the skeletal muscle Ca^{2+} current. Depletion of $\alpha_2\delta$-1 with siRNA accelerates L-type Ca^{2+} current activation by shifting the balance from mainly slowly activating channels to mainly fast activating channels. Hence in skeletal muscle $\alpha_2\delta$-1 is neither required for membrane expression/targeting of the channel into the triads nor for normal EC coupling. Instead, $\alpha_2\delta$-1 is a critical determinant of the characteristic slow L-type current kinetics. More recently, other roles for the $\alpha_2\delta$-1 subunit unrelated to L-type Ca^{2+} channel function such as extracellular signalling in muscle development have also been proposed (Garcia et al., 2008).

1.8.3.2 γ subunit

The calcium channel γ subunits comprise an eight-member protein family that shares a common topology consisting of four transmembrane domains and intracellular N- and C-termini. Although the first γ subunit was identified as an auxiliary subunit of a voltage-dependent calcium channel, a review of phylogenetic, bioinformatic, and functional studies indicates that they are a functionally diverse protein family. Three distinct cellular functions have been proposed for members of the γ subunit family including regulation of VGCC expression and function, regulation of AMPA receptor gating and trafficking and, most recently, regulation of cellular aggregation (Chen et al., 2007).

γ_1 and γ_6 isoforms conforms to the original description of the protein family and seem to act primarily as subunits of calcium channels expressed in muscle. The 25.1 kD γ_1 subunit is exclusively expressed in skeletal muscle (Jay et al., 1990). Co-expression of γ_1 with α_{1C} in heterologous systems indicated that γ_1 is not involved in membrane expression of the channel but has an inhibitory effect on calcium currents (Eberst et al., 1997). γ_1 knock-out mice are viable and show no abnormal phenotype (Freise et al., 2000). Thus, γ_1 is not essential for EC-coupling or any other vital function. Like $\alpha_2\delta$-1, γ_1 is targeted to the surface membrane in the absence of α_{1s}, but requires the pore-forming subunit for its association with the channel complex (Arikkath et al., 2003). Functional analysis of γ_1- null myotubes and muscle fibers showed that amplitudes and voltage-dependence of L-type Ca^{2+} currents and depolarization-induced Ca^{2+} release from the SR were not altered (Ursu et al., 2004). However, detailed analysis found that the γ1 subunit accelerates current inactivation (Freise et al., 2000), causes a

hyperpolarizing shift in the voltage-dependence of inactivation and significantly reduces HVA calcium current density (Arikkath et al., 2003, Freise et al., 2000, Held et al., 2002). Studies have also shown that the γ_1 subunit of the DHPR functions as an endogenous Ca^{2+} antagonist and it has been proposed that its task may be to minimize Ca^{2+} entry and Ca^{2+} release under stress-induced conditions favoring plasmalemmal depolarization (Andronache et al., 2007). Thus, the role of the γ_1 subunit in skeletal muscle EC-coupling is to increase the voltage-sensitivity of inactivation and consequently to limit both calcium influx and, more importantly, calcium release in EC-coupling.

1.9 β subunit

1.9.1 History and nomenclature

The β subunit was first identified in 1987 and was classified as a 54 kD auxiliary subunit of the DHPR because of its association with the purified skeletal dihydropyridine receptor (Takahashi et al., 1987). The protein was partially sequenced and the gene encoding the skeletal muscle isoform of this subunit, subsequently termed β_{1a}, was cloned (Ruth et al., 1989). Three subsequent β subunit genes, $Ca_v\beta_2$, β_3 and β_4, were identified by homology and cloned (Perez-Reyes et al., 1992, Castellano et al., 1993a, Castellano et al., 1993b, Hullin et al., 1992). According to the HUGO/GDB nomenclature, the genes encoding the β subunits are referred to as CACNB1–4 and numerous splice variants for each gene are known (Table 1-3). Notably, all four isoforms are expressed in the brain. In addition, each β subunit is differentially expressed in other tissue types. β_{1a} is a distinct β_1 variant that is uniquely associated with the skeletal muscle voltage-gated L-type calcium channel.

Among the auxiliary subunits, β is unique in that it is located entirely in the cytoplasm where it acts as the most potent regulator of channel function and expression.

Table 1-3 Ca^{2+} Channel β subunit – Classification and Tissue distribution

Subunit isoform	HUGO/GDB gene nomenclature	Tissue distribution
β1	CACNB1	β1a – skeletal muscle β1b - brain
β2	CACNB2	Heart, lung ,trachea, aorta, brain
β3	CACNB3	Smooth muscle, trachea, aorta, lung, brain
β4	CACNB4	brain

1.9.2 Structural modularity of the β subunit

All β subunits possess a common structure consisting of five domains (**Figure 1-18**). Homology modelling and X-ray crystallographic studies have shown that these proteins consist of a core structure made up of a Src homology 3 (SH3) domain and a guanylate kinase (GK)-like domain (**Figure 1-19**). This core module is highly conserved amongst the four isoforms (Chen et al., 2004, Van Petegem et al., 2004, Opatowsky et al., 2004) while the region connecting these two domains (Hook region) and the N- and C-termini are relatively unconserved and are subject to alternative splicing. The core domain of the β subunits is similar to a group of scaffolding proteins dubbed Membrane-Associated GUanylate Kinases (MAGUKs) which contain several protein-protein interaction domains and are involved in the assembly of multiprotein complexes. (Dolphin, 2003, Hanlon et al., 1999)

The GK domain of the β subunit is enzymatically inactive due to the absence of an ATP binding motif (Kistner et al., 1995), but it interacts with the SH3 domain to form a

Figure 1-18 Schematic Domain modules of Ca^{2+} Channel β subunits. The SH3 and guanylate kinase (GK) domains are conserved in all β subunits with the greatest sequence variability observed in the N and C termini and the Hook region.

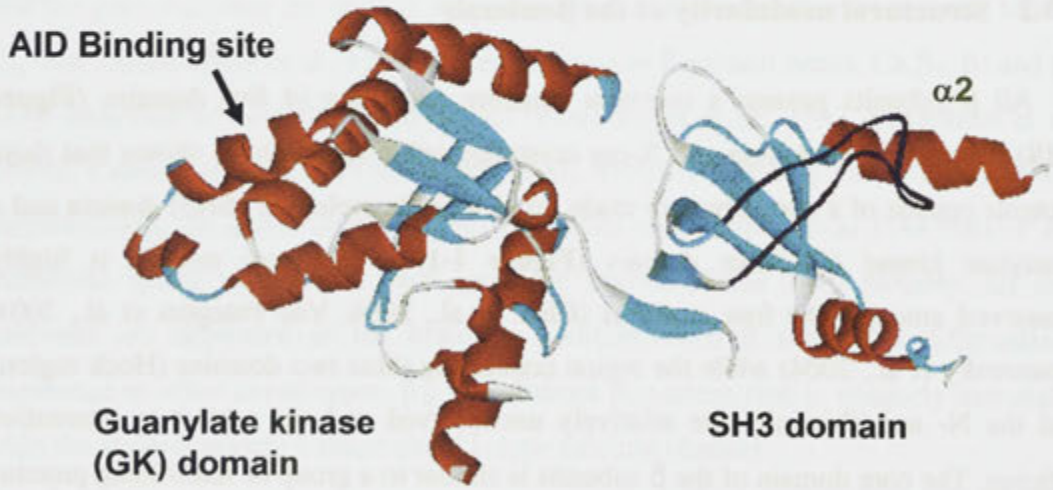

Figure 1-19 Crystal structure of the β3 core protein (Chen et al, 2004). The molecule is made up of a guanylate kinase (GK) and SH3 domain. An α_1 binding partner AID has been located on the GK domain. The loop highlighted in bold represents a potential SH3 binding site which is predicted to be occluded by helix α2. The Hook region is not visible due to poor electron density.

stable core. So far, crystallographic analysis of the β subunit has only been carried out on this central core region containing a short (β3, β4) or absent (β2) Hook sequence (Chen et al., 2004, Opatowsky et al., 2004, Van Petegem et al., 2004). In fact the β2 structure was partially solved by co-crystalisation of separate SH3 and GK domains (minus the Hook region). The non-conserved N-terminal, C-terminal and Hook region have been shown to be exposed in a protease sensitive manner (Opatowsky et al., 2003) and no crystallographic data are available on these regions presumably due to their dynamic nature. It is noteworthy that unlike true MAGUK proteins which contain PDZ domains upstream to their SH3 domains, no comparable PDZ regions have been identified in the β subunits. The Hook region of MAGUK proteins has been shown to be involved in docking with other proteins (Chishti, 1998) whereas no such binding partners are yet to be attributed to the Hook region of the β subunit. The non-conserved C-terminal tail of the β subunit is highly divergent amongst the different isoforms, and is predicted to have less secondary structure (Hanlon et al., 1999).

The β subunit associates predominantly with the α1 subunit through a highly conserved high affinity interaction between the Alpha Interaction Domain (AID) in the I-II loop of the α1 subunit and the GK domain of the β subunit (**Figure 1-19**). All three X-ray structure studies investigated the binding of the AID peptide to the β subunit core and provided similar evidence that the interaction site of AID is located in a deep groove on the GK domain called the AID-binding pocket (ABP) (Van Petegem et al., 2004, Chen et al., 2004, Opatowsky et al., 2004). Binding of the AID peptide does not significantly alter the core structure of the β subunit (Chen et al., 2004). The binding affinity of the β subunits to either the AID peptide or the full length I–II linker has been determined for a variety of combinations of subunits and shown, using several methods, to be in the low nanomolar range (Richards et al., 2004). In addition to this high affinity interaction, two other lower affinity β subunit interaction sites have also been identified on the C-terminus (Qin et al., 1997, Walker et al., 1999) and the N-terminus (Stephens et al., 2000) of the α1 subunit. These interactions are isoform specific and involve the GK domain and the carboxyl terminal of the β subunit.

1.9.3 The SH3 Domain of the β subunit

Although the GK domain of the β_{1a} subunit is responsible for the high affinity binding to the AID, *the functional significance of the other structural motif, the SH3 domain, remains unclear.*

SH3 domains were first described as a polypeptide fragment conserved between the N-terminus of a Src family tyrosine kinase and blocks of sequences in the adaptor protein Crk (Mayer et al., 1988). Hence it was named Src homology 3 (SH3) domain. The human genome encodes approximately 300 such domains and it is one of the most prevalent families of protein modules found in nature (Karkkainen et al., 2006). SH3 domains are involved in a plethora of important cellular processes including intracellular signalling and cell-environment communication, cytoskeletal rearrangements and cell movement, cell growth and differentiation, protein trafficking and degradation, and immune responses (Mayer et al., 1988, Zarrinpar et al., 2003).

SH3 domains contain approximately 60 residues and share significant sequence identity and a common structure featuring a five-stranded ant-parallel beta-sheet. The majority of SH3 domains characterized to date bind proline-rich sequences containing a core element, PxxP, where x denotes any amino acid, through a set of conserved residues (Yu et al., 1994, Musacchio et al., 1992). Chen et al, employed combinatorial peptide libraries to identify SH3-binding motifs and found that proline-rich peptides selected by SH3 domains could be classified into two related, yet distinct groups named classes I and II , respectively (Chen et al., 1993). The consensus sequences for these two classes of motifs are represented as the following : [R/K]xXPxXP (class I) and XPxXPx[R/K] (class II), where the capital 'X' signifies a non-glycine, hydrophobic residue while the lower 'x' denotes any naturally occurring amino acid. These peptides bind with an affinity of between 1- 100 μM.

Crystallographic studies have shown that the arrangement of the first four β-strands of the β subunit SH3 are similar to canonical SH3 domains. However the fifth β-strand is separated by an unstructured central Hook region which gives the SH3 domain of the β subunit a 'split architecture'. In addition, two long helices that are absent in canonical SH3 domains are appended to the SH3 domains of the β subunit (**Figure 1-19**)(Chen et al., 2004, Van Petegem et al., 2004).

Within the β subunit SH3 domain, there is good sequence homology amongst the residues noted to form the hallmark proline binding residues of all SH3 domains (**Figure 1-20**) (Hanlon et al., 1999). Although the crystal structures have shown this putative polyproline binding site to be occluded, this does not preclude the possibility of dynamic structural rearrangements exposing these interaction sites for binding. Indeed such an interaction has been shown to occur between the β2a subunit and a GTPase involved in receptor-mediated endocytosis (Gonzalez-Gutierrez et al., 2007). Also, SH3 domain binding sites have been identified in the cardiac α1 II-III loop and C-terminal (Dubuis et al., 2006). Hence it is interesting to note the presence of SH3 domain binding motifs in the critical C region of the skeletal α_{1s} II-III loop (**Figure 1-21**). *An α_{1s} II-III loop/β_{1a}-SH3 interaction raises a possibility that the β_{1a} subunit may regulate or be part of the physical coupling between the DHPR α_{1s} subunit and the RyR1 in skeletal EC coupling.*

1.9.4 Role in membrane expression and modulation of calcium channels

The β subunit has a marked effect on DHPR channel expression and modulation of the pore forming α_1 subunit. A number of research groups have shown that over-expression of the β subunit increased the density of endogenous calcium currents, indicating an increase in the functional expression of HVA α1 subunits (Colecraft et al., 2002, Neuhuber et al., 1998, Raghib et al., 2001). The β subunit aids in the trafficking of α_1 to the plasma membrane, partly by its ability to mask an endoplasmic reticulum retention signal in the α1 subunit (Bichet et al., 2000). According to He et al, the AID-GK domain interaction is necessary for β-subunit stimulated P/Q type Ca^{2+} channel surface expression and the GK domain alone can carry out this function (He et al., 2007).

In addition to its role in membrane trafficking, the β subunit modulates a host of biophysical properties of the L-type Ca^{2+} channel with characteristics specific to the α_1-β combination. The β subunit can accomplish these dual functions independently, as illustrated by its ability to modulate the biophysical properties of channels in the presence of a mutation in the AID region, which disrupts its ability to enhance membrane trafficking of α_1 (Gerster et al., 1999). It has been suggested that this is due to the ability of some β subunits to associate with other intracellular loops of the

```
β3   ..........................................60 VAFAVRTNVSYCGVLDEEC
β4   ..........................................92 VAFAVKTNVSYCGALDEDV
β2a  ..........................................60 VAFAVRTNVRYSAAQEDDV
β1a  .........................................101 VAFAVRTNVGYNPSPGDEV

β3   PVQGSGVNFEAKDFLHIKEKYSNDWWIGRLVKEGGDIAFIPS 120.....
β4   PVPSTAISFDAKDFLHIKEKYNNDWWIGRLVKEGCEIGFIPS 152.....
β2a  PVPGMAISFEAKDFLHVKEKFNNDWWIGRLVKEGCEIGFIPS 120.....
β1a  PVQGVAITFEPKDFLHIKEKYNNDWWIGRLVKEGCEVGFIPS 161.....

β3   .....170 PYDVVP 176.....
β4   .....211 PYDVVP 217.....
β2a  .....219 PYDVVP 225.....
β1a  .....267 PYDVVP 273.....
```

Figure 1-20 Amino acid sequence alignment of SH3 domains within Ca^{2+} channel β subunit isoforms. Regions with the highest greatest sequence homology are shown with red denoting conserved residues for all isoforms.

```
.....666EAESLTSAQKAKAEERKRRKMSRGLPDKTEEEKSVM
AKKLEQKPKGEGIPTTAKLKVDEFESNVNEVKDPYPSADFPG
DDEEDEPEIPVSPRPRPLAELQLKEKAVPIPEASSFFIFSPTN
KVRVL791.....
```

Figure 1-21 Sequence of the DHPR α_{1s} II-III loop. The critical C region is highlighted in blue and the proline residues in the putative SH3 binding sites are shown in red.

channel through weaker interactions. The independent functions support a model in which the conserved high-affinity binding of the β-subunit to the AID anchors it to the α1 subunit and facilitates low affinity interactions of other β-subunit domains/regions with different parts of the α1 subunit, which in turn are responsible for the modulation of gating (He et al., 2007, Van Petegem et al., 2008).

All four β subunit isoforms shift the voltage-dependent activation of all high voltage activated VGCCs to more negative potentials. In contrast, steady state inactivation properties reveal differences between the effects of different β subunits and particular α_1 subunits. In general, the β1, β3, and β4 subunits expressed with α1 result in channels inactivating at more negative potentials and acceleration of the inactivation kinetics. On the other hand, partly due to palmitoylation of two cysteines in its N-terminus, the rat and human β_{2a} subunit shifts the voltage dependence of inactivation to more positive potentials and dramatically slows the kinetics of inactivation (He et al., 2007). Furthermore, the β core containing the SH3-Hook-GK module governs the modulatory effects on activation kinetics and the Hook region and the N-terminus (especially the distal variable region) are critical for modulating inactivation (He et al., 2007, Richards et al., 2007). However, Hidalgo et al have recently reported that the structural determinants of inhibition of inactivation by β2a are encoded not in variable regions but rather within the GK domain (Gonzalez-Gutierrez et al., 2008). Although the C-terminus constitutes a large portion of the β subunits, the deletion of it did not have any effect on activation or inactivation of, at least, $Ca_v2.1$ channels (He et al., 2007).

Regulation of L-type Ca^{2+}channels also occurs through modification of the β subunits and/or its interactions with other proteins. β_{2a} is a substrate for protein kinase A, and phosphorylation of β_{2a} is important for the ability of protein kinase A to stimulate the currents generated by the $\alpha_1$1.2 channels in mammalian expression systems and in cardiac myocytes. The β subunit also plays a role in the modulation of the $\alpha_1$2.2 channels through the mitogen-activated protein kinase (MAPK) pathway (Fitzgerald, 2002). Gem is a small Ras related G protein that has a high affinity for the β subunit, the binding of which interferes with the β subunit's ability to traffic the α1 to the plasma membrane (Beguin et al., 2001).

1.9.5 Gene knockout studies and disease

The significance of the β subunit is emphasised by diseases associated with its knockout and through mutations. Knock-out of the β1 isoform (CACNB1), present in skeletal muscle as β_{1a} and in heart and brain as β_{1b}, results in a lethal phenotype. Homozygous β1 -/- mice show reduced skeletal muscle mass with structural abnormalities and die at birth from respiratory failure. Interestingly heterozygotes are asymptomatic, indicating that there is normally a sufficient excess of β1 subunit, such that loss of 50% has no effect (Strube et al., 1996).

Deletion of the Cavβ2 gene (CACNB2) gives rise to an embryonic lethal phenotype, underlining the essential role of β_2 in cardiac contraction (Ball et al., 2002). In contrast, knock-out of the β_3 isoform (CACNB3) does not result in a major phenotype, indicating that other β subunits are able to substitute for its function. The lethargic mouse is a spontaneous mutation in the gene encoding the β4 subunit (CACNB4). This causes a premature stop codon resulting in no detectable protein as it is a null mutation. Lethargic mice exhibit ataxia, lethargic behavior and spontaneous focal motor seizures. (Burgess et al., 1999) Mutations in the Cavβ4 subunit gene have been found in patients with idiopathic generalized epilepsy and episodic ataxia (Escayg et al., 2000). In cardiac myopathy associated with failed cardiac myografts, there was a large reduction in β subunit mRNA and protein by up to 80%, and the major species detected was β_{1b} (Hullin et al., 1999). There was also an increase in the amount of truncated relative to full-length β3 transcript in human left ventricular tissue showing ischaemic cardiomyopathy, compared to non-failing tissue (Hullin et al., 2003).

1.9.6 $Ca_v\beta$ subunit in skeletal muscle

The β_{1a} isoform is specific to skeletal muscle. It is a 58 kD protein consisting of 524 amino acid residues (**Figure 1-22**). Similar to other isoforms, it has five domains including the conserved SH3 and GK domains and has also been shown to perform a dual role as a chaperone and modulator of the α_{1s} subunit (Bichet et al., 2000, Gerster et al., 1999). Consistent with its role in membrane expression of the α_{1s} subunit, patch-clamp analyses of β_{1a}-null myotubes show that their L-type calcium currents are strongly decreased (Strube et al., 1996). Although these observations indicate a failure

of EC-coupling due to a reduction of voltage sensors, further experiments have shown a direct role of the β subunit in the transmission of the signal from the voltage sensor (α_{1s}) to the Ca^{2+} release channel (RyR1) (Sheridan et al., 2004, Beurg et al., 1999). β1-null myotubes transfected with the cardiac β_{2a} isoform show cardiac-type EC coupling and deletion/chimeric studies of β_{1a} and β_{2a} in knock-out cells have identified a region in the C-terminus of β_{1a} that enables skeletal type EC coupling. In this study, the deletion of 35 residues of β_{1a} at the C-terminus produced a fivefold reduction in the maximum amplitude of the Ca^{2+} transients (Beurg et al., 1999, **Figure 1-22**). A further study by the same group identified a heptad repeat (repeated at seven residue intervals) of hydrophobic residues (L478, V485, V492) contained within the last 47 residues of the β_{1a} subunit (β_{1a} 478 – 524) as being essential for skeletal type EC-coupling (Sheridan et al., 2004). It was also shown that the β_{1a} is able to bind to a cluster of positively charged residues (3495-3502) in the foot region of the RyR1 and that this interaction strengthens EC-coupling (Cheng et al., 2005). It is of interest that the region of the RyR1 involved in the binding with β_{1a} subunit is immediately adjacent to a variably spliced region implicated in myotonic dystrophy which also has a significant influence on EC coupling (Kimura et al., 2007). These results reinforce the interesting question about the precise role of β_{1a} in skeletal EC coupling.

The recent analysis of a novel β-null zebrafish mutant "*Relaxed*" has demonstrated that the lack of EC-coupling in this system is caused by the disruption in the structural network involving the DHPR and the RyR1s (Schredelseker et al., 2008, Schredelseker et al., 2005). The authors suggest that β_{1a} may act as a scaffolding protein and that at least in skeletal muscle cells, the reduced number of channels in the membrane may result from a decreased stabilization in the signalling complex rather than from reduced

1 MVQKSGMSRGPYPPSQEIPMEVFDPSPQGKYSKRKGRFKRSDGSTSSDTT
51 SNSFVRQGSAESYTSRPS DSDVSLE EDREALRKEAE RQALAQLEKAKTKP
101 VAFAVRT NVGYN PSPGDEVPVQGVAITFEPKDFLHI KEKYNNDWW IGRLV
151 K EGCEVGF I PSPVKLDSLRL LQEQTLRQNRLSSSKSGDNSSSSLGDVVTG
201 TR RPTP PASGNEMTNFAFELDPLE LEEEEAELGE HGGSAKTSVSSVTTPP
251 PHGKRIPF FKKTEHVP PY DVVPSMRPI I LVGPSLKGYEVTDM MQKALFDF
301 LKH RFDGRIS I TRVTAD I SLAKRSVLN NPSKH I I I ERSNT RSSLAEVQSE
351 I E R I E LARTLQLVALDADT I NH PAQ LSKTS LAP I I VY I K I TSPKV LQRL
401 I KSRGKSQSKH LNVQ I AASEKLAQCPPEMFD I I LDENQLEDACEH LAEYL
451 EAYWKATH PPSSTPPN PLLN RTMATAALAASPAPVSN LQVQVLTSLRRNL
501 SFWGGLEASPRGGDAVAQPQEHAM

Figure 1-22 The amino acid sequence of the skeletal isoform of beta subunit. The SH3 domain is shown in purple, GK domain in green and the Hook region in orange. Amino acids of the heptad repeat are denoted in red. The 35- residue C-terminal tail shown to be important for skeletal EC-coupling is highlighted in yellow.

trafficking to the membrane (Obermair et al., 2008b). However, fluorescent protein-tagged β_{1a} subunits failed to colocalize with RyR1 in dysgenic myotubes indicating that triad-targeting of β_{1a} may require an association with α1s (Leuranguer et al., 2006). Further study on the β_1-null zebrafish *relaxed* larvae and isolated myotubes also failed to show an effect on tetrad formation and skeletal EC-coupling upon mutation of the hydrophobic heptad repeat residues in the β_{1a} C-terminal tail (Dayal et al., 2010). This is contrary to the observations made by Sheridan et al (2004) in mouse fetal myotubes.

1.9.7 The role of β_{1a} subunit in skeletal EC coupling?

All $Ca_v\beta$ subunit isoforms play a vital role in the membrane expression and modulation of HVA calcium channels. However, the presence of DHPRs in freeze-fracture replicas obtained from the muscle of β_{1a} null zebra fish (relaxed) mutants suggests that trafficking the α_{1s} subunits to the triad junctions is not the only role of the β_{1a} subunit. In particular, the β_{1a} subunit is essential for the structural organization of the DHPR complex into tetrads in the t-tubule opposite RyR1 in the SR, thus enabling skeletal type EC coupling. However, the exact molecular mechanism of how the β_{1a} subunit participates in the skeletal EC coupling process remains unresolved.

Of the 5 domains of the β_{1a} subunit, the GK domain alone can carry out the α_{1s} targeting role of β_{1a}. But the role of the β_{1a}-SH3 domain is less well understood. The DHPR β subunit belongs to a class of MAGUK proteins which are scaffolding/clustering proteins. The presence of SH3 binding motifs in the critical region of the α_{1s} II-III loop raises the possibility that a β_{1a}-SH3/α_{1s} II-III loop interaction may play a role in clustering the DHPRs into a tetrad formation apposing the RyR1. Furthermore, the β_{1a} C terminal tail has been shown to be important for skeletal type EC coupling. It is also known that the β_{1a} subunit and its 35-residue C terminal tail are able to bind to RyR1. *This raises the possibility that the β_{1a} subunit may not only support tetrad formation but possibly may be a component of the trigger mechanism for SR Ca^{2+} release.*

Therefore the author hypothesize that the skeletal isoform of the β subunit (β_{1a}) not only plays a role in membrane targeting and modulation of α_{1s}, but acts as a conduit in the transmission of the EC-coupling signal from the DHPR to the Ryanodine receptor in skeletal muscle.

1.10 This thesis

The first objective of this study is to investigate the interaction between the DHPR β_{1a} subunit and the α_{1s} II-III loop and to identify regions involved in this interaction. The second objective is to investigate the structure of the 35-residue C-terminal tail of the β_{1a} subunit and to identify residues important for the modulation of RyR1.

The second chapter of this thesis describes the general materials and methods used in this study whereas methods specific to a given experiment will be detailed in the relevant chapter. Chapter three of this thesis describes the development of the protocol for cloning, expression and purification of the full length recombinant β_{1a} subunit for the use of downstream experiments. Chapter four details the investigation of the interaction between the β_{1a}-SH3 domain and the α_{1s} II-III loop and the identification of regions involved in this interaction. Chapter five looks into the structure of the 35-residue C terminal tail of the β_{1a} subunit and chapter six investigates the functional effects of mutating a predicted binding site in the C terminal tail on RyR1. Chapter 7 presents a general summary and discussion of the results obtained in this study.

Chapter 2 General Materials and Methods

These materials and methods are those used in general sample and solution preparation in the course of experimental procedures. Materials and methods specific to a technique are detailed in the relevant chapters.

2.1 Materials

All chemicals and reagents used in this study were of analytical grade unless otherwise stated. Buffer recipes and stock solutions used for each method are given in Appendix Table A.1. All reagents are listed in Appendix Table A.2.

All primers for PCR amplification and mutagenesis were obtained from GeneWorks (Australia).

2.2 Methods

All general methods used in this project are detailed below:

2.2.1 Peptide synthesis

Peptides used in this study were synthesized by the ACRF Biomolecular Resource Facility (BRF), JCSMR, ANU on a CEM Liberty Microwave peptide synthesizer. Synthesis was performed using Fmoc chemistry and solid phase peptide synthesis (SPPS) techniques. Peptides were purified using HPLC (SHIMADZU, Japan) and the homogeneity of the synthetic peptides was checked by mass spectroscopy (MALDI TOF/TOF™ Model 4800, Applied Biosystems, USA).

1 mM stock solutions of the peptides were prepared (in distilled water or relevant buffer depending on the downstream application) by weighing out the equivalent amount based on the calculated molecular weight (Prot Param- Gasteiger et al., 2005). The precise concentration of the peptide solutions were confirmed by a modified BCA assay method (Kapoor et al., 2009).

2.2.2 Plasmid Construction

All proteins used in this study were cloned in an in-house histidine ubiquitin expression vector pHUE (Catanzariti et al., 2004, Baker et al., 2005) unless otherwise specified.

The **H**istidine-tagged **U**biquitin **E**xpression vector, pHUE, (Fig. 2-1) was constructed by modifying the pET15b vector (Novagen) containing an ampicillin resistance marker and a T7 RNA polymerase promoter. This is an efficient *Escherichia coli*-based expression system where the protein of interest is expressed as a fusion to a 8 kDa, poly-histidine-tagged ubiquitin, enabling a simple one-step purification of the fusion protein by immobilized metal affinity chromatography (IMAC). A poly-histidine-tagged catalytic core of a mouse deubiquitylating enzyme, Usp2cc, is then used to cleave the ubiquitin tag from the desired protein. This allows the selective removal of the protease from the cleavage reaction, along with the cleaved ubiquitin, any uncleaved fusion protein, and any copurified contaminants using a second IMAC, leaving the desired protein as the only soluble product.

This system has the added advantage that deubiquitylating enzymes (DUBs) do not cleave non-specific sequences and do not leave additional amino acids at the N-terminus of the protein of interest. Cleavage occurs precisely after the final glycine residue at the carboxyl terminal of ubiquitin irrespective of the amino acid immediately following, with the sole exception of proline.

2.2.3 Polymerase Chain Reaction (PCR)

Amplification of genes for the purpose of constructing protein expression vectors was carried out using Phusion®High Fidelity PCR kit (NEB) according to the manufacturers' instructions. All other PCR reagents were obtained from Promega, USA. Molecular biology-grade water (DNase, RNase, and nucleic acid free) was used in all steps and solutions.

Routine PCR amplification was carried out as follows: The PCR mix (20µl) was made up of 1x PCR buffer, 1.75 mM $MgCl_2$, 0.2 mM dNTPs, 2U Taq DNA polymerase, 5ng template DNA and 0.3 pmole oligonucleotide primers. The mixture was cycled 33 times in a PTC-200 DNA Engine (MJ Research, USA). The following general cycling

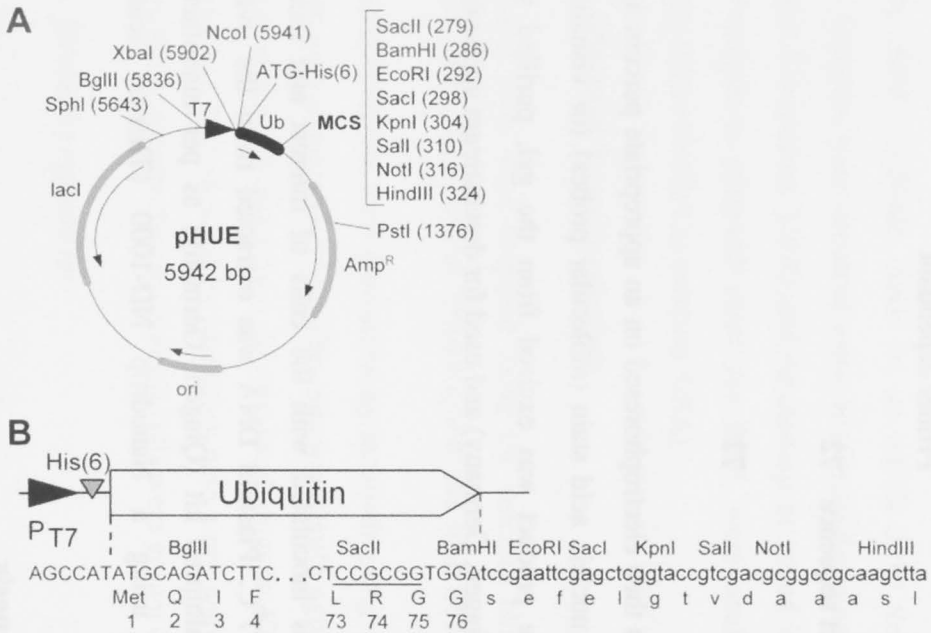

Figure 2-1 (*A*) **Plasmid map of pHUE** showing the ubiquitin (Ub) coding region (black box), the T7 polymerase promoter (black triangle), and other regions (shaded boxes). Arrows indicate the direction of transcription. Restriction enzyme recognition sites within the multiple cloning site (MCS) are listed and other useful recognition sites in the vector backbone are also shown (unique, except BglII); locations are given relative to the start codon upstream of the his-tag, ATG = 1. *(His)6*, poly histidine tag; *Amp*^{r}, β-lactamase gene; *ori*, colE1 origin of replication; *lacI*, lacI repressor gene. (*B*) DNA and encoded protein sequence of the 5′ and 3′ end of the ubiquitin coding region showing the engineered SacII site (underlined) within codons Leu 73, Arg 74, and Gly 75, and the 3′ polylinker. Restriction sites and protein translation are given above and under the DNA sequence, respectively (Baker et al., 2005).

parameters were used and the annealing temperature and extension time was adjusted according to the primer composition and template length, respectively.

	Time (s)	Temperature (^{0} C)
Initialization	120	95
Denaturation	20	95
Annealing	18	Primer dependant
Extension	60/ kb product sequence	72
Final extension	300	72

5 – 10 µl of PCR reaction was then electrophoresed on an appropriate percent agarose gel containing SYBR®Green nucleic acid stain (molecular probes) for visualization. Following electrophoresis, the product was excised from the gel, purified with a Qiaquick Gel Extraction kit (Qiagen, Germany) and used for downstream applications.

2.2.4 DNA extraction

5 ml of LB/amp (A.1.1) was inoculated with the cells of interest and incubated overnight with agitation at 37^{0}C. Plasmid DNA was extracted from the overnight culture using the QIAprep miniprep kit (Qiagen, Germany) as per manufacturers' instructions and quantified using a Nanodrop ND-1000 (Thermo scientific) spectrophotometer.

2.2.5 Site directed mutagenesis

Mutagenesis was carried out using a PCR based Phusion^{TM} site-directed mutagenesis kit (Finnzymes, Finland). The 25 µl PCR mix consisted of 1x High Fidelity (HF) buffer, 0.2 mM dNTPs, 1U Phusion DNA Polymerase, 0.5 pmol primers (forward and reverse) and 0.4 ng/µl DNA template. Reactions were carried out according to the manufacturer's instructions in a PTC-200 DNA Engine (MJ Research, USA). The mutated plasmid was digested with 1U *DpnI* (New England BioLabs) at 37°C for

30min. The digested PCR product was immediately transformed into *E. coli* DH5α strain and streaked on a pre-warmed LB/amp-agar plate and incubated overnight at 37°C. A single colony was picked from this plate and inoculated into 5ml of LB/amp (A.1.1) and incubated overnight at 37°C. Plasmids were purified from the overnight culture using QIAprep Miniprep Kit as per manufacturer's protocol (Qiagen, Germany) and sequenced (2.2.6.) to verify the presence of the desired mutation.

2.2.6 DNA sequencing

Automated DNA sequencing was carried out by the ACRF Biomolecular Resource Facility (BRF), JCSMR, ANU on an ABI® 3730 Sequencer (Applied Biosystems, USA). Samples were prepared using BigDye® Terminator v3.1 Cycle Sequencing Kit (Applied Biosystems, USA) and cleaned-up as stated in the manufacturer's protocol. DNA sequences retrieved from the BRF, were analysed using Sequencher® 4.8 software (Gene Codes Corporation, USA).

2.2.7 Plasmid Transformation

Competent cells were prepared using the calcium chloride method (Sambrook and Russell, 2001), dispensed in 100µl aliquots and snap frozen before storage at -70°C.

All transformations were performed by incubating 2ng of plasmid DNA with a 100 µl of respective competent cells. The mix was gently agitated by carefully pipetting the solution on ice, followed by a 30 min incubation at 4°C. The plasmid/competent cell mix was then heat shocked by spreading onto a pre-warmed (37°C) LB/amp-agar plate (A.1.1). Subsequently the transformed cells were grown overnight at 37°C.

2.2.8 Protein expression

All incubations were carried out at 37^0C unless otherwise noted.

First, an LB/amp agar plate (A.1.2) was streaked with the relevant *E.coli* host strain containing the plasmid of interest and incubated overnight. A single colony from this streak plate was then inoculated into 5 ml of LB/amp starter culture and again incubated overnight. The LB/amp starter culture was then inoculated to 400ml of LB/amp broth in a 2 litre flask and incubated with agitation until A_{600} (absorbance at 600 nm) reached approximately 0.8 – 1.0 (Cary 100 UV-vis spectrophotometer). Protein expression was

induced by the addition of 0.1 – 0.4 mM IPTG (A.2.26) and incubation was continued for another 3 – 4 hours. The exact concentration of IPTG and the temperature and time of protein expression were optimized for each protein individually. Following protein expression, the cells were harvested in 500 ml-Drypin bottles (Du Pont Instruments, USA) by centrifuging at 5000 rpm (4400g) for 20min at 4°C in a SLA3000 rotor (Sorval RC-5B Refrigerated Superspeed Centrifuge, Du Pont Instruments, USA). The cell pellets were stored at -20^{0}C.

2.2.9 Protein purification by IMAC (Immobilized metal affinity chromatography)

Initial purification of proteins used in this study was carried out by immobilized metal affinity chromatography using a Ni-NTA agarose resin produced in-house according to (Hochuli, 1990).

2.2.9.1 Non-denaturing purification (Native)

All steps were carried out at 4^{0}C unless otherwise noted.

The *E.coli* cell pellet was thawed on ice and re-suspended in lysis Buffer A (A.1.4) at 5 ml per gram wet weight. Cells were lysed by sonication on ice using six 30s bursts at 300W with a 30s cooling period between each burst (Branson Sonifier, USA). The cell lysate was spun down in 50 ml-polycarbonate tubes (DuPont Instruments, USA) in a SS34 rotor (Sorval RC-5B Refrigerated Superspeed Centrifuge, Du Pont Instruments, USA) at 15000 rpm (10 000 g) for 30min.

The supernatant was added to a 50% slurry of Ni-NTA agarose resin pre-equilibrated in wash buffer A (A.1.5). Based on the binding capacity of the resin, Ni-NTA agarose was used at 0.5 ml bed volume per 400 ml of original culture (Hochuli, 1990). The mix was incubated on a slow-rotating wheel for 1 hour. Following incubation, the resin was spun down at 1500 rpm (453 g) in a benchtop centrifuge (Eppendorf Centrifuge Model 5810R, Eppendorf, USA) for 5 min. The supernatant was discarded and the resin was washed by centrifugation with 10 bed volumes of wash buffer A (A.1.5). After the final wash, the resin was transferred to a 10 ml polypropylene column and the fusion protein was eluted using elution buffer A (A.1.6). The eluate was collected in 2 ml fractions and 10 µl samples of the fractions were resolved on a 12% SDS-polyacrylamide gel

(2.2.10). The gel was stained with coomassie blue (2.2.10) and the fractions containing the band of interest were pooled together.

The 6xhis-ubiquitin tag was removed by digesting the fusion protein with a ubiquitin-specific protease, Usp2cc, in the presence of 1mM DTT. The Usp2cc to fusion protein ratio was 1:200 (v:v). Digestion was carried out overnight followed by dialysis into buffer A (A.1.3) in order to remove the excess imidazole. The excised 6xhis-ubiquitin tag was removed by incubating the digested recombinant protein with a 50% slurry of Ni-NTA resin for 1h on a slow-rotating wheel. The resin was spun down at 1500 rpm (453 g) for 5min in a benchtop centrifuge (Eppendorf Centrifuge Model 5810R, Eppendorf, USA). The supernatant containing the native recombinant protein was stored at -20^{0}C.

2.2.9.2 Denaturing purification

All steps were carried out at room temperature (24^{0}C) unless otherwise noted.

The *E.coli* cell pellet was thawed on ice and re-suspended in Buffer B containing 8M Urea (A.1.7) at 5 ml per gram wet weight. Cells were lysed by sonication using six 30s bursts at 300W with a 30s cooling period between each burst (Branson Sonifier, USA). The cell lysate was spun down in 50 ml-polycarbonate tubes (DuPont Instruments, USA) in a SS34 rotor (Sorval RC-5B Refrigerated Superspeed Centrifuge, Du Pont Instruments, USA) at 15000 rpm (10 000 g) for 30min.

The supernatant was added to a 50% slurry of Ni-NTA agarose resin pre-equilibrated in buffer B (A.1.7). Based on the binding capacity of the resin, 0.5 ml bed volume of Ni-NTA agarose was used per 400 ml of original culture (Hochuli, 1990). The mix was incubated on a slow-rotating wheel for 1 hour. Following incubation, the resin was spun down at 1500 rpm (453 g) in a benchtop centrifuge (Eppendorf Centrifuge Model 5810R, Eppendorf, USA) for 5min. The supernatant was discarded and the resin was washed by centrifugation with 10 bed volumes of buffer B (A.1.7). After the final wash, the resin was transferred to a 10 ml polypropylene column and the fusion protein was eluted using elution buffer B (A.1.8). The eluate was collected in 2 ml fractions and 10 µl samples of the fractions were resolved on a 12% SDS-polyacrylamide gel (2.2.10). The gel was stained with coomassie blue (2.2.10) and the fractions containing the band of interest were pooled together.

The pooled fractions were diluted 3 fold with buffer A (A.1.3) in order to bring down the concentration of urea to 2.6 M. The urea concentration was lowered in order to preserve the activity of the ubiquitin protease. Usp2cc was added to the fusion protein at a ratio of 1:200 (v:v) and digestion was carried out overnight at 30^0C in the presence of 1mM DTT. The digested sample was concentrated down to approximately 2 ml using a 10 kDa cutoff AMICON® Ultra filter concentrator (Millipore, USA) according to the manufacturer's instructions. The concentrated sample was then diluted ten fold with buffer B (A.1.7) to bring the imidazole concentration down to 50 mM. The excised 6xhis-ubiquitin tag was removed by incubating the cleaved recombinant protein with a 50% slurry of Ni-NTA resin for 1h on a slow-rotating wheel. The resin was spun down at 1500rpm (453 g) for 5 min in a benchtop centrifuge (Eppendorf Centrifuge Model 5810R, Eppendorf, USA). The supernatant containing the denatured recombinant protein was stored at -4^0C.

2.2.10 Denaturing (SDS) Polyacrylamide Gel Electrophoresis (PAGE)

One-dimensional SDS-PAGE was used to analyse and visualise the proteins used in this study. 1 mM thick Tris-Glycine (A.1-9,10,11) gels varying from 7% - 12% were used according to the molecular weight of the analysed protein. Samples were mixed with sample loading buffer (A.1.12) at a ratio of 1:3 and boiled for 5 min. Electrophoresis was carried out using a Bio-Rad Mini PROTEAN 3 cell (Bio-Rad Laboratories, USA) attached to a Bio-Rad 100/500 power supply (Bio-rad Laboratories, USA) at 200V constant voltage.

BenchMark™ Pre-stained markers (Invitrogen) were used as protein standards unless otherwise noted.

The resolved proteins were visualised by Coomassie Blue R-250 staining. The gels were removed from the electrophoresis apparatus, placed in a container with the staining solution and gently agitated on a platform shaker for approximately 20 min. The staining solution was decanted and the gels briefly rinsed with deionized water to remove excess stain. Ten gel volumes of destaining solution (A.1.13) were added and the gels were destained by slow agitation on a platform shaker until the background was clear and the protein bands visible. The gels were documented by digital imaging on a flat bed scanner.

2.2.11 Protein Quantitation

The concentration of recombinant proteins used in this study was measured using the BCA assay (Smith et al., 1985) which measures the formation of Cu^{+} from Cu^{2+} by the Biuret complex in alkaline solutions of proteins using bicinchoninic acid (BCA). The assay was conducted according to the manufacture's protocol using the Thermo Scientific Pierce BCA Protein assay kit.

Spectrophotometric determination of absorbance at 280 nm (A_{280}) was used when a rapid estimation of protein concentration was required. Absorbance was measured on a Nanodrop ND-1000 (Thermo scientific) spectrophotometer.

Protein concentration was calculated according to the Beer-Lambert law:

$$A = \varepsilon \times l \times c$$

Where ε is the molar absorption coefficient ($M^{-1}cm^{-1}$) and *l* is the cell path length (cm). The molar absorption coefficient of a protein at 280 nm, ε_{280} (in $M^{-1}cm^{-1}$), was calculated using the following equation:

$$\varepsilon_{280} = (5500 \times n_{Trp}) + (1490 \times n_{Tyr}) + (125 \times n_{s-s})$$

where the numbers are the molar absorbances for tryptophan (Trp), tyrosine (Tyr), and cystine (i.e., the disulfide bond, S-S), and n_{Trp} = number of Trp residues, n_{Tyr} = number of Tyr residues, and n_{S-S} = number of disulfide bonds in the protein.

2.2.12 Circular Dichroism (CD) spectroscopy

Circular dichroism is the difference in the absorption of left-handed circularly polarised light (L-CPL) and right-handed circularly polarised light (R-CPL) and occurs when a molecule contains one or more chiral chromophores. It is used to monitor changes in the conformation of biopolymers and is used mainly for studying changes in the secondary and tertiary structure of proteins and peptides.

CD data was aquired on a Chirascan™ Circular Dichroism Spectrometer (Applied Photophysics Ltd, UK). Samples were prepared at 1mg/ml in 10mM sodium phosphate buffer, pH 8.0. Spectra were measured at 20^{0} C over the range of 320 – 180 nm at a scan rate of 1 nm/s. For all measurements, a cell with 0.1 path length was used. The CD

spectra were corrected for buffer contributions and an average of three scans was subjected to a smoothing function using the proprietary software of the manufacturer. Deconvolution calculations on the resulting spectrum were computed by the secondary structure prediction software, K2D2 (Perez-Iratxeta and Andrade-Navarro, 2008).

Chapter 3 Expression and Purification of the recombinant DHPR-β_{1a} subunit

3.1 Introduction

Since the DHPR β subunit was first cloned, much attention has been focused on its role in the function of voltage gated calcium channels (VGCCs). Two major findings have emerged during this period. First, the β subunit facilitates the proper localization and trafficking of the VGCC and in particular the pore forming α_1 subunit to the plasma membrane (Bichet et al. 2000; He et al. 2007). Second, the β subunit acts as an important modulator of the channel's electrophysiological properties (Richards et al. 2004; He et al. 2007).

The β subunit associates with the α_1 subunit through a region in the loop between trans-membrane domains I and II known as the alpha interaction domain (AID). Further structural, biochemical and electrophysiological studies have shown that the second conserved motif of the β subunit, the GK domain, is responsible for binding to the α_1 subunit. Although this high affinity AID-GK interaction can account for many of the functional properties of the β subunit, other lower affinity interactions have been shown to contribute to the modulatory properties of this subunit. Notably, the variable C-terminus of the β_{1a} isoform has been shown to contribute to skeletal type EC-coupling (Beurg et al. 1999; Sheridan et al. 2004). It has also been shown through pull-down experiments that the β_{1a} subunit is able to bind to a stretch of positively charged residues of the RyR1 (Cheng et al. 2005).

Four different isoforms of β-subunits ($\beta_1 - \beta_4$) have been identified, each with multiple splice variants (Arikkath et al. 2003; Dolphin 2003). All four β isoforms contain five regions (N-terminus, C-terminus, Hook region, SH3 and GK domain - **Figure 1-18**), with the second and fourth (SH3 and GK domain) being highly conserved (68–92% identity) and the others highly variable among the four β-isoforms (Hanlon et al. 1999). So far, crystallographic analysis has only been carried out on this central core region containing a short (β3, β4) or absent (β2) Hook sequence (Chen et al. 2004; Opatowsky et al. 2004; Van Petegem et al. 2004) (Table 3-1). In two of these studies the core region

Table 3-1 – Summary of existing crystallographic studies on the β subunit. SH3 – Src Homology 3 domain, GK Guanylate kinase-like domain, AID – alpha interaction domain

β subunit isoform	Crystallised region	Summary	Reference
	Full length β subunit 		
β_3 (Rat)	SH3, Hook and GK domain  SH3, Hook and Gk domain in complex with AID 	β-SH3 - has 5 beta strands similar to canonical SH3 domains, but its 4th and 5th b strands are separated by the Hook region. The loop between 1st and 2nd b strands (RT-Src loop) is much longer and shields the putative PXXP- motif binding residues. Hook region - 13 amino-terminal residues form an α-helix (α2), but the remaining residues are disordered. β-GK - overall structure is similar to canonical GK domains, but catalytically inative. AID binding – AID binds to the "AID-binding pocket" in the GK domain.Binding does not cause significant structural changes of the β-subunit core	Chen *et al* 2004
β_4 (Rat)	SH3, Hook and GK domain 	Similar to β_3	

Table 3-1 continued on next page

Table 3-1 (continued from previous page)

β_{2a} (Rat)	SH3 and GK domain. No Hook region. SH3 GK SH3 and Gk domain in complex with AID SH3 GK	SH3 and GK domains have been co-crystallized together. The Hook region is absent. Structure of the β_{2a}-SH3 and GK domains similar to β_3 and β_4 core domains.	Van Petegem *et al.* 2004
β_{2a} (Rabbit)	SH3 and GK domain. No Hook region. SH3 GK SH3 and GK domain in complex with AID SH3 GK	SH3 and GK domains have been co-crystallized together. The Hook region is absent. Structure of the β_{2a}-SH3 and GK domains similar to β_3 and β_4 core domains.	Opatowsky *et al.* 2004

of the rabbit β_{2a} isoform was crystallised alone and together with the AID region of the α_1 subunit. In the third study the core regions of the β_3 and β_4 isoforms were crystallised alone and together in complex with AID. So far no crystallographic data are available of the full length protein of any of the β isoforms. Also no crystallographic structures are available of the core region or the full length β_{1a} isoform which has been implicated in skeletal type EC-coupling.

3.2 Aim

The aim of the work presented in this chapter was to generate the full length recombinant β_{1a} subunit for the investigation of its interactions with the α_{1s} II-III loop and the RyR1. An additional aim was to enable crystallographic studies of the recombinant protein.

3.3 Materials and Methods

3.3.1 Plasmid Construction

The β_{1a} subunit isoform is encoded by 1890 nucleotide base pairs and consists of 524 amino acids. It has a calculated (ProtParam - (Gasteiger et al. 2005)) molecular weight of 57817.4 Daltons.

A GST-β_{1a}-His vector generated by inserting six histidines in tandem into a pGEX-2T vector (Amersham Pharmacia) containing a full-length β_{1a} (GenBank accession no. NM_031173) was kindly provided by Cheng *et al* (University of Wisconsin School of Medicine, Madison, USA). The β_{1a} insert was amplified (Ch.2.2.3) and sequenced (Ch 2.2.6) to check its integrity. Sequencing results of the original clone showed a "gc" to "cg" mutation which changed an arginine to a proline residue at position 78. This mutation was corrected by site-directed mutagenesis (Ch. 2.2.5). The insert was then amplified from the original construct and inserted into the in-house vector pHUE (Ch.2.2.2) as detailed below. This enabled the generation of a recombinant protein with a minimum of additional residues at either end. The presence of the ubiquitin tag was also expected to assist in the solubilisation and folding of the recombinant protein.

Primers, β_{1a} forward (β_{1a}-F) and reverse (β_{1a}-R) (GeneWorks, Australia) were designed to incorporate *BamHI* and *HindIII* restriction sites to the amplified β_{1a} gene. These sites were chosen due to the presence of a *SacII* restriction site within the β_{1a} sequence. This resulted in the addition of an extra residue (serine) to the β_{1a}- N-terminus (**Figure 3-1**).

PCR amplification was performed using the Phusion®High Fidelity kit (NEB) according to the manufacturers' instructions. The amplified product was analysed on an agarose gel, excised and purified (Ch. 2.2.4). The purified product was ligated into a pGEM-T-easy (Promega) vector system according to the manufacturer's instructions. This was done in order to facilitate a more efficient restriction digestion of the insert. The ligated product was transformed (Ch.2.2.7) into XL1-blue cells and positive transformants were identified by blue-white screening (Miller 1978). A single positive colony was inoculated into 5ml of LB/amp (A.1.1) and plasmid DNA was extracted from the overnight culture (Ch.2.2.4).

Following extraction, the plasmid DNA was double digested with 0.5 IU each of *BamHI* (NEB) and *HindIII* (NEB) restriction enzymes in the presence of NEB buffer 2 at 37 ^{0} C for 1 hour. The digested insert was resolved on an agarose gel and purified with a QIAQUICK gel extraction kit (Qiagen, Germany). The pHUE vector was simultaneously digested with *BamHI* and *HindIII* enzymes as above. The linearised vector was mixed with purified β_{1a} insert in a ratio of 1:3 and ligated in the presence of 1x ligation buffer (Promega, USA) and 3 Weiss Units of T4 DNA ligase (Promega, USA). The vector/insert mix was incubated overnight at 4^0C. The ligated product was transformed (Ch.2.2.7) into *E.coli* BL21 (DE3) competent cells and grown overnight at 37^0C. Cells from eight single colonies were picked and directly amplified by PCR (Ch.2.2.3.) using the β_{1a}-F (forward) and β_{1a}-R (reverse) primers to check for the presence of the insert. DNA was extracted (Ch.2.2.4) from one positive colony of cells and sequenced (Ch.2.2.6) to confirm the presence and the integrity of the β_{1a} insert sequence. Once confirmed, glycerol stocks of the clone, His-Ub-β_{1a} were prepared by mixing 800 µl of overnight culture with 200 µl of sterile 75% glycerol. The stocks were stored at -70^0C.

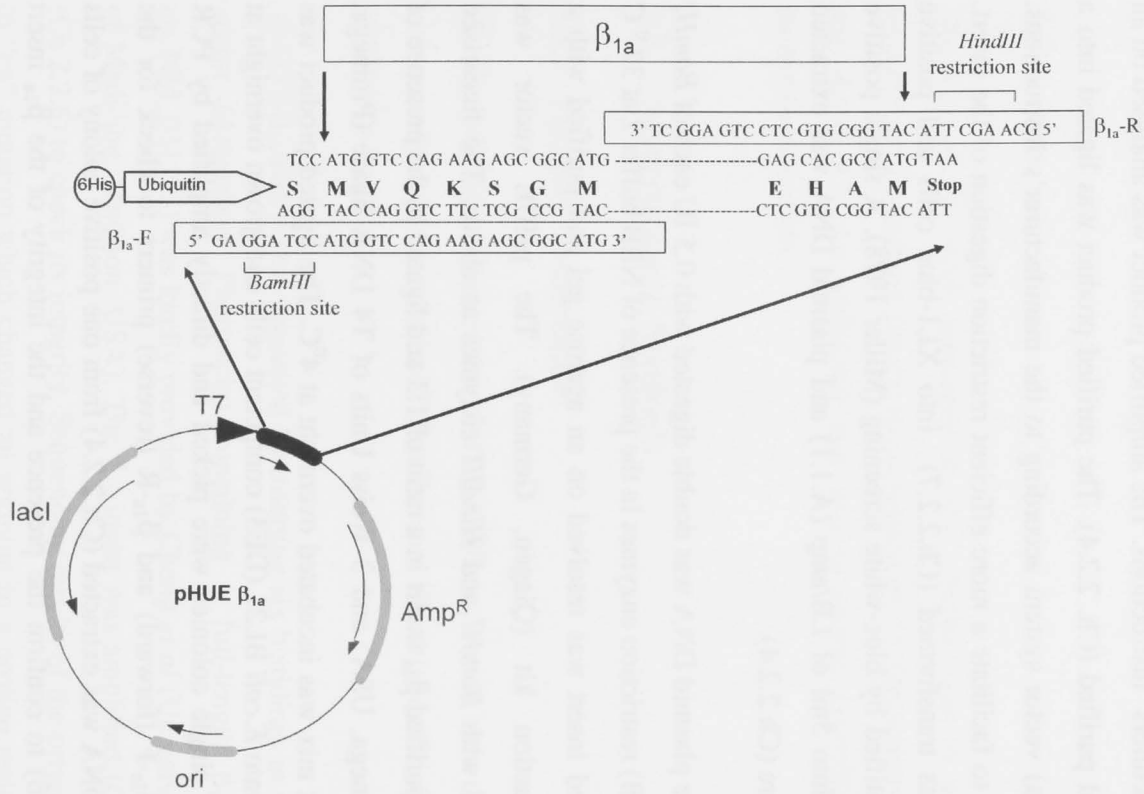

Figure 3-1 6Xhis-ubiquitin-β_{1a} construct. The protein sequence was amplified with β_{1a}-F and β_{1a}-R primers and inserted into the pHUE vector using *BamHI* and *HindIII* restriction sites (Adapted from Baker et al. 2005).

3.3.2 Protein Expression

Bacterial growth was carried out as described in Ch.2.2.8, but scaled up to 4.8 litres of culture. The culture was induced with 0.1 mM IPTG at an A_{600} (absorbance at 600 nm) of 0.8 and the protein was expressed for 2 hours at 37^0C.

3.3.3 Purification

Initial purification of the His-Ub-β_{1a} protein was carried out by IMAC (immobilized Metal Affinity Chromatography) under denaturing conditions using a Ni-NTA resin as described in chapter 2.2.9.2. Due to the persistent presence of contaminants and degradation products after IMAC, further purification of the protein was carried out by a method of preparatory electrophoresis using the Bio-Rad Prep Cell model 491 (Bio-Rad laboratories, USA).

3.3.3.1 Preparatory Electrophoresis

The Model 491 Prep Cell (Bio-Rad laboratories, USA) is an apparatus designed to purify proteins or nucleic acids from complex mixtures by continuous-elution electrophoresis (**Figure 3-2**). During a run, samples are electrophoresed through a cylindrical gel. As molecules migrate through the gel matrix, they separate into ring shaped bands. Individual bands migrate off the bottom of the gel where they pass directly into the elution chamber for collection. The elution chamber consists of a thin polyethylene frit. A dialysis membrane, directly underneath the elution frit, traps protein within the chamber. Elution buffer enters the chamber around the perimeter of a specially designed gasket. Buffer is drawn radially inward to an elution tube in the centre of the cooling core by a peristaltic pump. The peristaltic pump drives separated proteins to a fraction collector. To assure that separated molecules migrate in compact, parallel bands, temperature gradients across the gel are minimized. The temperatures of the internal and external surfaces of the gel are equalized by continuously pumping lower electrophoresis buffer through the central cooling core by means of the buffer recirculation pump.

Running conditions (gel pore size, gel length and gel tube diameter) for preparative SDS-PAGE of the partially purified β_{1a} subunit were optimized to give the maximum separation between the band of interest and its nearest contaminant. This was done by

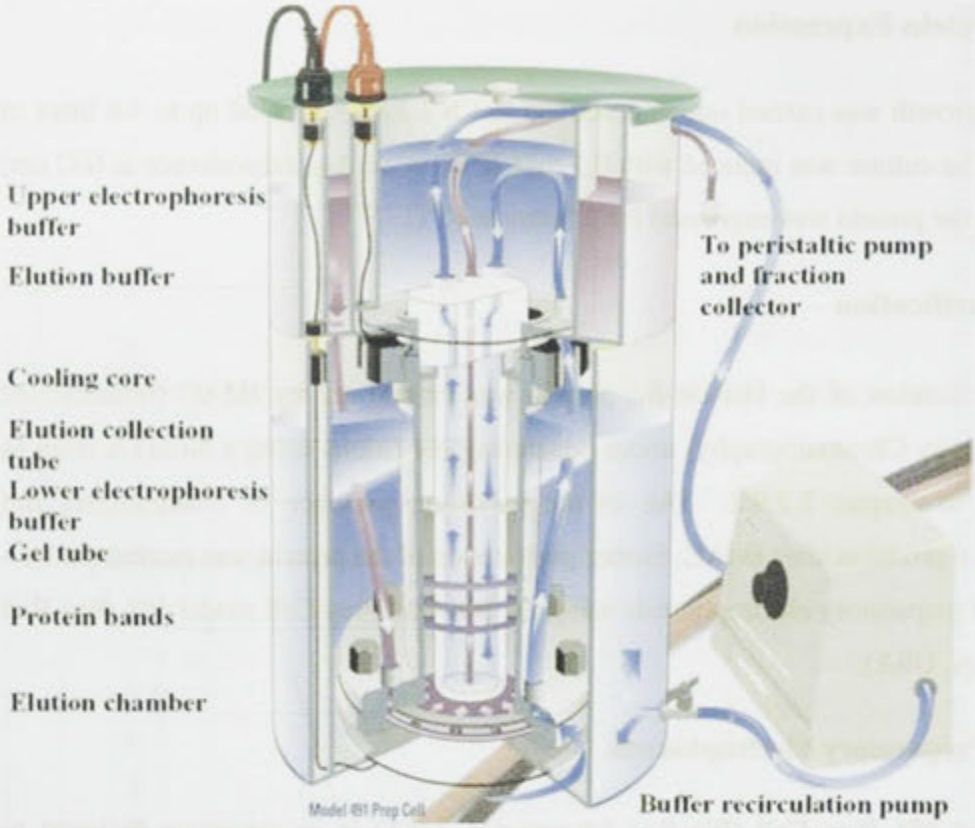

Figure 3-2 Schematic diagram illustrating the major components of the apparatus used for preparatory electrophoresis (Bio-Rad Prep Cell 491 Manual, Bio-Rad laboratories).

scouting runs on analytical mini-gels (ch 2.2.1). A 10 cm, 7% Tris-glycine resolving gel and a 2 cm, 6 % stacking gel gave the maximum resolution. These gels were poured on to the 2.8 cm diameter gel assembly tube of the Prep cell apparatus according to the manufacturers' instructions.

The partially purified β_{1a} protein was concentrated down to approximately 2 ml (10mg/ml) using a 10 kDa cut off AMICON® Ultra filter concentrator (Millipore, USA). The concentrated sample was mixed with 1 ml of denaturing sample loading dye, (A.1.12) boiled for 5 min and loaded on to the preparative gel. The Prep Cell apparatus was assembled according to the manufactures' instructions and electrophoresis was carried out at 4^0C at a constant current of 40mA. A Tris-glycine buffer containing 0.1% SDS (A.1.11) was used both as the running and elution buffers. Fractions of 4 ml were collected after the dye front eluted (Gilson Model 201 Fraction collector. Gilson Inc.).

The eluted fractions were analysed on analytical mini-gels (Ch.2.2.10) and the fractions containing the band of interest were pooled together. Ice-cold acetone was added to the pooled sample at a ratio of 5:1 (v:v) in order to precipitate the protein from the buffer containing SDS. The proteins were precipitated overnight at -20^{0}C and were spun down at 4000 rpm (Eppendorf Centrifuge Model 5810R, Eppendorf, USA) at 4°C for 30min. A vacuum desiccator was used to remove excess acetone and the desiccated protein was dissolved in 1ml of Buffer A (A.1.3) containing 6M guanidine hydrochloride. This sample was then refolded to its native form by dialysing into Buffer A at 4°C overnight. The refolded and purified protein was quantified (Ch.2.2.11), aliquoted and stored at -70^{0}C.

3.3.4 Western blotting

Western blotting was carried out on a Bio-Rad Mini-Trans-Blot Cell (Bio-Rad Laboratories, USA). Following SDS-PAGE (2.2.10), the gels were equilibrated in transfer buffer (A.1.14). A sandwich of two sponges, six pieces of filter paper and a 50cm^2 nitrocellulose membrane (TransBlot® Transfer Medium, Bio-Rad Laboratories, USA), were also pre-soaked in transfer buffer (A.1.14). The gel containing the protein (s) to be transferred was placed on the nitrocellulose membrane and sandwiched between the filter paper and the sponges and secured in the plastic gel holder cassette. The assembled cassette was then placed in the tank containing transfer buffer (A.1.14) such that the membrane was positioned on the anode side of the gel. Transfer was performed at 100v constant voltage for 1.5 hours.

Following transfer, the membrane containing the transferred proteins was removed and blocked for 1 hour with blocking buffer (A.1.15) at room temperature with agitation on a platform shaker.

Anti-β_{1a} monoclonal antibody, VD2(1)B12 (Developmental Studies Hybridoma Bank, University of Iowa, Department of Biological Sciences, Iowa City, IA 52242) was diluted 1:3000 (v:v) with blocking buffer. The diluted antibody was added to the membrane and incubated in a sealed plastic bag at room temperature for 1 hour with gentle agitation. The membrane was washed 4 times with an excess of blocking buffer (A.1.15), with each wash lasting 15 minutes. The blotted membrane was then incubated for another hour with horse radish peroxidise (HRP) conjugated-goat anti-mouse antibody (DakoCytomation, Denmark), diluted 1:10000 (v:v) with blocking buffer. The

membrane was washed again as before and treated with ECL detection reagent (GE Healthcare, UK) for 1min. The treated membrane was later exposed to X-ray film (FUJI Medical X-Ray Film, Fuji Photo Film, Japan) for 1min. Exposed film was later developed on an automated film developer (Kodak X-OMAT 1000 Processor, KODAK, Japan).

3.3.5 Circular Dichroism (CD) spectroscopy

The purified β_{1a} sample was dialysed into 10mM sodium phosphate buffer, pH 8.0 and CD was performed as described in Ch.2.2.12.

3.3.6 Mass spectrometry

The band of interest was excised from a SDS-PAGE gel and subjected to tryptic digestion. The resulting fragments were analysed on a MALDI TOF/TOF™ model 4800 mass spectrometer(Applied Biosystems) at the ACRF Biomolecular Resource Facility (BRF), JCSMR, ANU. The masses of peptides generated by enzymatic cleavage were then matched with peptides generated by theoretical cleavage of the protein using the search program MASCOT (Matrix Science).

3.4 Results

3.4.1 Protein Expression

During the process of expression and purification of the full length β_{1a} subunit, problems were encountered due to auto-cleaving of the histidine-ubiquitin tag and protein degradation. Therefore, many different conditions and experimental protocols were tried in a bid to optimise the expression and purification of this protein.

In order to reduce auto-cleaving of the fusion protein, expression was trialed at room temperature (24^0C) for different time intervals and at 4^0C overnight. Expression was also attempted by auto induction using the Studier method (Studier 2005). Maximum yield of recombinant protein was obtained by expressing the protein for 2 hours at 37^0C following induction with 0.1 mM IPTG.

3.4.2 Purification

Purification of the β_{1a} subunit was initially tried out by IMAC (immobilized Metal Affinity Chromatography) under native conditions (Ch.2.2.9.1). However, a higher yield of recombinant protein was obtained by purifying under denaturing conditions (Ch.2.2.9.2). Due to the persistent presence of contaminants and degradation products after IMAC, further purification of the protein was necessary (**Figure 3-3**). This was initially tried out using an anion-exchange column (Mono Q HR 5/5) on the AKTA™ (GE life sciences) FPLC (fast performance liquid chromatography) system. FPLC was carried out under varying buffer conditions, but the results were only partially successful. Although over 95% of contaminants were dispelled, two bands (denoted β_{1a}-upper and β_{1a}-lower) corresponding to the expected molecular weight were inseparable using FPLC. These bands were successfully separated by preparatory electrophoresis (**Figure 3-4**) where a purity of over 95% and a yield of approximately 2 mg per purification were achieved (**Figure 3-5**).

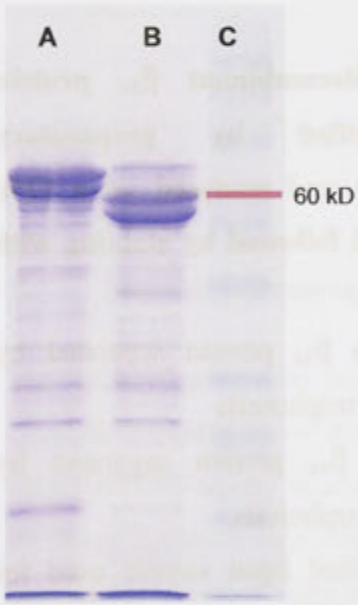

Figure 3-3 IMAC purified (chapter 2.2.9.2) Recombinant β_{1a} protein analysed on a 12 % SDS-PAGE gel followed by staining with coomassie blue.

A). 6Xhis-ub-β_{1a}. The fusion protein eluted from the Ni-NTA resin

B) Cleaved β_{1a} protein. The 6Xhis-Ub tag has been cleaved with ubiquitin protease and removed by re-binding to the Ni-NTA resin.

C) BenchMark™ prestained protein ladder (Invitrogen)

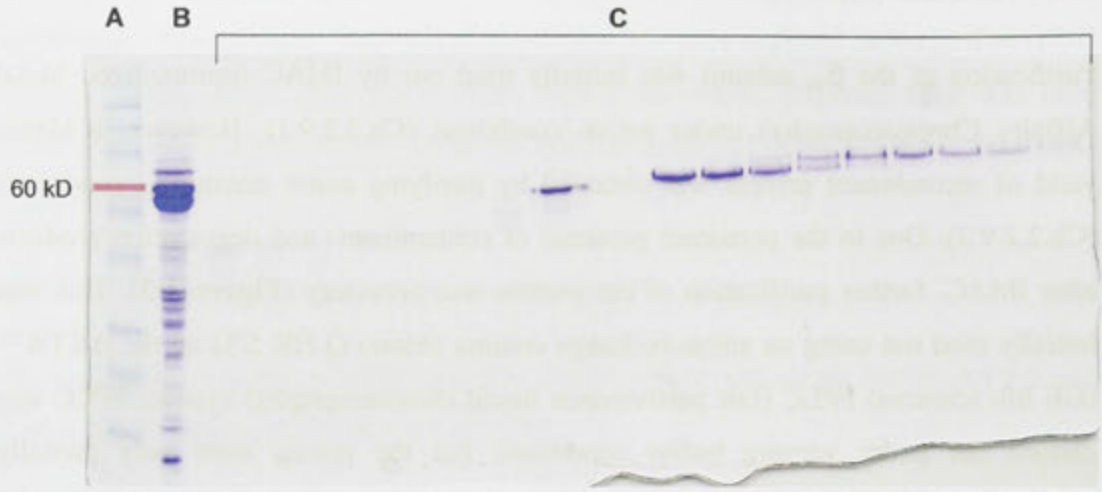

Figure 3-4 Further purification of the β_{1a} protein by preparatory electrophoresis using the Bio-Rad Prep Cell 491. (7 % SDS-PAGE gel coomassie stained) **A)** BenchMark™ prestained protein ladder (Invitrogen) **B)** IMAC purified β_{1a} input sample **C)** Eluted fractions containing the separated protein bands.

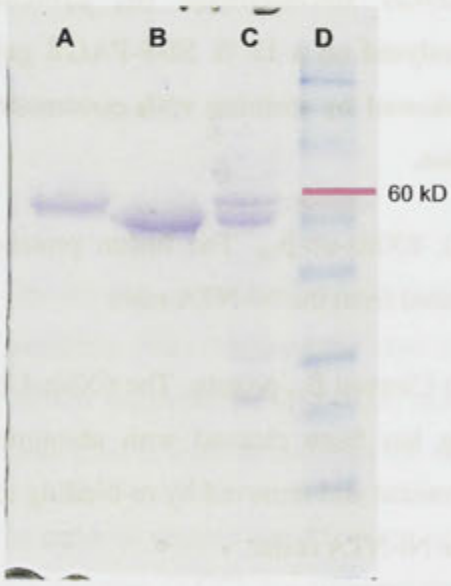

Figure 3-5 Recombinant β_{1a} protein further purified by preparatory electrophoresis and analysed on a 12% SDS-PAGE gel followed by staining with coomassie blue.

A) Full length β_{1a} protein separated by preparatory electrophoresis

B) Truncated β_{1a} protein separated by preparatory electrphoresis

C) IMAC purified input sample used for preparatory electrophoresis

D) BenchMark™ prestained protein ladder (Invitrogen)

3.4.3 Western blotting

Both β_{1a}-upper and β_{1a}-lower bands migrated at the expected molecular weight of ~58 kD on a 10% SDS-PAGE gel and were recognized by the anti-β_{1a} monoclonal antibody, VD2(1)B12, indicating that the β_{1a}-lower band was most likely a truncated product of the full length β_{1a} subunit (**Figure 3-6**).

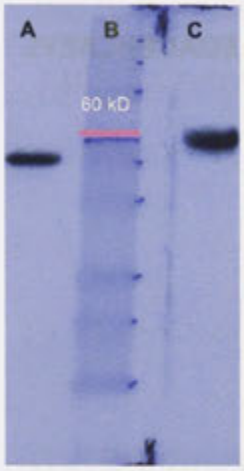

Figure 3-6 Western blot of the bands separated by preparatory electrophoresis and probed with anti-β_{1a} monoclonal antibody. Both bands are positively identified by the antibody indicating the presence of the epitope in both proteins. (proteins analysed on a 12 % SDS-PAGE gel)

A). β_{1a} lower band

B) BenchMark™ prestained protein ladder (Invitrogen)

C) β_{1a} upper band

3.4.4 Mass spectrometry

Mass spectrometry was performed on the β_{1a}-upper and β_{1a}-lower bands in order to estimate the integrity of the proteins (**Figure 3-7**). Peptide finger print mass mapping (MASCOT by Matrix Science) gave a coverage of 39% for the upper band and 60% for the lower band. A nine residue peptide was not matched from the N-terminal end of both bands. At the C terminal end of the lower band, no peptides were matched to the last 53 residues. Considering that the sequence coverage is 60% for this band, the absence of the peptides are most likely due to truncation of this region. However, in the upper band peptides was matched up to residue 511 indicating the integrity of this region. The inability to match the N-terminal 9 residue peptide and the C-terminal 13 residue peptide of the upper band could be due truncation of the residues or more likely it could be due to an artifact of the method. This needs to be investigated further.

A

```
  1 MVQKSGMSRGPYPPSQEIPMEVFDPSPQGKYSKRKGRFKRSDGSTSSDTT
 51 SNSFVRQGSAESYTSRPSDSDVSLEEDREALRKEAE RQALAQLEKAKTKP
101 VAFAVRT NVGYN PSPGDEVPVQGVAITFEPKDFLHI KEKYNNDWW IGRLV
151 K EGCEVGF I PSPVKLDSLRL LQEQTLRQNRLSSSKSGDNSSSSLGDVVTG
201 TR RPTP PASGNEMTNFAFELDPLE LEEEEAELGE HGGSAKTSVSSVTTPP
251 PHGKRIPF FKKTEHVP PY DVVPSMRPI I LVGPSLKGYEVTDM MQKALFDF
301 LKH RFDGRIS I TRVTAD I SLAKRSVLN NPSKH I I I ERSNT RSSLAEVQSE
351 I E R I E LARTLQLVALDADT I NH PAQ LSKTS LAP I I VY I K I TSPKVLQRL
401 I KSRGKSQSKH LNVQ I AASEKLAQCPPEMFD I I LDENQLEDACEHLAEYL
451 EAYWKATH PPSSTPPN PLLN RTMATAALAASPAPVSNLQVQVLTSLRRNL
501 SFWGGLEASPRGGDAVAQPQEHAM
```

B

```
  1 MVQKSGMSRGPYPPSQEIPMEVFDPSPQGKYSKRKGRFKRSDGSTSSDTT
 51 SNSFVRQGSAESYTSRPSDSDVSLEEDREALRKEAE RQALAQLEKAKTKP
101 VAFAVRT NVGYN PSPGDEVPVQGVAITFEPKDFLHI KEKYNNDWW IGRLV
151 K EGCEVGF I PSPVKLDSLRL LQEQTLRQNRLSSSKSGDNSSSSLGDVVTG
201 TR RPTP PASGNEMTNFAFELDPLE LEEEEAELGE HGGSAKTSVSSVTTPP
251 PHGKRIPF FKKTEHVP PY DVVPSMRPI I LVGPSLKGYEVTDM MQKALFDF
301 LKH RFDGRIS I TRVTAD I SLAKRSVLN NPSKH I I I ERSNT RSSLAEVQSE
351 I E R I E LARTLQLVALDADT I NH PAQ LSKTS LAP I I VY I K I TSPKVLQRL
401 I KSRGKSQSKH LNVQ I AASEKLAQCPPEMFD I I LDENQLEDACEHLAEYL
451 EAYWKATH PPSSTPPN PLLN RTMATAALAASPAPVSNLQVQVLTSLRRNL
501 SFWGGLEASPRGGDAVAQPQEHAM
```

Figure 3-7 Mass spectrometry results of the β_{1a}-upper (A) and β_{1a}-lower bands (B). The masses of peptides generated by enzymatic cleavage matched with peptides generated by theoretical cleavage of the protein using the search program MASCOT (Matrix Science). The matched peptides are highlighted in red. **A)** Upper band – sequence coverage – 39 % **B)** Lower band – sequence coverage – 60%

Although the peptide coverage for the upper band is only 39%, the protein migrates at the expected molecular weight of 60 kD in a 12% SDS PAGE gel **(Figure 3-8)** indicating that the protein is full length or close to that. Therefore, the β_{1a}-upper band will be referred to as the recombinant full length β_{1a} protein.

3.4.5 Circular Dichroism (CD) spectroscopy

CD spectroscopy of the purified and refolded (3.3.3) full length β_{1a} (β_{1a}-upper) subunit (**Figure 3-8**) was carried out in order to verify the presence of secondary structure. The resulting spectrum contained a maximum at 191 nm followed by minima at 209 and 226 nm (**Figure 3-9**). Deconvolution calculations on the resulting spectrum were computed

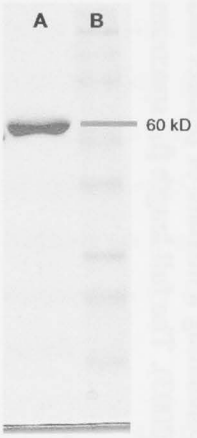

Figure 3-8 Recombinantly expressed and purified full length β_{1a} protein analysed on a 12 % SDS-PAGE gel followed by coomassie staining.

A) 10 μg of purified full length β_{1a} protein

B) BenchMark™ prestained protein ladder (Invitrogen)

by the secondary structure prediction software, K2D2 (Perez-Iratxeta and Andrade-Navarro, 2008).software predicted 17.94 % helical content and 26.38 % β-strand. These results are consistant with published data for full length β_{2a} and β_3 (~35% β-sheet, ~15% α helix) which have over 90% similarity with β_{1a} in the SH3 and GK domains (**Figure 3-9**). The full length β_{1a} CD spectrum indicates a protein of mixed secondary structure as evidenced by crystallographic studies of the core region of other β isoforms (Opatowsky et al. 2003; Chen et al. 2004; Van Petegem et al. 2004). Sequence analysis and proteolytic studies (Opatowsky et al. 2003) indicate that the relatively long N, C termini and the Hook region of all β isoforms have a random coil formation.

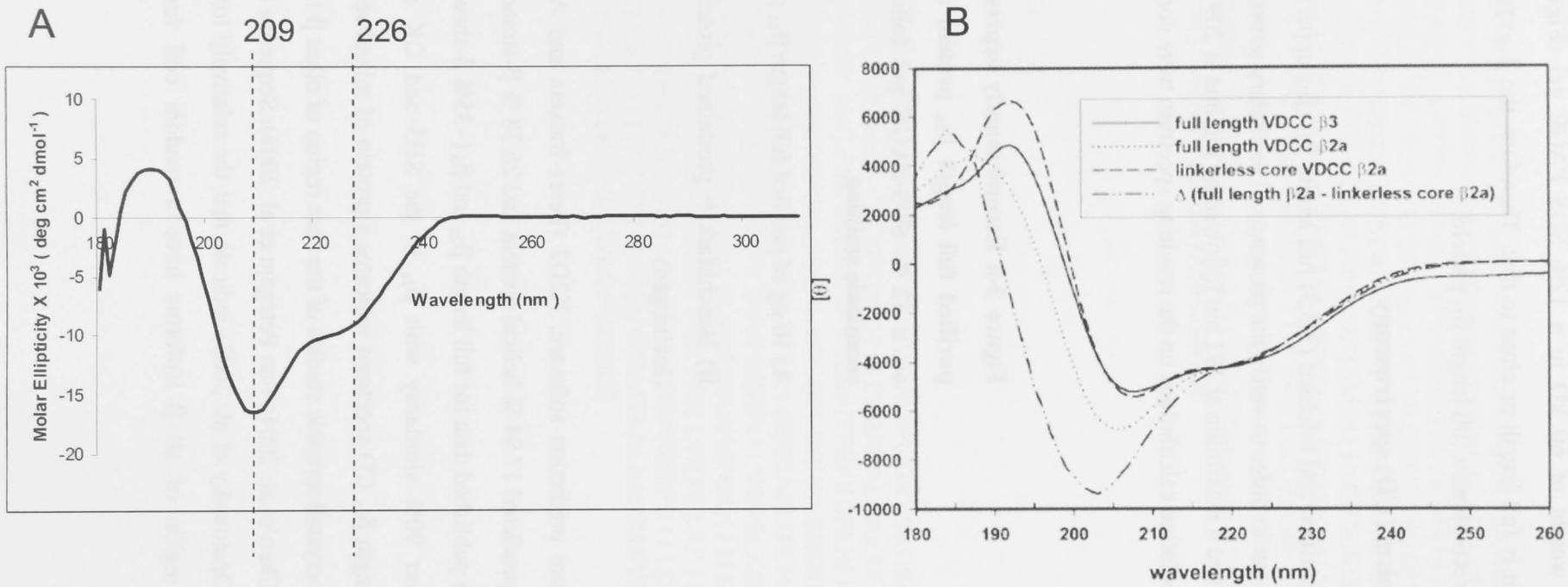

Figure 3-9 Comparison of Circular dichroism (CD) spectra of full length β_{1a} subunit, β_{2a} and β_3. **A**) CD spectrum of the purified and refolded β_{1a} protein. The spectrum shows a maximum at 191 nm followed by minima at 209 and 226 nm. Deconvolution calculations point to ~ 26 % β sheet and ~ 18 % α-helix. This is indicative of a protein containing a mixture of β-sheet and α-helical structure. **B)** CD spectra for full length β_{2a}, β_3, β_{2a} core and β_{2a} minus the linkerless core (Opatowsky et al. 2003). The full length β_{1a} spectrum shows a strong similarity to the full length β_3 spectrum.

3.5 Discussion

The expression and purification of the β_{1a} subunit posed many challenges. This was mainly due to the proteolytic cleavage of the fusion protein which gave rise to many degradation products and hence a low yield. Consequently the development of the expression and purification protocol required extensive optimisation at each step of the experiment.

The first obstacle was faced during the expression of the fusion protein. Although the protein was expressed in a protease deficient host (E.coli BL21- DE3), degradation of the protein was still apparent. In addition to degradation, auto-cleaving of the 6Xhis-ubiquitin tag was also a problem. The presence of the ubiquitin tag was expected to assist in the solubility of the fusion protein, but in this instance it did not prevent a large amount of the protein from being expressed as inclusion bodies. In order to combat these problems, expression was tried out at many different temperatures (37^0C, 24^0C, 4^0C) and at different time points (2, 4, 6 hours and over-night). Different methods of induction (Studier method) were also tried. But the long induction period used in this method seemed to increase degradation and resulted in a low yield. A short period of expression (2 hrs) at 37^0C produced the least amount of degradation and the maximum yield.

Purification of the fusion protein by IMAC under native conditions gave a minimum yield. Auto-cleaving of the 6Xhis-ubiquitin tag appeared to be a continuous process and wasn't retarded by the presence of protease inhibitors in the lysis buffer (A.1.4). Progressive auto-cleaving of the tag significantly reduced the amount of fusion protein that was bound to the Ni-NTA resin thus reducing the yield. This problem was overcome by purifying the protein under denaturing conditions. The reduction of auto-cleaving and the improvement in yield of fusion protein was most likely due to the proteases being inactivated under denaturing conditions. After initial purification of the fusion protein using the tag, subsequent cleavage of the his-ubiquitin tag was carried out in the presence of 2.6M urea which allowed the activity of the ubiquitin protease (Ch.2.2.9.2) but discouraged further proteolysis. Further purification steps were continued under denaturing conditions since the protein appeared to be extremely prone to degradation.

The fusion protein purified by IMAC still contained numerous contaminants and degradation products (**Figure 3-3**). Efforts to improve purity by varying the imidazole concentration in the buffers and the quantity of resin were unsuccessful. This was probably due to two problems : 1) weak binding of the β_{1a} fusion protein to the resin. A very low (10 mM) concentration of imidazole was sufficient to elute the protein off the resin. This precluded the use of higher concentrations of imidazole in the lysis and wash buffers to prevent non-specific binding. 2) the presence of the 6Xhis-ubiquitin tag in most degradation products which resulted in co-purification of these with the fusion protein.

The biggest challenge for further purification of the protein was posed by the presence of two major bands of almost equal intensity that migrated (12% SDS-PAGE) very closely together at the expected molecular weight of ~ 60 kD (**Figure 3-3**). Further purification was first tried out by FPLC (Fast Performance Liquid Chromatography) using an anion exchange column (Mono-Q, Amersham-Pharmacia). Anion exchange chromatography was carried out using buffers of different ionic strengths and composition. Although the protein was cleared of most contaminants the two bands of interest were inseparable using this method. This was probably due to the fact that these proteins were closely related and had very similar isoelectric points (Pi).

The most successful result was obtained by using a method of preparatory electrophoresis (3.3.3.1) based on mass difference and the different migratory patterns of these two bands (**Figure 3-4**). Using this method the two proteins were separated and purified to over 95 % purity (**Figure 3-8**).

Both purified bands were positively identified by the anti-β_{1a} antibody, VD2(1)B12, which indicated that these two proteins were indeed closely related and contained the epitope recognized by the antibody (**Figure 3-6**). Finally, peptide mapping and mass spectrometry (3.3.6) of these bands confirmed that the lower band was a truncated product of the full length protein which corresponded to the upper band.

Hence, the isolated upper band was refolded to its native state and circular dichroism (CD) spectra were obtained of the refolded full length protein (**Figure 3-9**). These spectra indicated a mixture of secondary structural elements (3.4.4) which are consistant with the available crystallographic data and suggested a correctly folded protein.

The β_{1a} subunit is a 57817.4 dalton protein consisting of 524 amino acid residues. By sequence homology mapping to the published structural studies (Chen et al. 2004; Opatowsky et al. 2004; Van Petegem et al. 2004) using other β isoforms (β_{2a}, β_3 and β_4), β_{1a} is also predicted to contain two, well ordered, structural domains (SH3 and GK). The Hook region within the SH3 domain and the N and C termini of this protein are predicted to have a random coil structure. The exposed nature of these random coil elements most likely predisposes this protein to proteolysis. Previous structural studies expressing other isoforms of this protein have indeed alluded to this fact (Opatowsky et al. 2003; Van Petegem et al. 2004). Hence the challenges faced during the expression and purification of this protein were not entirely unexpected.

The purified β_{1a} protein was used to examine its interactions with the α_{1s} II-III loop and the RyR1. Future directions will be to further optimise the purification protocol to obtain a sufficient yield to perform crystallographic studies.

Chapter 4 Interactions between the DHPR-β_{1a} subunit and the α_{1s} II-III loop

4.1 Introduction

Unlike cardiac-type EC coupling, skeletal-type EC coupling does not require an influx of Ca^{2+} through the DHPR L-type-Ca^{2+} channel. For this reason, it is thought that transmission of the EC coupling signal from the voltage sensing skeletal DHPR to the RyR1 depends on conformational coupling between these two multimeric complexes (Ch.1.5.2). This idea is supported by a number of studies, the most significant of which was provided by ultrastructural studies of Franzini-Armstrong and colleagues who revealed that DHPRs are arranged into groups of four ("tetrads") and that these tetrads were arranged in register with the four subunits of every other RyR1 (Franzini-Armstrong et al., 1998)(**Figure 1-6**). Subsequent work showed that the distance between DHPRs within tetrads is decreased by exposure to concentrations of ryanodine sufficient to lock RyR1 in a non-conducting state, hence demonstrating that skeletal DHPRs are linked (directly or indirectly) to RyR1s (Paolini et al., 2004).

The absence of either the α_{1s} or the β_{1a} subunit of the DHPRs produce an EC coupling-dead phenotype in which mice deficient in either subunit die perinatally as a consequence of respiratory paralysis. The almost identical phenotype of β_{1a}-null and dysgenic mice (α_{1s} null) have been explained by the inability of α_{1s} to be trafficked to triad junctions in the absence of β_{1a} (Coronado et al., 2004). However, studies on β_{1a}-null zebrafish (relaxed) mutants indicate that the lack of β_{1a} does not prevent triad targeting of the α_{1s} subunit but precludes the skeletal muscle-specific arrangement of DHPR particles opposite the RyR1 (Schredelseker et al., 2009). This suggests that trafficking of the α_{1s} subunit to triad junctions is not the only role of β_{1a} and that the links between DHPRs and RyR1 that result in tetrad formation and skeletal type EC coupling require the presence of the β_{1a} subunit.

The β subunit has a modular structure consisting of 5 regions – an N-terminus, C-terminus, SH3 and guanylate kinase (GK) domains connected by a Hook region (**Figure 1-18**). The existence of an SH3-Hook-GK module places the β subunit in a

family of proteins called the membrane-associated guanylate kinases (MAGUKS). MAGUKs, which include proteins such as PSD95, SAP97, CASK, Shank and Homer, function as scaffold molecules that play a key role in organizing multiprotein complexes. The Ca^{2+} channel β subunit differs from canonical MAGUK proteins in that it does not contain a well-defined PDZ domain. But considering its overall similarity to other MAGUK proteins, it is not surprising that the β_{1a} subunit is involved in the organisation of tetrad complexes in skeletal musle (Schredelseker et al., 2005, Schredelseker et al., 2009)

However, the exact molecular interactions that result in the isoform specific role of the β_{1a} subunit in tetrad formation and skeletal type EC coupling remain unclear. The β subunit induced trafficking of the α_1 to the triad junction has been attributed to the high affinity (3-76 nM) interaction between the AID (alpha interaction domain) of the I-II loop of the α_1 subunit and the highly conserved GK domain of the β subunit (He et al., 2007, Richards et al., 2004). But the functional role of the SH3 domain is less understood.

Canonical SH3 domains mediate specific protein-protein interactions by binding to proline-rich motifs in target proteins through an aromatic patch formed by a cluster of highly conserved hydrophobic residues (Zarrinpar et al., 2003). The SH3 domains are composed of five sequential β strands (β1- β5) arranged into two orthogonally packed sheets (Larson and Davidson, 2000). The Ca^{2+} channel β-SH3 has a similar fold as classical SH3 domains, but its last two β strands are separated by a Hook region (Chen et al., 2004)(**Figure 1-18**). This split configuration is also shared by other MAGUK proteins such as PSD-95 (McGee et al., 2001). Like canonical SH3 domains, the β-SH3 also contains a well-preserved proline-rich motif-binding site and therefore has the potential to bind proteins containing such motifs. However, in the crystal structures, this binding site is partly occluded by the α_2 helix which is situated near the N-terminus of the Hook region and the RT-Src loop connecting the first and second β strands (**Figure 4-1**)(Chen et al., 2004). Thus access to this site requires movement of these two regions. Such conformational changes are conceivable around the long and flexible Hook region and would expose the proline-rich motif-binding site of the β-SH3 domain for interaction with proline-rich motifs of neighbouring molecules. Such an interaction has in fact been documented *in vitro* between the SH3 domain of β_{2a} and a poly-proline

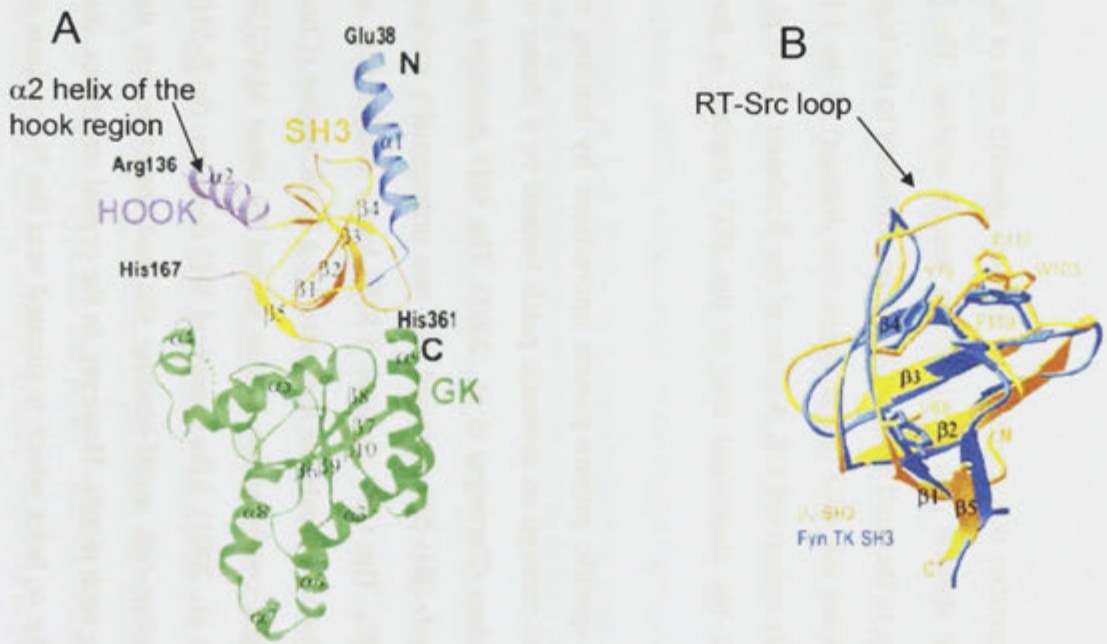

Figure 4-1 Crystallographic structure of the β_3 core showing the α_2 helix of the Hook region and the RT-Src loop. A) The Hook region is in purple. The arrow points to the α_2 helix. The SH3 domain is depicted in orange. B) The β_3-SH3 domain (orange) is superimposed on the Fyn TK SH3 domain (blue). The arrow points to the RT-Src loop between the 1st and 2nd β strands of the β_3 SH3 domain, which is predicted to occlude the potential polyproline-motif binding site in β_3 (P119,W103,Y70, V68 and F117). Adapted from (Chen et al., 2004)

motif of the protein, Dynamin (Gonzalez-Gutierrez et al., 2007). However, the β_{2a} fragment used in this study lacked the fifth β strand of the SH3 domain and the Hook region, which hinders access to the proline-rich motif binding site of β-SH3.

Assuming that dynamic re-arrangments around the flexible Hook region can expose the proline-rich motif binding site of β_{1a}-SH3, we proceeded to search for potential proline-rich binding motifs in its neighbouring molecules. It was noted that functional SH3 binding sites have already been identified in the α_{1c} (cardiac) II-III loop (Dubuis et al., 2006). Therefore it was of interest to investigate the α_{1s} (skeletal) II-III loop for similar SH3 binding motifs, as several *in vivo* studies have unequivocally demonstrated that the II-III loop of the α_{1s} subunit plays a key role in transmitting the EC coupling signal to RyR1 (Ch.1.8.2.1).

Investigation of the α_{1s} II-III loop sequence by ELM (Eukaryotic Linear Motif resource-http://elm.eu.org (Gould et al.)), a resource for identifying candidate functional motifs in proteins, revealed three such potential binding sites (**Figure 4-2**). It was interesting to note that all three predicted proline-rich motifs were contained in the C-region of the α_{1s} II-III loop. The C-region of the α_{1s} II-III loop has been shown to be critical for skeletal type EC-coupling and it has been proposed that the C-region may interact in some manner with RyR1 (Ch.1.8.2.1). More specifically, four skeletal-specific residues (critical residues) within the C region (A739, F741, P742 and D744) have been identified as being essential for skeletal type EC coupling (Kugler et al., 2004). However, the precise mechanism of the interaction between the α_{1s} II-III loop and the RyR1 remains a topic of contention and despite over a decade of intense research the site of its interaction with RyR1 has not been established. This may be because the link between the α_{1s} II-III loop and RyR1 is in fact through the β_{1a} subunit.

4.2 Aim

The aim of the work presented in this chapter is to investigate the role of the β_{1a}-SH3 domain as a potential binding site for the α_{1s} II-III loop. This includes the identification of key residues in the II-III loop involved in this interaction *in vitro*.

A)

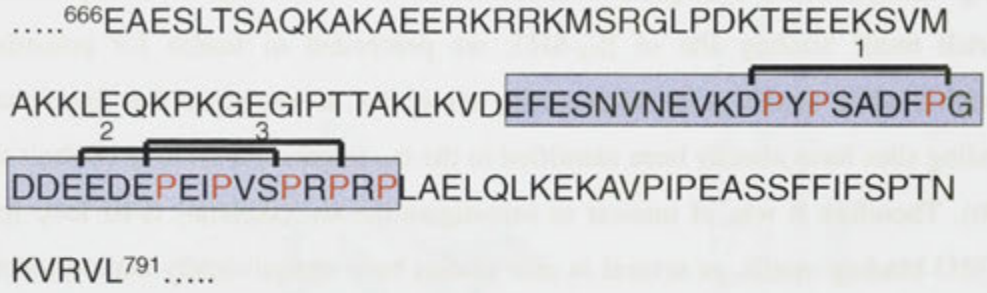

B)

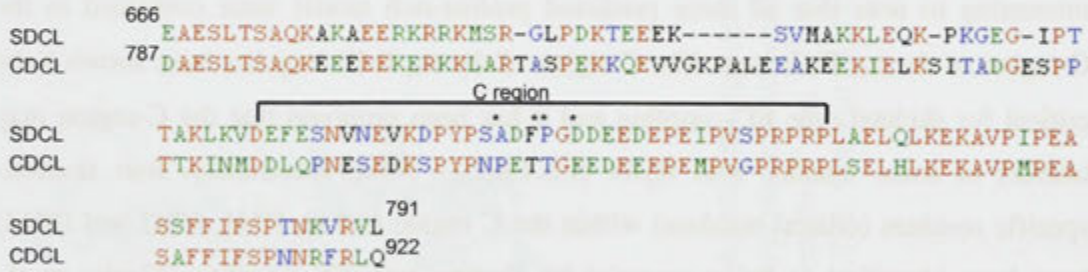

Figure 4-2 **A) 1,2,3 - Potential SH3 binding motifs in the α_{1s} II-III loop as identified by ELM** (Eukaryotic Linear Motif search tool - http://elm.eu.org) The C region of the II-III loop is enclosed in blue and the proline residues are highlighted in red.

B) Alignment of the α_{1s} II-III loop (SDCL) with the α_{1c} II-III loop (CDCL). Exact matches are in red, highly similar residues in green and dissimilar residues in blue. Very different or non-aligning residues are in black. " * " - residues critical for skeletal type EC-coupling. The C region is enclosed.

4.3 Materials and Methods

4.3.1 Expression of proteins and synthesis of peptides

4.3.1.1 Peptides used in this study (Table 4-1)

Peptides were synthesized as described in the general methods section (Ch. 2.2.1). In the peptide nomenclature the α_{1s} II-III loop is referred to as "SDCL" (**S**keletal **D**ihydropyridine receptor **C**ytoplasmic **L**oop) and the α_{1c} II-III loop as "CDCL" (**C**ardiac **D**ihydropyridine receptor **C**ytoplasmic **L**oop).

4.3.1.2 Peptide and protein quantitation

The precise concentration of peptides and proteins used in this study was determined as described in chapter 2.2.1 and 2.2.11 respectively.

4.3.1.3 β_{1a} subunit

The recombinant β_{1a} subunit was prepared as described in Chapter 3.3.3.

4.3.1.4 α_{1S} II-III loop

The His-Ub-α_{1s} II-III loop construct (Cui, Karunasekara et al., 2005) was transformed in to *E.coli* BL 21 (DE3) strain and bacterial growth was carried out in 4.8 litres of LB/amp (A.1.1). The culture was induced with 0.1 mM IPTG at an A_{600} (absorbance at 600 nm) of ~0.9 – 1.0 and the protein was expressed for 4 hrs at 37^0C.

The protein was initially purified by IMAC (immobilized Metal Affinity Chromatography) under native conditions using a Ni-NTA resin as described in Chapter 2.2.9.1. This was followed by further purification using preparatory electrophoresis under native conditions on the Bio-rad 491 prep cell (Bio-Rad laboratories, USA) (Cui, Karunasekara et al., 2005). The purified sample was eluted in 25 mM Tris, 192 mM glycine pH 8.3. The eluted sample was concentrated, dialysed against buffer A (A.1.3) and stored at -70^0 C.

The expression and purification of the circularized II-III loop was carried out by Dr. Han-Shen Tae (Tae et al., 2009).

Table 4-1 Peptides used in this study (see figure 1-4b for full sequence of SDCL and its alignment with CDCL)

Name	Description	Sequence
Peptides derived from α_{1S} II-III loop (SDCL)		
SDCL Peptide A	A region of the α_{1s} II-III loop	^{671}TSAQKAKAEERKRRKMSRGL^{690}
SDCL Peptide C	Proline rich C region of the α_{1s} II-III loop	^{720}LKVDEFESNVNEVKD**P**Y**P**SADF**P**GDDEEDE**P**EI **P**VS**P**R**P**R**P**LAELQ^{765}
SDCL Peptide C P-A mutant	C region of the α_{1s} II-III loop with all prolines mutated to alanine residues	^{720}LKVDEFESNVNEVKD**A**Y**A**SADF**A**GDDEEDE**A**E I**A**VS**A**R**A**R**A**LAELQ^{765}
SDCL Scrambled Peptide C	Scrambled sequence of α_{1s} II-III loop C region	IPEQNEDPEKSANDPSYLVVEPLRGFEPSEFDPVLD EKPVDEDRPA
SDCL Peptide C1	N-terminus of α_{1s} II-III loop C region	^{720}LKVDEFESNVNEVKD**P**Y**P**SADF**P**GD^{743}
SDCL Peptide C2	Middle of α_{1s} II-III loop C region	^{730}NEVKD**P**Y**P**SADF**P**GDDEEDE**P**EI^{751}
SDCL Peptide C3	C-terminus of α_{1s} II-III loop C region	^{739}DF**P**GDDEEDE**P**EI**P**VS**P**R**P**R**P**LAEL^{764}
SDCL Peptide C3 short	Short peptide derived from the C region (SDCL peptide C) of the α_{1s} II-III loop containing the canonical SH3 binding motif, PXXP.	^{748}DE**P**EI**P**VS**P**R**P**R**P**LAEL^{764}
SDCL Peptide C3 short P-A mutant	SDCL peptide C3 with all prolines mutated to alanines	^{748}DE**A**EI**A**VS**A**R**A**R**A**LAEL^{764}

Table 4-1 continued from previous page

SDCL Peptide C4	Short peptide derived from the C region (SDCL peptide C) of the α_{1s} II-III loop containing the critical residues shown to be essential for skeletal type EC coupling..	^{732}KDPYPS**A**D**FP**G**D**D^{744}
SDCL Peptide C4 A to P	SDCL peptide C4 A739 mutated to its cardiac residue	^{732}KDPYPS**P**DFPGDD^{744}
SDCL Peptide C4 F to T	SDCL peptide C4 F741 mutated to its cardiac residue	^{732}KDPYPSAD**T**PGDD^{744}
SDCL Peptide C4 P to T	SDCL peptide C4 P742 mutated to its cardiac residue	^{732}KDPYPSADF**T**GDD^{744}
SDCL Peptide C4 D to E	SDCL peptide C4 P742 mutated to its cardiac residue	^{732}KDPYPSADFPG**E**D^{744}
Peptides derived from α_{1C} II-III loop (CDCL)		
CDCL Peptide C	Cardiac equivalent of the α_{1s} II-III loop	^{851}INMDDLQ**P**NESEDKS**P**Y**P**N**P**ETTGEEDEEE**P**EM **P**VG**P**R**P**R**P**LSEL^{895}
CDCL Peptide C3	Cardiac equivalent of SDCL peptide C3	^{879}EE**P**EM**P**VG**P**R**P**R**P**LSEL^{895}
CDCL Peptide C4	Cardiac equivalent of SDCL peptide C4	^{864}KSPYPN**P**E**TT**G**E**E^{876}
Peptides derived from α_{1S} I-II loop		
AID	Alpha Interaction Domain of the α_{1s} I-II loop	^{357}QQLEEDLRGYMSWITQGE^{374}
Peptides derived from β_{1a} subunit		
Short SH3	β_{1a} SH3 domain minus the Hook region and 5 th β-strand.	^{98}TKPVAFAVRTNVGYNPSPGDEVPVQGVAITFEP KDFLHIKEKYNNDWWIGRLVKEGCEVGFIPS^{161}

4.3.1.5 SH3 domain

Plasmid construction

The β_{1a}-SH3 domain including the intervening Hook region extends from Valine 101 to Proline 272. In order to facilitate tertiary folding, the recombinant SH3 domain was cloned from Alanine 96 to Valine 280. The resulting protein was encoded by 555 nucleotide base pairs and consisted of 185 amino acids with a calculated (ProtParam -(Gasteiger et al., 2005) molecular weight of 20294.9 Daltons.

Primers, SH3 forward (SH3-F) and reverse (SH3-R) (GeneWorks, Australia) were designed to incorporate *SacII* and *HindIII* restriction sites to the amplified SH3 sequence. The SH3 sequence was amplified from the His-Ub-β_{1a} (3.3.1.1.) template and re-cloned into the pHUE vector (Ch.2.2.2)

PCR amplification was performed using the Phusion®High Fidelity kit (NEB) according to the manufacturer's instructions. The amplified product was analysed on an agarose gel, excised and purified (Ch. 2.2.3) The purified product was ligated into a pGEM-T-easy (Promega) vector system according to the manufacturer's instructions. This was done in order to facilitate a more efficient restriction digestion of the insert. The ligated product was transformed (Ch.2.2.7) into XL1-blue cells and positive transformants were identified by blue-white screening (Miller, 1978). A single positive colony was inoculated into 5ml of LB/amp (A.1.1) and plasmid DNA was extracted from the overnight culture (ch.2.2.4.).

Following extraction, the plasmid DNA was double digested with 0.5 IU each of *SacII* (NEB) and *HindIII* (NEB) restriction enzymes in the presence of NEB buffer 2 at 37 ^{0} C for 1 hour. The digested insert was resolved on an agarose gel and purified with a QIAQUICK gel extraction kit (Qiagen, Germany). The pHUE vector was simultaneously digested with *SacII* and *HindIII* enzymes as above. The linearised vector was mixed with purified SH3 insert in a ratio of 1:3 and ligated in the presence of 1x ligation buffer (Promega, USA) and 3 Weiss Units of T4 DNA ligase (Promega, USA). The vector/insert mix was incubated overnight at 4^0C. The ligated product was transformed (Ch.2.2.7) into *E.coli* BL21 (DE3) competent cells and grown overnight at 37^0C. Cells from eight single colonies were picked and directly amplified by PCR (Ch.2.2.3) using the SH3-F (forward) and SH3-R (reverse) primers to check for the

presence of the insert. DNA was extracted (Ch.2.2.4) from one positive colony of cells and sequenced (Ch.2.2.6) to confirm the presence and the integrity of the SH3 insert sequence. Once confirmed, glycerol stocks of the clone, His-Ub-SH3 were prepared by mixing 800 µl of overnight culture with 200 µl of sterile 75% glycerol. The stocks were stored at -70^{0}C.

Protein expression and Purification

Bacterial growth was carried out as described in chapter 2.2.8, but scaled up to 2.4 litres of culture. The culture was induced with 0.1 mM IPTG at an A_{600} (absorbance at 600 nm) of 0.8 and the protein was expressed for 3 hrs at 37^{0}C.

The protein was purified by IMAC (immobilized metal affinity chromatography) under de-naturing conditions using Ni-NTA resin as described in chapter 2.2.9.2. The purified protein was refolded by dialysing against buffer A (A.1.3) and the presence of secondary structure was checked by circular dichroism as described in chapter 2.2.12. The purified and refolded protein was stored at -70^0 C.

4.3.2 Tryptophan fluorescence quenching spectroscopy

Tryptophan fluorescence quenching spectroscopy was used in this study for the detection and quantification of protein-protein interactions. Fluorescence measurements offer a range of advantages, one of which enables this technique to be performed with only small amounts of protein. Hence it was the method of choice for this study due to the constraints posed by the complexity of purification and limited availability of purified recombinant proteins. Also the presence of the interacting partners in free solution as a first method avoids the complication of coupling to a matrix such as encountered in surface plasmon resonance where steric hindrance of the binding surface could occur. ITC (Isothermal calorimetry) was also considered for binding measurments, however the limited protein material meant that this technique was only used sparingly.

The fluorescence of a protein is characterized by its excitation and emission spectra and corresponding emission maximum (λ_{max}), as well as by its quantum yield and anisotropy. These parameters depend on the local environment of the fluorophore and therefore can change upon its interaction with another protein or ligand. As a result,

these characteristics can be used to measure the extent of complex formation involving a given protein. To determine binding parameters, the change in fluorescence that results from the interaction is monitored while the concentration of one of the reaction partners is varied. The signal employed could be fluorescence intensity, anisotropy, fluorescence resonance energy transfer (FRET), or change in fluorescence intensity as a function of accessibility to a quencher molecule for the complex as compared with the unbound protein (Groemping, 2005).

Tryptophan is the dominant amino acid contributor to the fluorescence spectrum of a protein. Upon binding to another protein or ligand, a decrease in fluorescence intensity due to direct quenching of the tryptophan fluorescence by the bound protein/ligand can occur (Kelly et al., 1976). The phenomenon of fluorescence quenching by a bound protein or ligand was used as a measure of binding interaction between β_{1a}/β_{1a}-SH3 and α_{1S}/α_{1C} II-III loops and its peptide derivatives in this study. The α_{1S}/α_{1C} II-III loops and their peptide derivatives contain one tyrosine residue but do not contain any tryptophan residues. Hence the contribution of the titrants to the overall fluorescence intensity was minimal.

Spectroscopy was carried out using a LS50B Luminescence Spectrophotometer (Perkin Elmer, USA). The excitation slit width was set at 10 nm and the emission slit width was varied between 5 to 10 nm depending on the tryptophan composition of the protein. The cut-off filter was set at 290 nm. The excitation and emission wavelengths were set to 280nm and 340 nm, respectively. All peptides and proteins were prepared in buffer A (A.1.3) which was degassed and filtered prior to use. The protein to be quenched was placed in a quartz cuvette (Spectrosil® Far UV Quartz cuvette, Starna Cells Inc.,) at a concentration of 0.5 to 5 μM. Quenchers were titrated into the cuvette and mixed gently by pipetting. The signal was allowed to stabilize before acquisition of data after each titration step. Titration was carried out at 24^0C.

The emission spectrum was monitored from 290 – 450nm and the maximum fluorescence intensity at 340nm was taken into account for the estimation of the dissociation constant (K_d). The contribution of quencher to the fluorescence signal was measured by titrating the quencher to buffer and subtracting this value(F_{add}) from the observed fluorescence (F_{obs}):

$F_{corr1} = F_{obs} - F_{add}$

The fluorescence values were then corrected for the dilution effect arising from the quencher:

$F_{corr2} = F_{corr1} (V_0 + dV) / V_0$

Here, F_{corr1} is the fluorescence observed prior to correction for dilution effects (and after correction for the fluorescence contribution of quencher) V_0 is the total volume of protein in the cuvette at the beginning of the experiment, and dV is the total volume of quencher solution added during titration.

F_{corr2} was expressed as relative fluorescence intensity (F_{340}) and a non-linear regression plot with the relative F_{340} as a function of quencher concentration (μM) was generated using GraphPad PRISM® (GraphPad Software, USA). The dissociation constant (Kd) was derived from Equation 4-1.

Equation 4- 1

$$Y = F_0 - \frac{F_0 - F_s}{2E_0}\left(E_0 + X + K_d - \sqrt{(E_0 + X + K_d)^2 - 4E_0 X}\right)$$

Where;

F_0 is the initial fluorescence of protein without quencher

F_s is the final fluorescence of protein

E_0 is the concentration of protein to be quenched

K_d is the dissociation constant

Stoichiometry is 1:1

Statistical analysis – Dissociation constant (K_d) is presented as mean ± SEM. The significance of differences was tested using Student's t-test for paired data. A P value of < 0.05 was considered significant.

4.4 Results

4.4.1 β_{1a} subunit

The recombinant β_{1a} subunit was purified and its integrity was confirmed as described in chapter 3 (**Figure 4-3**).

4.4.2 α_{1s} II-III loop

The recombinant α_{1s} II-III loop was expressed and purified (**Figure 4-3**) and the 126 residue protein showed the same migratory pattern on a 12% SDS-PAGE gel as previously published results (Lu et al., 1994, Dulhunty et al., 2005). This is higher than its predicted molecular mass of 14.13 kD (Gasteiger et al., 2005).

4.4.3 SH3 domain

4.4.3.1 Protein Expression and purification

The SH3 domain was purified and a yield of approximately 2 mg per purification was obtained from a 2.4 litre culture. The purified protein migrated at the expected molecular weight of ~20 kD on a 12% SDS-PAGE gel (**Figure 4-3**).

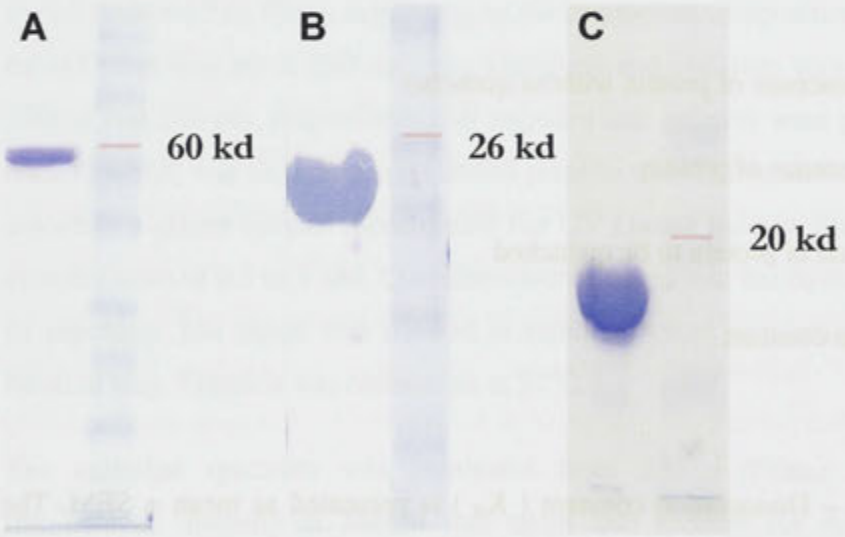

Figure 4-3 Purified recombinant proteins used for binding experiments. 12% SDS-PAGE coomassie stained gel. **A)** – Full length β_{1a} subunit, **B)** - β_{1a}-SH3 domain, **C)** - α_{1s} II-III loop. Right hand lane of each gel is a protein marker (BenchMark™ prestained- Invitrogen). Pink band corresponds to the molecular weight noted.

4.4.3.2 Circular Dichroism (CD) spectroscopy

CD spectroscopy of the purified SH3 domain was carried out in order to verify the presence of secondary structure. The resulting spectrum contained a maximum at 193 nm followed by minima at 213 and 221 nm. When compared to a reference spectrum of poly-L-lysine in α-helical, β sheet and random coil conformations (Greenfield, 2006), the shift of the first minimum to the right (>210 nm) and the second minimum to the left (<225) is indicative of a conformation containing a higher proportion of β sheet (**Figure 4-4**). Furthermore, analysis of the spectrum by the deconvolution software, K2D2 (Perez-Iratxeta and Andrade-Navarro, 2008) predicted 39.37 % β-strand and a 11.52 % α helix. This is expected from a domain largely consisting of β-strands (Chen et al., 2004). The remaining percentage of structure could be attributed to the relatively long intervening Hook region that is predicted to be random coil.

4.4.4 Tryptophan fluorescence quenching spectroscopy

4.4.4.1 The β_{1a} subunit binds to the AID (alpha interaction domain) of the α_{1s} I-II loop

Firstly, the well-established interaction between the DHPR I-II loop (AID peptide) and β_{1a} was examined in order to assess the robustness of tryptophan fluorescence quenching as a method to measure binding interactions. β_{1a} subunit (50 nM) was titrated with an increasing concentration of AID peptide (Table 4-1) starting from 5 nM until the signal reached saturation. The resulting binding affinity, K_d, was calculated using equation 4-1 as described in section 4.3.2. The AID peptide bound to the β_{1a} subunit with an affinity (K_d) of 15.2 ± 1.8 nM **(Figure 4-5)**. This agrees with published values (3 -76 nM) for this interaction which have been determined for other β isoforms and AID peptides using different techniques (Richards et al., 2004).

4.4.4.2 The β_{1a} subunit and the β_{1a}-SH3 domain binds to the α_{1s} II-III loop

An interaction between the β_{1a} subunit and the α_{1s} subunit II-III loop was investigated using tryptophan fluorescence quenching spectroscopy as described in section 4.3.2. The β_{1a} subunit (0.5 μM) was titrated with an increasing concentration of α_{1s} II-III loop until the signal reached saturation (**Figure 4-6**). The fluorescence intensity at 340 nm

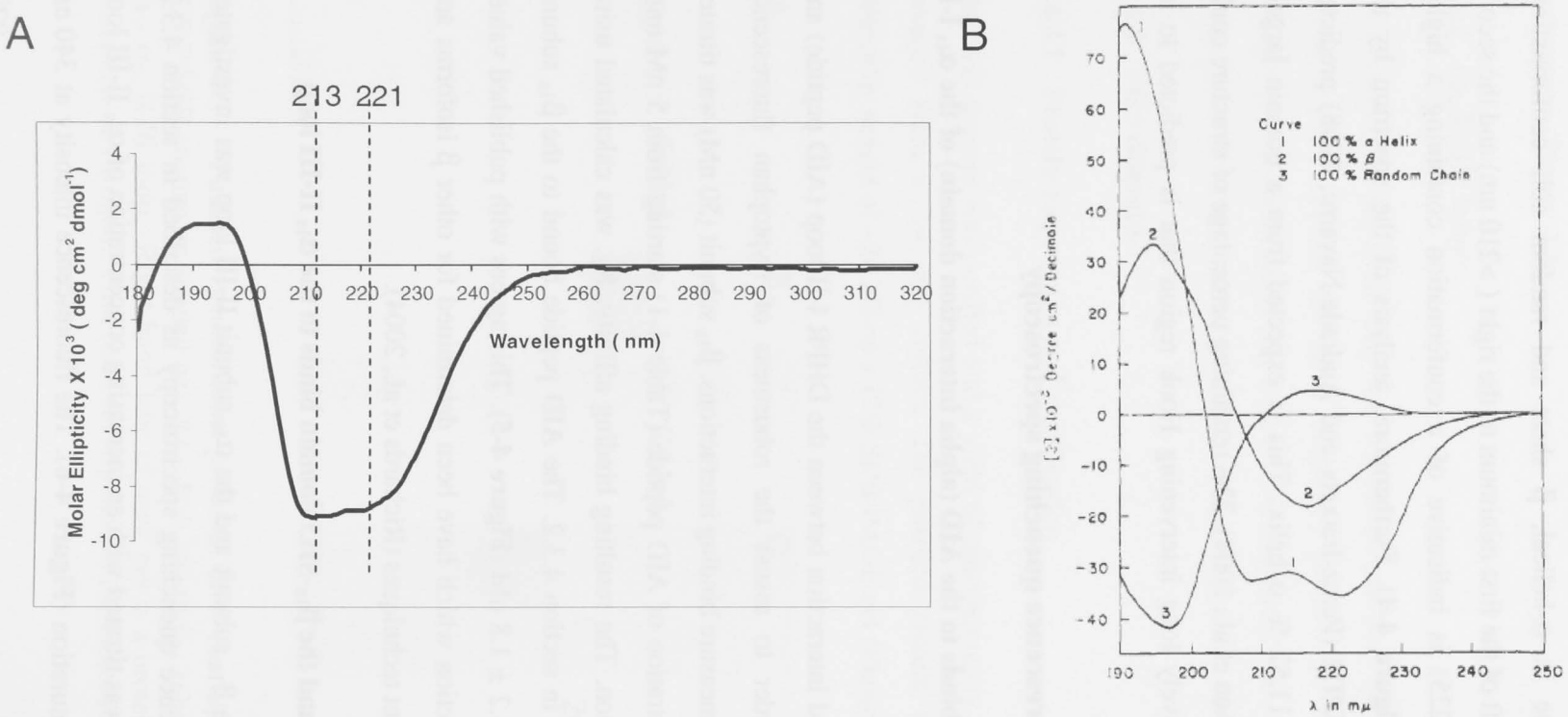

Figure 4-4 Circular dichroism (CD) spectrum of the recombinant β_{1a}-SH3 domain. A) The spectrum shows a maximum at 193 nm followed by minima at 213 and 221 nm. The shift of the first minimum to the right (>210 nm) and the second minimum to the left (<225) is indicative of a more β sheet conformation. This would be expected from a domain largely consisting of β-strand and a Hook region consisting mostly of random coil. B) reference spectrum of poly-L-lysine in 1- 100%α-helical, 2-100% β sheet and 3 -100 % random coil conformations (Greenfield, 2006).

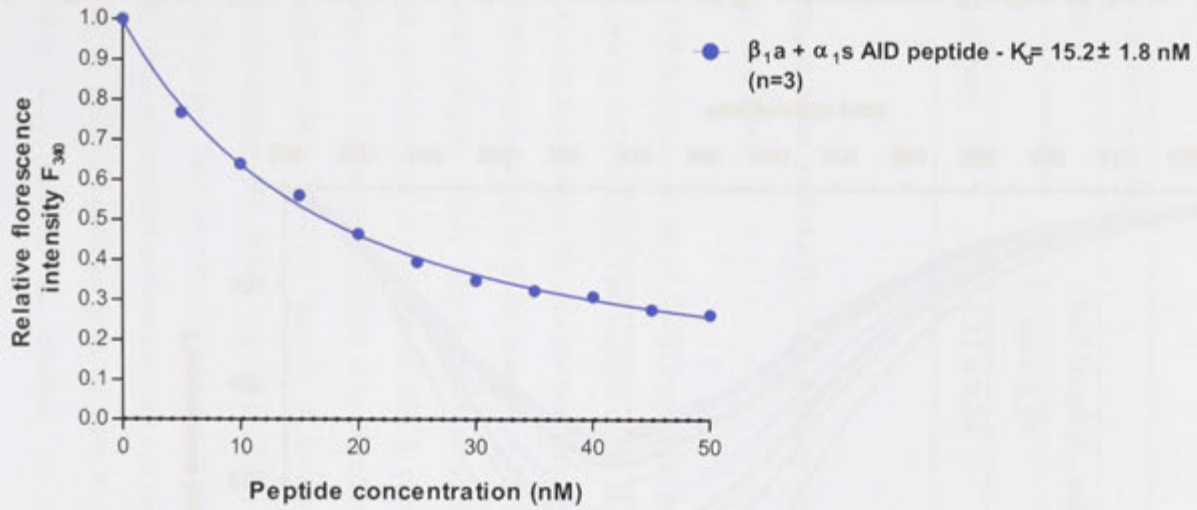

Figure 4-5 The β_{1a} subunit binds to the Alpha Interaction Domain (AID) peptide of the α_{1s} I-II loop . Non-linear regression curve with the relative F_{340} as a function of the concentration of the titrant. The full length β_{1a} bound to the α_{1s} I-II loop AID peptide with an affinity (Kd) of 15.2 ± 1.8 nM. The K_d was calculated from equation 4-1. The K_d value is the Mean ± SEM (n=3)

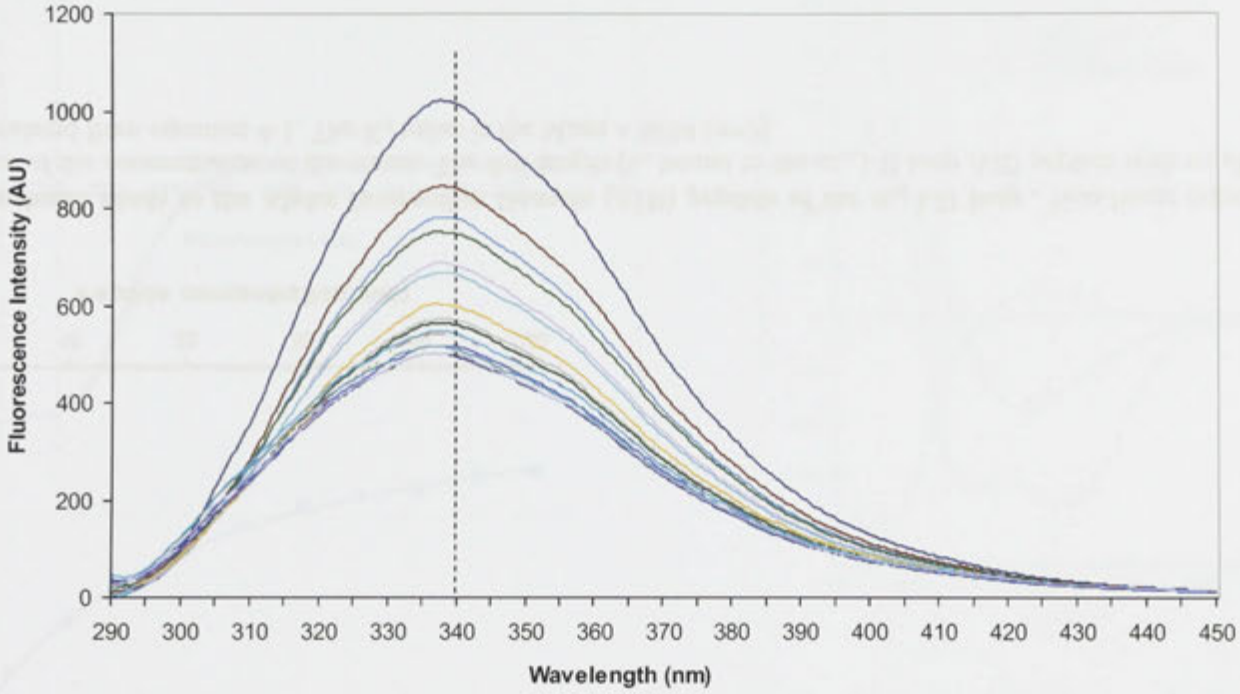

Figure 4-6 Quenching of the tryptophan emission spectrum of β_{1a} subunit upon binding of the α_{1s} II-III loop. 0.5 μM of β_{1a} subunit was titrated with an increasing concentration of α_{1s} II-III loop. The florescence intensity at 340 nm was quenched from ~1000 AU to ~450 AU (Au-arbitrary units). The dashed line indicates the fluorescence intensity at 340 nm.

was quenched from ~1000 AU to ~450 AU. Titration of buffer to β_{1a} and titration of α_{1s}II-III loop to BSA (Bovine Serum Albumin) were used as control experiments. The α_{1s} II-III loop bound to β_{1a} with an affinity (K_d) of 2.46 ± 0.37 μM (**Figure 4-7,** Table 4-2). The same experiment was repeated with the recombinant SH3 domain and a similar affinity (K_d) of 2.57 ± 0.15 μM (**Figure 4-7,** Table 4-2) was obtained.

An interaction between the circularized α_{1s} II-III loop and the β_{1a} subunit as well as the isolated SH3 domain was also investigated. Both interactions showed a binding affinity similar to the non-circularized α_{1s} II-III loop (Table 4-2).

Table 4-2

Dissociation Constant K_d (μM)		
Peptide/Protein	Full length β_{1a} subunit	SH3 domain
α_{1s} II-III loop	2.46 ± 0.37	2.57 ± 0.15
Circular α_{1s} II-III loop	3.32 ± 0.24	2.50 ± 0.25

4.4.4.3 The β_{1a} subunit and the β_{1a}-SH3 domain binds to the critical C-region of the α_{1s} II-III loop

To determine which regions of the α_{1s} II-III loop were responsible for the binding to the full length β_{1a} and its SH3 domain, two regions of the II-III loop were investigated – the A region which does not contain any proline residues and the C region which contain 3 proline-rich motifs as predicted by ELM, a resource for identifying candidate functional motifs in proteins (**Figure 4-2a**). The β_{1a} subunit at a concentration of 0.5 μM was titrated with an increasing concentration of SDCL peptide A (Table 4-3) and SDCL peptide C (Table 4-3). The binding affinity was calculated as described in section 4.3.2. The binding affinity (K_d) of SDCL peptide A to the β_{1a} subunit was significantly ($P = 0.007$) weaker compared to SDCL peptide C (Table 4-3). Binding of SDCL peptide A and peptide C to the SH3 domain showed a similar trend ($P = 0.005$, **Figure 4-8**, Table 4-3). The same experiment performed with a scrambled peptide C (Table 4-3) or a mutant peptide C, where all prolines were mutated to alanines (SDCL peptide C, P-A mutant – Table 4-3) showed no binding to either β_{1a} or SH3 domain.

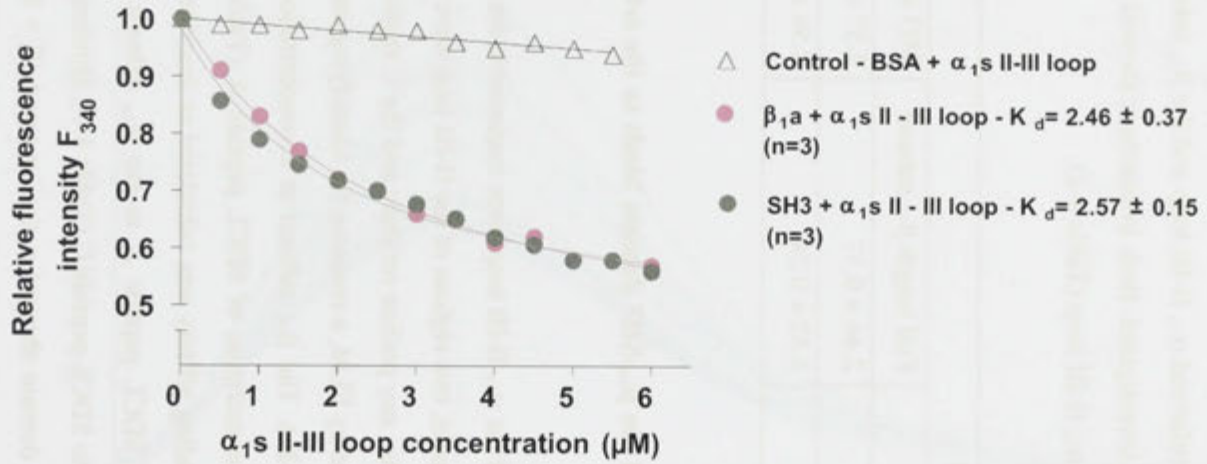

Figure 4-7 The β_{1a} subunit and the isolated SH3 domain binds to the α_{1s} II-III loop. Non-linear regression curve with the relative F_{340} as a function of the concentration of the titrant. The full length β_{1a} bound to the α_{1s} II-III loop with an affinity (Kd) of 2.46 ± 0.37. The SH3 domain bound to the α_{1s} II-III loop with an affinity (Kd) of 2.57 ± 0.15. The K_d was calculated from equation 4-1. The K_d value is the Mean ± SEM (n=3)

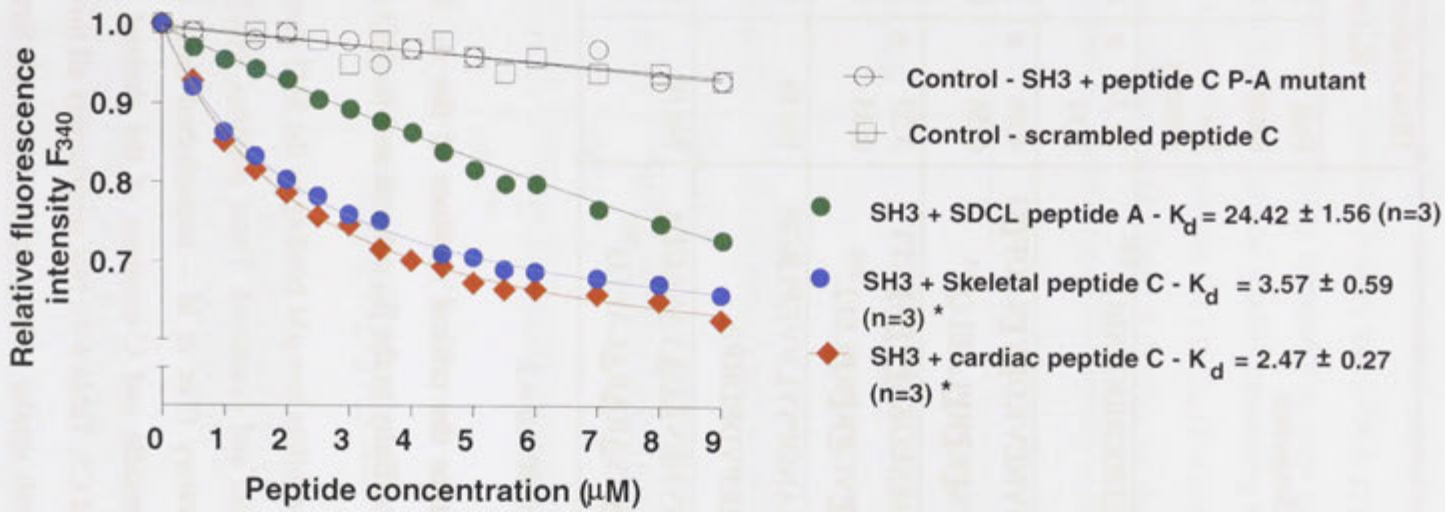

Figure 4-8 The β_{1a} SH3 domain binds to the C region of the α_{1s} II-III loop with higher affinity. Non-linear regression curve with the relative F_{340} as a function of the concentration of the titrant. The SH3 domain bound to the α_{1s} II-III loop C-region with an affinity (K_d) of 3.57 ± 0.59, to the α_{1c} II-III loop C-region with an affinity (K_d) of 2.47 ± 0.27 and to the α_{1s} II-III loop A region with an affinity (K_d) of 24.42 ± 1.56. The K_d was calculated from equation 4-1. The K_d value is the Mean ± SEM. * compared to SDCL peptide A. $P < 0.007$

The binding of the C region of the cardiac (α_{1c}) II-III loop (CDCL peptide C, Table 4-3) to the β_{1a} and SH3 domain was also investigated. This interaction showed a similar binding affinity to the C region of the skeletal (α_{1s}) II-III loop (**Figure 4-8**, Table 4-3).

Table 4-3

Peptide/Protein	Sequence	Dissociation Constant K_d (μM)	
		Full length β_{1a} subunit	SH3 domain
SDCL peptide A	^{671}TSAQKAKAEERKRRKMSRGL^{690}	27.33 ± 2.31	24.42 ± 1.56
SDCL peptide C	^{720}LKVDEFESNVNEVKD**P**Y**P**SADF**P**G DDEEDE**P**EI**P**VS**P**R**P**R**P**LAELQ^{765}	4.86 ± 0.56 *	3.57 ± 0.59*
CDCL peptide C	^{851}INMDDLQ**P**NESEDKS**P**Y**P**N**P**ETT GEEDEEE**P**EM**P**VG**P**R**P**R**P**LSEL^{895}	3.53 ± 0.43	2.47 ± 0.20
SDCL scrambled peptide C	IPEQNEDPEKSANDPSYLVVEPLRGF EPSEFDPVLDEKPVDEDRPA	No fit	No fit
SDCL peptide C, P-A mutant	^{720}LKVDEFESNVNEVKD**A**Y**A**SADF**A** GDDEEDE**A**EI**A**VS**A**R**A**R**A**LAELQ^{765}	No fit	No fit

* compared to SDCL peptide A. $P < 0.007$, $n = 3$

4.4.4.4 Proline rich sequence within the critical residues of the α_{1s} II-III loop C region bind with higher affinity to the β_{1a} subunit and its SH3 domain

Since the C region of the II-III loop exhibits low μM binding to the SH3 domain of β_{1a}, this region was divided into segments and examined. These peptides which had been previously synthesized in our laboratory (Tae *et al* – unpublished data) correspond approximately to the N-terminus, middle and C-terminus of the skeletal II-III loop C region (SDCL peptides C1, C2 and C3, Table 4-4). Not surprisingly all three peptides bound to β_{1a} and its SH3 domain with similar affinity (table 4-4) as all three peptides contained predicted SH3-binding proline-rich motifs.

Based on these results four peptides were synthesized corresponding to two proline rich sequences (**Figure 4-9**) of the α_{1s} and α_{1c} II-III loop C regions – SDCL peptide C3short, SDCL peptide C4, CDCL peptide C3 and CDCL peptide C4 (Table 4-4). Binding of these peptides to the β_{1a} subunit and the SH3 domain was carried out as described in section 4.3.2. The cardiac and skeletal peptides containing the second proline rich sequence (SDCL peptide C3 short and CDCL peptide C3) bound to β_{1a} and the SH3 domain with similar affinity compared to each other (**Figure 4-9**, Table 4-4). But the binding affinity of the cardiac version containing the first proline rich sequence (SDCL peptide C4 and CDCL peptide C4) to β_{1a} ($P = 0.005$) and the SH3 ($P = 0.009$) domain was weaker (**Figure 4-10**, Table 4-4) than its skeletal counterpart (which contain the critical residues for skeletal type EC-coupling – Chap 1.8.2.1).

Table 4-4

Peptide/Protein	Sequence	Dissociation Constant K_d (μM)	
		Full length β_{1a} subunit	SH3 domain
SDCL peptide C1	^{720}LKVDEFESNVNEVKD**P**Y**P**SAD F**P**GD^{743}	4.63 ± 0.12	4.53 ± 0.27
SDCL peptide C2	^{730}NEVKD**P**Y**P**SADF**P**GDDEED E**P**EI^{751}	5.00 ± 0.80	2.05 ± 0.55
SDCL peptide C3	^{739}DF**P**GDDEEDE**P**EI**P**VS**P**R**P**R**P**L AEL^{764}	5.16 ± 0.29	6.22 ± 0.37
SDCL peptide C3 Short	^{748}DE**P**EI**P**VS**P**R**P**R**P**LAEL^{764}	5.39 ± 0.87	3.75 ± 0.15
CDCL peptide C3	^{879}EE**P**EM**P**VG**P**R**P**R**P**LSEL^{895}	4.55 ± 0.25	3.60 ± 0.32
SDCL peptide C4	^{732}KDPYPS**A**D**FP**G**D**D^{744}	3.63 ± 0.24*	2.60 ± 0.36*
CDCL peptide C4	^{864}KSPYPN**P**E**TT**G**E**E^{876}	14.07 ± 1.87	19.43 ± 3.60

* compared to CDCL peptide C4. $P < 0.01$, $n = 3$

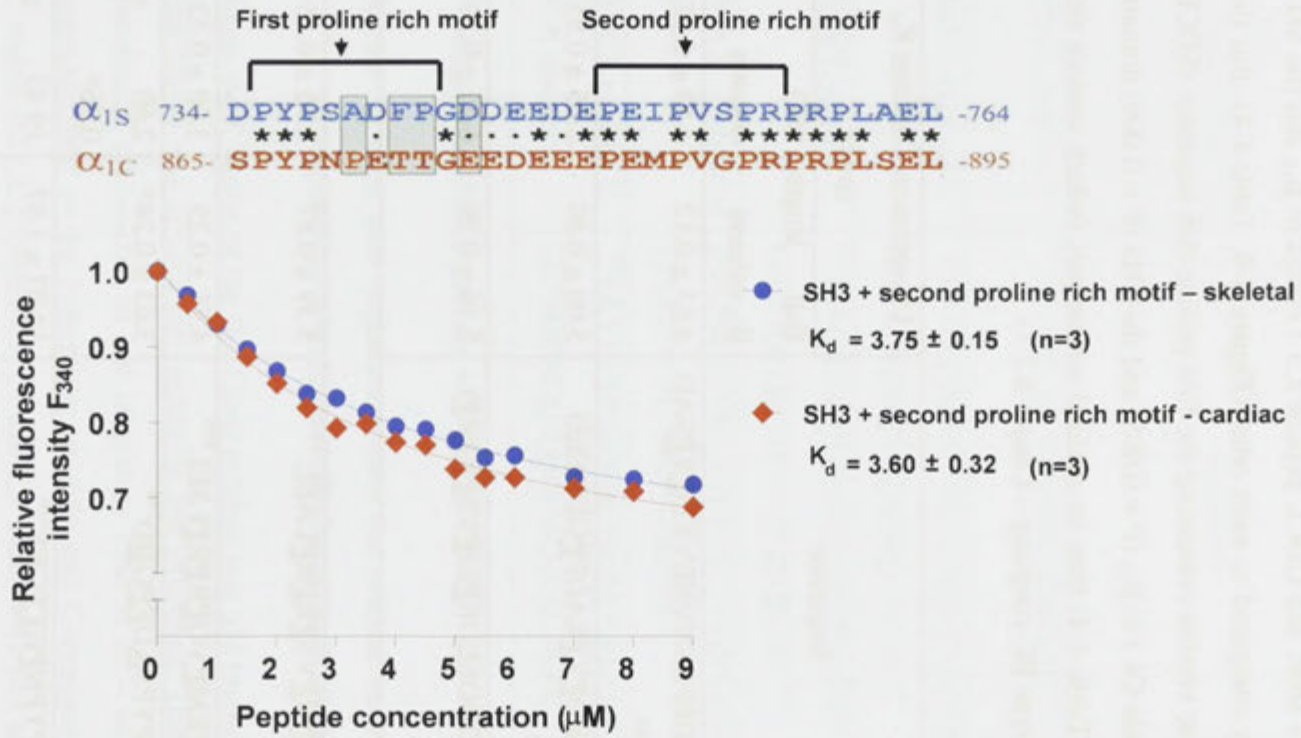

Figure 4-9 The β_{1a} SH3 domain binds with similar affinity to the second proline rich motif of both α_{1s} and α_{1c} II-III loop C-regions. Non-linear regression curve with the relative F_{340} as a function of the concentration of the titrant. The SH3 domain bound to the second proline rich motif of the α_{1s} II-III loop C-region (SDCL peptide C3 short) with an affinity (K_d) of 3.75 ± 0.15 and to its cardiac counterpart (CDCL peptide C3) with an affinity (K_d) of 3.60 ± 0.32. The K_d was calculated from equation 4-1. The K_d value is the Mean ± SEM.

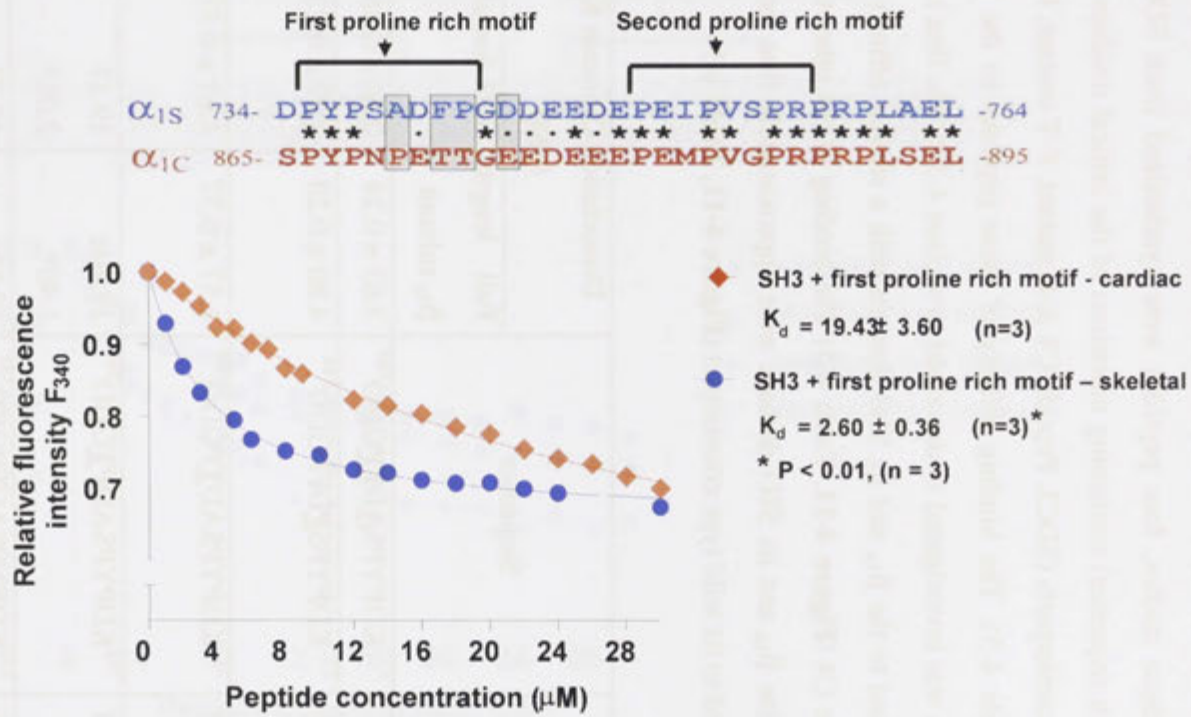

Figure 4-10 The β_{1a} SH3 domain binds with higher affinity to the first proline rich sequence adjacent to the critical residues of skeletal type EC-coupling. Non-linear regression curve with the relative F_{340} as a function of the concentration of the titrant. The SH3 domain bound to the first proline rich motif of the α_{1s} II-III loop C-region (SDCL peptide C4) with an affinity (K_d) of 2.60 ± 0.36 and to its cardiac counterpart (CDCL peptide C4) with an affinity (K_d) of 19.43 ± 3.60. The K_d was calculated from equation 4-1. The K_d value is the Mean ± SEM. P = 0.009 (n=3)

4.4.4.5 Residues P742 and D744 of the α_{1s} II-III loop C region are important for binding to the β_{1a} and SH3 domain

Studies by Kugler *et al* (Kugler et al., 2004) showed that four skeletal specific "critical" residues (A739, F741, P742 and D744) were important for skeletal type EC-coupling (Chap.1.8.2.1). Based on these studies, four peptides were synthesized from SDCL peptide C4 (first proline rich sequence) containing mutations of the critical residues of the C region to its cardiac counterparts (SDCL Peptide C4 A-P mutant, F-T mutant, P-T mutant, D-E mutant – Table 4-5). The binding affinity of these peptides to the β_{1a} subunit and its SH3 domain was investigated as described in section 4.3.2. The first two mutants (A-P and F-T) bound to the β_{1a} and its SH3 domain with a similar affinity as the wild type SDCL peptide C4 (**Figure 4-11**, Table 4-5) The binding of the other two mutants (P-T and D-E) to the β_{1a} and its SH3 domain were approximately five times weaker ($P \approx 0.001$) compared to its wild type counterpart (**Figure 4-11,** Table 4-5).

Table 4-5

Peptide/Protein	Sequence	Dissociation Constant K_d (μM)	
		Full length β_{1a} subunit	SH3 domain
SDCL peptide C4 WT	^{732}KDPYPS**A**D**FP**G**D**D^{744}	3.63 ± 0.24	2.60 ± 0.36
SDCL peptide C4 A-P mutant	^{732}KDPYPS**P**DFPGDD^{744}	4.80 ± 0.20	2.27 ± 0.23
SDCL peptide C4 F-T mutant	^{732}KDPYPSAD**T**PGDD^{744}	4.57 ± 0.37	4.63 ± 0.33
SDCL peptide C4 P-T mutant	^{732}KDPYPSADF**T**GDD^{744}	19.80± 1.40*	19.37 ± 2.06*
SDCL peptide C4 D-E mutant	^{732}KDPYPSADFPG**E**D^{744}	13.85± 1.75*	15.77 ± 1.03*

* compared to wild type SDCL peptide C4. $P < 0.002$, $n = 3$

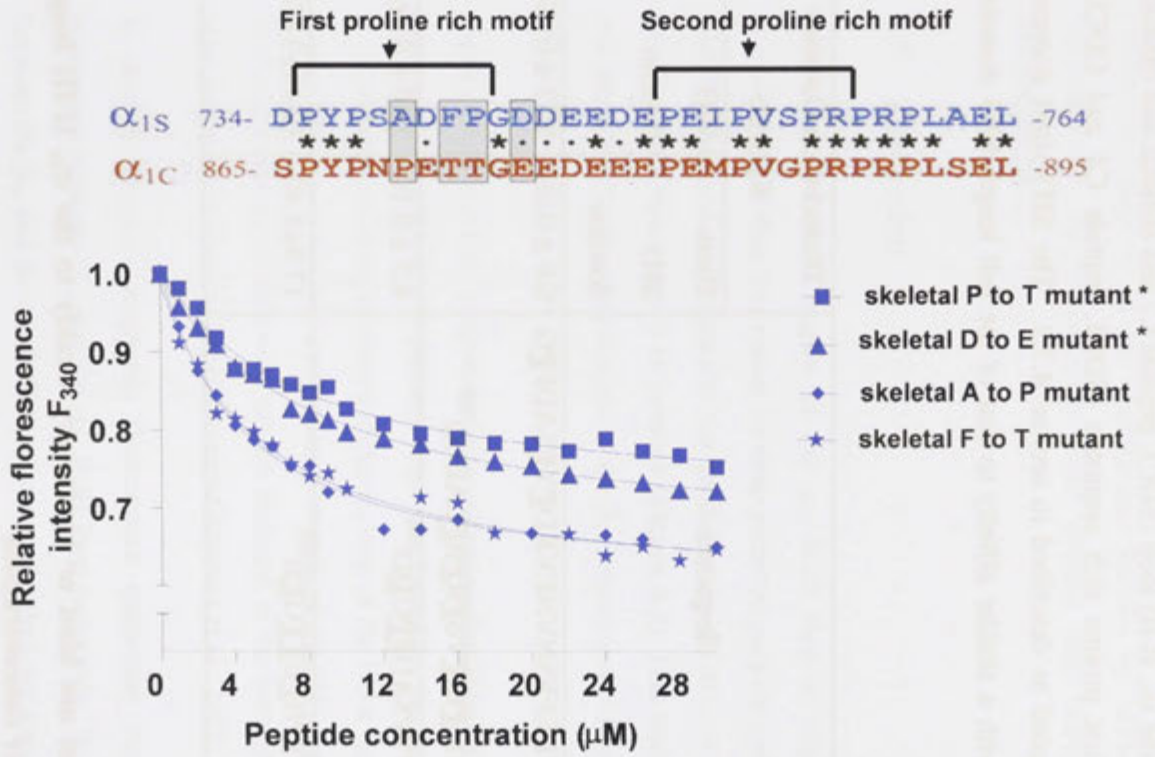

Figure 4-11 Residues P742 and D744 of the α_{1s} II-III loop C region are important for binding to the β_{1a}-SH3 domain. Non-linear regression curve with the relative F_{340} as a function of the concentration of the titrant. Mutation of P742 and D744 to its cardiac counter parts reduced the binding affinity by approximately 5 fold compared to wild type. The K_d was calculated from equation 4-1. The K_d value is the Mean ± SEM. * compared to wild type SDCL peptide C4. $P < 0.002$, $n = 3$

4.4.4.6 The β_{1a}-SH3 domain minus the Hook region (short SH3) binds to the α_{1s} II-III loop C region

Attempts to produce a recombinant SH3 lacking the intervening Hook region and the fifth β-strand of the domain were as yet unsuccessful. Hence, a peptide encompassing this region was synthesized as described in chapter 2.2.1. The binding affinities of this peptide to the C region of the α_{1s} II-III loop (SDCL peptide C) and skeletal and cardiac peptides containing the first proline rich sequence (SDCL peptide C4 and CDCL peptide C4) were investigated as described in section 4.3.2. The SH3 short domain bound to these peptides with a similar affinity to that of the full length SH3 domain (Table 4-7).

Table 4-7

Peptide/Protein	Sequence	Dissociation Constant K_d (μM)	
		Short-SH3 domain	SH3 domain
SDCL peptide C	^{720}LKVDEFESNVNEVKD**P**Y**P**SADF**P**G DDEEDE**P**EI**P**VS**P**R**P**R**P**LAELQ^{765}	6.0 ± 0.20	3.57 ± 0.59
SDCL peptide C4	^{732}KDPYPS**A**D**FP**G**D**D^{744}	4.5 ± 0.10	2.60 ± 0.36
CDCL peptide C4	^{864}KSPYPN**P**E**TT**G**E**E^{876}	17.9±1.40	19.43±3.60

4.4.4.7 The β_{1a}-SH3 does not bind or binds very weakly to the α_{1s} II-III loop C-region at higher concentrations

The interaction between the recombinant β_{1a}-SH3 domain and the α_{1s} II-III loop C region peptide was investigated using ITC (Isothermal calorimetry) by Dr.N. Norris (Biomolecular structure group, JCSMR, ANU). In order to carry out these measurements, the C region peptide was titrated into β_{1a}-SH3 domain which was used a

concentrations >100 μM. Under these conditions no binding was detected between the β_{1a}-SH3 domain and the C region peptide. Hence tryptophan fluorescence quenching was also carried out at higher concentrations (50 μM β_{1a}-SH3 - the maximum possible concentration that gives a measurable emission spectrum) of β_{1a}-SH3 domain in the cuvette and the resulting binding constant was over a thousand times weaker(K_d > 4 mM)**(Figure 4-11)** in comparison to when the experiment was carried out at 1 uM. Further investigation of the recombinant protein by SDS-PAGE (Dr. N. Norris) indicates that the recombinant SH3 domain may form multimers at higher concentrations.

4.5 Discussion

It is clear that the C-region of the α_{1s} II-III loop is important for skeletal type EC-coupling. Within this region lie three potential poly-proline binding motifs with the potential to bind SH3 domains (as predicted by ELM – a resource for identifying candidate functional motifs in proteins (**Figure 4-2**). This study investigated whether it was possible that the SH3 domain of the β_{1a} subunit could interact with the C-region of the α_{1s} II-III loop *in vitro*.

Previous structural investigations have suggested that interactions between the β–SH3 domains and polyproline partners were not possible due to the binding site on the β1a-SH3 domain being occluded by the α_2 loop of the Hook region and the RT-Src loop connecting two of the four continuous β strands of the SH3 domain (Chen et al., 2004). However previous studies with various isoforms of the beta subunit have indicated that such interactions are possible (Gonzalez-Gutierrez et al., 2007, Dubuis et al., 2006).

In this investigation tryptopan fluorescence quenching experiments show that an interaction between β_{1a} and the α_{1s} II-III loop is feasible. Given that *in vitro* binding between the β_{1a} and the α_{1s} II-III loop was established, we sought to identify the regions within these proteins responsible for binding.

Firstly, the well characterized binding between the β_{1a} subunit and the AID (alpha interaction domain) peptide was used to validate the method. The AID peptide bound to the β_{1a} subunit with an affinity (K_d) of 15.2 ± 1.8 nM indicating a tight interaction.

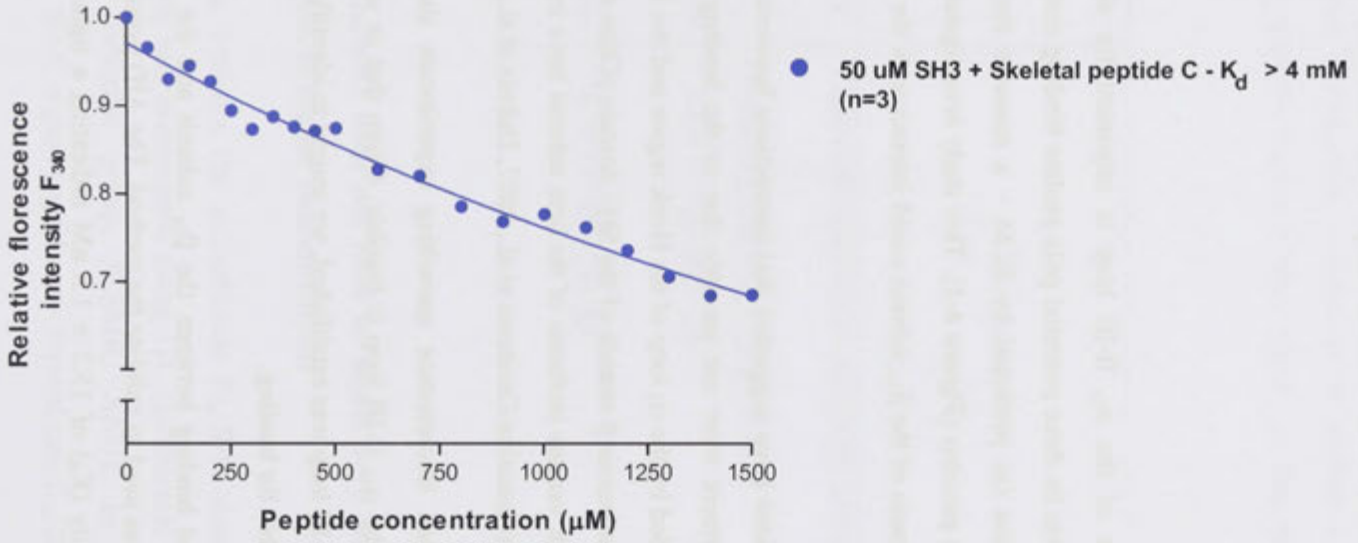

Figure 4-11 At higher concentrations (50 uM), the β_{1a}-SH3 domain shows negligible binding to the α_{1s} II-III loop C region. Non-linear regression curve with the relative F_{340} as a function of the concentration of the titrant. At 50 uM, β_{1a} SH3 domain bound to the α_{1s} II-II loop C region with an affinity (Kd) of >4 mM. The K_d was calculated from equation 4-1. The K_d value is the Mean ± SEM (n=3)

Although there are no published values for the isoform specific (skeletal) β_{1a}-AID interaction, the obtained binding constant falls within the range of reported values (3-76 nM) for other β isoforms.

As predicted the full length β_{1a} subunit and the SH3 domain in isolation were able to bind to the α_{1s} II-III loop with an affinity in the low micro-molar (~2 μM) range. SH3 domains in general are known to bind with affinities ranging from 1-100 μM (Kaneko T et al., 2008). Hence the value obtained for the β_{1a}-α_{1s} II-III loop interaction is within the lower end of this spectrum. Binding was also investigated with the circularized form of the α_{1s} II-III loop which more closely mimics the II-III loop's position in the cytoplasmic membrane. The circular II-III loop bound to the β_{1a} subunit and the SH3 domain with a similar affinity as the linear II-III loop. Hence, any structural modifications (Tae et al., 2011) caused by circularisation of the loop do not appear to affect its binding to the β_{1a} subunit.

The proline rich SH3 binding motifs in the II–III loop are located in its C region. Hence it is not surprising that the C region bound to the β_{1a} subunit and the SH3 domain with significantly higher affinity than the A region which do not contain such binding motifs. Furthermore, mutating all proline residues in the C-region to alanines completely abolished its binding to β_{1a} and the SH3 domain signifying that the proline residues were essential for this interaction.

The interaction between the β_{1a} subunit and its SH3 domain was also probed with the C-region of the α_{1c} (cardiac) II-III loop which also contain the predicted proline rich SH3 binding motifs. The C-region of the α_{1c} II-III loop also bound to the β_{1a} and its SH3 domain with a similar affinity as the C region of the skeletal loop. This is probably due to the almost identical compositions of the second and third predicted SH3 binding motifs between the cardiac and skeletal isoforms (**Figure 4-2B**). However, it is notable that the residues encompassing the first predicted SH3 binding motif are very different between the two isoforms (**Figure 4-2B**). It is these residues (A739, F741, P742 and D744) in the skeletal isoform that have been shown to be important for skeletal type EC-coupling (Kugler et al., 2004).

In order to dissect which sections of the skeletal II-III loop C region was involved in the interaction with the β_{1a} SH3 domain, scouting experiments were first conducted with

three pre-existing peptides corresponding to the N-terminus, middle and the C-terminus of the C-region. Not surprisingly all three peptides bound to the β_{1a} subunit and its SH3 domain with similar affinity as all three peptides contained elements of the predicted poly-proline binding motifs.

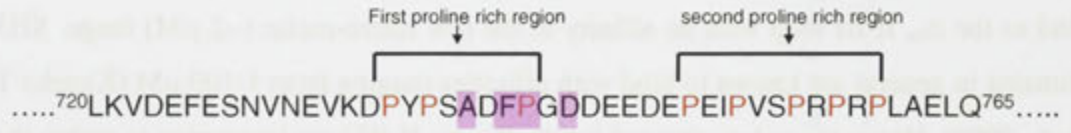

Figure 4-12 Two proline-rich sequences in the C-region of the α_{1s} II-III loop. Proline residues are in red. Residues shown to be important for skeletal type EC-coupling are highlighted in pink. (The second proline rich region consists of the second and third predicted proline-rich motifs - Figure 4-2)

Therefore, binding to the SH3 domain (and β_{1a}) was investigated using both cardiac and skeletal versions of peptides corresponding to two separate proline rich sequences of the C region - SDCL C3 short, CDCL C3, corresponding to the second and third predicted motifs and SDCL C4 and CDCL C4, corresponding to the first predicted polyproline motif (**Figure 4-2 and Figure 4-12**) The second and third predicted polyproline motifs were considerd as one as there are minimal differences in this region between the skeletal and cardiac isoforms. Both cardiac and the skeletal versions of the second proline rich sequence (**Figure 4-12**) bound with similar affinity to the SH3 domain and the full length β_{1a} subunit. But the skeletal version of the first proline rich sequence (encompassing the skeletal specific critical residues, **Figure 4-12**) bound with approximately five times greater affinity than its cardiac counterpart. It is known that although the proline residues are generally essential for SH3 domain binding, the specificity of the interaction is governed by the surrounding residues (Kaneko T et al., 2008). In this case the skeletal specific residues located within the proline rich sequence appear to confer the increased affinity to the skeletal version of the peptide.

Next, experiments were conducted to clarify which of these skeletal specific residues (A739, F741, P742 and D744), if any, were responsible for the increase in affinity. Mutant peptides were synthesized where each residue in turn was mutated to its cardiac counterpart. Mutating A739 or F741 did not alter the binding affinity of the peptide compared to the wild type (SDCL C4). But mutating P742 or D744 reduced its binding affinity approximately five times compared to the wild type. Hence these two residues appear to be important for the skeletal specific binding of the first proline rich motif of

the C-region. The loss of a proline residue could weaken the affinity of this peptide (SDCL C4 P-T) to the SH3 domain although the gain of a proline residue in mutating A739 (SDCL C4 A-P) did not seem to increase its affinity compared to the wild type. Aspartic acid (D) is a residue which commonly follows SH3 binding motifs (Kaneko T et al., 2008), hence weakening of the binding affinity upon its mutation is possible.

The SH3 domain of the β_{1a} subunit has a split architecture (Van Petegem et al., 2004, Chen et al., 2004) where the fifth β-strand of the domain is separated by a largely unstructured Hook region. Hence the recombinant SH3 domain produced in this study included the Hook region. Experiments to generate a recombinant SH3 domain minus the Hook region are in progress. In the interim, a peptide was synthesized corresponding to the SH3 domain minus the Hook region and the fifth β strand (SH3 short). This peptide produced similar binding affinities as its full length counterpart with the skeletal II-III loop C-region and its first proline rich region, both skeletal and cardiac. Previous structural studies on different β isoforms have predicted that the α_2 helix of the Hook region occludes the polyproline binding site of the β–SH3 domains (Chen et al., 2004). But, in this *in vitro* study, the absence (or presence) of the Hook region or the fifth β strand did not significantly affect the binding affinity of the β_{1a}-SH3 domain to the α_{1s} II-III loop. This could be due to structural differences between the skeletal isoform of the β subunit and the isoforms used in the structural studies or it could be that the labile Hook region shifts to allow a β_{1a}-SH3 – II-III loop interaction.

Further to binding experiments by tryptophan fluorescence quenching, a series of experiments using ITC (Isothermal calorimetry) suggest that the interaction between the β_{1a}-SH3 domain and the α_{1s} II-III loop is concentration dependant. Upon further investigation it was revealed that the recombinant SH3 domain appears to form multimers at higher concentrations. This is not entirely surprising considering the role of SH3 domains (and membrane associated guanylate kinases –MAGUKs in general) as protein clustering/oligomerisation modules (McGee et al., 2001). It may also be that the β_{1a}-SH3/α_{1s} II-III loop interaction is only possible at lower concentrations. This will require further investigation.

This study investigated the interaction between the β_{1a}-SH3 domain and the α_{1s} II-III loop *in vitro*. However, the *in vivo* role of the SH3 domains in L-type calcium channels

remains unclear. Lately studies have emerged using a β_{1a} null zebra fish mutant system, where the SH3 domain of the β_{1a} subunit has been shown to be important for skeletal type EC-coupling (Dayal *et al* – unpublished data, Gordan Research Conference on EC-Coupling 2009). Therefore the *in vitro* data on the interaction between the β_{1a}-SH3 domain and the α_{1s} II-III loop presented here represent a starting point for further investigations *in vivo*.

Chapter 5 Structural analysis of the DHPR β_{1a} subunit C-terminal tail

5.1 Introduction

Conformational coupling between the dihydropyridine receptor in the T-tubular membrane and the ryanodine receptor Ca^{2+} release channel in the sarcoplasmic reticulum forms the basis of EC-coupling in skeletal muscle. Although a combination of electrophysiological, morphological and biochemical approaches provide a solid foundation for the notion that protein-protein interactions link the skeletal DHPR and RyR1, the exact mechanism of this coupling process remains unresolved.

The pore forming α_{1s} subunit and the accessory β_{1a} subunit of the DHPR are essential for skeletal type EC-coupling, with the absence of these subunits resulting in a lethal phenotype due to respiratory paralysis. Lack of β_{1a} also gives rise to reduced membrane expression of α_{1s}, reduction of its charge movement and the disruption of the arrangement of DHPRs in groups of four (tetrads) opposing RyR1. Although triad expression and facilitation of charge movement are functions common to a number of β isoforms, the skeletal specific ultrastructural arrangement of DHPRs opposite every other RyR1 is an exclusive feature of the β_{1a} isoform (Schredelseker et al., 2009).

As has been discussed in detail in chapter 1.9.2, the β subunit consists of five well defined regions – the N-terminus, C-terminus, Hook region, SH3 and guanylate kinase (GK) domains. The GK and the SH3 domains of the β subunits are relatively well conserved among the four β isoforms . Hence the highly variable amino-terminus, carboxyl terminus and the Hook region maybe involved in the isoform-specific functions of the β subunits. In the β_{1a} isoform, deletion of the amino-terminal and the Hook region was found to have little effect on EC-coupling (Beurg et al., 1999). However the deletion of 35 residues of β_{1a} at the C-terminus resulted in a fivefold reduction in the maximum amplitude of the Ca^{2+} transients (Beurg et al., 1999). This same group showed that the purified full length β_{1a} subunit is able to bind to a fragment of the RyR1 *in-vitro* (Cheng et al., 2005). The binding site for the DHPR β_{1a} subunit has been mapped to the M^{3201} to W^{3661} region of RyR1 and the strength of this interaction was shown to be controlled by a cluster of positively charged residues (K^{3495}KKRR_

R^{3502}) within this region. These findings indicate that β_{1a} is able to interact with the RyR1 and that the end 35 residues of its carboxyl terminus are important for skeletal type EC-coupling. This region may be responsible for the DHPR tetrad formation opposite the RyR1 or it may be a component of the trigger mechanism for SR Ca^{2+} release in skeletal muscle.

Although the crystal structures of the core region (GK/SH3), of three β isoforms (β_{2a}, β_3 and β_4) have been published (Chen et al., 2004, Van Petegem et al., 2004, Opatowsky et al., 2004), no structural data exist on its variable regions – the C-terminus, N-terminus and the Hook region. This is presumably due to the disordered nature of these regions. Hence an alternative approach of investigating their structure is by examining specific regions and this study represents a starting point in gaining an insight into the function of these variable fragments, in particular, the β_{1a} C-terminus.

5.2 Aim

Investigate the structure of the 35-residue C-terminal tail of the DHPR β_{1a} subunit and identify structural elements that may facilitate its interaction with RyR1.

5.3 Materials and Methods

5.3.1 Peptide synthesis

A peptide corresponding to the 35-residue C-terminal tail of the β_{1a} subunit (**Figure 5-1**), hereafter referred to as β_{1a}-C35, and its mutants were synthesized and purified as described in Chapter 2.2.1.

...^{490}**VQVLTSLRRNLSFWGGLEASPRGGDAVAQPQEHAM**^{524}

Figure 5-1 **β_{1a}-C35 peptide**. Sequence of C-terminal 35 residues of β_{1a} which has been shown to be important for skeletal type EC-coupling (Beurg et al., 1999).

5.3.2 Solution State Nuclear Magnetic Resonance (NMR) Spectroscopy

5.3.2.1 Introduction

The NMR phenomenon is based on the fact that nuclei of atoms have magnetic properties that can be utilized to yield chemical information. Each atom has distinct

quantum mechanical properties of spin. In some atoms (eg ^{12}C,^{16}O,^{32}S) these spins are paired and cancel each other out so that the nucleus of the atom has no overall spin. However, nuclei with an odd mass or odd atomic number (^{1}H, ^{13}C, ^{15}N) have "nuclear spin". The overall spin of the charged nucleus generates a magnetic dipole along the spin axis, and the intrinsic magnitude of this dipole is a fundamental nuclear property called the nuclear magnetic moment. In quantum mechanical terms, the nuclear magnetic moment of a nucleus can align with an externally applied magnetic field, either spin aligned or spin opposed. In NMR, a radio frequency pulse is used to "flip" the alignment of nuclear spins from the low energy spin aligned state to the higher energy spin opposed state. For a given type of nucleus, this precession (rotation) frequency (resonance) is proportional to the strength of the external magnetic field.

Within a molecule, a nucleus of a given type, for example a proton (^{1}H nucleus), will have a slightly different precession frequency depending on its location in the molecule. The molecular framework of a molecule (the chemical bonds between atoms) induces slight changes in the magnetic field experienced by the nuclei in that molecule. This is because the electrons that constitute chemical bonds also interact with the magnetic field, and act to "shield" the nuclei from the field. The more electron density associated with a particular nucleus, the greater the shielding from the static magnetic field and the lower the resonance frequency. Conversely, a nucleus bonded to an electronegative atom has a reduced electron density. Such a nucleus is said to be deshielded and experiences a greater proportion of the static magnetic field; consequently, its NMR transition is of higher energy. The concept of chemical shift is used to explain the difference in the precession frequency of the nucleus of interest compared to that of a standard reference molecule (for example, 5,5-dimethylsilapentanesulfonate (DSS)). Because the difference in precession frequency is proportional to the magnetic field, this number is divided by the precession frequency of the reference. The resulting numbers are small and are expressed in parts per million (ppm). The chemical shift is one of the fundamental NMR parameters and is associated with a particular atom in a defined molecule or complex under defined experimental conditions (Keeler, 2005).

Chemical shifts in proteins are also influenced by non-covalent interactions, specifically hydrogen bonding and the proximity and relative orientation of carbonyl groups and aromatic rings. These influences on the chemical shift reflect the local environment of a

nucleus in a protein and are thus a function of the secondary and tertiary folded structures (Wurthrich, 1986).

5.3.2.2 Types of ^{1}H NMR experiments

Two types of NMR experiments were used to determine the structure of the β_{1a}-C35 peptide - ^{1}H TOCSY and ^{1}H NOESY. Total correlation spectroscopy (TOCSY) spectra provide information regarding connections of ^{1}H atoms through chemical bonds. In a TOCSY experiment, magnetization is dispersed over a complete spin system of an amino acid by successive scalar coupling (coupling between two nuclear spins mediated by electrons participating in the bond (s) connecting the nuclei). The TOCSY experiment correlates all connected protons of a spin system. Thus a characteristic pattern of signals results for each amino acid from which it can be identified based on known chemical shift values for hydrogen atoms located in the side chains.

While TOCSY experiments provide information relating to ^{1}H atoms connected through chemical bonds, Nuclear Overhauser Effect Spectroscopy (NOESY) spectra provide information relating to the relative closeness in space of ^{1}H atoms. The NOESY experiment is crucial for the determination of protein structure. It uses the dipolar interaction of spins (the Nuclear Overhauser effect, NOE) for the correlation of protons. The correlation between two protons depends on the distance between them, but normally a signal is only observed if their distance is smaller than 5 Å. The strength of the NOE signal is proportional to the inverse sixth power of the distance between the atoms, $1/r^6$, with r being the distance between the protons. The NOESY experiment correlates all protons which are close enough, including protons which are distant in the amino acid sequence but close in space due to tertiary structure (Martin and Zekter, 1988, Wurthrich, 1986).

Apart from NOE effects, additional NMR parameters including coupling constants, temperature co-efficients and chemical shift indexes (CSI) can be used to aid in the structural elucidation of a protein molecule.

5.3.2.3 Coupling Constants

$^3J_{NH\text{-}\alpha H}$ coupling constants are measurements relating to the polypeptide backbone dihedral angle (Φ – torsion angle around the N-αC bond) and can provide local

structural information. In homonuclear ^{1}H experiments $^{3}J_{NH-\alpha H}$ coupling constants can be derived from splitting patterns observed in 1 or 2-dimensional experiments. The measurement itself is a frequency difference (Hz). Generally, residues that are involved in alpha helical secondary structure have been found to contain coupling constants of < 6 Hz, while residues involved in beta sheet secondary structure have coupling constants > 8 Hz. Coupling constants between 6 and 8 Hz are typically from unstructured proteins or peptides.

5.3.2.4 Temperature Co-efficient

It has been known since the early years of peptide NMR that the chemical shifts of amide proton resonances are temperature dependant (Ohnishi and Orry, 1969). In general, they shift upfield as the temperature increases and this is conventionally described as a negative temperature coefficient. If a residue is involved in some form of secondary structure, backbone hydrogen bonding will be present. This hydrogen bonding contributes an extra level of stability to the structure of the peptide and will be affected by the additional energy imparted by an increase in temperature. The value of the amide proton temperature coefficient has therefore been used widely as an indicator that the amide proton is involved in intra-molecular hydrogen bonding (Andersen et al., 1992, Skalicky et al., 1994, Dyson et al., 1988). For this study, a value greater than -5 ppb/K is taken to indicate the presence of secondary structure. The temperature coefficient of each residue can be determined by quantifying the difference in amide chemical shift values obtained over a set temperature range. This information is then presented as a difference in parts per billion per degree of temperature change (ppb/K). For this study, the temperature co-efficient of each residue was obtained over a range of 280 – 291 ^{0}K.

5.3.2.5 Alpha Hydrogen Chemical shift index

Pioneering studies by Wishart et al. have demonstrated that ^{1}H NMR chemical shifts are strongly dependent on the character and nature of protein secondary structure (Wishart et al., 1991). In particular, it has been found that the ^{1}H NMR chemical shift of the alpha-CH proton of all 20 naturally occurring amino acids experiences an upfield shift (with respect to the random coil value) when in a helical configuration and a comparable downfield shift when in a beta-strand extended configuration. Proteins

containing alpha helical secondary structure exhibited a mean ^1H upfield shift of 0.39 ppm, from the random coil value, while the ^1H chemical shift was found to move downfield by an average of 0.37 ppm when the residue is contained in a beta-strand or extended configuration. On the basis of these observations, the identity, extent, and location of secondary structural elements in proteins can be determined based on the alpha-CH ^1H resonance assignments (Wishart et al., 1992). In this study ^1H CSI (Chemical Shift Index) were measured and are presented as shifts +1 or -1 respectively. An ^1H CSI of -1 refers to a shift of more than 0.1 ppm downfield, while +1 refers to a shift of more than 0.1 ppm upfield, from the assignments determined for random coil structures (Wishart and Nip, 1998). Values of <-1 are suggestive of alpha helical secondary structures, whereas values of >+1 will most likely represent residues participating in beta sheet secondary structure.

5.3.2.6 Methodology

NMR samples were prepared to a concentration of ~ 2 mM in an H_2O solution consisting of 10% D_2O and 90% H_2O. The peptides were adjusted to a pH of ~ 5.8 using small amounts of dilute hydrochloric acid. DSS (5,5-dimethylsilapentanesulfonate) was added to a final concentration of 0.2 mM as an internal reference.

The NMR spectral data was acquired by Dr. Marco Casarotto and Dr.Yanfang Cui of the Biomolecular structure group. Spectra were acquired on a Avance 600 (Bruker BioSpin) spectrometer with a spectral width of 6000 Hz. Spectra were obtained using a pulse width of 7 – 10 μs (90^0) and acquisition time of 0.130 s, collecting 4096 data points and 512 increments of 32 transients. NOESY spectra (mixing time of 200-500 ms) and TOCSY spectra (mixing time of 70 ms) were acquired at 280 K, 285 K or 291 K and used for the assignment of the ^1H-NMR resonances. Suppression of the H_2O resonance for the NOESY spectra was achieved using pulse field gradients while a pre-saturation pulse was employed for the TOCSY experiments. Two-dimensional data were acquired, processed and analysed using Topspin™ (Bruker BioSpin) software. The graphical NMR assignment and intergration program "Sparky" was also used for analysis (Goddard and Kneller). Data sets were zero-filled to 4096 by 2048 and multiplied by a phase-shifted gaussian function in both dimensions prior to

transformation. 1-dimensional ^1H spectra were obtained in an attempt to derive $^3J_{NH-\alpha H}$ coupling constants.

5.3.3 Circular Dichroism (CD) spectroscopy

A 1 mg/ml solution of β_{1a}-C35 peptide was prepared in distilled water and CD was performed as described in Ch.2.2.12.

5.4 Results

5.4.1 NMR structural studies

Proton assignments for all 35 residues of the β_{1a}-C35 peptide were carried out using the ^1H TOCSY (**Figure 5-2**) and the ^1H NOESY (**Figure 5-3**) spectra obtained at 280 ^0K.

The connectivity of a given amino acid in the sequence (i) to its following residue (i+1) can be monitored in the NOESY spectrum because the distance of the amide proton of (i+1) to the H_α, H_β, or H_γ protons of (i) is smaller than 5 Å in almost every case. Therefore, sequential cross signals to $H^\alpha(i)$, $H^\beta(i)$ etc. are observed at the frequency of $H_N(i+1)$ (**Figure 5-4**). These inter-residual cross signals can be distinguished from the intra-residual connectivities by comparing the 2D NOESY (through space information - ch-5.3.2.2) with the 2D TOCSY (through bond information – ch-5.3.2.2) spectrum (**Figure 5-4**). A series of these sequential connectivities between $H\alpha(i)$ and $H_N(i+1)$ determines the order (i, i+1, i+2,...) of the amino acid sequence. The chain of sequential connectivites is however interrupted by proline residues because these have no amide proton. Therefore, no $H_N(i)$-$H\alpha(i-1)$ cross signal will be observed. However, if the proline (i) is in its trans conformation, the sequential $H_N(i-1)$-$H\delta$ (i) and $H\alpha(i-1)$-$H\delta(i)$ cross signals can be observed. The proton assignments for the β_{1a}-C35 peptide carried out as described above are presented in table 5-1.

Following the sequential assignment of residues, the NOESY spectrum was examined for secondary structural elements. Certain NOE profiles can be related to secondary structural elements. For example, alpha helices are characterized by short distances between certain protons on sequentially neighbouring residues (e.g., between backbone amide protons (dNN) as well as between beta protons of residue i and the amide protons of residue i+1 (dβN)). Helical conformations result in short distances between the alpha

proton of residue i and the amide proton of residues i+3 and to a lesser extent i+4 and i+2. These i+2, i+3, and i+4 NOEs are collectively referred to as medium range NOEs

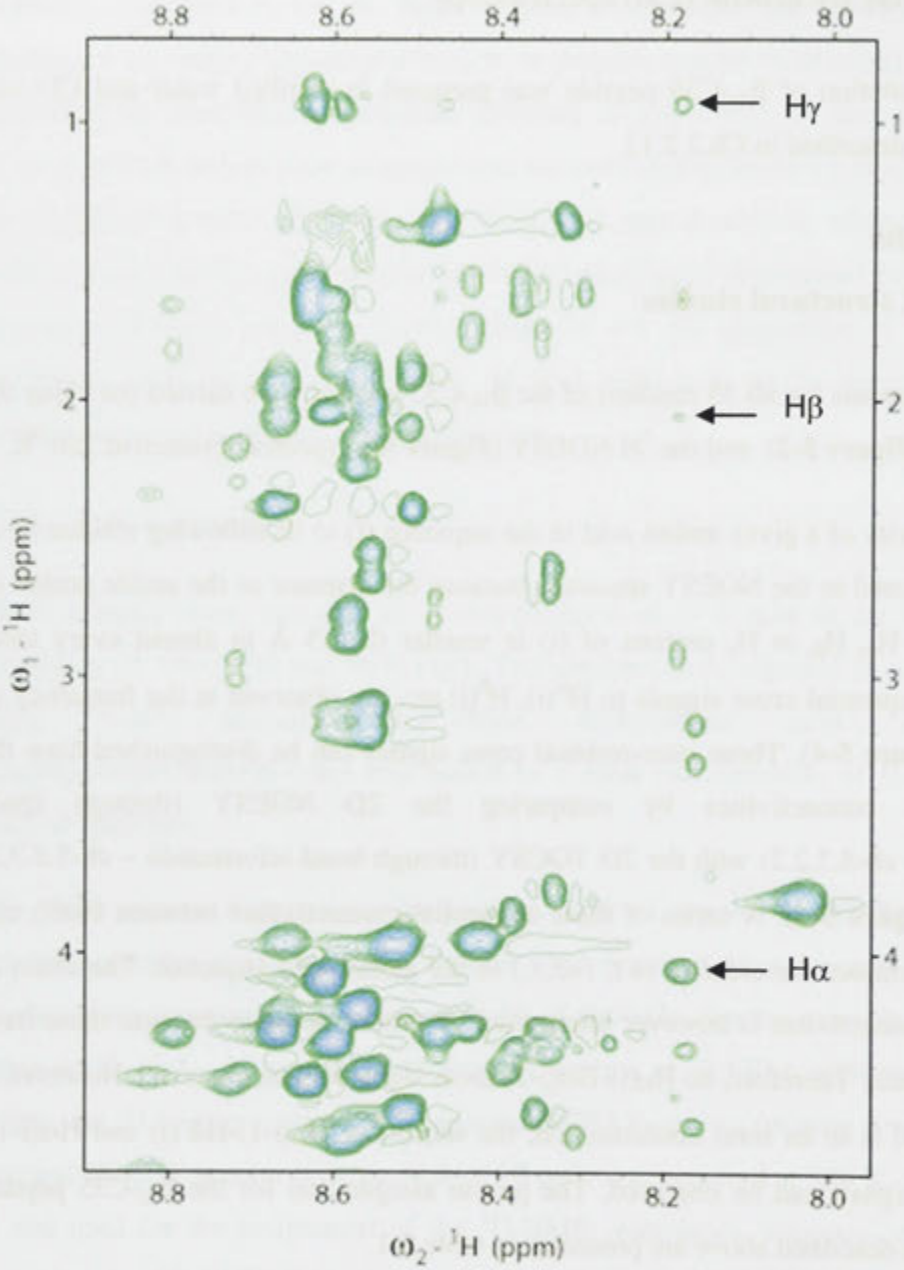

Figure 5-2 Finger print region of the TOCSY spectrum for β_{1a}-C35 peptide. Arrows point to H_α, H_β, and H_γ protons of Valine[516] as an example of a characteristic spin system of an amino acid residue.

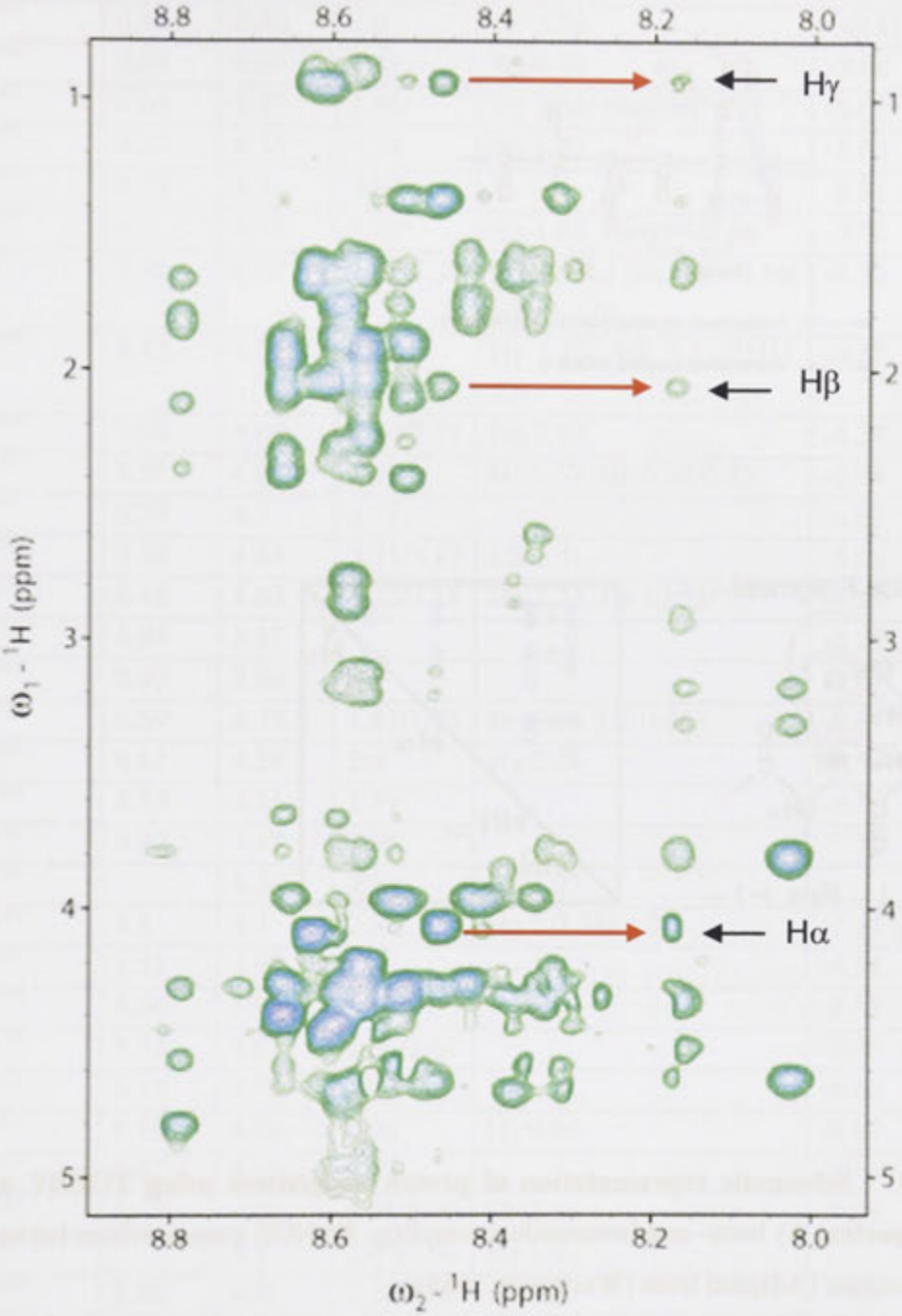

Figure 5-3 Finger print region of the NOESY spectrum for β_{1a}-C35 peptide. Red arrows point to NOEs from the H_N of A^{517} to H_α, H_β, and H_γ protons of Valine[516] as an example of NOE connectivities.

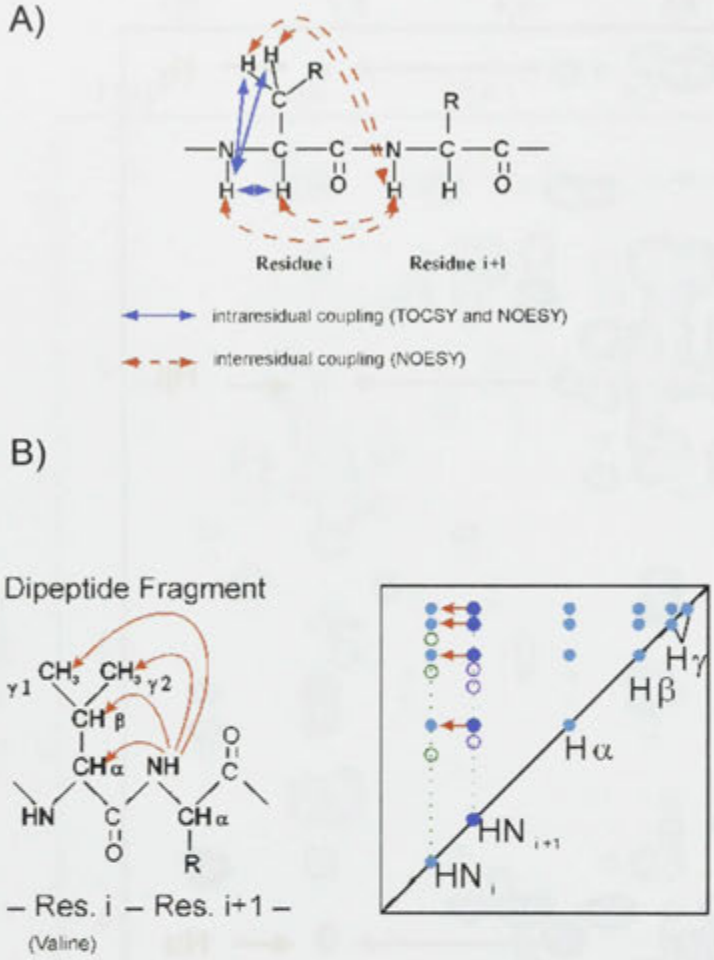

Figure 5-4 Schematic representation of proton assignment using TOCSY and NOESY spectra. A) Inter- and intraresidual coupling. B) NOE connectivities between adjacent residues (Adapted from (Wurthrich, 1986).

Residue	NH	Hα	Hβ	Other	Temp.Co.(ppb/K)
V^{490}	8.58	4.12	1.69	Hγ 0.95	-9.04
Q^{491}	8.82	4.46	2.0	Hγ 2.34	-10.81
V^{492}	8.62	4.66	1.88	Hγ 0.94	-9.66
L^{493}	8.63	4.47	1.64	Hγ 1.64, Hδ 0.86	-6.01
T^{494}	8.26	4.33	4.24	Hγ 1.22	-5.03
S^{495}	8.39	4.3	3.87		-5.71
L^{496}	8.3	4.35	1.62	Hγ 1.62, Hδ 0.93/0.86	-5.36
R^{497}	8.35	4.27	1.82/1.75	Hγ 1.63/1.58, Hδ 3.16, HH11 7.01	-4.32
R^{498}	8.43	4.28	1.75	Hγ 1.57, Hδ 3.1, HH11 7.0	-4.37
N^{499}	8.58	4.64	2.86/2.78	Hδ 7.23	-4.29
L^{500}	8.37	4.35	1.64	Hγ 1.57, Hδ 0.92/0.85	-5.78
S^{501}	8.33	4.3	3.78		-6.63
F^{502}	8.56	4.44	3.21/3.12	Hδ 7.01	-5.02
W^{503}	8.16	4.63	3.32/3.18	Hδ 7.23, Hε 10.23/7.5	-4.53
G^{504}	8.04	3.81			-6.25
G^{505}	8.43	3.96			-7.37
L^{506}	8.59	4.37	1.87/1.75	Hγ 1.64, Hδ 0.94	-8.87
E^{507}	8.61	4.29	2.0	Hγ 2.24	-8.57
A^{508}	8.53	4.25	1.39		-9.12
S^{509}	8.42	4.45	3.95		-7.71
P^{510}		4.34	2.28	Hγ 2.03	
R^{511}	8.8	4.3	2.3/2.7	Hγ 2.0, Hδ 3.2	-7.47
G^{512}	8.53	3.97			-8.31
G^{513}	8.66	3.96			-8.07
D^{514}	8.32	4.67	2.68/2.61		-8.93
A^{515}	8.32	4.29	1.36		-8.66
V^{516}	8.18	4.06	2.06	Hγ 0.94	-8.81
A^{517}	8.47	4.29	1.37		-10.69
Q^{518}	8.67	4.28	1.95/2.06	Hγ 2.38	-9.29
P^{519}		4.4	2.07/2.00	Hγ 1.9	
Q^{520}	8.48	4.38	2.10/2.07	Hγ 2.27	-9.08
E^{521}	8.57	4.24	2.06	Hγ 2.24	-9.15
H^{522}	8.60	4.57	3.2/3.13		-10.65
A^{523}	8.47	4.29	1.37		-11.96
M^{524}	8.56	4.44	2.55/2.65	Hγ 2.02/2.12	-9.24

Table 5-1 Proton assignment (p.p.m.) for the β_{1a}-C35 peptide at pH 5.8 and 280 ^{0}K and temperature coefficients (p.p.b./ ^{0}K).

while NOEs connecting residues separated by more than 5 residues are referred to as long range. Extended conformations (e.g., beta strands) on the other hand, are characterized by short sequential, dαN, distances. The formation of sheets also result in short distances between protons on adjacent strands. This information is summarised in **Figure 5-5**.

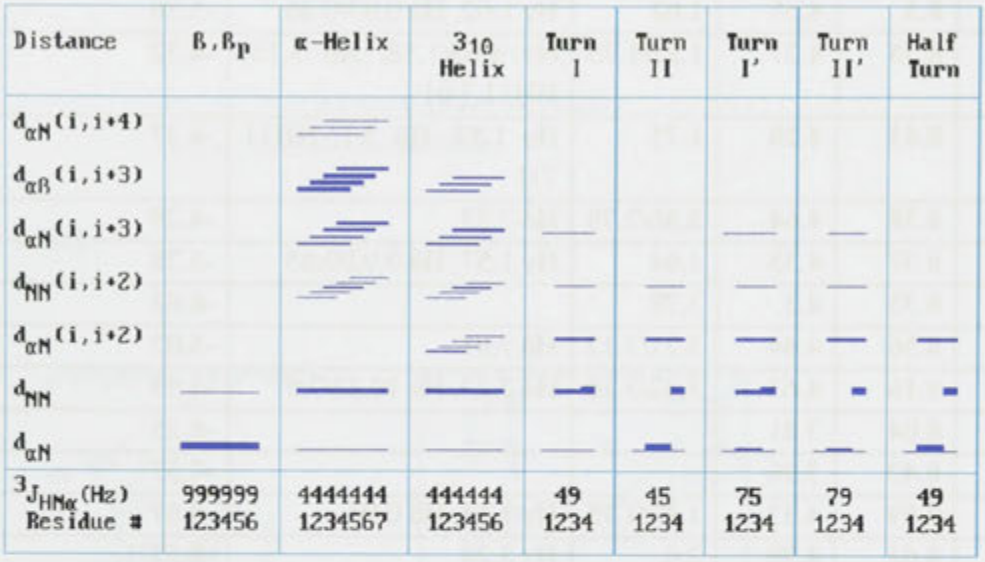

Figure 5-5 Survey of the sequential and medium range proton-proton NOE's and the spin-spin coupling constants 3JHNa in some common secondary structures. The numbers at the bottom represent the amino acid residues in the given secondary structure and the values of the 3JHNα coupling constant. Short proton-proton distances are indicated by lines linking the residues that contain the hydrogen atoms involved. The thickness of the line is proportional to the intensity of the NOE (Wurthrich, 1986).

Examination of the H_N-H_N region of the NOESY spectrum of β_{1a}-C35 revealed a stretch of sequential short range NOEs from residues L^{493} to G^{504} (**Figure 5-6**) indicating the presence of a helical secondary structure within this portion of the peptide. Other short and medium range NOEs were also detected which supported a helical element within this region of β_{1a}-C35. They are: 1) medium strength NOEs between the alpha proton of residue i and the beta proton of residues i+3 ($d_{\alpha\beta(i,i+3)}$) stretching from residues L^{493} to L^{496} and N^{499} to L^{506} 2) weak NOEs between the alpha proton of residue i and the amide proton of residues i+3 ($d_{\alpha N(i,i+3)}$) stretching from residues L^{494} to L^{506} and 3) weak NOEs between the alpha proton of residue i and the amide proton of residues i+2 ($d_{\alpha N(i,i+2)}$) stretching from residues R^{497} to G^{505}. These results are summarised in **figure 5-7**.

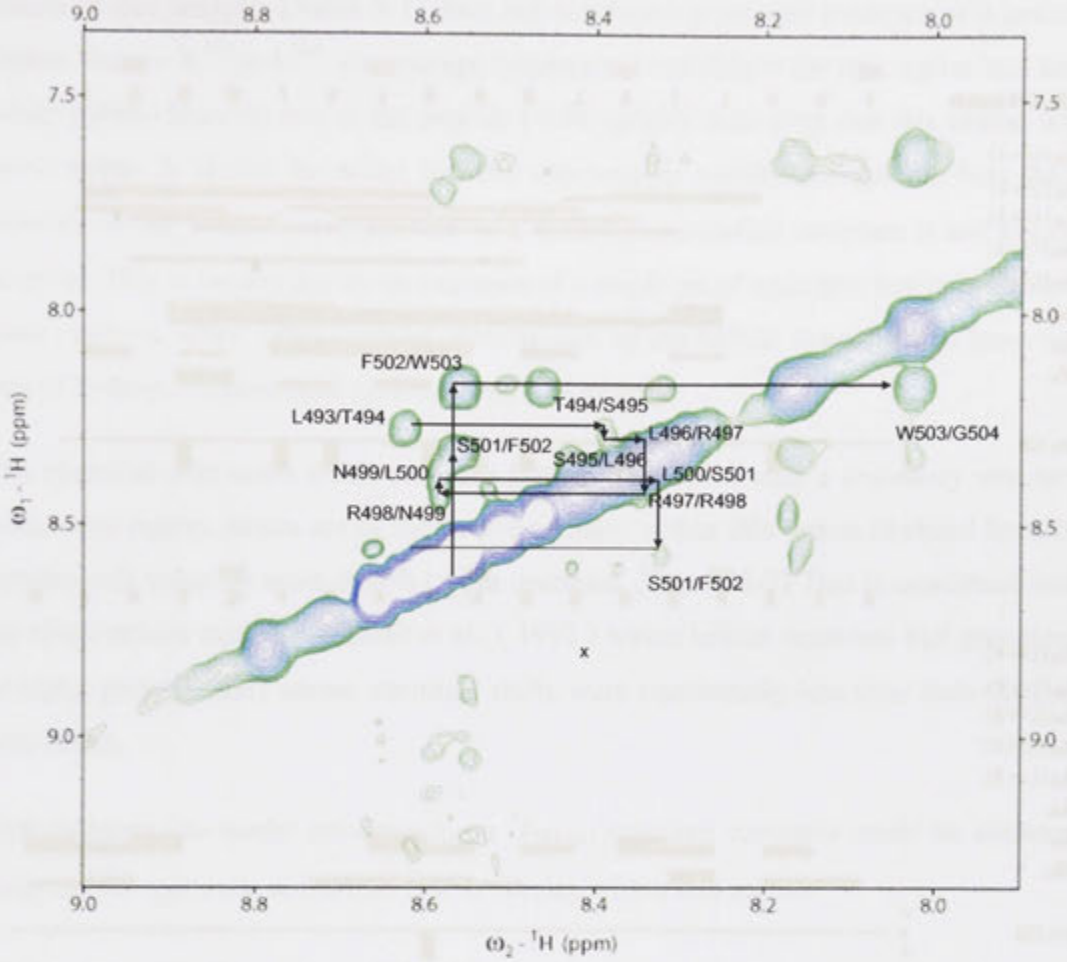

Figure 5-6 Amide-amide (HN-H_N) region of the NOESY spectrum of β_{1a}-C35 peptide. Strong and continuous cross peaks are shown and labelled.

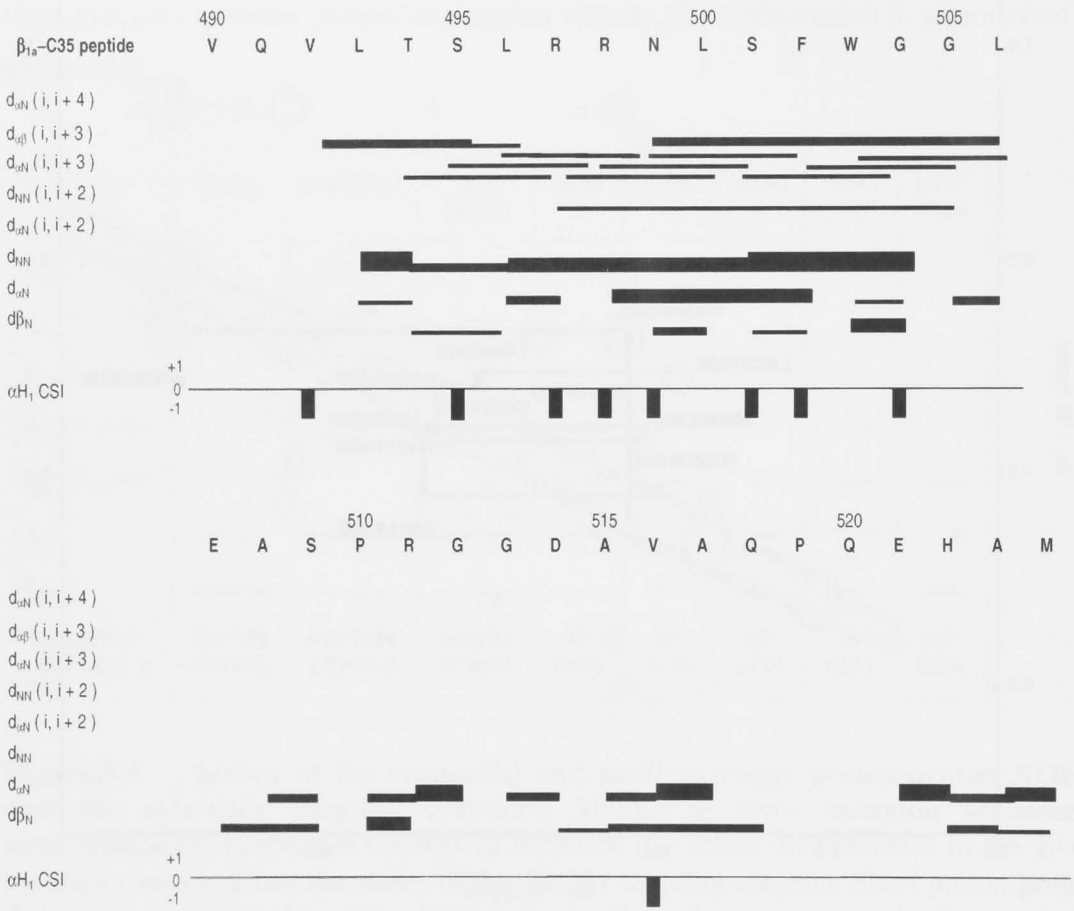

Figure 5-7 Summary of sequential and medium range proton-proton NOEs and ^{1}H CSI (chemical shift index) for β_{1a}-C35. NOE connectivities are classified as strong, medium, weak or absent and are represented by the thickness (or absence) of a bar connecting the residues in question. A CSI value of +1 or -1 has been assigned for residues whose αH chemical shift deviates from tabulated random coil values by more than 0.1 ppm, downfield or upfield respectively. Values of <-1 are suggestive of alpha helical secondary structures (Wishart et al., 1991, ch - 5.3.2.5).

Next, in order to confirm the presence of an α helix, other indicators of secondary structure characteristics such as $^3J_{NH\text{-}\alpha H}$ coupling constants, temperature coefficients and chemical shift indexes (CSI) were examined.

Analysis of the temperature coefficients (ch-5.3.2.4) of the β_{1a}-C35 peptide was carried out by comparing the ^{1}H TOCSY spectra obtained at 280, 285 and 291 ^{0}K. Although the results of this analysis (Table 5-1) does not conclusively provide evidence of a helical region from ~ L^{493} to L^{506}, the average temperature coefficient for this region was less (-5.21 ppb/K) than the rest of the peptide (-9.00 ppb/K) indicating that this region was more stable. It should be noted that the temperature coefficients for the first three residues of the N- or C-terminal end of a α helical secondary structure is not always accurate. This is largely due to the presence of a single set of hydrogen bonds in the first three residues, while other residues forming part of the helical structure will have two sets of hydrogen bonds, both upstream and downstream.

The chemical shift index (CSI) provided further support for such a secondary structure within this region. Seven out of the twelve residues within this region deviated from its random coil value by more than 0.1 ppm upstream (**Figure 5-7**) This is consistent with the observations made by Wishart et al., (1992) where helical segments had groupings of alpha protons (αH) whose chemical shifts were consistently less than their random coil values.

Unfortunately, no useful information on $^{3}J_{NH\text{-}\alpha H}$ coupling constants could be obtained from the 1D spectrum of β_{1a}-C35 due to overlap within this region.

5.4.2 Circular Dichroism (CD) spectroscopy

CD spectroscopy of the β_{1a}-C35 peptide was also carried out to investigate its overall secondary structure content. The resulting spectrum contained a single minimum at 198 nm and indicated a mostly random coil structure when compared to a reference spectrum (Greenfield, 2006) of poly-L-lysine in α-helical, β sheet and random coil conformations (**Figure 5-8**). However, it should be noted that circular dichroism is not a reliable technique short peptides as only well formed secondary structures can be quantitatively characterized by this method (Reed and Reed, 1997).

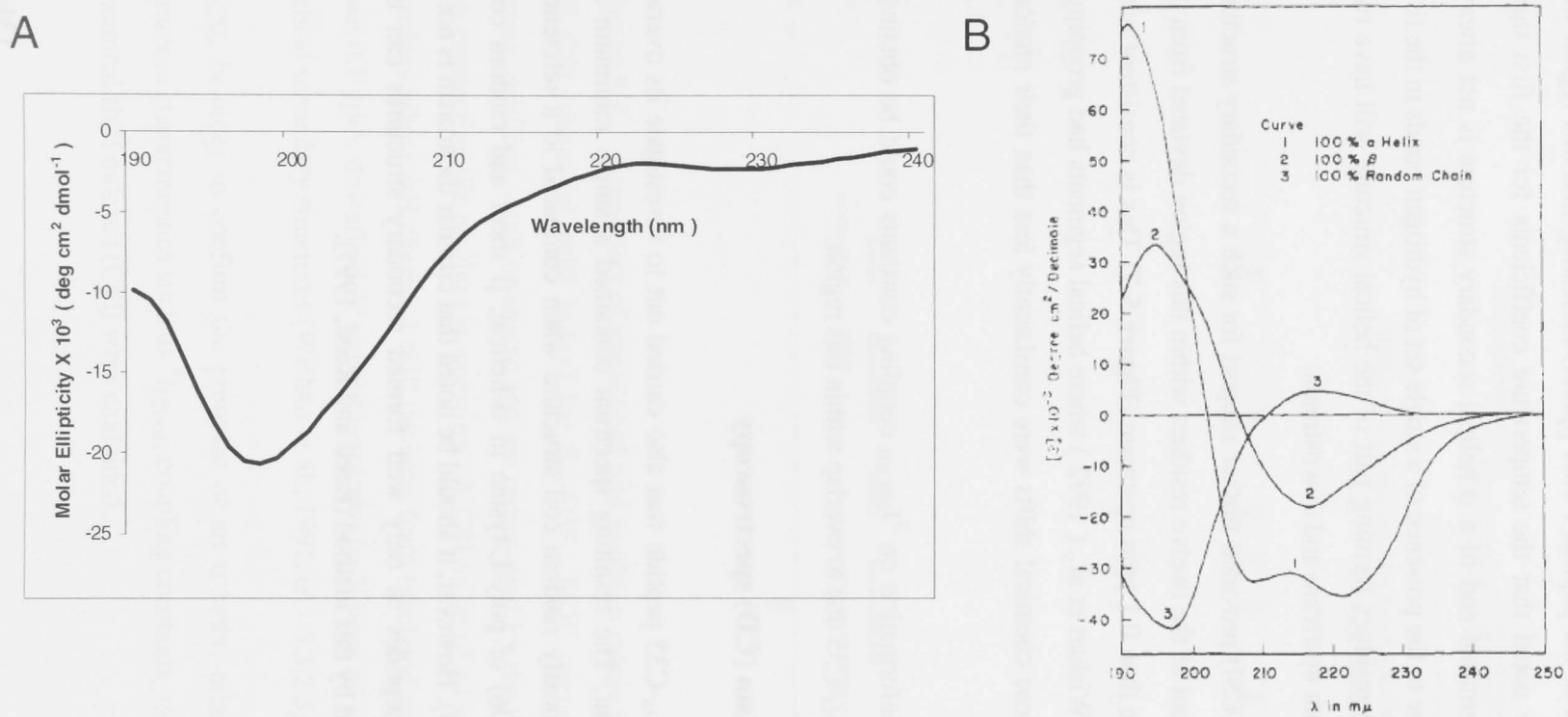

Figure 5-8 Circular dichroism studies of β_{1a}-C35 peptide. A) CD spectrum of the β_{1a}-C35 peptide in water at 25 ^{0}C and pH ~5.8. The spectrum shows a minimum at 198 nm and a mostly random coil structure **B)** reference spectrum of poly-L-lysine in 1- 100%α-helical, 2-100% β sheet and 3 - 100 % random coil conformations (Greenfield, 2006)

5.4.3 Structure of the β_{1a}-C35 peptide and design of mutant peptides

The structural information obtained from NMR studies showed that the β_{1a}-C35 peptide contains a helical region extending from approximately L^{493} through to L^{506}. Based on these results a model structure of the β_{1a}-C35 peptide was generated by Dr. Marco Casarotto (Biomolecular Structure Group) using a molecular modeling software (Insight II – Molecular Simulations, MSI,). This model structure revealed four hydrophobic residues, L^{493}, L^{496}, $L^{500}$and W^{503}, forming one face of the helical region (**Figure 5-9**).

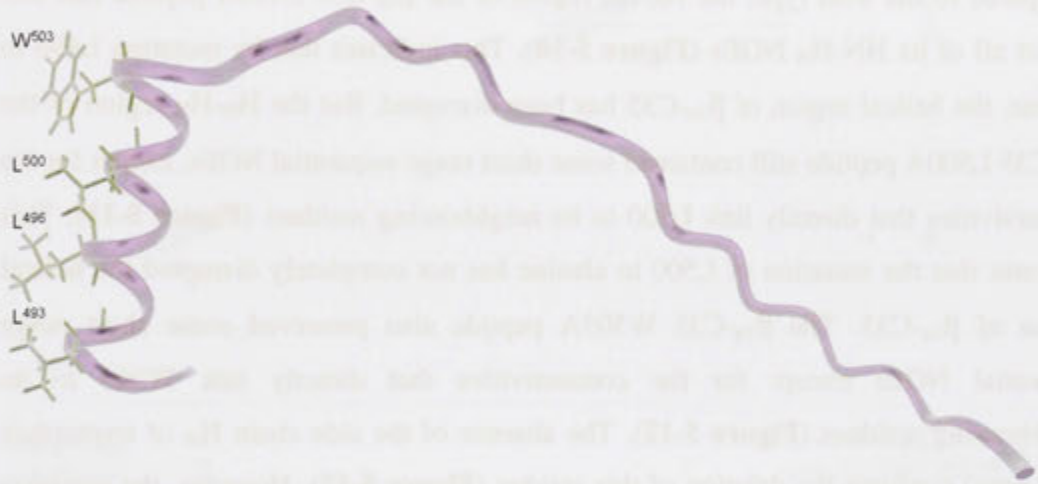

Figure 5-9 Model structure of β_{1a}-C35 peptide. The backbone structure is presented as a ribbon diagram and the residues forming a hydrophobic surface in the helical region are shown as stick models (Dr.Marco Casarotto – Biomolecular Structure group, JCSMR).

It is possible that the hydrophobic surface formed by these residues are involved in the interactions with neighbouring molecules such as the RyR1. Therefore, in order to investigate the role, if any, of these hydrophobic residues in the structure and function of the C-terminal tail of the β_{1a} subunit, L^{496}, $L^{500}$and W^{503} were mutated to alanines. Residue L^{493} was not selected for mutation as it is too close to the N-terminus of the peptide. Four peptides were synthesized where the first three consisted of individual mutations in L^{496}, L^{500} and W^{503} (β_{1a}-C35 L496A, β_{1a}-C35 L500A and β_{1a}-C35 W503A). The fourth peptide consisted of simultaneous mutations of all three residues to alanines (β_{1a}-C35 L497/L500/W503 A). In order to characterize the structure of these peptides, solutions were prepared as described in ch-5.3.2.6 and their NOESY spectra were obtained at 280 ^{0}K and compared to the wild type.

5.4.4 Comparison of the H_N-H_N region of the β_{1a}-C35 mutant peptides

For a peptide or protein with a α helical secondary structure, a significant amount of the secondary structural information (short range sequential NOEs) is contained in the H_N-H_N region of the NOESY spectrum. Hence, a quick but reliable method of determining whether the α helix has been maintained is by monitoring the H_N-H_N NOE pattern in the NOESY spectrum. Therefore the H_N-H_N region of the mutant peptides were compared to that of the wild type and examined for any changes in NOE connectivities.

Compared to the wild type, the H_N-H_N region of the β_{1a}-C35 L496A peptide had lost almost all of its HN-H_N NOEs (**Figure 5-10**). This indicates that by mutating L496 to alanine, the helical region of β_{1a}-C35 has been disrupted. But the H_N-H_N region of the β_{1a}-C35 L500A peptide still contained some short range sequential NOEs, except for the connectivities that directly link L500 to its neighbouring residues (**Figure 5-11**). This indicates that the mutation of L500 to alanine has not completely disrupted the helical region of β_{1a}-C35. The β_{1a}-C35 W503A peptide also preserved some short range sequential NOEs except for the connectivities that directly link W503 to its neighbouring residues (**Figure 5-12**). The absence of the side chain H_N of tryptophan (~10 ppm) confirms the deletion of this residue (**Figure 5-12**). However, the mutation of W503 to alanine, has also not completely disrupted the helical region of β_{1a}-C35.

Interestingly, the H_N-H_N region of the triple mutant peptide, β_{1a}-C35 L496/L500/W503A, still contain some short range sequential NOEs (**Figure 5-13**) This indicates that despite the mutation of three residues to alanines, a significant proportion of the helical structure of this region (L^{493} to G^{504}) of β_{1a}-C35 is maintained.

5.5 Discussion

Previous studies have shown that the β_{1a} subunit is able to bind to the RyR1 and that the end 35 residues of its carboxyl terminus was important for skeletal type EC-coupling (Beurg et al., 1999). More recent studies by affinity chromatography has shown that a peptide corresponding to this C-terminal region is able to bind to RyR1 (Rebbeck et al.,2011). But the currently available crystal structure studies (Chen et al., 2004, Opatowsky et al., 2004, Van Petegem et al., 2004) of the β subunit do not contain any data on its variable regions, which includes the C-terminus. This study investigated the

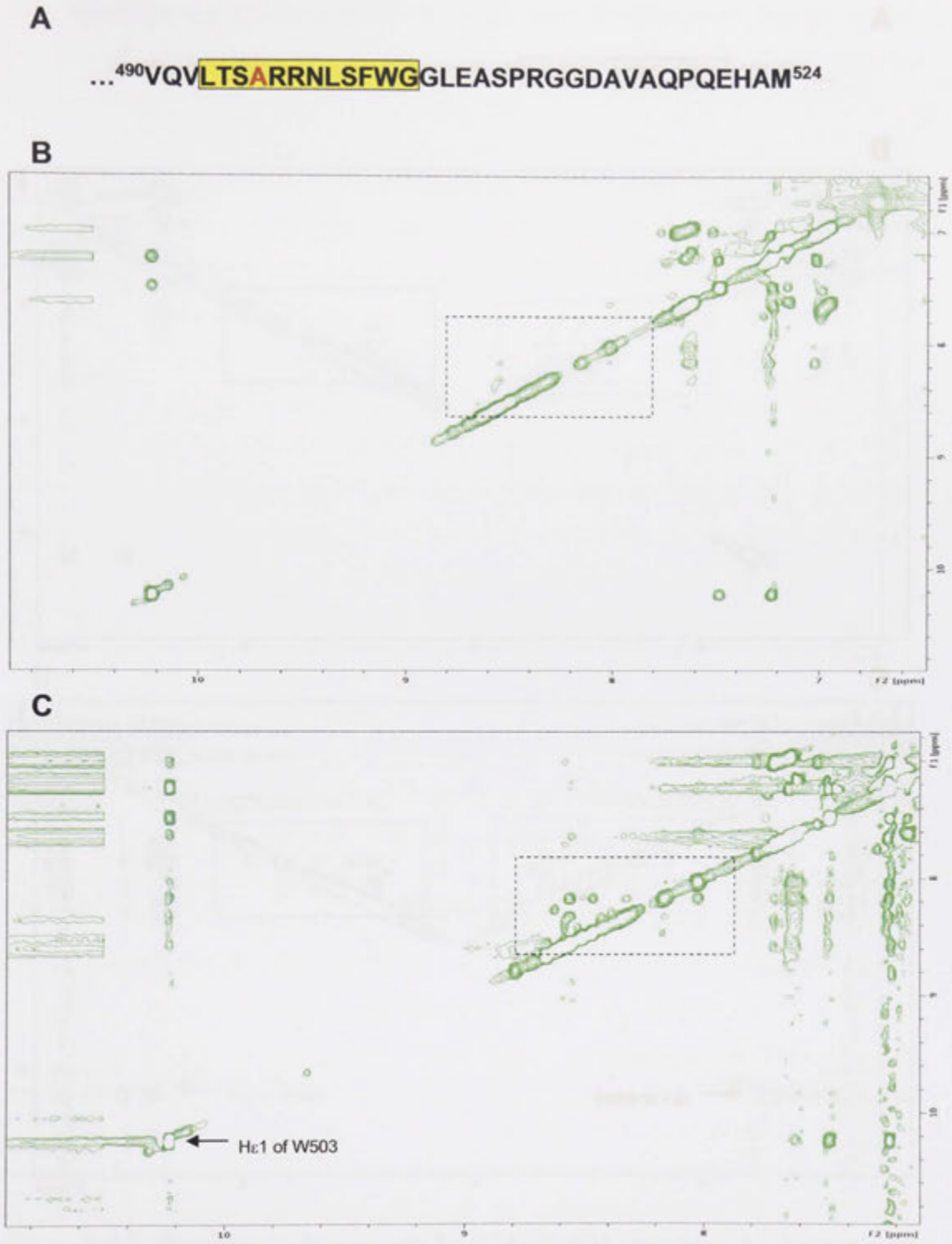

Figure 5-10 Structural changes of β_{1a}-C35 L496A peptide. A) Sequence of peptide. L496 to A mutation is in red. The helical region is highlighted in yellow. **B)** The H_N-H_N region (enclosed) has lost most NOE connectivities indicating disruption of the helical region. **C)** The H_N-H_N region of wild type β_{1a}-C35 (enclosed) showing sequential short range NOEs indicative of a helical region. Arrow points to the side chain H_N of W503. Both spectra are presented at a comparable contour level.

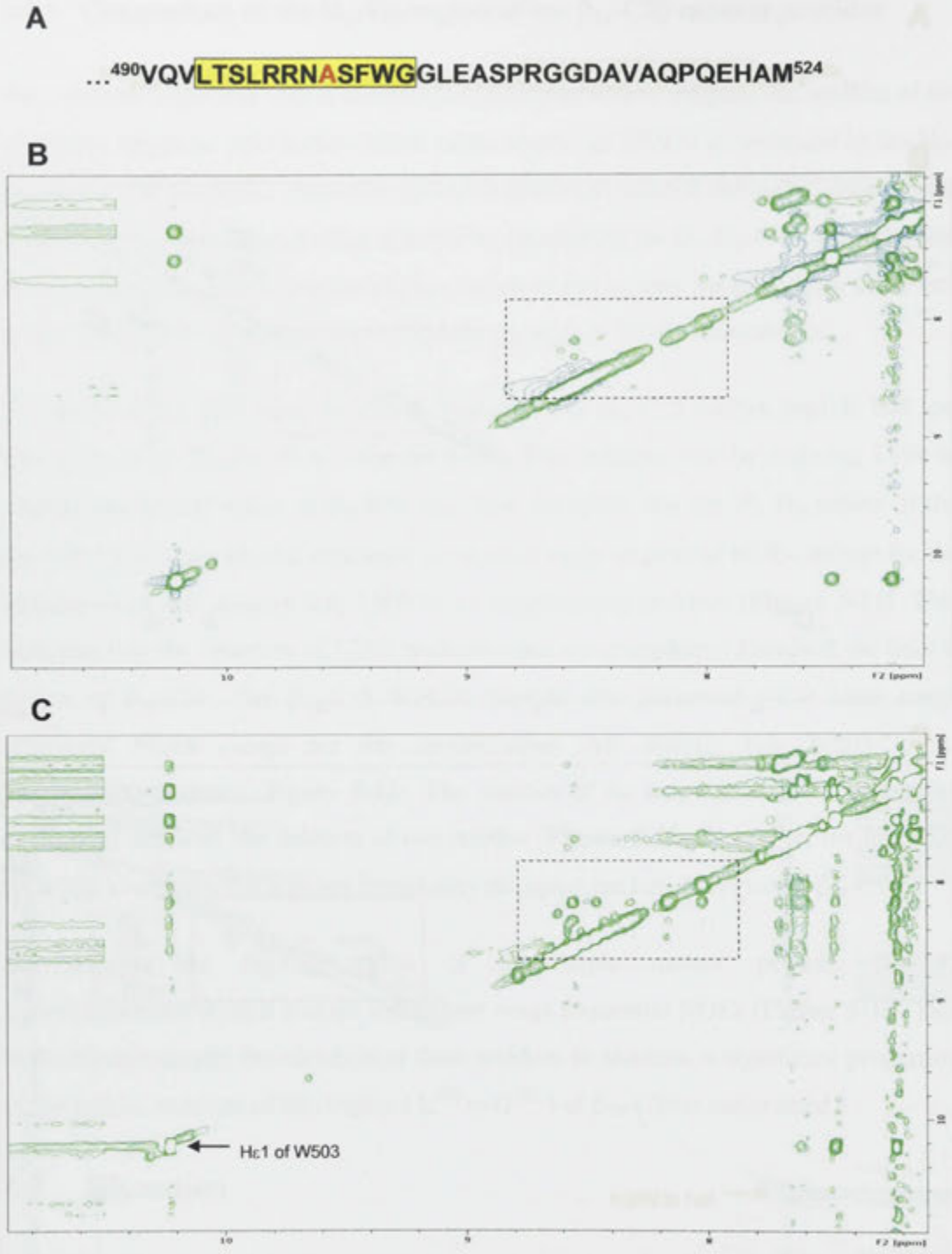

Figure 5-11 Structural changes of β_{1a}-C35 L500A peptide. A) Sequence of peptide. L500 to A mutation is in red. The helical region is highlighted in yellow. **B)** The H_N-H_N region (enclosed) has retained some NOE connectivities indicating that the helical region is not completely disrupted. **C)** The H_N-H_N region of wild type β_{1a}-C35 (enclosed) showing sequential short range NOEs indicative of a helical region. Arrow points to the side chain HN of W503. Both spectra are presented at a comparable contour level.

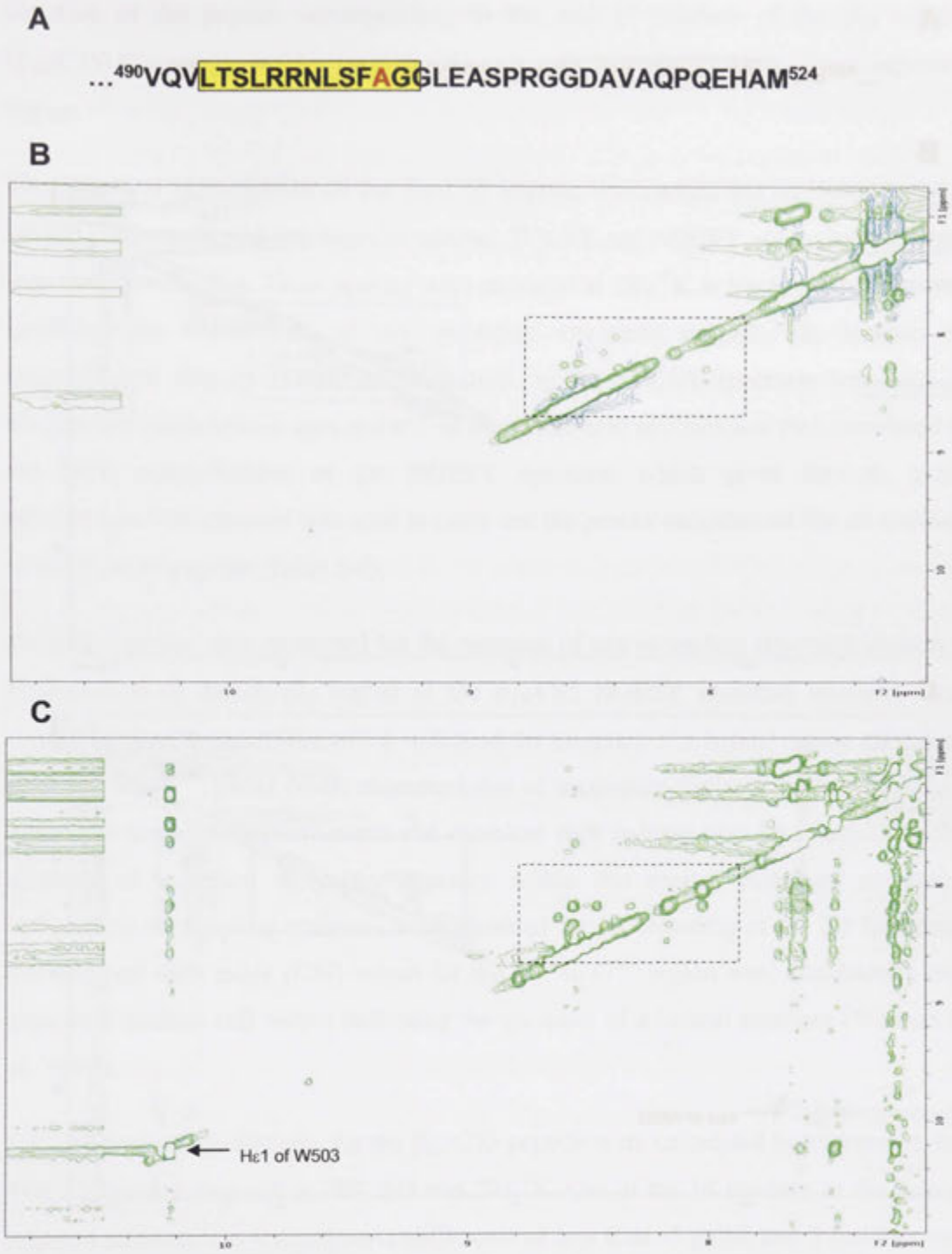

Figure 5-12 Structural changes of β_{1a}-C35 W503A peptide. A) Sequence of peptide. W503 to A mutation is in red. The helical region is highlighted in yellow. **B)** The H_N-H_N region (enclosed) has retained some NOE connectivities indicating that the helical region is not completely disrupted. Note the absence of side chain H_N of W503. C) The H_N-H_N region of wild type β_{1a}-C35 (enclosed) showing sequential short range NOEs indicative of a helical region. Arrow points to the side chain HN of W503. Both spectra are presented at a comparable contour level.

A

...[490]VQVLTSARRNASFAGGLEASPRGGDAVAQPQEHAM[524]

B

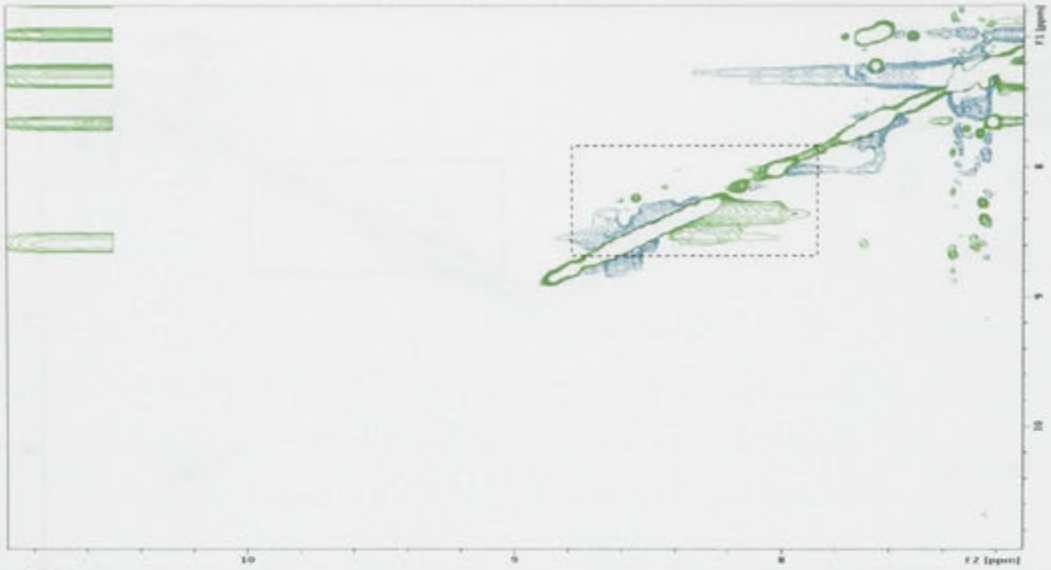

C

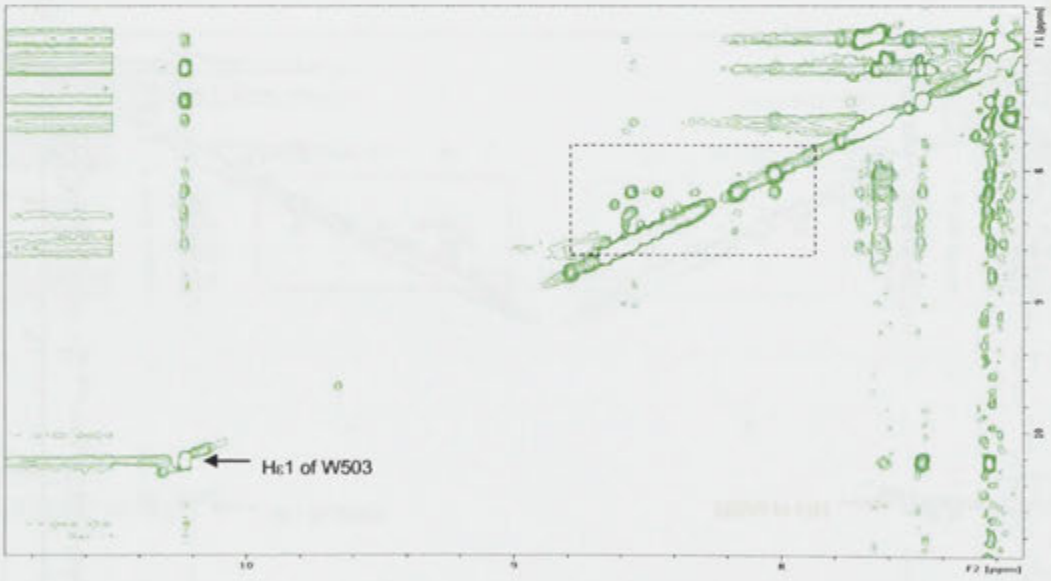

Figure 5-13 Structural changes of β_{1a}-C35 L496/L500/W503A peptide. A) Sequence of peptide. Mutated residues are in red. The helical region is highlighted in yellow. **B)** Despite the triple mutation, the H_N-H_N region (enclosed) has retained some NOE connectivities indicating that the helical region is still somewhat intact. Note the absence of side chain H_N of W503. **C)** The H_N-H_N region of wild type β_{1a}-C35 (enclosed) showing sequential short range NOEs indicative of a helical region. Arrow points to the side chain HN of W503. Both spectra are presented at a comparable contour level.

structure of the peptide corresponding to the end 35 residues of the β_{1a} subunit (β_{1a}-C35) C-terminus in an attempt to gain an insight in to the structure of this important region.

The structural investigation of the β_{1a}-C35 peptide was carried out by 2-dimensional NMR spectroscopy and two types of spectra, TOCSY and NOESY, were used to obtain structural information. These spectra were acquired at 280 ^{0}K as the lower temperature facilitates the stabilisation of any secondary structures present. The transfer of magnetisation through bonds, which is seen on the TOCSY spectrum was used to identify the characteristic spin systems of the amino acid residues and then correlated to the NOE connectivities of the NOESY spectrum which gives through space information. This process was used to carry out the proton assignments for all residues of the β_{1a}-C35 peptide (Table 5-1).

Next, the spectra were examined for the presence of any secondary structural elements. Examination of the H_N-H_N region of the β_{1a}-C35 NOESY spectrum revealed clear sequential short range NOEs which indicated the presence of a helical region extending from L^{493} to G^{506}. Other NMR characteristics of secondary structure such as coupling constants, temperature coefficients and chemical shift indexes also lend support to the presence of a helical secondary structure within this region. Although no useful information on coupling constants were obtained due to crowding of the 1D spectrum, the chemical shift index (CSI) values for the L^{493} to G^{504} region were consistently less than their random coil values indicating the presence of a helical structure (Wishart et al., 1992).

The temperature coefficients for the β_{1a}-C35 peptide were calculated by comparing the TOCSY spectra acquired at 280, 285 and 291 ^{0}K. Out of the 14 residues in the helical region 4 residues had temperature coefficients of less than -5 ppb/k and 5 residues had temperature coefficients of around -5 ppb/k. On average, the temperature coefficients for the L^{493} to G^{506} region were lower than for the rest of the peptide (Table 5-1). According to previous studies (Andersen et al., 1992, Dyson et al., 1988, Skalicky et al., 1994), a value greater than -5 ppb/K for each residue is taken to indicate the presence of secondary structure. The lower than expected temperature coefficients for some residues in the L^{493} - G^{504} region indicates that it forms a nascent helix (an inter-converting mixture of random coil and structured peptide) which is increasingly unstable at higher

temperatures. This is supported by circular dichroism (CD) spectroscopy results (conducted at 20 ^{0}C – 293 ^{0}K) which shows the β_{1a}-C35 peptide to be mostly random coil at this temperature. In the absence of a rigid helical region, the determination of a 3-D solution structure of the β_{1a}-C35 peptide was not pursued. Instead a model structure was generated based on the NOE connectivies and other indicators of secondary structure obtained by NMR studies (**Figure 5-7 and Figure 5-9**).

Based on the findings of NMR studies, the β_{1a}-C35 peptide was found to have a nascent helix type structure in the region of L^{493} to G^{504}. Closer examination of this region revealed a group of hydrophobic residues of which (L^{496}, L^{500} and W^{503}) were most likely to form a hydrophobic surface which may interact with neighbouring molecules such as the RyR1. Therefore, in order to investigate the role, if any, of these residues in the structure and function of the C-terminal tail of the β_{1a} subunit, they were mutated to alanine residues. NMR studies of the mutated peptides showed that the mutation of L^{500} or W^{503} to alanines did not completely disrupt the helical structure of the L^{493} - G^{504} region of β_{1a}-C35. The mutation of L496 to alanine caused a significant disruption to this helical region and this residue may therefore be important for the stability of the helical L^{493} - G^{504} region of β_{1a}-C35. Interestingly, the simultaneous mutation of all three residues to alanines did not cause a complete disruption of the helical region. This maybe due to the fact that alanines themselves have a propensity for helix formation and therefore the presence of three alanine residues in conducive positions facilitates the formation of a helical secondary structure (Pace and Scholtz, 1998).

In summary, NMR studies of a peptide corresponding to the end 35 residues of the β_{1a} C-terminus revealed that it contained a nascent helical region which may form a hydrophobic surface that is involved in the binding with the RyR1. Within this region, three hydrophobic residues which were capable of forming a binding surface were mutated to alanines and the structural implications were examined. In the following chapter the ability of the β_{1a}-C35 peptide to interact with the RyR1 and the functional impact of mutating the hydrophobic residues involved in the helical region will be examined.

Chapter 6 Functional interactions between the DHPR-β_{1a} C-terminal tail and the skeletal ryanodine receptor

6.1 Introduction

The process of excitation-contraction (EC) coupling in skeletal muscle does not depend on Ca^{2+} entry from the extracellular compartment. Therefore it is widely accepted that a physical interaction between the dihydropyridine receptor (DHPR) voltage sensor in the transverse tubule membrane and the ryanodine receptor (RyR) Ca^{2+} release channel in the closely opposed SR membrane leads to skeletal type EC-coupling (Bannister, 2007, Beam and Bannister, 2010).

Of the five subunits of the DHPR, the skeletal isoforms of the membrane spanning α_{1S} subunit and the cytoplasmic β_{1a} subunit are essential for EC coupling in skeletal muscle. In the α_{1s} subunit, the intracellular II-III loop forms a minimal essential region for transmitting the EC-coupling signal from the DHPR to the RyR1 (Grabner et al., 1999, Beam and Bannister, 2010). Hence the deletion of this region abolishes skeletal type EC-coupling.

One essential role of the β subunit is to traffic the DHPR α_{1s} subunit to the t-tubular membrane. The trafficking depends on the well characterised binding of the guanylate kinase (GK) domain of the β_{1a} subunit to the I-II loop of the α_{1S} subunit. In addition to this essential role, there are several findings which suggest that the β_{1a} subunit may play a direct role in the physical EC coupling process. Firstly, deletion of the end 35 residues of the C-terminal tail of β_{1a} leads to a significant reduction in depolarization induced Ca^{2+} release from the SR through the RyR (in β_{1a}-null mouse myotubes transfected with mutant β_{1a} c-DNA). This C-terminal modification does not appear to affect targeting of the DHPR to RyR1 (Beurg et al., 1999). A direct interaction between the β_{1a} subunit and RyR1 is also demonstrated by affinity chromatography and the β_{1a} binding site on the RyR1 fragments was localised to a small cluster of basic residues K^{3494}-R^{3502} (Cheng et al., 2005). Interruption of binding of β_{1a} by deletion or substitution of these basic residues resulted in a significant reduction in depolarisation-induced Ca^{2+} release. Finally expression of the β_{1a} subunit in β_{1a}–null zebrafish restored targeting of the DHPR to the triad junction and physical skeletal EC coupling. However expression of

the cardiac/neuronal β_{2a} or housefly β_M subunits restored triad targeting of the DHPR, but not physical coupling (Schredelseker et al., 2009). These results could be explained by a direct contribution of β_{1a} to EC coupling or by an allosteric influence of β_{1a} on the precise geometry (tetrad formation) of the DHPR opposite RyR1 in the surface/SR junction that reduced the efficacy of EC coupling (Schredelseker et al., 2009).

Although a combination of electrophysiological, morphological and biochemical approaches provide a solid foundation for the notion that protein-protein interactions link the skeletal DHPR and RyR1 *in vivo*, the exact mechanism of this coupling process at a molecular level remains unresolved. Studies carried out in the previous chapter examined the structure of a peptide corresponding to the end 35 residues of the β_{1a} C-terminus and investigated the structural consequences of mutating three hydrophobic residues which were capable of forming a binding surface with RyR1. This study explores the ability of the full length β_{1a} subunit as well as its C-terminal tail peptide and its mutants to interact with the gating mechanism of a RyR1 channel embedded in an artificial lipid bilayer.

6.2 Aim

Examine the functional interactions between the isolated RyR1 channel and the full length β_{1a} subunit and its 35 residue C-terminal tail (β_{1a}-C35). It is also the aim of this study to explore the functional effects on RyR1 of mutating three hydrophobic residues in the helical region of the C-terminal peptide.

6.3 Materials and Methods

6.3.1 Expression and purification of full length recombinant β_{1a} subunit

The recombinant β_{1a} subunit was prepared as described in Chapter 3.3.3.

6.3.2 Peptide synthesis

Peptides used in this study (Table 6-1) were synthesized as described in the general methods section (Ch. 2.2.1).

Table 6-1 Peptides used in this study. Mutated residues are in bold and underlined

Peptide	Sequence
β_{1a}-C35 (wild type)	^{490}VQVLTS**L**RRN**L**SF**W**GGLEASPRGGDAVAQPQEHAM^{524}
β_{1a}-C35 L496A	^{490}VQVLTS**A**RRNLSFWGGLEASPRGGDAVAQPQEHAM^{524}
β_{1a}-C35 L500A	^{490}VQVLTSLRRN**A**SFWGGLEASPRGGDAVAQPQEHAM^{524}
β_{1a}-C35 W503A	^{490}VQVLTSLRRNLSF**A**GGLEASPRGGDAVAQPQEHAM^{524}
β_{1a}-C35 L496/L500/W503 A	^{490}VQVLTS**A**RRN**A**SF**A**GGLEASPRGGDAVAQPQEHAM^{524}

6.3.3 Peptide and protein quantitation

The precise concentration of peptides and proteins used in this study was determined as described in chapter 2.2.1 and 2.2.11 respectively.

6.3.4 Planar bilayer recordings of ryanodine receptor channels

6.3.4.1 Introduction

In ion channel reconstitution studies using planar bilayers, a lipid membrane is formed across a small aperture that interconnects two chambers that are filled with aqueous solutions. A ryanodine receptor channel is embedded in this artificial lipid bilayer and its activity is recorded.

6.3.4.2 Preparation of samples

All stock solutions of proteins and peptides were prepared in *cis* solution. Full length recombinant β_{1a} protein was buffer exchanged to *cis* solution using Zeba™ desalting column (Thermo Scientific, USA) as per manufactures instructions.

6.3.4.3 Preparation of SR vesicles

Native skeletal sarcoplamic (SR) vesicles were isolated from the back and leg muscles of New Zealand white rabbits. The procedures were carried out by Mrs. Suzy Pace and Mrs. Joan Stivala from the JCSMR Muscle Research Group based on the method by (Inui et al., 1987), with minor modifications (Ahern et al., 1994, Ahern et al., 1997).

Diced muscle tissue from the rabbit was snap frozen and later homogenized in a Waring blender (Waring Products, USA) for 1 min in a homogenizing buffer consisting of 5mM imidazole, 300mM sucrose, pH 7.4 and a cocktail of protease inhibitors (1mM benzamadine, 0.5mM PMSF, 3μM anti-calpain I, 3μM anti-calpain II, 1μM leupeptin and 1μM pepstatin A). The homogenate was then centrifuged at 9000 RPM for 20min in a SLA1500 rotor (Sorval RC-5B Refrigerated Superspeed Centrifuge, Du Pont Instruments, USA). The pellet was resuspended in the homogenizing buffer followed by another round of homogenization and centrifugation as described above.

Next, the supernatant was filtered through four layers of cotton gauze and was centrifuged at 30000RPM in a Ti-45 rotor (Beckman L8-70 Ultracentrifuge, Beckman Instruments, Australia) for 1 – 2h at 4°C. The pellet was collected and resuspended in 42ml of homogenising buffer in a Dounce Teflon homogeniser (Edwards Instrument, Australia). Several millilitres of the sample was loaded onto a discontinuous sucrose density gradient comprising of 4 ml of 45% (w:v), 7 ml of 38% (w:v), 7 ml of 34% (w:v), 7 ml of 32% (w:v) and 4 ml of 27% (w:v) sucrose layer. Sucrose solutions were prepared in a diluting buffer containing 20 mM imidazole, pH 7.4 and a cocktail of protease inhibitors as described above. The sucrose gradient was centrifuged overnight at 20000RPM in a SW28 rotor (Beckman L8-70 Ultracentrifuge, Beckman Instruments, Australia) at 4°C. Sucrose density bands at the 34 – 38% (band 3) and 38 – 45% (band 4) interface were collected and diluted with two volumes of diluting buffer. Finally, the diluted fractions were centrifuged at 4°C for 1h at 32000RPM in a Ti-45 rotor (Beckman L8-70 Ultracentrifuge, Beckman Instruments, Australia). The final pellet was resuspended in homogenizing buffer to a final concentration of approximately 20 mg/ml, divided into 15 μl aliquots and snap frozen before storage at -70°C.

6.3.4.4 Lipid mixture

An artificial lipid mix of phosphatidylethanolamine (PE) and phosphatidylcholine (PC) at a ratio of 4:1 was nitrogen-dried prior to dilution with n-decane to a final concentration of 50 mg/ml.

6.3.4.5 Bilayer solutions

The *cis* and *trans* solutions used for lipid bilayer experiments consisted of: *cis*: 20 mM CsCl, 230 mM $CsCH_3O_3S$, 10 mM TES and 1 mM [Ca^{2+}]; and *trans*: 20 mM CsCl, 30 mM $CsCH_3O_3S$, 10 mM TES and 1 mM [Ca^{2+}]. Each solution was adjusted to a pH of 7.4 with 4 M CsOH. BAPTA was used to chelate Ca^{2+} and to adjust the Ca^{2+} concentration. The purity of BAPTA was accessed using a Ca^{2+} electrode.

6.3.4.6 The bilayer setup

A planar bilayer technique (Laver, D.,2001) requires the presence of aqueous solution on each side of the bilayer. Therefore, two interconnected solution chambers are formed using a cup and a cup holder (**Figure 6-1**). The cup contains one of the reservoirs, while the unoccupied well in the cup holder forms the second reservoir. The cup is made of a lipophilic substance called Delrin, and contains a ~ 100 µm aperture across which a bilayer is painted. The reservoir to which SR vesicles are added is known as the *cis* chamber and is voltage clamped at +40 or -40 mV. The opposing chamber, known as the *trans* chamber, is grounded. The potentials are expressed according to standard physiological convention as $V_{cis} - V_{trans}$.

Both reservoirs were filled with 0.8 ml of *cis* and *trans* solutions (6.3.4.5) respectively and the artificial lipid mix (6.3.4.4) was smeared across the aperture in the Delrin cup using a flame-polished glass pipette. Next, 10 µg/ml of native skeletal SR vesicles was added into the *cis* chamber whilst stirring. In general channels incorporated with their cytoplasmic surface of the SR facing the *cis* solution and this was confirmed by characteristic changes in channel activity with changes in cytoplasmic ATP and Ca^{2+}

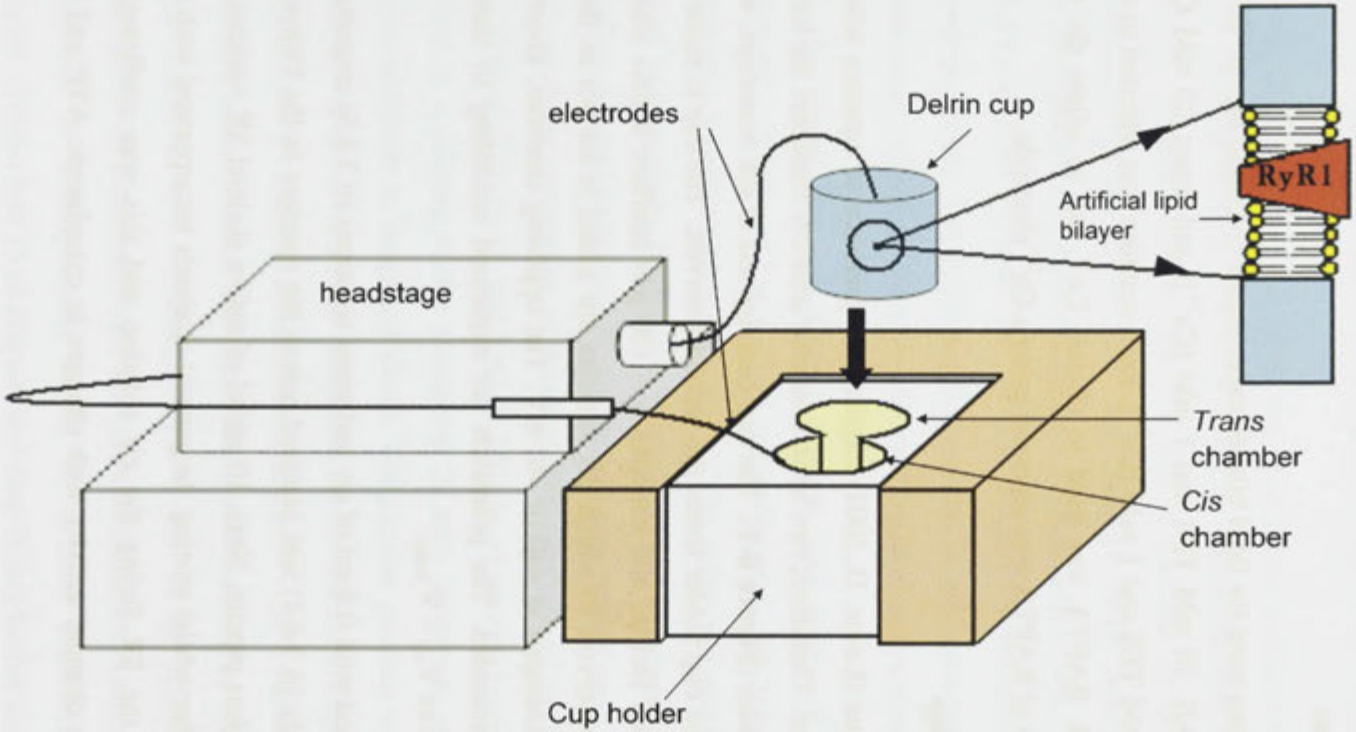

Figure 6-1 Bilayer setup. The deldrin cup fits into one well of the cup holder with the aperture facing the adjacent well. An artificial lipid bilayer is painted across this aperture. A brass block holds the cup holder in place. The gold pins of the electrodes are connected to the headstage as shown. The other ends of the electrodes, encased in agar bridges, rest within the cup or the cup holder. The electrode that rests in the cup is usually connected to the ground of the headstage and is called the *trans* electrode, while the electrode that rests in the unoccupied well of the cup holder is connected to the input of the headstage and is referred to as the *cis* electrode. A patch clamp amplifier receives input from and sends output to the head stage. The whole set up is encased in a faraday cage to reduce electrical noise.

concentration in the *cis* chamber. After channel incorporation, 200 mM $CsCH_3O_3S$ was added to the *trans* chamber to achieve solutions that were symmetrical (with respect to [Cs^+], [Cl-] and [CH_3O_3S]). The *cis* [Ca^{2+}] was then reduced to 10 μM by the addition of 1 mM BAPTA to the *cis* chamberCa^{2+} added to the cytoplasmic side of RyR1, has a biphasic effect on RyR1 channel activity. The threshold concentration for channel activation is approximately 100 nM with a maximum in the range of 10 – 100 μM, whereas high concentrations (mM) of Ca^{2+} almost entirely inhibits the channel (Meissner et al., 1986, Smith et al., 1988, Meissner, 2002, Fessenden et al., 2004). Addition of ATP to the cytoplasmic side of RyR1, in the presence of low concentrations (nM) of Ca^{2+} stimulates the RyR1 channel activity. In addition, cytoplasmic ATP elicits persistent channel activation at high concentrations (mM) of Ca^{2+} (Meissner, 1984, Meissner et al., 1986, Smith et al., 1988). Ruthenium red applied at micromolar concentrations to the *cis* chamber, specifically blocks the RyR1 channel (Smith et al., 1988, Ma, 1993, Xu et al., 1999). These characteristic responses of RyR1 to its agonists (Ca^{2+} and ATP) or antagonist (ruthenium red) were used to confirm the identity of the channel.

6.3.4.7 Single Channel recordings

Ryanodine receptor 1 (RyR1) channel activity was recorded using an Axopatch 200 amplifier (Molecular Devices, USA). Voltage was applied to the *cis* chamber while the *trans* chamber was held at ground and the *cis* voltage changed every 30 s between +40 mV and 40 mV. Current was recorded continuously throughout the experiment at 5 kHz and was filtered at 1 kHz. Proteins/peptides were added into the *cis* chamber to desired concentrations whilst stirring and were followed by recordings for several minutes under each condition. The washout step of the *cis* chamber was performed with approximately 10 ml of *cis* solution. Additional recordings were carried out before the addition of an approximately 1 mM ruthenium red to the *cis* chamber at the end of the experiment. Experiments were conducted at 23 ± 2°C.

6.3.4.8 Single Channel analysis

Single channel parameters were obtained using an in-house software Channel 2, developed by Prof. P.W. Gage and M. Smith (John Curtin School of Medical Research). Channel parameters were measured from 90s of channel activity at each potential, before and after the addition of the peptide. The following parameters were determined;

open probability (P_o), Fractional mean current ($I'f$), mean open time (T_o; ms) and mean closed time (T_c;ms), open frequency (F_o) which are defined by the following equations:

Open probability (Po) = $T_{open}/T_{total\ time}$

Fractional Mean Current (I'f) = I' / I_{max}

Mean open time (T_o; ms) = T_{open} / n

Mean closed time (T_c; ms) = T_{closed} / n

Open frequency (F_o) = n / T_{time}

Where T_{open} is the total channel open time; T_{closed} is the total channel closed time, n is the total number of channel openings, $T_{total\ time}$ is the total duration of the analysed record; I', mean current, an average of the current from all data points obtained during a recording period and I_{max}, maximal current of the analysed record.

RyR1 activity was quantified by calculating either or both: the probability that the channel would be open at any one time, i.e. open probability (P_o), or the average current as a function of the maximum current ($I'f$).

$I'f$ is approximately equal to P_o and it has been shown that P_o and $I'f$ values obtained from a record of a single channel with a high open probability are very similar (Beard et al., 2008). P_o most accurately quantifies RyR1 channel activity when only one channel is active in a bilayer, but $I'f$ is the most accurate measure of RyR1 activity when more than one channel is active. Since $I'f$ is approximately equal to P_o, all channel activity (measured as $I'f$ or P_o) is included in the average P_o presented in this thesis. To measure P_o, a threshold was set outside the noise at ~20% of the maximum open conductance, I_{max}, and currents exceeding the threshold were detected as channel openings. The closed threshold was placed above baseline noise. All analyses were corrected for baseline variation using an in-house program Baseline (developed by Dr. D. R. Laver).

6.3.4.9 Statistical analysis

Average data are given as mean ± SEM. Statistical significance was evaluated using paired or unpaired Student's t-test as appropriate or ANOVA. Numbers of

observations (n) are given in Tables and Figure legends. If there were separate sets of control data for each concentration of protein, ANOVA and the Mahalanobis test was used. To reduce effects of variability in control open probability (P_oc), and to evaluate test parameters after protein addition (P_ot), data were expressed as the difference between the $\log_{10} P_oc$ and $\log_{10} P_ot$ for each channel (e.g. $\log_{10} P_oc - \log_{10} P_ot$). The difference from control was assessed with a paired t-test applied to $\log_{10} P_{oC}$ and $\log_{10} P_ot$. The difference between each concentration was assessed using ANOVA on $\log_{10} P_oc - \log_{10} P_ot$ at each concentration with the multidimensional Mahalanobis test. The difference between $\log_{10} - P_oc - \log_{10} P_ot$ at +40 mV and at -40 mV at each concentration was assessed using the Student's t-test. A *P* value of <0.05 was considered significant for all tests.

6.4 Results

6.4.1 The effect of full length β_{1a} subunit on RyR1 channel activity

The effect of adding the full length β_{1a} subunit to a RyR1 channel embedded in an artificial lipid bilayer was investigated by Dr. Esther Gallant (Muscle research Group, JCSMR).

The recombinant (Ch.3.3.1) β_{1a} subunit (expressed and purified by the author of this thesis) was added to the cytoplasmic (*cis*) side of a single RyR1 channel in a lipid bilayer. Each RyR1 channel was exposed to one concentration of β_{1a} for 15 to 20 min and the protein was then removed by perfusion. The cytoplasmic (*cis*) [Ca^{2+}] in this experiment was 10μM, and the luminal (*trans*) [Ca^{2+}] was 1mM.

A strong increase in activity was apparent within 1min of addition of only 10nM of the protein and this was maintained until the *cis* chamber was perfused to remove the β_{1a} subunit. Activity fell towards control levels following perfusion (**Figure 6-2**). However the effect of β_{1a} was not always reversible within the lifetime of the bilayer (10 to 20min

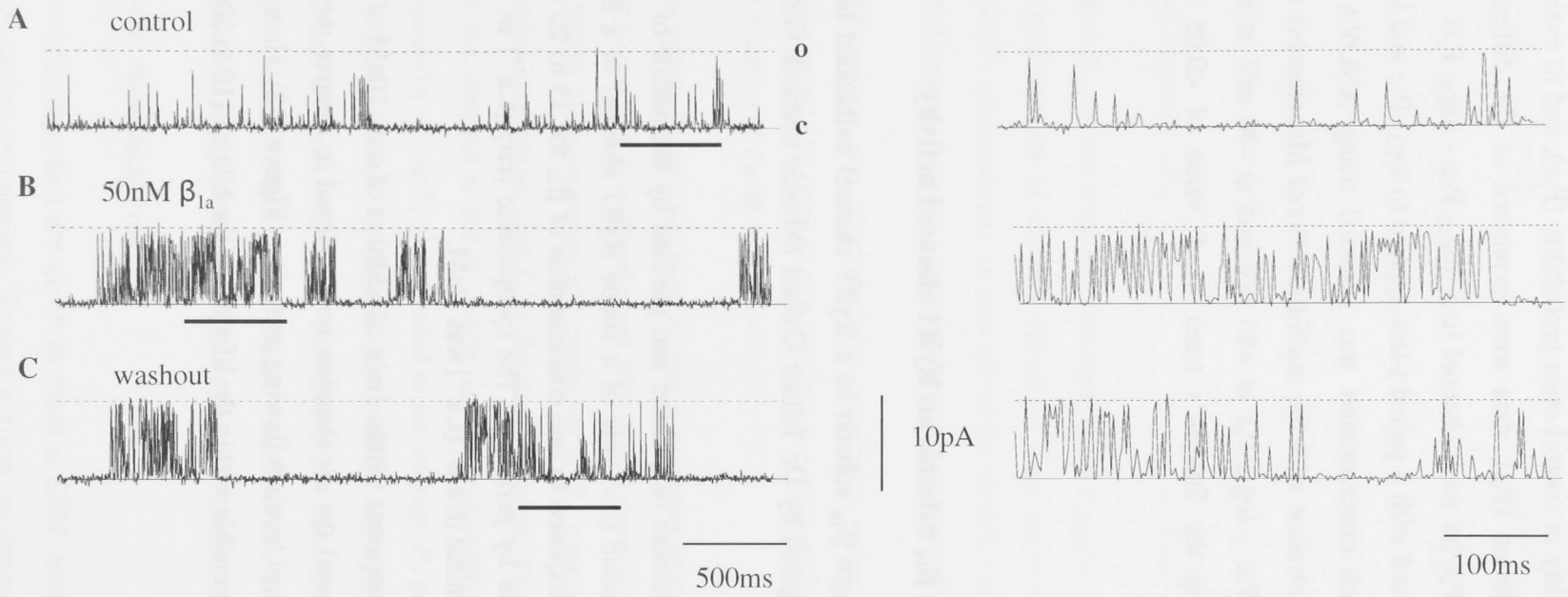

Figure 6-2 Effect of full length β_{1a} on RyR1 channel activity A) control recording before the addition of β_{1a} **B)** addition of 50 nM β_{1a} – channel activity increases **C)** washout - channel activity decreases but does not completely return to control levels. The left panel shows 3 s recordings of representative channel activity at +40 mV and the right panel shows expansions of data underlined by thick black lines in the 3 s records to illustrate the changes in open duration. "o" – maximum open current indicated by broken lines. "c" – zero current (closed state of channel) indicated by continuous lines. Channel records obtained from Dr. Esther Gallant (Muscle research Group. JCSMR).

after perfusion) with only 15 of 27 channels showing a decrease in activity after washout of ≥10nM of the β_{1a} subunit.

The effects of the full length β_{1a} on channel activity were similar at +40 mV and at -40 mV. There was an average 2.3±0.4 -fold increase in P_o at +40 mV and an average 3.8±1.0 at -40 mV after adding 100 nM β_{1a} subunit (i.e. the average of P_{ot}/P_{oc} for individual channels). Thus measurements at +40 mV and -40 mV were combined in all average data. There was a significant increase in average relative open probability (open probability of each channel in the presence of the subunit compared with its internal control before exposure to protein, i.e. log P_{ot}-log P_{oc}) with protein concentrations

≥10nM (**Figure 6-3A**). The increase in open probability was primarily due to a significant prolongation of open times (**Figure 6-3B**) with abbreviation of closed times (**Figure 6-3C**).

Buffer alone, added at the same volume as that added with 1μM protein, had no effect on channel activity (first bar in each graph, Figure **6-3A-C**).

6.4.2 The effect of the 35-residue C terminal tail of β_{1a} (β_{1a}-C35) on RyR1 channel activity

Preliminary investigations into the effects of adding the native β_{1a}-C35 peptide to a RyR1 channel embedded in an artificial lipid bilayer were carried out by the author of this thesis. Further investigations into this interaction was undertaken by Ms. Robyn Rebbeck from the Muscle Research Group, JCSMR (Rebbeck et al., 2011).

As with the full length protein, the β_{1a}-C35 peptide was added to the cytoplasmic (*cis*) side of a single RyR1 channel in a lipid bilayer and the experiments were performed with 10 μM cytoplasmic (*cis*) Ca^{2+} and 1mM luminal (*trans*) Ca^{2+}. Each RyR1 channel was exposed to one concentration of the peptide for 15 to 20 min and then removed by perfusion.

The β_{1a}-C35 peptide was as effective as the full length protein in increasing native RyR1 channel activity (**Figure 6-4**). Concentrations as low as 100 pM in the cytoplasmic (*cis*) solution caused a substantial increase in activity in 5 of 7 individual channels (**Figure 6-5A**), although the average increase in open probability at this

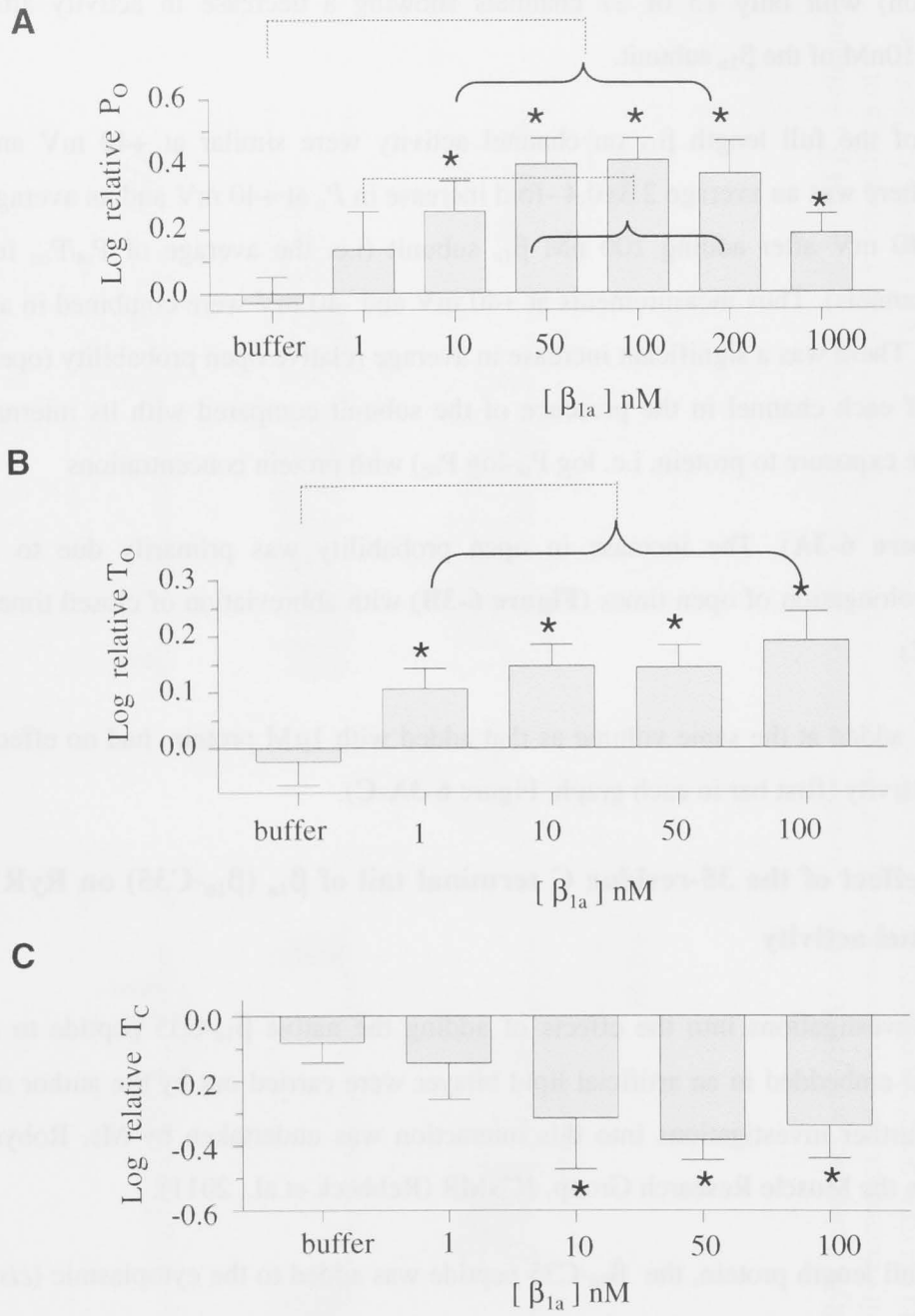

Figure 6-3 Changes in RyR1 channel activity parameters upon the addition of full length β_{1a}. A) Relative P_O (log rel P_O) is the average of differences between the $\log_{10}$ of P_O in the presence of the β_{1a} subunit ($\log P_{OB}$) and $\log_{10}$ of the control P_O ($\log P_{OC}$) for each channel, with P_O measured over 180 s. **B)** The relative mean open time (log rel T_O) is $\log T_{OB}$-$\log T_{OC}$. **C)** The relative mean closed time (log rel T_C) is $\log T_{CB}$-$\log T_{CC}$. N = 5–8 experiments for each bin in A-C. Asterisks indicate significant changes from control induced by the β_{1a} protein. The broken lines indicate significant differences between each bin under the horizontal bracket and data at the far end of the line. A P value of <0.05 was considered significant. Data obtained from Dr. Esther Gallant (Muscle research Group. JCSMR).

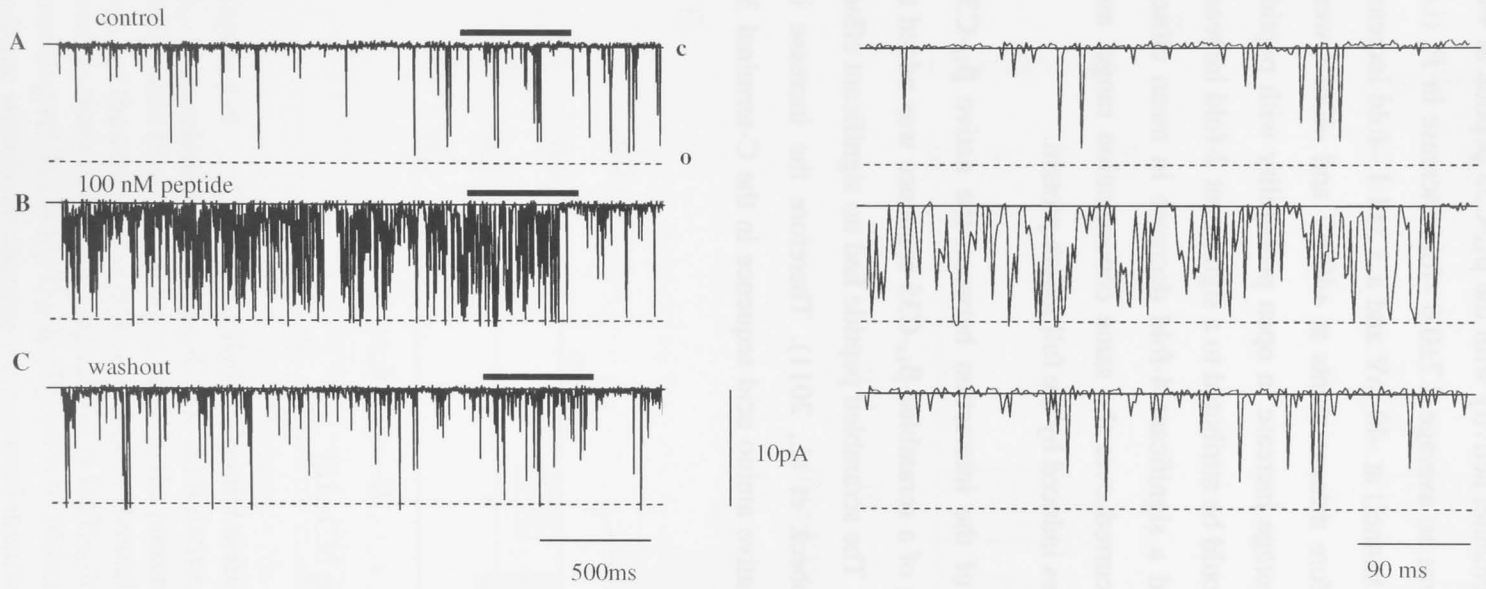

Figure 6-4 Effect of β_{1a}-C35 peptide on RyR1 channel activity A) control recording before the addition of β_{1a}-C35 peptide **B)** addition of 10 nM β_{1a}-C35 peptide – channel activity increases **C)** washout - channel activity decreases but does not completely return to control levels. The left panel shows 3 s recordings of representative channel activity at -40 mV and the right panel shows expansions of data underlined by thick black lines in the 3 s records to illustrate the changes in open duration. "o" – maximum open current indicated by broken lines. "c" – zero current (closed state of channel) indicated by continuous lines.

concentration was not statistically significant. Similar to the full length protein, the effects of the peptide were not easily reversible, with a clear decrease in activity seen in only 9 of 18 channels following washout of ≥10 nM of the peptide.

As with full length β_{1a}, the changes in channel activity with the β_{1a}-C35 peptide at +40 mV and -40 mV were similar. There was an average 2.7±0.6 –fold increase in P_o (i.e. average of P_{ot}/P_{oC} for each individual channel) at -40 mV and a 3.3±1.1 –fold increase at +40mV with 100nM peptide. Therefore measurements at +40mV and -40mV were combined in the average data. The average increase in open probability with peptide concentrations ≥10nM (**Figure 6-5A**) could be attributed to a significant 2-fold increase in mean open time (**Figure 6-5B**), and a significant 4-fold decrease in mean closed time(**Figure 6-5C**). These changes occurred over the same concentration range, and were similar in magnitude, to the changes induced by the full length protein.

In order to determine the specificity of the interaction between the native β_{1a}-C35 peptide and RyR1, a peptide consisting of a scrambled β_{1a}-C35 sequence was added to the cytoplasmic side of RyR1 channels. The scrambled peptide had no significant effect on channel activity (**Figure 6-6**, Rebbeck et al., 2011). Therefore the increase in channel activity required the specific native amino acid sequence in the C-terminal 35 residues of the β_{1a} subunit.

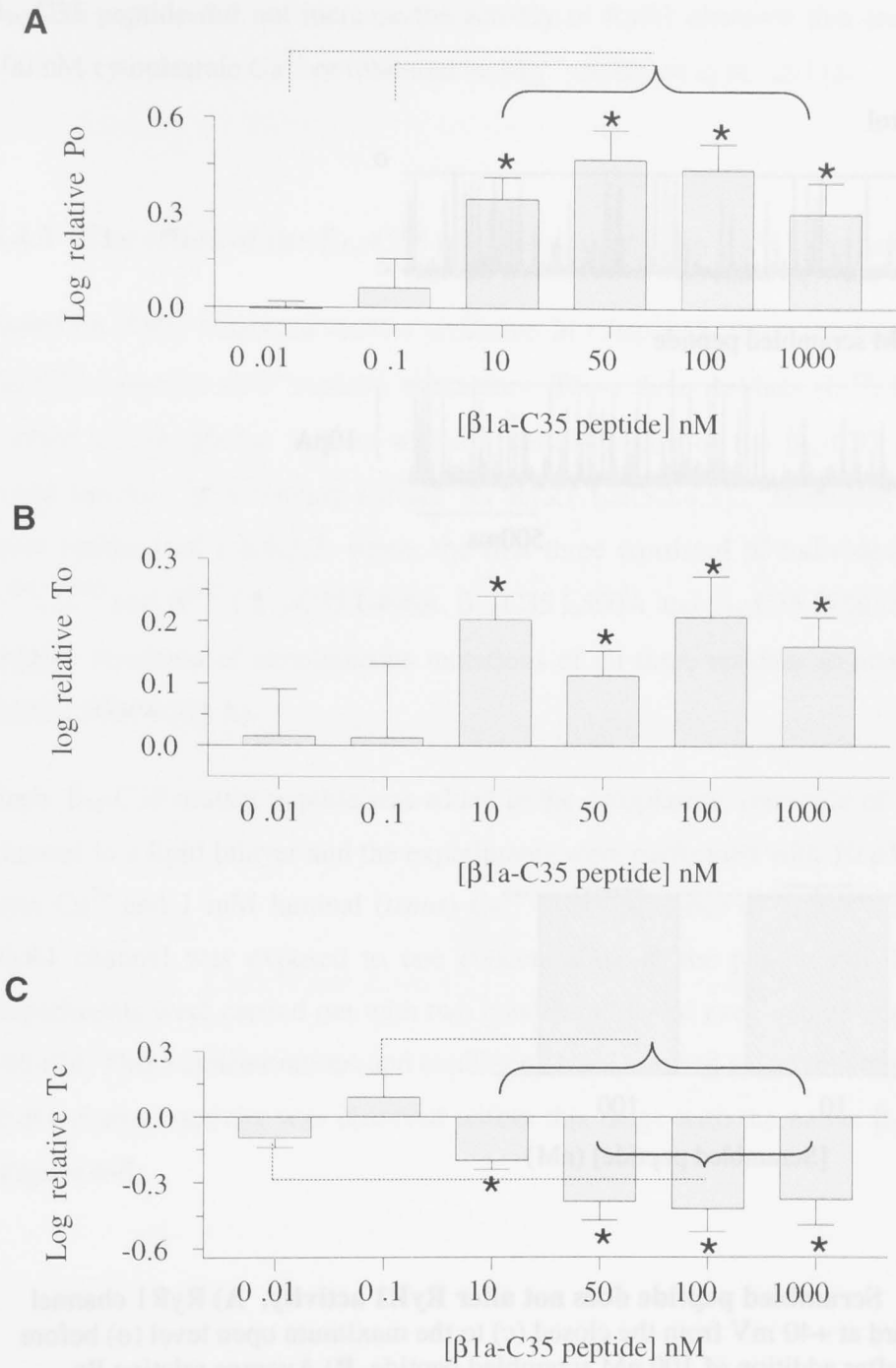

Figure 6-5 Changes in RyR1 channel activity parameters upon the addition of β_{1a}-C terminal peptide (β_{1a}-C35). A) Relative P_O (log rel P_O) is the average of differences between the $\log_{10}$ of P_O in the presence of the β_{1a}-C35 peptide ($\log P_{OB}$) and $\log_{10}$ of the control P_O ($\log P_{OC}$) for each channel, with P_O measured over 180 s. **B)** The relative mean open time (log rel T_O) is $\log T_{OB}$-$\log T_{OC}$. **C)** The relative mean closed time (log rel T_C) is $\log T_{CB}$-$\log T_{CC}$. N = 5–10 experiments for each bin in A-C. Asterisks indicate significant changes from control induced by the β_{1a}-C35 peptide. The broken lines indicate significant differences between each bin under the horizontal bracket and data at the far end of the line. A P value of <0.05 was considered significant. Data obtained from Ms. Robyn Rebbeck (Muscle research Group. JCSMR).

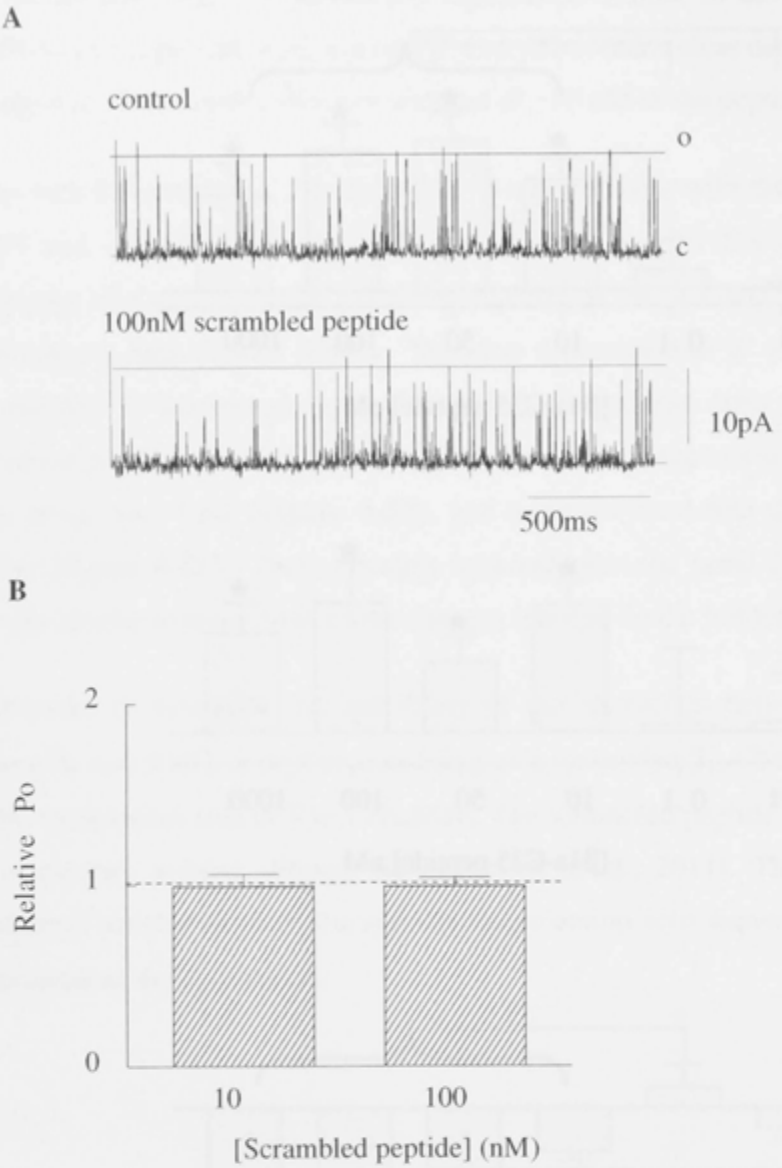

Figure 6-6 Scrambled peptide does not alter RyR1 activity. A) RyR1 channel opening upward at +40 mV from the closed (c) to the maximum open level (o) before (control) and after addition of 100 nM scrambled peptide. **B**) Average relative Po (PoP/PoC) after exposure to 10 and 100 nM scrambled peptide (N = 7 experiments) Data obtained from Ms. Robyn Rebbeck (Muscle research Group. JCSMR).

The interaction between the β_{1a}-C35 peptide and RyR1 was also investigated in the presence of 2 mM ATP (and 10 μM Ca^{2+}) in the cytoplasmic (*cis*) solution. The changes seen in channel gating characteristics and the concentration-dependence of the changes in the presence of 2 mM ATP were very similar to those described for the full-length β_{1a} subunit and for the β_{1a}-C35 peptide in the absence of ATP (Rebbeck et al., 2011). Further experiments performed with varying Ca^{2+} and Mg^{2+} concentrations indicated the

β_{1a}-C35 peptide did not increase the activity of RyR1 channels that are inactive with 100 nM cytoplasmic Ca^{2+} or inhibited be Mg^{2+} (Rebbeck et al., 2011).

6.4.3 The effect of the β_{1a}-C35 mutant peptides on RyR1 channel activity

Based on NMR structural studies presented in Chapter 5, three residues of the native β_{1a}-C35 sequence were mutated to alanines. These three residues (L^{496}, L^{500} and W^{503}) formed a hydrophobic surface within a helical region of the β_{1a}-C35 peptide which could function as a binding surface for RyR1 (ch.5.3.4.3). Therefore, four peptides were synthesized (ch.6.3.2) where the first three consisted of individual mutations in L^{496}, L^{500} and W^{503} (β_{1a}-C35 L496A, β_{1a}-C35 L500A and β_{1a}-C35 W503A). The fourth peptide consisted of simultaneous mutations of all three residues to alanines (β_{1a}-C35 L496/L500/W503 A).

Each β_{1a}-C35 mutant peptide was added to the cytoplasmic (*cis*) side of a single RyR1 channel in a lipid bilayer and the experiments were performed with 10 μM cytoplasmic (*cis*) Ca^{2+} and 1 mM luminal (*trans*) Ca^{2+} in the presence of 2 mM *(cis)* ATP. Each RyR1 channel was exposed to one concentration of the peptide for 15 to 20 min. Experiments were carried out with two concentrations of each mutant peptide – 10 and 100 nM. These concentrations and conditions were selected as the maximum increase in RyR1 channel activity was observed within this range with the native β_{1a}-C35 peptide (**Figure 6-5**).

Unlike the native β_{1a}-C35 peptide, the mutant peptides showed a voltage dependence in their effect on the ryanodine receptor. The simultaneous mutation of all three hydrophobic residues to alanines (β_{1a}-C35 L496/L500/W503 A) resulted in an inhibitory effect on RyR1 (**Figure 6-7**).

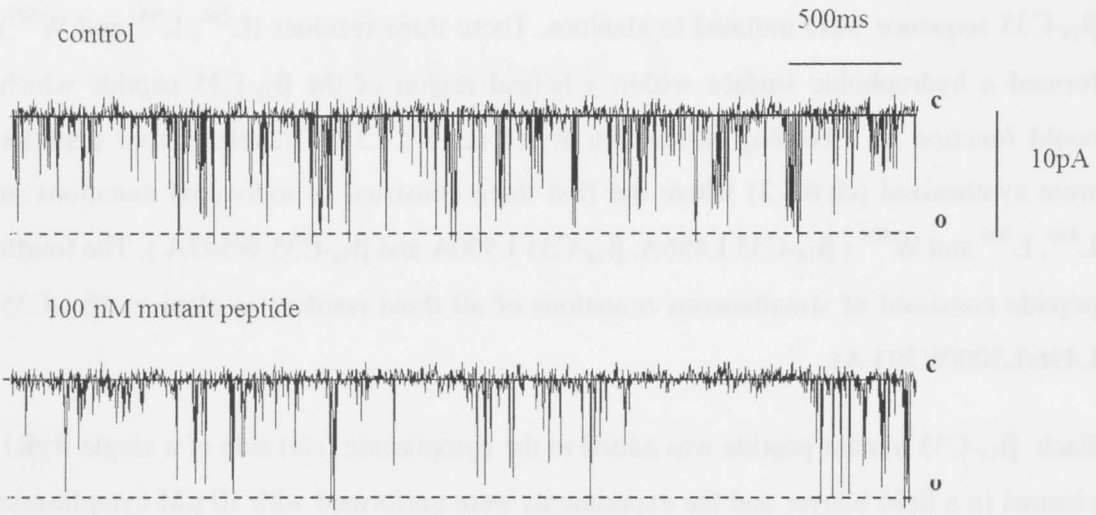

Figure 6-7 Triple mutant peptide, β_{1a}-C35 L496/L500/W503 A inhibits RyR1 activity. 3 s recordings of representative channel activity at - 40 mV. RyR1 channel opening downward at - 40 mV from the closed (c) to the maximum open level (o) before (control) and after addition of 100 nM peptide.

At +40 mV the triple mutant peptide caused an inhibition of the ryanodine receptor at both 10 and 100 nM. At -40 mV it was unable to activate the RyR1 at 10 nM and showed an inhibitory effect at 100 nM (**Figure 6-8**). The inhibitory effect caused by the triple mutant at +40 mV was due to a 2 fold increase in mean closed times (T_c) and a >0.5 fold decrease in mean open frequency. This was seen at both concentrations of 10 nM and 100 nM. At -40 mV, the inhibitory effect was mostly due to >2 fold decrease in the mean open frequency (**Figure 6-9**).

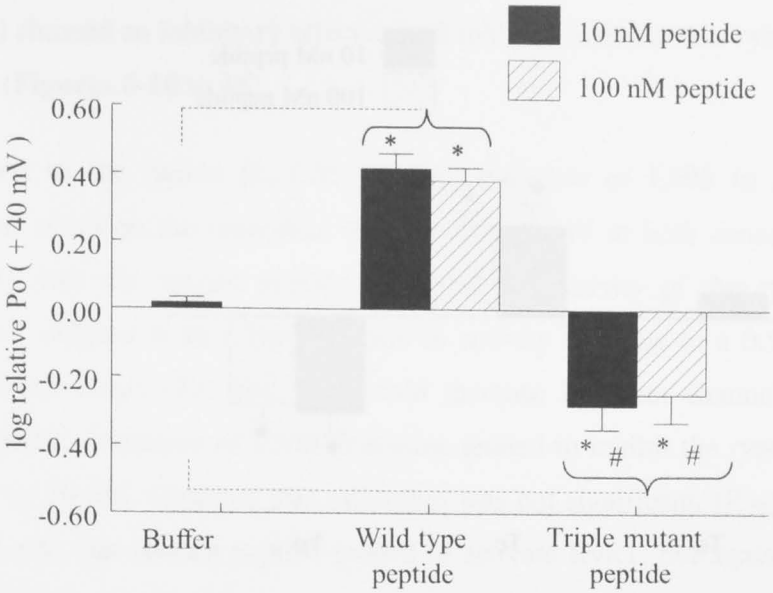

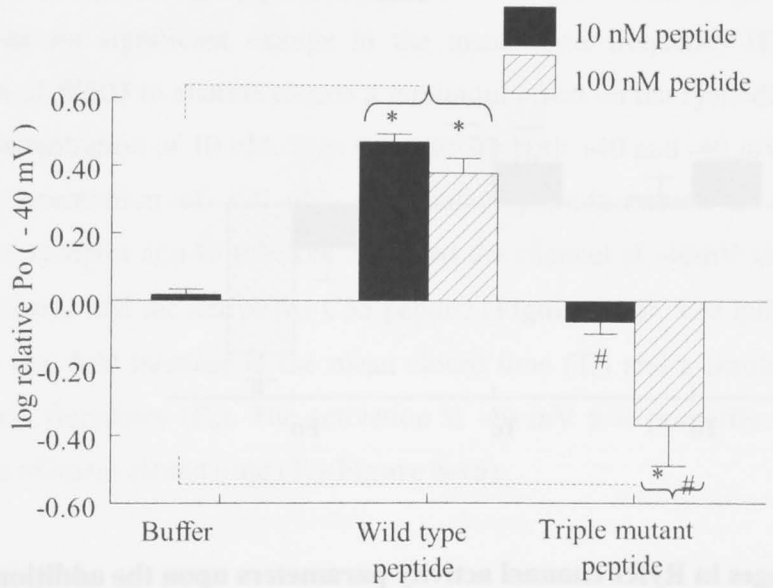

Figure 6-8 Changes in log relative open probability of RyR1 upon the addition of the triple mutant peptide β_{1a}-C35 L496/L500/W503 A . Relative P_O (log rel P_O) is the average of differences between the $\log_{10}$ of P_O in the presence of the mutant peptide ($\log P_{OB}$) and $\log_{10}$ of the control P_O ($\log P_{OC}$) for each channel, with P_O measured over 180 s. **A)** The triple mutant peptide inhibits the channel at +40 mV. **B)** The triple mutant peptide inhibits the channel at – 40 mV and 100 nM ($N = 5$ in each bin). "*" indicate significant changes from control induced by the mutant peptide. "#" indicates significant differences between the mutant peptide and the wild type. The broken lines indicate significant differences between each bin under the horizontal bracket and buffer. A P value of <0.05 was considered significant. Results are means ±SEM.

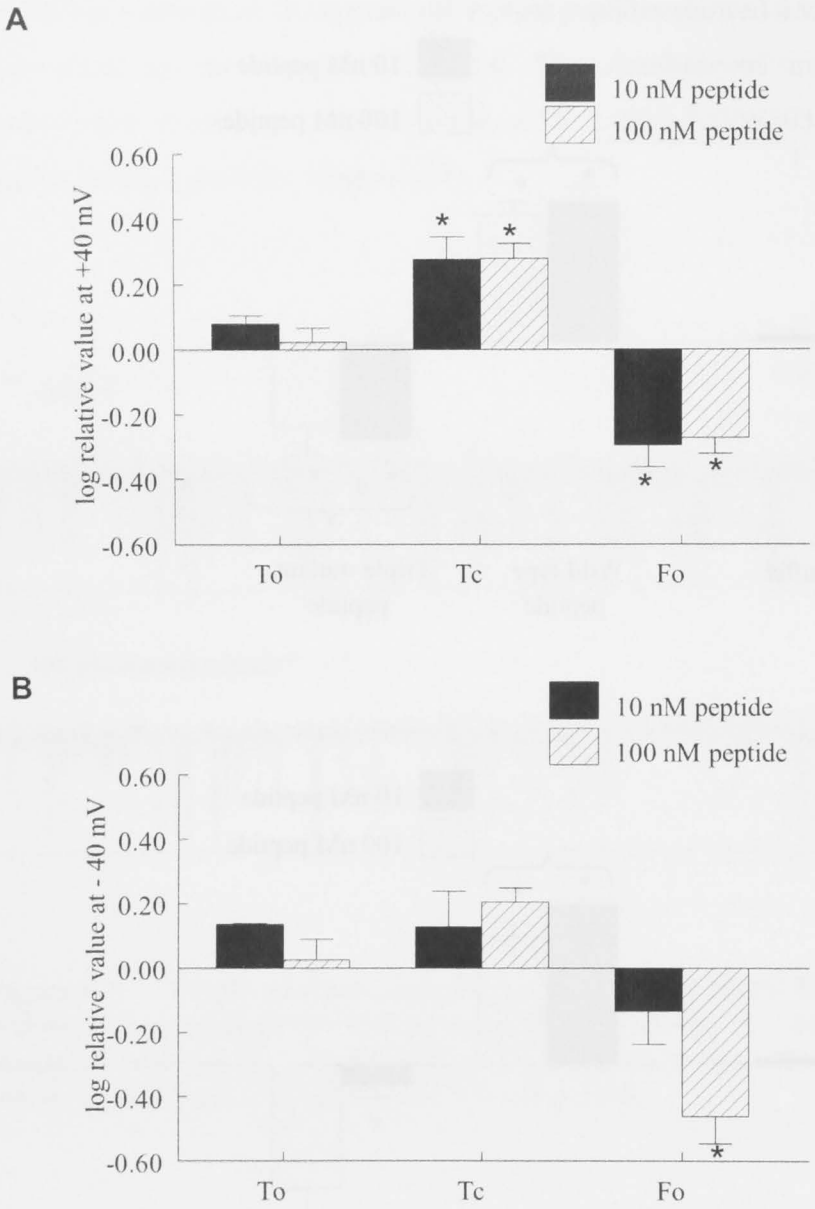

Figure 6-9 Changes in RyR1 channel activity parameters upon the addition of the triple mutant peptide β_{1a}-C35 L496/L500/W503 A. Relative mean open time, T_O (log rel T_O) is the average of differences between the $\log_{10}$ of T_O in the presence of the mutant peptide ($\log T_{OB}$) and $\log_{10}$ of the control T_O ($\log T_{OC}$) for each channel, with T_O measured over 180 s.The relative mean closed time (log rel T_C) is $\log T_{CB}$-$\log T_{CC}$. The relative mean open frequency (log rel F_O) is log F_{OB}-$\log F_{OC}$. **A)** There is a statistically significant increase in Tc and a decrease in Fo leading to inhibition of RyR1 at +40 mV. **B)** There is a statistically significant decrease in Fo leading to inhibition of the channel upon the addition of 100 nM of the triple mutant peptide at -40 mV. (N = 5 experiments for each bin) "*" indicate significant changes from control induced by the mutant peptide. A P value of <0.05 was considered significant. Results are means ±SEM.

Overall, all three single mutant peptides (β_{1a}-C35 L496A, β_{1a}-C35 L500A and β_{1a}-C35 W503A) showed an inhibitory effect at +40 mV, but activated the ryanodine receptor at -40 mV (**Figures 6-10 to 15**).

Compared to the native β_{1a}-C35 peptide, mutation of L496 to alanine caused a minimum effect on the ryanodine receptor at +40 mV at both concentrations (10 and 100 nM). But the mutant peptide increased the activity of the ryanodine receptor at -40 mV (**Figure 6-10**). This increase in activity was due to a 0.5 fold decrease in mean closed times (Tc) and a 1.5 fold increase in mean channel open frequency (**Figure 6-11**). Mutation of L500 to alanine tended to inhibit the ryanodine receptor at +40 mV at 10 nM. However this inhibition was not significant. ($P = 0.06$). At 100 nM and +40 mV, this mutant peptide tended to activate RyR1, but again the increase was not significant. At -40 mV, the mutant peptide, β_{1a}-C35 L500A activated the ryanodine receptor at both concentrations similar to the native β_{1a}-C35 peptide (**Figure 6-12**). This activation was primarily due to an >0.6 fold decrease in the mean closed time (T_c). There was no significant change in the mean open frequency (F_o)(**Figure 6-13**) Mutation of W503 to alanine caused a minimum effect on the ryanodine receptor at the lower concentration of 10 nM. This was true for both +40 and -40 mV. However at the higher concentration of 100 nM, this mutant peptide caused an inhibition of the ryanodine receptor at +40 mV, but activated the channel at -40mV similar to the other single mutants and the native β_{1a}-C35 peptide (**Figure 6-14**). The inhibitory effect was due to a two fold increase in the mean closed time (T_c) and a similar decrease in the mean open frequency (F_o). The activation at -40 mV was primarily due to a 0.7 fold reduction of mean closed time (T_c)(**Figure 6-15**).

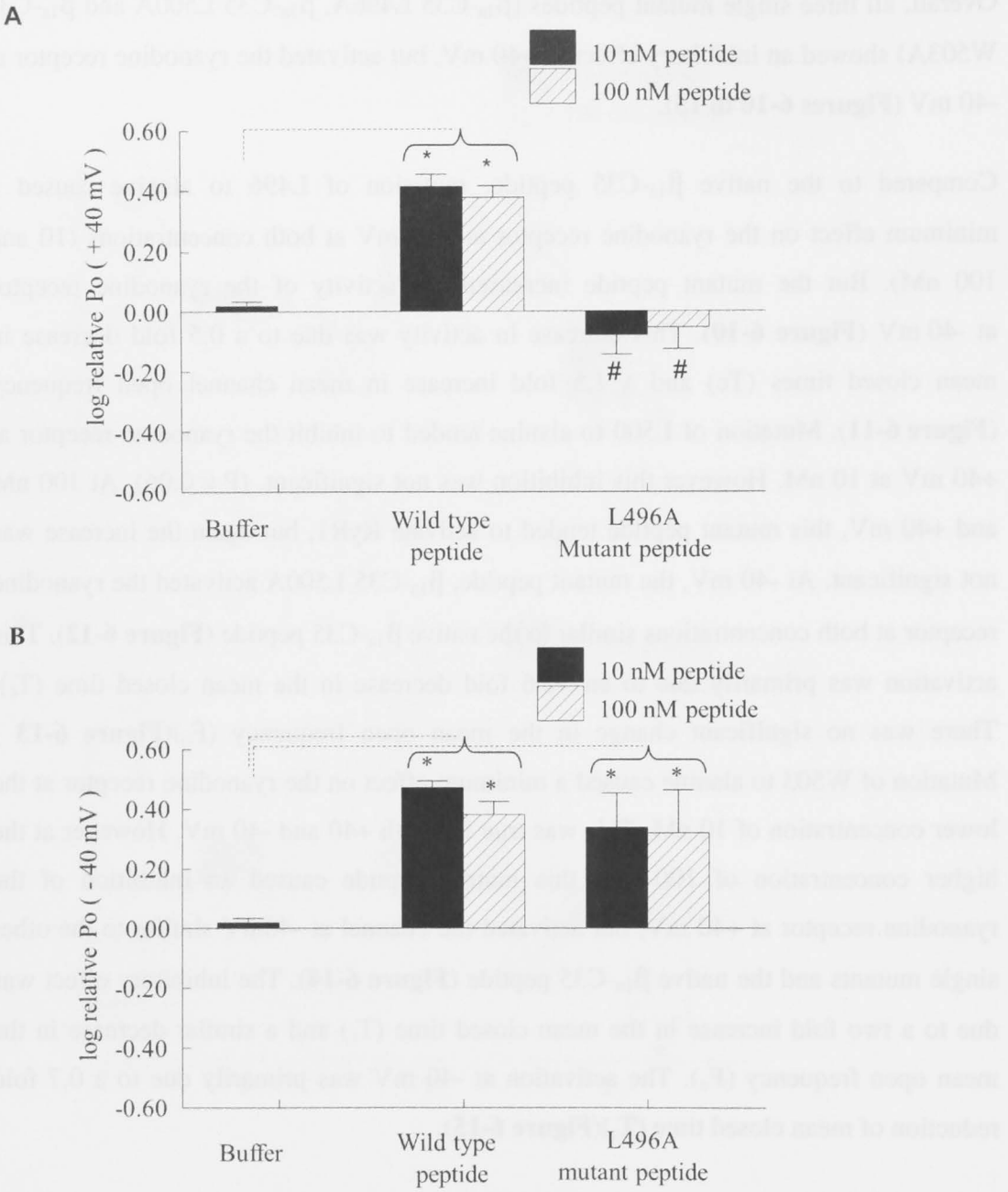

Figure 6-10 Changes in log relative open probability of RyR1 upon the addition of the mutant peptide β_{1a}-C35 L496A . Relative P_O (log rel P_O) is the average of differences between the $\log_{10}$ of P_O in the presence of the mutant peptide ($\log P_{OB}$) and $\log_{10}$ of the control P_O ($\log P_{OC}$) for each channel, with P_O measured over 180 s. **A)** Mutant peptide L496A does not activate the channel at +40 mV. **B)** Mutant peptide L496A activates the channel at – 40 mV. (N = 5 in each bin). "*" indicate significant changes from control induced by the mutant peptide. "#" indicates significant differences between the mutant peptide and the wild type. The broken lines indicate significant differences between each bin under the horizontal bracket and buffer. A P value of <0.05 was considered significant. Results are means ±SEM.

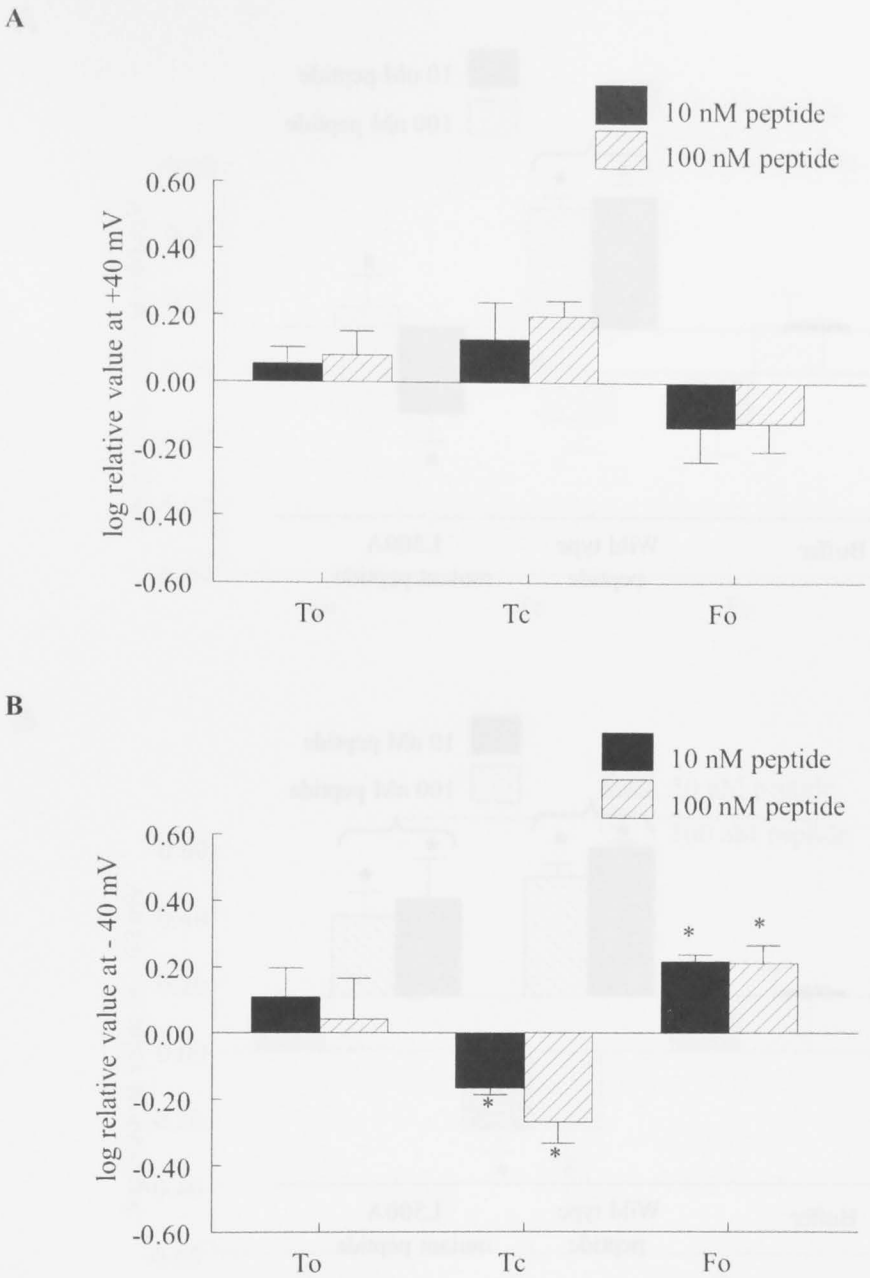

Figure 6-11 Changes in RyR1 channel activity parameters upon the addition of the mutant peptide β_{1a}-C35 L496A . Relative mean open time, T_O (log rel T_O) is the average of differences between the $\log_{10}$ of T_O in the presence of the mutant peptide ($\log T_{OB}$) and $\log_{10}$ of the control T_O ($\log T_{OC}$) for each channel, with T_O measured over 180 s.The relative mean closed time (log rel T_C) is $\log T_{CB}$-$\log T_{CC}$. The relative mean open frequency (log rel F_O) is log F_{OB}-$\log F_{OC}$. **A)** There is no significant change in any of the parameters upon the addition of L496A peptide at +40 mV. **B)** There is a statistically significant decrease in Tc and and increase in Fo leading to activation of the channel at -40 mV. (N = 5 experiments for each bin) "*" indicate significant changes from control induced by the mutant peptide. A P value of <0.05 was considered significant. Results are means ±SEM.

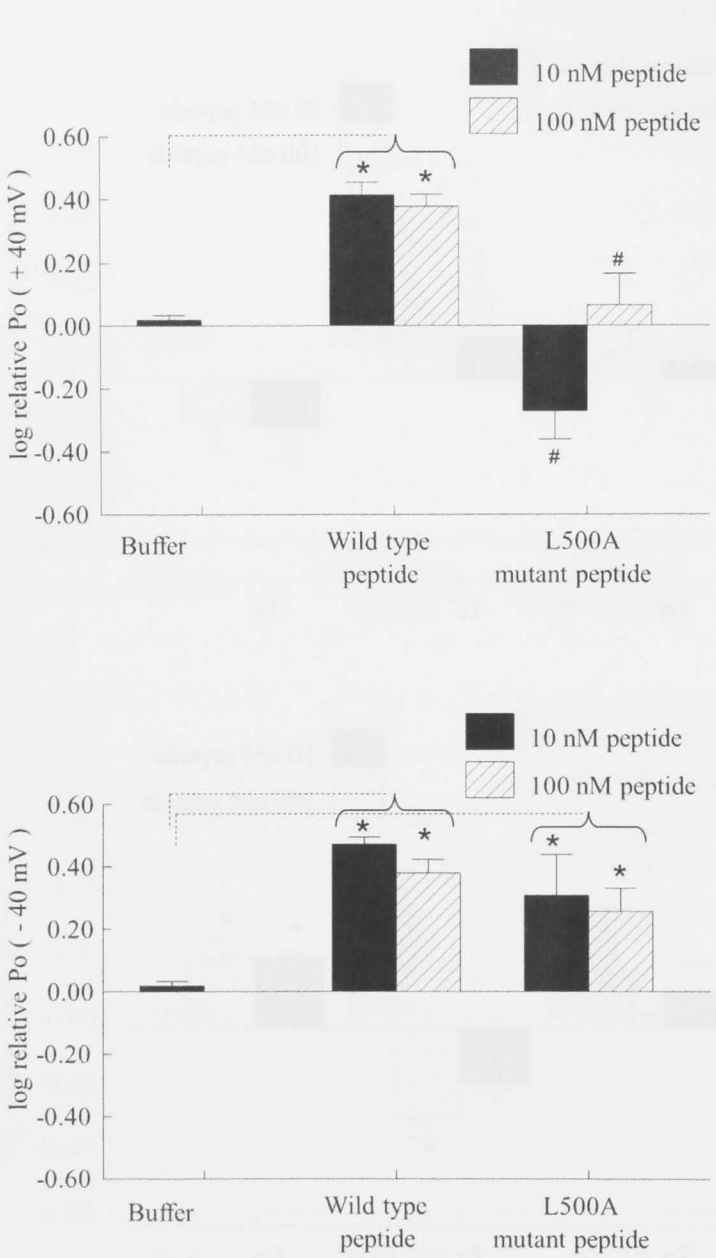

Figure 6-12 Changes in log relative open probability of RyR1 upon the addition of the mutant peptide β_{1a}-C35 L500A . Relative P_O (log rel P_O) is the average of differences between the $\log_{10}$ of P_O in the presence of the mutant peptide ($\log P_{OB}$) and $\log_{10}$ of the control P_O ($\log P_{OC}$) for each channel, with P_O measured over 180 s. **A)** Mutant peptide L500A does not activate the channel at +40 mV. **B)** Mutant peptide L500A activates the channel at – 40 mV. ($N = 5$ in each bin). "*" indicate significant changes from control induced by the mutant peptide. "#" indicates significant differences between the mutant peptide and the wild type. The broken lines indicate significant differences between each bin under the horizontal bracket and buffer. A P value of <0.05 was considered significant. Results are means ±SEM.

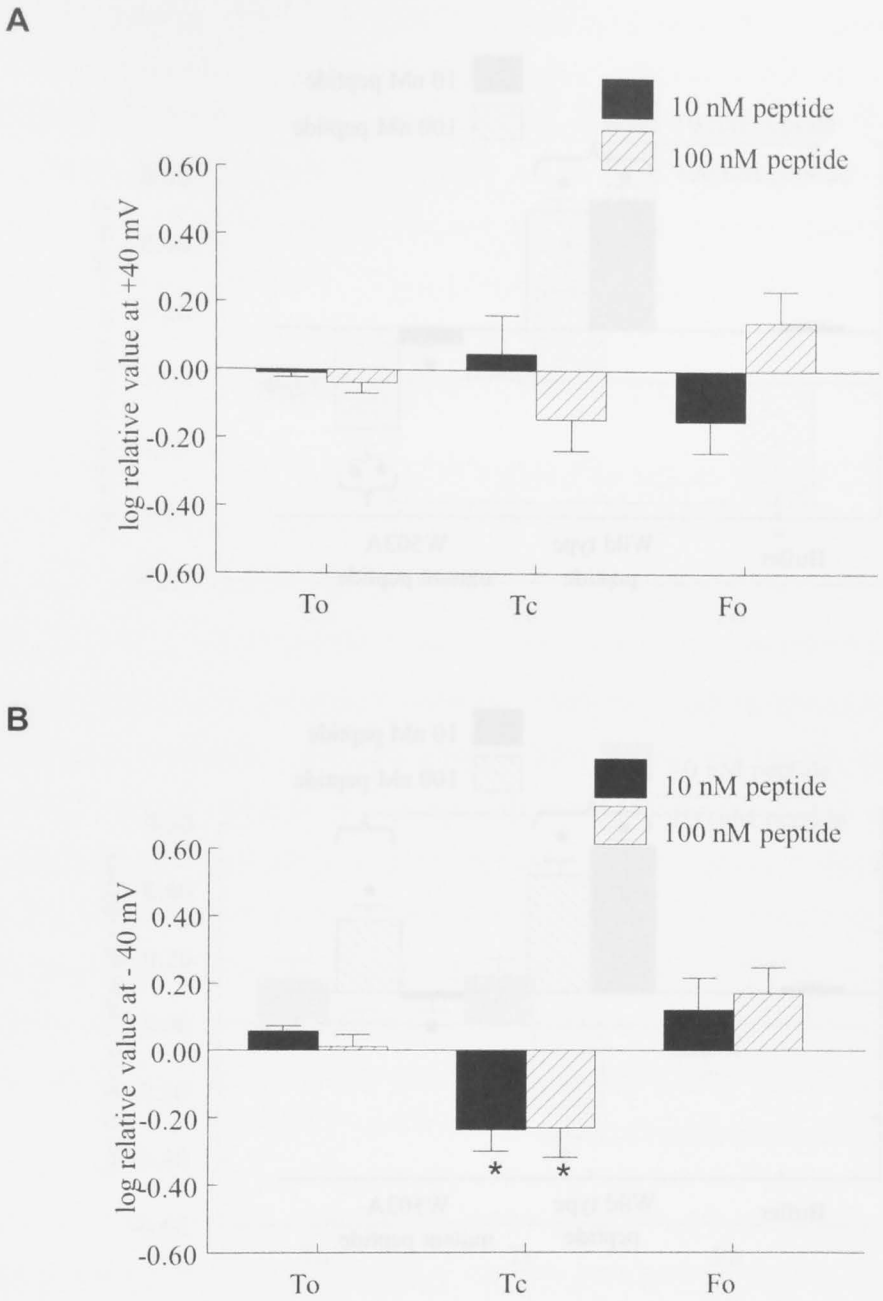

Figure 6-13 Changes in RyR1 channel activity parameters upon the addition of the mutant peptide β_{1a}-C35 L500A . Relative mean open time, T_O (log rel T_O) is the average of differences between the $\log_{10}$ of T_O in the presence of the mutant peptide ($\log T_{OB}$) and $\log_{10}$ of the control T_O ($\log T_{OC}$) for each channel, with T_O measured over 180 s.The relative mean closed time (log rel T_C) is $\log T_{CB}$-$\log T_{CC}$. The relative mean open frequency (log rel F_O) is log F_{OB}-$\log F_{OC}$. **A)** There is no significant change in any of the parameters upon the addition of L500A peptide at +40 mV. **B)** There is a statistically significant decrease in Tc leading to activation of the channel at -40 mV. (N = 5 experiments for each bin) "*" indicate significant changes from control induced by the mutant peptide. A P value of <0.05 was considered significant. Results are means ±SEM.

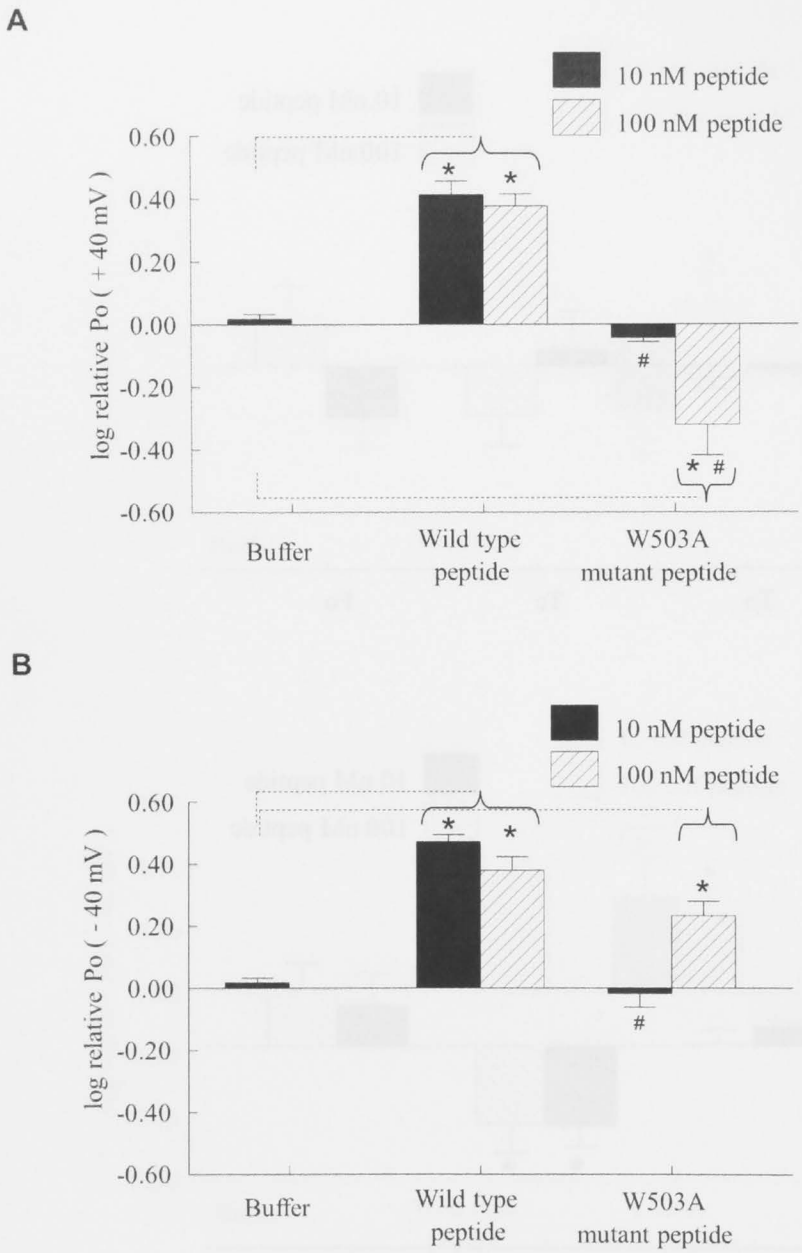

Figure 6-14 Changes in log relative open probability of RyR1 upon the addition of the mutant peptide β_{1a}-C35 W503A . Relative P_O (log rel P_O) is the average of differences between the $\log_{10}$ of P_O in the presence of the mutant peptide ($\log P_{OB}$) and $\log_{10}$ of the control P_O ($\log P_{OC}$) for each channel, with P_O measured over 180 s. **A)** Mutant peptide W503A does not activate the channel at +40 mV. It inhibits the channel at 100 nM **B)** Mutant peptide W503A activates the channel at – 40 mV and 100 nM ($N = 5$ in each bin). "*" indicate significant changes from control induced by the mutant peptide. "#" indicates significant differences between the mutant peptide and the wild type. The broken lines indicate significant differences between each bin under the horizontal bracket and buffer. A P value of <0.05 was considered significant. Results are means ±SEM.

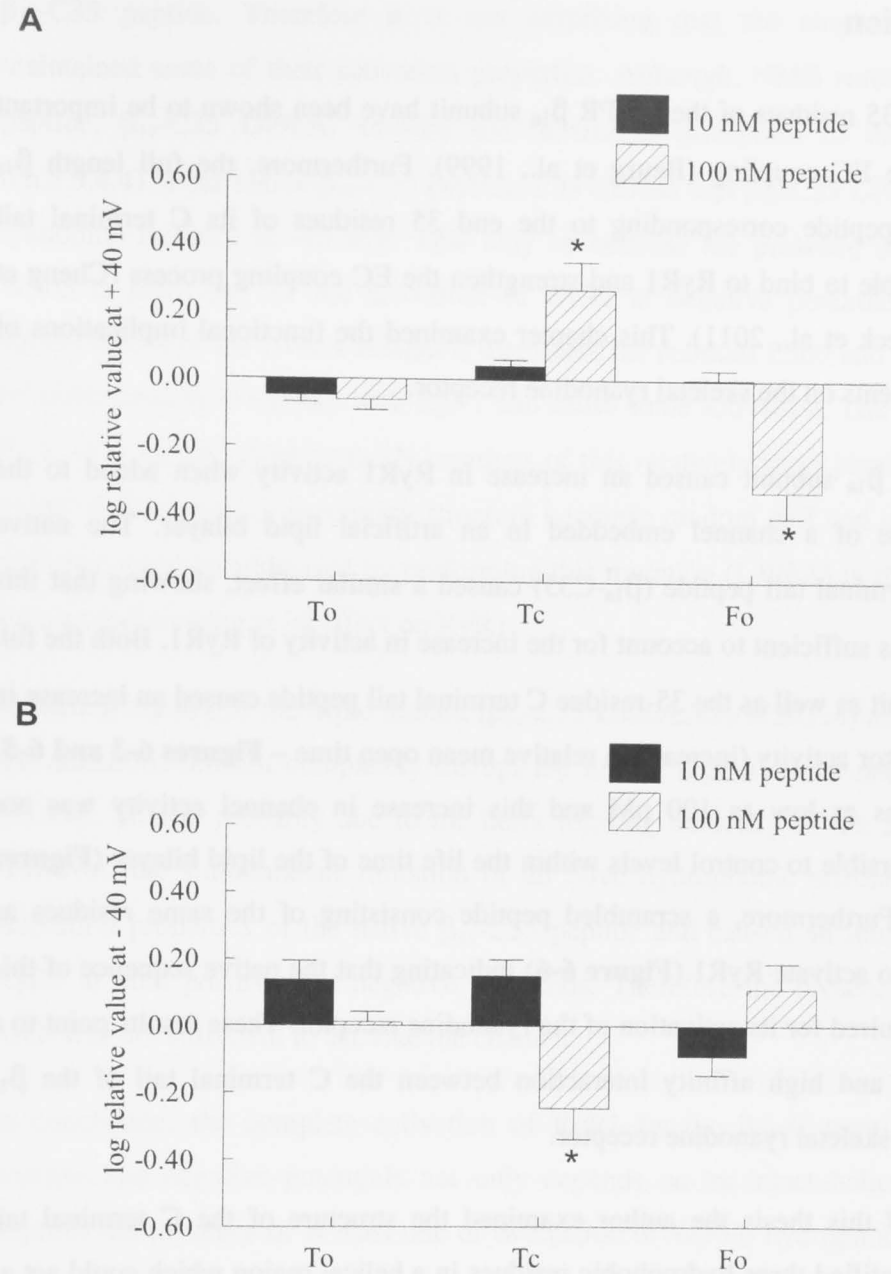

Figure 6-15 Changes in RyR1 channel activity parameters upon the addition of the mutant peptide β_{1a}-C35 W503A . Relative mean open time, T_O (log rel T_O) is the average of differences between the $\log_{10}$ of T_O in the presence of the mutant peptide ($\log T_{OB}$) and $\log_{10}$ of the control T_O ($\log T_{OC}$) for each channel, with T_O measured over 180 s.The relative mean closed time (log rel T_C) is $\log T_{CB}$-$\log T_{CC}$. The relative mean open frequency (log rel F_O) is log F_{OB}-$\log F_{OC}$. **A)** There is a statistically significant increase in Tc and a decrease in Fo leading to inhibition of RyR1 upon the addition of 100 nM W503A peptide at +40 mV. **B)** There is a statistically significant decrease in Tc leading to activation of the channel upon the addition of 100 nM W503A peptide at -40 mV. (N = 5 experiments for each bin) "*" indicate significant changes from control induced by the mutant peptide. A P value of <0.05 was considered significant. Results are means ±SEM.

6.5 Discussion

The C-terminal 35 residues of the DHPR β_{1a} subunit have been shown to be important for skeletal type EC coupling (Beurg et al., 1999). Furthermore, the full length β_{1a} subunit, and a peptide corresponding to the end 35 residues of its C terminal tail (β_{1a}-C35) are able to bind to RyR1 and strengthen the EC coupling process (Cheng et al., 2005, Rebbeck et al., 2011). This chapter examined the functional implications of these binding events on the skeletal ryanodine receptor.

The full length β_{1a} subunit caused an increase in RyR1 activity when added to the cytoplasmic side of a channel embedded in an artificial lipid bilayer. The native 35-residue C terminal tail peptide (β_{1a}-C35) caused a similar effect, showing that this region of β_{1a} was sufficient to account for the increase in activity of RyR1. Both the full length β_{1a} subunit as well as the 35-residue C terminal tail peptide caused an increase in ryanodine receptor activity (increase in relative mean open time – **Figures 6-3 and 6-5**) at concentrations as low as 100 pM and this increase in channel activity was not completely reversible to control levels within the life time of the lipid bilayer (**Figures 6-2 and 6-4**). Furthermore, a scrambled peptide consisting of the same residues as β_{1a}-C35 failed to activate RyR1 (**Figure 6-6**) indicating that the native sequence of this peptide was required for its activation of the ryanodine receptor. These results point to a highly specific and high affinity interaction between the C terminal tail of the β_{1a} subunit and the skeletal ryanodine receptor.

In chapter 5 of this thesis the author examined the structure of the C terminal tail peptide and identified three hydrophobic residues in a helical region which could act as a binding surface for the ryanodine receptor. Overall, the mutation of these residues to uncharged neutral residues (alanines), altered the functional interaction between the β_{1a} C-35 peptide and the ryanodine receptor. Unlike the native β_{1a}-C35 peptide which showed similar activation at positive and negative potentials, single mutations of each residue (table 6-1) resulted in a voltage dependence of its effect on the ryanodine receptor. The single mutant peptides (β_{1a}-C35 L496A, β_{1a}-C35 L500A and β_{1a}-C35 W503A) lost their ability to activate RyR1 at +40 mV while maintaining activation at -40 mV. Structural studies of the mutant peptides (ch. 5.3.4.4) indicated that, except for L496A, the mutations did not completely disrupt the helical region seen in the native

β_{1a}-C35 peptide. Therefore it is not surprising that the single mutant peptides maintained some of their activation properties. Although, NMR studies of the mutant peptide, β_{1a}-C35 L496A, showed the maximum disruption to the helical region (ch.5.3.4.4) of the native β_{1a}-C35 peptide, it is curious that β_{1a}-C35 L496A activated the ryanodine receptor at -40 mV. This may be because the presence of either L500 or W503 is sufficient for the activation of RyR1 at negative potentials. Although the helical region of the L496A mutant is disrupted, the residues L500 and W503 could still be labile enough to interact with RyR1 and cause some activation. The helical region of β_{1a}-C35 is located close to the N-terminus of this relatively short peptide, which in the event of disruption of secondary structure becomes random coil and more labile. This question could be addressed by performing this mutation (L496A) in the full length β_{1a} subunit and looking at its effect on RyR1.

Structural studies of the triple mutant (β_{1a}-C35 L496/L500/W503 A) also indicated that the mutations did not completely disrupt the helical region of the native peptide (ch. 5.3.4.4). This is probably due to the helix forming tendency of the alanine residues. However, the simultaneous mutation of all three hydrophobic residues abolished the activation properties of the native β_{1a}-C35 peptide and caused an inhibitory effect on RyR1 at both positive and negative potentials. Therefore the presence of helicity by itself was not sufficient to activate the channel.

In conclusion, the complete activation of RyR1 by the β_{1a} C terminal tail at both positive and negative potentials not only depends on an intact helical structure but requires the presence of at least one of two (L500 or W503) hydrophobic residues that participates in forming a hydrophobic surface in β_{1a}-C35 peptide. The importance of the helical region of the β_{1a} C- terminal for the interaction with RyR1 will be better evaluated by performing these mutations in the full length β_{1a} subunit in future experiments.

Chapter 7 Discussion

Excitation-contraction (EC) coupling in skeletal muscle is critically dependent on the close interaction of two distinct Ca^{2+} channels, the voltage dependent 1,4-dihydropyridine receptor (DHPR) in the sarcolemma and the type-1 ryanodine receptor (RyR1) in the sarcoplasmic reticulum (SR). Specifically, the DHPR responds to membrane depolarization which results in the opening of RyR1 and the release of Ca^{2+} from the SR which consequently induces muscle contraction. Although the DHPR can function as a calcium channel, skeletal type EC coupling does not require the entry of extracellular Ca^{2+}, leading to the notion that physical protein-protein interactions link the DHPR and RyR1. This idea is supported by the fact that the DHPRs in skeletal muscle are arranged in groups of four ("tetrads") such that each DHPR within a tetrad is apposed to one of the four, identical subunits of RyR1 (Block et al., 1988). Although a wealth of knowledge about the skeletal DHPR-RyR1 interaction has been generated during the last two decades, the exact molecular details of this interaction remains elusive.

Of the five subunits of the DHPR, the skeletal isoforms of the membrane spanning α_{1s} subunit and the cytoplasmic β_{1a} subunit are essential for the skeletal muscle EC coupling process. A region in the α_{1s} subunit consisting of amino acid residues 724-760 in the loop between the second and third trans-membrane domains (II-III loop) form a minimal essential region for transmitting the EC coupling signal from DHPR to the RyR1 Ca^{2+} release complex in the SR membrane. Deletion/mutation of this region abolishes skeletal-type EC coupling (Grabner et al., 1999).

The beta-subunit of the DHPR plays a dual role in chaperoning the α_{1s} subunit to the t-tubular membrane and modulating their gating. This targeting depends on a well characterized, high affinity binding between the guanylate kinase (GK) domain of the beta subunit and the I-II loop of the α_1 subunit (Chen et al., 2004). This interaction anchors the beta subunit to the α_1 subunit, enabling α_1- β pair-specific low-affinity interactions involving the N-terminus, Hook region and C-terminus, which confer on each of the four beta-subunit subfamilies its distinctive modulatory properties (He et al., 2007).

However, the exact role of the SH3 domain of the β subunit remains a mystery. Furthermore, in addition to its modulatory properties, several studies suggest that the skeletal isoform of the β_{1a} subunit (β_{1a}) may play a direct role in skeletal type EC-coupling. The β_{1a} subunit has an essential role in targeting the α_{1s} into a precise tetrad formation apposing alternate type 1 ryanodine receptors (Schredelseker et al., 2005). Also, the β_{1a} subunit was shown to bind the skeletal ryanodine receptor and deletion of its end 35 residues led to a significant reduction in depolarization induced Ca^{2+} release from the SR through RyR1 (Cheng et al., 2005, Beurg et al., 1999). Therefore, the aim of this study was to investigate the molecular interactions of the β_{1a} subunit and its SH3 domain and the 35-residue β_{1a} C terminal tail in the mechanical coupling between the skeletal DHPR and the ryanodine receptor.

7.1 Recombinant β_{1a} subunit

Although the structure of the core domains (SH3 and GK domains) of several beta isoforms (β_{2a} and β_3) have been elucidated, no such structural information exist for the skeletal isoform of the beta subunit. Hence, the first step of this study was to recombinantly express and purify the full length β_{1a} subunit to homogeneity with a view of elucidating its structure. However, due to the protease sensitive nature of the protein, obtaining a yield sufficient for further structural studies was not feasible. The existing structural data on the core region indicate that the well conserved GK and SH3 domains contain a high degree of secondary structure whereas the Hook region, N and C-termini show a high degree of motility. The unstructured nature of the terminal ends of the protein would certainly predispose it to proteolytic activity. Therefore it is not surprising that no structural information exists so far of any of the full length beta subunit isoforms.

7.2 Interaction between β_{1a}-SH3 domain and the α_{1s} II-III loop

The recombinant, full length β_{1a} subunit and its SH3 domain were used to probe the β_{1a} interaction with the α_{1s} subunit. Since SH3 domains are known to interact with poly-proline rich motifs, and such motifs are present in the C region (minimal essential region for skeletal type EC coupling - residues 724-760) of the α_{1s} II- III loop, the

possibility of an interaction between the β_{1a}-SH3 domain and the II-III loop was explored. The α_{1s} II-III loop and a peptide corresponding to its C region bound to the full length β_{1a} subunit and its SH3 domain with an affinity of ~ 2 μM. Mutation of the proline residues to alanines and scrambling the sequence of the C region peptide abolished this binding, confirming that the native sequence of the α_{1s} II-III loop C region was required for binding to the β_{1a}-SH3. Previous crystallographic studies on the β_{2a} and β_3 isoforms had suggested that such an interaction between β-SH3 domains and a poly-proline motif was not possible because the binding site in the SH3 domain is occluded by the RT-Src loop and the α_2 helix of the Hook region (**Figure 4-1**). However it is possible that the interaction described in chapter 4 of this thesis is a skeletal specific interaction that can occur due to structural differences specific to the SH3 domain of the β_{1a} isoform. Alternatively, it is possible that under certain conditions the highly flexible RT-Src loop and/or the α_2 helix may shift, in such way as to expose the poly-proline binding site.

This study further narrowed down the interaction between the β_{1a}-SH3 domain and the α_{1s} II-III loop, to two poly proline motifs in the critical C region. Although both poly-proline rich motifs bound with similar affinity to β_{1a}-SH3, the second motif encompassing four skeletal specific residues was favoured compared to its cardiac counterpart (**Figure 4-9**, table 4-4). Of these essential skeletal residues, mutation of P742 and D744 to its cardiac counterparts reduced the binding affinity between the skeletal specific poly proline motif (motif 1) of the α_{1s} II-III loop and the β_{1a}-SH3 domain by approximately five fold (**Figure 4-10**, table 4-5). It is established that the specificity of protein-protein interactions between canonical SH3 domains and poly-proline rich motifs are governed not exclusively by the prolines themselves but by the surrounding residues (Kaneko T et al., 2008). It appears that the specificity of the interaction between the α_{1s} II-III loop and the β_{1a}-SH3 domain could be controlled by two skeletal specific residues, P742 and D744. This is significant as *in vivo* studies have shown that these skeletal specific residues (A739, F741, P742 and D744) are important for skeletal type EC coupling (Kugler et al., 2004). In the study by Kuglar *et al.*, A739 and F741 were involved in bi-directional coupling but P742 and D744 were only involved in orthograde coupling. . In this study (Kugler et al., 2004), the loss of skeletal type EC coupling due to the mutation of the skeletal specific residues to their cardiac

counterparts was attributed to the loss of random coil structure of the C-region which the authors deemed necessary for skeletal type EC-coupling. But the study by Kuglar *et al.* does not address the possible contributions of additional sites involved in the interaction with RyR1, and the authors acknowledge that "parts of α_{1s} outside the II-III loop and/or auxiliary DHPR subunits also participate directly or indirectly in the specific interaction with RyR1". Therefore it is possible that the effect of P742 and D744 in skeletal type EC coupling is in determining the specificity of the interaction between β_{1a}-SH3 domain and the α_{1s}-II-III loop.

But the question remains as to how this interaction participates in the skeletal EC coupling process. The DHPR β_{1a} belongs to a class of MAGUK proteins, which are scaffolding proteins that play a clustering role in protein interactions (McGee et al., 2001). The presence of two SH3 binding motifs in the skeletal II-III loop C region indicates the possibility of a β_{1a}-SH3 dimer acting as a linker and clustering the tetrad of α_{1s} subunits apposing the RyR1s in the triad junctions. In fact dimerization of the β_{1a}-SH3 was seen in this study when used at higher concentrations (ch.4.1.6.7) and ligand mediated dimerisation of the SH3 domain has been reported in several other studies (Miranda-Laferte et al., 2011). The clustering role of the SH3 domain could be exclusive to the skeletal II-III loop since it has two SH3 binding motifs of higher affinity in comparison to the cardiac. Tetrad formation has been shown to be an exclusive function of the β_{1a} subunit (Schredelseker et al., 2005). Therefore, it is tempting to speculate that tetrad formation may be linked to the clustering role of the β_{1a}-SH3 domain.

7.3 Structure and function of the 35-residue C terminal tail of the β_{1a} subunit

The full length β_{1a} subunit was previously shown to bind to RyR1 fragments (Cheng et al., 2005) and the end 35 residues of β_{1a} was shown to support EC-coupling (Beurg et al., 1999). A recent study has also shown that the full length β_{1a} subunit activates the skeletal ryanodine receptor and that a peptide corresponding to the C terminal 35 residues of β_{1a} (β_{1a}-C35) is able to bind to RyR1 and is sufficient to support this increase in channel activity (Rebbeck et al., 2011). The present study investigated the

structure of the β_{1a}-C35 peptide with the aim of understanding its binding to RyR1. NMR investigations of the β_{1a}-C35 revealed a mostly random coil peptide with a helical region extending from approximately L493 through to L506. Closer examination of this helical region showed four hydrophobic residues, L493, L496, L500and W503 (Figure 5-9), that could likely form a hydrophobic binding surface with RyR1. Interestingly, mutating three of these residues (L496, L500 and W503) simultaneously to alanines did not completely disrupt the helicity of this region, perhaps due to the inherent helix forming tendency of alanine residues. But the ability of this triple mutant peptide to activate RyR1 was abolished. In fact this peptide inhibited the skeletal ryanodine receptor. Also, individual mutations of two of these hydrophobic residues (L500 and W503) did not completely disrupt the helical structure of this region. But in contrast to β_{1a}-C35 wild type, these mutant peptides showed a voltage dependence in their interaction with RyR1. Although structural studies indicated that L496 was essential for the stability of the helical region of β_{1a}-C35, this peptide interacted with RyR1 in a similar manner to the other single mutants, L500A and W503A. These results indicate that the nature of the hydrophobic residues themselves, specifically L500 and W503, rather than the secondary structure of this region is important for binding to RyR1.

A more recent *in vivo* study conducted by Feng *et al.* also showed that the β_{1a} C terminal (terminal 38 residues) is essential for the functional interaction with RyR1 (Feng et al., 2011). However, in the Feng *et al.* study, the full length β_{1a} subunit showed an inhibitory effect on the skeletal ryanodine receptor. This discrepancy in results could be due to a species difference between the ryanodine receptor vesicles (mouse versus rabbit) used but a definitive answer needs further investigation. In the same study four leucine residues (L488, L493, L500 and L506) were mutated within and adjacent to the helical region of the β_{1a}-C terminal identified in the present work. These mutations led to a reduction of the inhibitory effect on RyR1 compared to the wild type β_{1a} subunit. It is of note that both studies, Feng *et al.* and the present study, identified L500 as being important for the functional interaction of the β_{1a} subunit with RyR1.

Another study by Sheridan *et al.* suggested that a hydrophobic heptad repeat in the β_{1a} C-terminal tail (L478, V485 and V492) was important for skeletal type EC coupling (Sheridan et al., 2004). However, alanine substitution of the hydrophobic heptad repeat residues that abolished voltage-dependant Ca^{2+} release in a mouse model did not alter

Ca^{2+} release in a zebra fish model (Dayal et al., 2010). Although this could be explained by species differences between the two tissues, the exact role of this heptad repeat in skeletal EC coupling remains contentious.

Although the above studies including those reported in this thesis have clearly identified the β_{1a} C-terminus as a critical element of β_{1a} function, FRET based studies do not support these results (Papadopoulos et al., 2004). The FRET efficiency of a CFP-YFP tandem construct fused to the β_{1a} C terminus was minimally affected by the presence of RyR1 and the fusion of this tag did not alter the percentage of myotubes that contracted in response to electrical stimulation. Moreover, EC coupling persisted after the binding of streptavidin to a biotin acceptor domain affixed to the β_{1a} C terminus (Lorenzon et al., 2004). These results may indicate that the β_{1a} C terminus is not essential for binding to RyR1. However these results could also be explained by the fact that the β_{1a} binding site involves hydrophobic residues remote from the extreme C terminus of β_{1a}. Studies conducted by Papadopoulos *et al.* also show that β_{1a} expressed without α_{1s} did not colocalise with RyR1s, suggesting that β_{1a} cannot bind to RyR1 in the absence of α_{1s}. However this could be explained by geometrical changes in the narrow triad junction that could occur in the absence of α_{1s}.

7.4 Role of the β_{1a} SH3 domain and the β_{1a} C terminus in skeletal EC coupling?

Recent *in vivo* studies in a β_{1a} null zebra fish model have shown that the β_{1a} SH3 domain is essential for skeletal type EC coupling. Specifically, the substitution of the β_{1a} N, Hook and C terminus on a *Musca domesticus* (which does not support EC coupling) background did not restore motility to β_{1a} null zebra fish larvae, whereas the addition of the SH3 domain restored motility (Grabner *et al.* personal communication). Further unpublished *in vivo* studies in β_{1a} null zebra fish myotubes suggest that the β_{1a}-SH3 domain and its C-terminus are essential for α_{1s} charge movement. Specifically, the substitution of β_{1a}-SH3 domain and the C terminus on a β_3 background (which show no charge movement) restored α_{1s} charge movement (Kumar et al., 2011). However the substitution of the β_{1a} N, Hook or the GK domain on a β_3 background did not restore α_{1s}

charge movement indicating that these regions were not involved in this particular role of the β_{1a} subunit.

This study shows that the SH3 domain of the β_{1a} subunit interacts with the critical region of the α_{1s} II-III loop *in vitro*. This interaction is localised to a proline rich motif encompassing four skeletal specific critical residues of the α_{1s} II-III loop. Of these four skeletal specific residues, P742 and D744 are important for this interaction.

The final 35 residues of the β_{1a} C terminal domain binds and activates the skeletal ryanodine receptor. A peptide corresponding to this region contains a helical region encompassing three hydrophobic residues (L496, L500and W503) which could act as a binding site for RyR1. Mutation of these hydrophobic residues to alanines did not completely destabilize the helical region however it abolished the ability of this peptide to activate the ryanodine receptor.

Therefore we propose a model where the β_{1a} SH3 domain binds to the α_{1s} II-III loop and clusters the DHPRs in the correct tetrad formation apposing RyR1. This skeletal specific tetrad formation facilitates charge movement upon depolarization which is in turn relayed through the β_{1a} C terminus to the RyR1 (**Figure 7-1**).

Some studies support a model where the β_{1a} subunit binds to the α_{1s} and acts as an allosteric modifier of the critical region of the II-III loop which binds to the ryanodine receptor and ultimately leads to skeletal type EC coupling (Schredelseker et al., 2009) However, such a binding site for the II-III loop in the RyR1 is yet to be identified. Moreover such a model also does not take into account the increasing body of evidence showing a direct interaction between the β_{1a} C terminus and the skeletal ryanodine receptor.

7.5 Conclusion

In conclusion, in this thesis the author has presented *in vitro* evidence of a possible pathway in the physical coupling between the DHPR and the RyR1 in skeletal EC coupling.

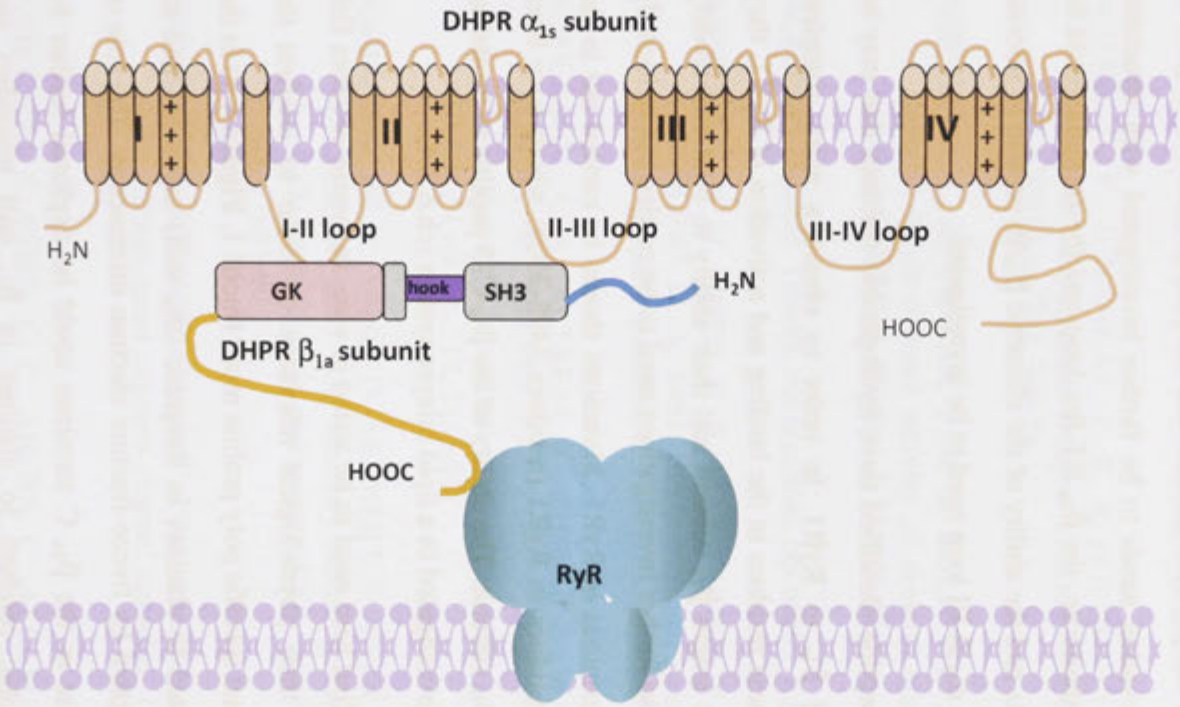

Figure 7-1 – Proposed model of EC coupling in skeletal muscle. The β_{1a}- SH3 domain binds to the α_{1s} II-III loop and clusters them in the correct tetrad formation apposing RyR1. This skeletal specific tetrad formation facilitates depolarisation induced charge movement which is in turn relayed through the β_{1a} C terminus to the RyR1.

7.6 Future directions

Structural studies of the β_{2a} and β_3 isoforms have indicated that the SH3 domains of the β subunits are unlikely to interact with proline rich motifs because the poly-proline binding site is occluded by the RT Src loop (between the 1st and 2nd β strands of the SH3domain) and α_2 helix of the Hook region. This study has shown that such an interaction is possible between the β_{1a}-SH3 domain and the poly-proline rich region of the α_{1s} II-III loop. This observation needs to be further investigated with structural studies of the β_{1a} isoform. Furthermore, the β_{1a} RT-Src loop and the α_2 helix could be substituted to its β_2 counterparts and the ability of the chimeric β_{1a}/β_2 protein to interact with poly-proline motifs of the α_{1s} II-III loop need to be investigated.

NMR studies of the β_{1a}-C35 peptide identified three hydrophobic residues that may be important for the binding of β_{1a} to RyR1. In order to obtain a more complete understanding of the role of these residues in the binding and activation of RyR1, they need to be mutated in the full length β_{1a} subunit and their ability to bind and modify RyR1 activity investigated. Also further investigations need to be carried out to identify the binding site of the β_{1a} C terminus in RyR1. Mutations should be carried out in the cluster of positively charged residues in RyR1 (residues 3495-3502) which have been shown to bind the full length β_{1a} subunit. The ability of the β_{1a}-C35 peptide to modulate these mutant RyR1s could be investigated in a lipid bilayer system (ch.6.3.4).

Finally, the interactions identified here need to be tested *in vivo*, in mouse or zebra fish models, in order to validate their physiological relevance. In order to confirm the clustering role of β_{1a}, the skeletal specific poly proline motif (motif 1, **Figure 4-9**) in the α_{1s} II-III loop could be mutated to alanines in dysgenic (α_{1s} null) myotubes and its ability to form tetrads investigated by freeze-fracture electron microscopy. The role of the putative RyR1 binding site in the β_{1a} C terminus could be explored further by mutating the three hydrophobic residues to alanines in β_{1a} null myotubes and investigating the effect on skeletal type EC coupling.

References

AHERN, C. A., ARIKKATH, J., VALLEJO, P., GURNETT, C. A., POWERS, P. A., CAMPBELL, K. P. & CORONADO, R. 2001. Intramembrane charge movements and excitation- contraction coupling expressed by two-domain fragments of the Ca2+ channel. *Proc Natl Acad Sci U S A,* 98, 6935-40.

AHERN, C. A., BHATTACHARYA, D., MORTENSON, L. & CORONADO, R. 2001. A component of excitation-contraction coupling triggered in the absence of the T671-L690 and L720-Q765 regions of the II-III loop of the dihydropyridine receptor alpha(1s) pore subunit. *Biophys J,* 81, 3294-307.

AHERN, G. P., JUNANKAR, P. R. & DULHUNTY, A. F. 1994. Single channel activity of the ryanodine receptor calcium release channel is modulated by FK-506. *FEBS Lett,* 352, 369-74.

AHERN, G. P., JUNANKAR, P. R. & DULHUNTY, A. F. 1997. Subconductance states in single-channel activity of skeletal muscle ryanodine receptors after removal of FKBP12. *Biophys J,* 72, 146-62.

ALLEN, P. D. 2009. Triadin, not essential, but useful. *J Physiol,* 587, 3123-4.

ANDERSEN, N. H., CHEN, C. P., MARSCHNER, T. M., KRYSTEK, S. R., JR. & BASSOLINO, D. A. 1992. Conformational isomerism of endothelin in acidic aqueous media: a quantitative NOESY analysis. *Biochemistry,* 31, 1280-95.

ANDERSON, A. A., ALTAFAJ, X., ZHENG, Z., WANG, Z. M., DELBONO, O., RONJAT, M., TREVES, S. & ZORZATO, F. 2006. The junctional SR protein JP-45 affects the functional expression of the voltage-dependent Ca2+ channel Cav1.1. *J Cell Sci,* 119, 2145-55.

ANDRONACHE, Z., URSU, D., LEHNERT, S., FREICHEL, M., FLOCKERZI, V. & MELZER, W. 2007. The auxiliary subunit gamma 1 of the skeletal muscle L-type Ca2+ channel is an endogenous Ca2+ antagonist. *Proc Natl Acad Sci U S A,* 104, 17885-90.

ARIKKATH, J. & CAMPBELL, K. P. 2003. Auxiliary subunits: essential components of the voltage-gated calcium channel complex. *Curr Opin Neurobiol,* 13, 298-307.

ARIKKATH, J., CHEN, C. C., AHERN, C., ALLAMAND, V., FLANAGAN, J. D., CORONADO, R., GREGG, R. G. & CAMPBELL, K. P. 2003. Gamma 1 subunit interactions within the skeletal muscle L-type voltage-gated calcium channels. *J Biol Chem,* 278, 1212-9.

AVILA, G. & DIRKSEN, R. T. 2000. Functional impact of the ryanodine receptor on the skeletal muscle L-type Ca(2+) channel. *J Gen Physiol,* 115, 467-80.

AVILA, G., LEE, E. H., PEREZ, C. F., ALLEN, P. D. & DIRKSEN, R. T. 2003. FKBP12 binding to RyR1 modulates excitation-contraction coupling in mouse skeletal myotubes. *The Journal of biological chemistry,* 278, 22600-8.

BAKER, R. T., CATANZARITI, A. M., KARUNASEKARA, Y., SOBOLEVA, T. A., SHARWOOD, R., WHITNEY, S. & BOARD, P. G. 2005. Using deubiquitylating enzymes as research tools. *Methods Enzymol,* 398, 540-54.

BALL, S. L., POWERS, P. A., SHIN, H. S., MORGANS, C. W., PEACHEY, N. S. & GREGG, R. G. 2002. Role of the beta(2) subunit of voltage-dependent calcium channels in the retinal outer plexiform layer. *Invest Ophthalmol Vis Sci,* 43, 1595-603.

BANNISTER, R. A. 2007. Bridging the myoplasmic gap: recent developments in skeletal muscle excitation-contraction coupling. *J Muscle Res Cell Motil,* 28, 275-83.

BANNISTER, R. A. & BEAM, K. G. 2005. The alpha1S N-terminus is not essential for bi-directional coupling with RyR1. *Biochem Biophys Res Commun,* 336, 134-41.

BANNISTER, R. A., PAPADOPOULOS, S., HAARMANN, C. S. & BEAM, K. G. 2009. Effects of inserting fluorescent proteins into the alpha1S II-III loop: insights into excitation-contraction coupling. *J Gen Physiol,* 134, 35-51.

BAUER, C. S., TRAN-VAN-MINH, A., KADURIN, I. & DOLPHIN, A. C. A new look at calcium channel [alpha]2[delta] subunits. *Current Opinion in Neurobiology,* In Press, Corrected Proof.

BEAM, K. G. & BANNISTER, R. A. 2010. Looking for answers to EC coupling's persistent questions. *J Gen Physiol,* 136, 7-12.

BEARD, N. A., LAVER, D. R. & DULHUNTY, A. F. 2004. Calsequestrin and the calcium release channel of skeletal and cardiac muscle. *Progress in biophysics and molecular biology,* 85, 33-69.

BEGUIN, P., NAGASHIMA, K., GONOI, T., SHIBASAKI, T., TAKAHASHI, K., KASHIMA, Y., OZAKI, N., GEERING, K., IWANAGA, T. & SEINO, S. 2001. Regulation of Ca2+ channel expression at the cell surface by the small G-protein kir/Gem. *Nature,* 411, 701-6.

BERRIDGE, M. J. 1993. Inositol trisphosphate and calcium signalling. *Nature,* 361, 315-25.

BEURG, M., AHERN, C. A., VALLEJO, P., CONKLIN, M. W., POWERS, P. A., GREGG, R. G. & CORONADO, R. 1999. Involvement of the carboxy-terminus region of the dihydropyridine receptor beta1a subunit in excitation-contraction coupling of skeletal muscle. *Biophys J,* 77, 2953-67.

BICHET, D., CORNET, V., GEIB, S., CARLIER, E., VOLSEN, S., HOSHI, T., MORI, Y. & DE WAARD, M. 2000. The I-II loop of the Ca2+ channel alpha1 subunit contains an endoplasmic reticulum retention signal antagonized by the beta subunit. *Neuron,* 25, 177-90.

BLOCK, B. A., IMAGAWA, T., CAMPBELL, K. P. & FRANZINI-ARMSTRONG, C. 1988. Structural evidence for direct interaction between the molecular components of the transverse tubule/sarcoplasmic reticulum junction in skeletal muscle. *J Cell Biol,* 107, 2587-600.

BORSOTTO, M., BARHANIN, J., FOSSET, M. & LAZDUNSKI, M. 1985. The 1,4-dihydropyridine receptor associated with the skeletal muscle voltage-dependent Ca2+ channel. Purification and subunit composition. *J Biol Chem,* 260, 14255-63.

BURGESS, D. L., BIDDLECOME, G. H., MCDONOUGH, S. I., DIAZ, M. E., ZILINSKI, C. A., BEAN, B. P., CAMPBELL, K. P. & NOEBELS, J. L. 1999. beta subunit reshuffling modifies N- and P/Q-type Ca2+ channel subunit compositions in lethargic mouse brain. *Mol Cell Neurosci,* 13, 293-311.

BURIGHEL, P., NUNZI, M. G. & SCHIAFFINO, S. 1977. A comparative study of the organization of the sarcotubular system in ascidian muscle. *Journal of Morphology,* 153, 205-223.

CANTI, C., NIETO-ROSTRO, M., FOUCAULT, I., HEBLICH, F., WRATTEN, J., RICHARDS, M. W., HENDRICH, J., DOUGLAS, L., PAGE, K. M., DAVIES, A. & DOLPHIN, A. C. 2005. The metal-ion-dependent adhesion site in the Von Willebrand factor-A domain of alpha2delta subunits is key to trafficking voltage-gated Ca2+ channels. *Proc Natl Acad Sci U S A,* 102, 11230-5.

CARBONNEAU, L., BHATTACHARYA, D., SHERIDAN, D. C. & CORONADO, R. 2005. Multiple loops of the dihydropyridine receptor pore subunit are required for full-scale excitation-contraction coupling in skeletal muscle. *Biophys J,* 89, 243-55.

CASAROTTO, M. G., GREEN, D., PACE, S., YOUNG, J. & DULHUNTY, A. F. 2004. Activating the ryanodine receptor with dihydropyridine receptor II-III loop segments: size and charge do matter. *Front Biosci,* 9, 2860-72.

CASTELLANO, A., WEI, X., BIRNBAUMER, L. & PEREZ-REYES, E. 1993. Cloning and expression of a neuronal calcium channel beta subunit. *J Biol Chem,* 268, 12359-66.

CASTELLANO, A., WEI, X., BIRNBAUMER, L. & PEREZ-REYES, E. 1993. Cloning and expression of a third calcium channel beta subunit. *J Biol Chem,* 268, 3450-5.

CATANZARITI, A. M., SOBOLEVA, T. A., JANS, D. A., BOARD, P. G. & BAKER, R. T. 2004. An efficient system for high-level expression and easy purification of authentic recombinant proteins. *Protein Sci,* 13, 1331-9.

CHELU, M. G., DANILA, C. I., GILMAN, C. P. & HAMILTON, S. L. 2004. Regulation of Ryanodine Receptors by FK506 Binding Proteins. *Trends in Cardiovascular Medicine,* 14, 227-234.

CHEN, J. K., LANE, W. S., BRAUER, A. W., TANAKA, A. & SCHREIBER, S. L. 1993. Biased combinatorial libraries: novel ligands for the SH3 domain of phosphatidylinositol 3-kinase. *Journal of the American Chemical Society,* 115, 12591-12592.

CHEN, R. S., DENG, T. C., GARCIA, T., SELLERS, Z. M. & BEST, P. M. 2007. Calcium channel gamma subunits: a functionally diverse protein family. *Cell Biochem Biophys,* 47, 178-86.

CHEN, Y. H., LI, M. H., ZHANG, Y., HE, L. L., YAMADA, Y., FITZMAURICE, A., SHEN, Y., ZHANG, H., TONG, L. & YANG, J. 2004. Structural basis of the alpha1-beta subunit interaction of voltage-gated Ca2+ channels. *Nature,* 429, 675-80.

CHENG, W., ALTAFAJ, X., RONJAT, M. & CORONADO, R. 2005. Interaction between the dihydropyridine receptor Ca2+ channel beta-subunit and ryanodine receptor type 1 strengthens excitation-contraction coupling. *Proc Natl Acad Sci U S A,* 102, 19225-30.

CHISHTI, A. H. 1998. Function of p55 and its nonerythroid homologues. *Curr Opin Hematol,* 5, 116-21.

COLECRAFT, H. M., ALSEIKHAN, B., TAKAHASHI, S. X., CHAUDHURI, D., MITTMAN, S., YEGNASUBRAMANIAN, V., ALVANIA, R. S., JOHNS, D. C., MARBAN, E. & YUE, D. T. 2002. Novel functional properties of Ca(2+) channel beta subunits revealed by their expression in adult rat heart cells. *J Physiol,* 541, 435-52.

CORNEA, R. L., NITU, F. R., SAMSÓ, M., THOMAS, D. D. & FRUEN, B. R. 2010. Mapping the Ryanodine Receptor FK506-binding Protein Subunit Using Fluorescence Resonance Energy Transfer. *Journal of Biological Chemistry,* 285, 19219-19226.

CORONADO, R., AHERN, C. A., SHERIDAN, D. C., CHENG, W., CARBONNEAU, L. & BHATTACHARYA, D. 2004. Functional equivalence of dihydropyridine receptor alpha1S and beta1a subunits in triggering excitation-contraction coupling in skeletal muscle. *Biol Res,* 37, 565-75.

CUI, Y., KARUNASEKARA, Y., HARVEY, P. J., BOARD, P. G., DULHUNTY, A. F. & CASAROTTO, M. G. 2005. 1H, 13C and 15N assignments for the II-III loop region of the skeletal dyhydropyridine receptor. *J Biomol NMR,* 32, 89-90.

CUI, Y., TAE, H.-S., NORRIS, N. C., KARUNASEKARA, Y., POULIQUIN, P., BOARD, P. G., DULHUNTY, A. F. & CASAROTTO, M. G. 2009. A dihydropyridine receptor [alpha]1s loop region critical for skeletal muscle contraction is intrinsically unstructured and binds to a SPRY domain of the type 1 ryanodine receptor. *The International Journal of Biochemistry & Cell Biology,* 41, 677-686.

CURTIS, B. M. & CATTERALL, W. A. 1984. Purification of the calcium antagonist receptor of the voltage-sensitive calcium channel from skeletal muscle transverse tubules. *Biochemistry,* 23, 2113-8.

DAVIES, A., KADURIN, I., ALVAREZ-LAVIADA, A., DOUGLAS, L., NIETO-ROSTRO, M., BAUER, C. S., PRATT, W. S. & DOLPHIN, A. C. 2010. The alpha2delta subunits of voltage-gated calcium channels form GPI-anchored proteins, a posttranslational modification essential for function. *Proc Natl Acad Sci U S A,* 107, 1654-9.

DAYAL, A., SCHREDELSEKER, J., FRANZINI-ARMSTRONG, C. & GRABNER, M. 2010. Skeletal muscle excitation-contraction coupling is independent of a conserved heptad repeat motif in the C-terminus of the DHPRbeta(1a) subunit. *Cell calcium,* 47, 500-6.

DE JONGH, K. S., WARNER, C. & CATTERALL, W. A. 1990. Subunits of purified calcium channels. Alpha 2 and delta are encoded by the same gene. *J Biol Chem,* 265, 14738-41.

DIRKSEN, R. T. 2002. Bi-directional coupling between dihydropyridine receptors and ryanodine receptors. *Frontiers in bioscience : a journal and virtual library,* 7, d659-70.

DIRKSEN, R. T. 2009. Checking your SOCCs and feet: the molecular mechanisms of Ca2+ entry in skeletal muscle. *The Journal of physiology,* 587, 3139-47.

DOLPHIN, A. C. 2003. β subunits of voltage-gated calcium channels. *J. Bioenerg. Biomembr,* 35, pp. 599-620.

DU, G. G., SANDHU, B., KHANNA, V. K., GUO, X. H. & MACLENNAN, D. H. 2002. Topology of the Ca2+ release channel of skeletal muscle sarcoplasmic reticulum (RyR1). *Proc Natl Acad Sci U S A,* 99, 16725-30.

DUBUIS, E., ROCKLIFFE, N., HUSSAIN, M., BOYETT, M., WRAY, D. & GAWLER, D. 2006. Evidence for multiple Src binding sites on the alpha1c L-type Ca2+ channel and their roles in activity regulation. *Cardiovasc Res,* 69, 391-401.

DULHUNTY, A., WEI, L. & BEARD, N. 2009. Junctin - the quiet achiever. *J Physiol,* 587, 3135-7.

DULHUNTY, A. F. 1984. Heterogeneity of T-tubule geometry in vertebrate skeletal muscle fibres. *J Muscle Res Cell Motil,* 5, 333-47.

DULHUNTY, A. F. 2006. Excitation-contraction coupling from the 1950s into the new millennium. *Clin Exp Pharmacol Physiol,* 33, 763-72.

DULHUNTY, A. F., KARUNASEKARA, Y., CURTIS, S. M., HARVEY, P. J., BOARD, P. G. & CASAROTTO, M. G. 2005. Role of some unconserved residues in the "C" region of the skeletal DHPR II-III loop. *Front Biosci,* 10, 1368-81.

DWORKIN, R. H., O'CONNOR, A. B., BACKONJA, M., FARRAR, J. T., FINNERUP, N. B., JENSEN, T. S., KALSO, E. A., LOESER, J. D., MIASKOWSKI, C., NURMIKKO, T. J., PORTENOY, R. K., RICE, A. S., STACEY, B. R., TREEDE, R. D., TURK, D. C. & WALLACE, M. S. 2007. Pharmacologic management of neuropathic pain: evidence-based recommendations. *Pain,* 132, 237-51.

DYSON, H. J., RANCE, M., HOUGHTEN, R. A., LERNER, R. A. & WRIGHT, P. E. 1988. Folding of immunogenic peptide fragments of proteins in water solution. I. Sequence requirements for the formation of a reverse turn. *J Mol Biol,* 201, 161-200.

EBERST, R., DAI, S., KLUGBAUER, N. & HOFMANN, F. 1997. Identification and functional characterization of a calcium channel gamma subunit. *Pflugers Arch,* 433, 633-7.

EHRLICH, B. E., KAFTAN, E., BEZPROZVANNAYA, S. & BEZPROZVANNY, I. 1994. The pharmacology of intracellular Ca(2+)-release channels. *Trends Pharmacol Sci,* 15, 145-9.

EL-HAYEK, R., ANTONIU, B., WANG, J., HAMILTON, S. L. & IKEMOTO, N. 1995. Identification of calcium release-triggering and blocking regions of the II-III loop of the skeletal muscle dihydropyridine receptor. *J Biol Chem,* 270, 22116-8.

ELLIS, S. B., WILLIAMS, M. E., WAYS, N. R., BRENNER, R., SHARP, A. H., LEUNG, A. T., CAMPBELL, K. P., MCKENNA, E., KOCH, W. J., HUI, A. & ET AL. 1988. Sequence and expression of mRNAs encoding the alpha 1 and alpha 2 subunits of a DHP-sensitive calcium channel. *Science,* 241, 1661-4.

ERTEL, E. A., CAMPBELL, K. P., HARPOLD, M. M., HOFMANN, F., MORI, Y., PEREZ-REYES, E., SCHWARTZ, A., SNUTCH, T. P., TANABE, T., BIRNBAUMER, L., TSIEN, R. W. & CATTERALL, W. A. 2000. Nomenclature of voltage-gated calcium channels. *Neuron,* 25, 533-5.

ESCAYG, A., DE WAARD, M., LEE, D. D., BICHET, D., WOLF, P., MAYER, T., JOHNSTON, J., BALOH, R., SANDER, T. & MEISLER, M. H. 2000. Coding and noncoding variation of the human calcium-channel beta4-subunit gene CACNB4 in patients with idiopathic generalized epilepsy and episodic ataxia. *Am J Hum Genet,* 66, 1531-9.

FATT, P. & KATZ, B. 1953. The electrical properties of crustacean muscle fibres. *The Journal of Physiology,* 120, 171-204.

FELIX, R., GURNETT, C. A., DE WAARD, M. & CAMPBELL, K. P. 1997. Dissection of functional domains of the voltage-dependent Ca2+ channel alpha2delta subunit. *J Neurosci,* 17, 6884-91.

FENG, W., KIM, T., D, A. P., N, P. I. & F, P. C. 2011. Role of C term tail of DHPR beta1a in the DHPR/RYR1 Interaction. *2011 Biophysical Society Meeting, Abstracts, Biophysical journal,* 100, 3194-Pos.

FENG, W., TU, J., YANG, T., VERNON, P. S., ALLEN, P. D., WORLEY, P. F. & PESSAH, I. N. 2002. Homer regulates gain of ryanodine receptor type 1 channel complex. *J Biol Chem,* 277, 44722-30.

FESSENDEN, J. D., FENG, W., PESSAH, I. N. & ALLEN, P. D. 2004. Mutational analysis of putative calcium binding motifs within the skeletal ryanodine receptor isoform, RyR1. *J Biol Chem,* 279, 53028-35.

FITZGERALD, E. M. 2002. The presence of Ca2+ channel beta subunit is required for mitogen-activated protein kinase (MAPK)-dependent modulation of alpha1B Ca2+ channels in COS-7 cells. *J Physiol,* 543, 425-37.

FLEISCHER, S., OGUNBUNMI, E. M., DIXON, M. C. & FLEER, E. A. 1985. Localization of Ca2+ release channels with ryanodine in junctional terminal cisternae of sarcoplasmic reticulum of fast skeletal muscle. *Proceedings of the National Academy of Sciences of the United States of America,* 82, 7256-9.

FLOCKERZI, V., OEKEN, H. J., HOFMANN, F., PELZER, D., CAVALIE, A. & TRAUTWEIN, W. 1986. Purified dihydropyridine-binding site from skeletal muscle t-tubules is a functional calcium channel. *Nature,* 323, 66-8.

FLUCHER, B. E. & FRANZINI-ARMSTRONG, C. 1996. Formation of junctions involved in excitation-contraction coupling in skeletal and cardiac muscle. *Proceedings of the National Academy of Sciences of the United States of America,* 93, 8101-6.

FLUCHER, B. E., KASIELKE, N. & GRABNER, M. 2000. The triad targeting signal of the skeletal muscle calcium channel is localized in the COOH terminus of the alpha(1S) subunit. *J Cell Biol,* 151, 467-78.

FLUCHER, B. E., PHILLIPS, J. L. & POWELL, J. A. 1991. Dihydropyridine receptor alpha subunits in normal and dysgenic muscle in vitro: expression of alpha 1 is required for proper targeting and distribution of alpha 2. *J Cell Biol,* 115, 1345-56.

FLUCHER, B. E., WEISS, R. G. & GRABNER, M. 2002. Cooperation of two-domain Ca(2+) channel fragments in triad targeting and restoration of excitation-contraction coupling in skeletal muscle. *Proc Natl Acad Sci U S A,* 99, 10167-72.

FOX, A. P., NOWYCKY, M. C. & TSIEN, R. W. 1987. Kinetic and pharmacological properties distinguishing three types of calcium currents in chick sensory neurones. *J Physiol,* 394, 149-72.

FRANZINI-ARMSTRONG 1999. The sarcoplasmic reticulum and the control of muscle contraction. *FASEB J.,* 13, 266S-270.

FRANZINI-ARMSTRONG, C. 1970. STUDIES OF THE TRIAD : I. Structure of the Junction in Frog Twitch Fibers. *The Journal of cell biology,* 47, 488-99.

FRANZINI-ARMSTRONG, C. & PROTASI, F. 1997. Ryanodine receptors of striated muscles: a complex channel capable of multiple interactions. *Physiol Rev,* 77, 699-729.

FRANZINI-ARMSTRONG, C., PROTASI, F. & RAMESH, V. 1998. Comparative ultrastructure of Ca2+ release units in skeletal and cardiac muscle. *Ann N Y Acad Sci,* 853, 20-30.

FRANZINI-ARMSTRONG, C., PROTASI, F. & RAMESH, V. 1999. Shape, size, and distribution of Ca(2+) release units and couplons in skeletal and cardiac muscles. *Biophys J,* 77, 1528-39.

FREISE, D., HELD, B., WISSENBACH, U., PFEIFER, A., TROST, C., HIMMERKUS, N., SCHWEIG, U., FREICHEL, M., BIEL, M., HOFMANN, F., HOTH, M. & FLOCKERZI, V. 2000. Absence of the gamma subunit of the skeletal muscle dihydropyridine receptor increases L-type Ca2+ currents and alters channel inactivation properties. *J Biol Chem,* 275, 14476-81.

FROEMMING, G. R., PETTE, D. & OHLENDIECK, K. 1999. The 90-kDa junctional sarcoplasmic reticulum protein forms an integral part of a supramolecular triad complex in skeletal muscle. *Biochem Biophys Res Commun,* 261, 603-9.

FULLER-BICER, G. A., VARADI, G., KOCH, S. E., ISHII, M., BODI, I., KADEER, N., MUTH, J. N., MIKALA, G., PETRASHEVSKAYA, N. N., JORDAN, M. A., ZHANG, S. P., QIN, N., FLORES, C. M., ISAACSOHN, I., VARADI, M., MORI, Y., JONES, W. K. & SCHWARTZ, A. 2009. Targeted disruption of the voltage-dependent calcium channel alpha2/delta-1-subunit. *Am J Physiol Heart Circ Physiol,* 297, H117-24.

GAO, B., SEKIDO, Y., MAXIMOV, A., SAAD, M., FORGACS, E., LATIF, F., WEI, M. H., LERMAN, M., LEE, J. H., PEREZ-REYES, E., BEZPROZVANNY, I. & MINNA, J. D. 2000. Functional properties of a new voltage-dependent calcium channel alpha(2)delta auxiliary subunit gene (CACNA2D2). *J Biol Chem,* 275, 12237-42.

GAO, L., TRIPATHY, A., LU, X. & MEISSNER, G. 1997. Evidence for a role of C-terminal amino acid residues in skeletal muscle Ca2+ release channel (ryanodine receptor) function. *FEBS Lett,* 412, 223-6.

GARCIA, J., TANABE, T. & BEAM, K. G. 1994. Relationship of calcium transients to calcium currents and charge movements in myotubes expressing skeletal and cardiac dihydropyridine receptors. *J Gen Physiol,* 103, 125-47.

GARCIA, K., NABHANI, T. & GARCIA, J. 2008. The calcium channel alpha2/delta1 subunit is involved in extracellular signalling. *J Physiol,* 586, 727-38.

GASTEIGER, E., HOOGLAND, C., GATTIKER, A., DUVAUD, S., WILKINS, M. R., APPEL, R. D. & BAIROCH, A. 2005. Protein Identification and Analysis Tools on the ExPASy Server. *The proteomics Protocols Handbook, Humana Press,* (In) John M. Walker (ed), 571-607.

GERSTER, U., NEUHUBER, B., GROSCHNER, K., STRIESSNIG, J. & FLUCHER, B. E. 1999. Current modulation and membrane targeting of the calcium channel alpha1C subunit are independent functions of the beta subunit. *J Physiol,* 517 (Pt 2), 353-68.

GODDARD, T. D. & KNELLER, D. G. Sparky 3.

GOMEZ-OSPINA, N., TSURUTA, F., BARRETO-CHANG, O., HU, L. & DOLMETSCH, R. 2006. The C terminus of the L-type voltage-gated calcium channel Ca(V)1.2 encodes a transcription factor. *Cell,* 127, 591-606.

GONZALEZ-GUTIERREZ, G., MIRANDA-LAFERTE, E., NEELY, A. & HIDALGO, P. 2007. The Src homology 3 domain of the beta-subunit of voltage-gated calcium channels promotes endocytosis via dynamin interaction. *J Biol Chem,* 282, 2156-62.

GONZALEZ-GUTIERREZ, G., MIRANDA-LAFERTE, E., NOTHMANN, D., SCHMIDT, S., NEELY, A. & HIDALGO, P. 2008. The guanylate kinase domain of the beta-subunit of voltage-gated calcium channels suffices to modulate gating. *Proc Natl Acad Sci U S A,* 105, 14198-203.

GOONASEKERA, S. A., BEARD, N. A., GROOM, L., KIMURA, T., LYFENKO, A. D., ROSENFELD, A., MARTY, I., DULHUNTY, A. F. & DIRKSEN, R. T. 2007. Triadin binding to the C-terminal luminal loop of the ryanodine receptor is important for skeletal muscle excitation contraction coupling. *J Gen Physiol,* 130, 365-78.

GOULD, C. M., DIELLA, F., VIA, A., PUNTERVOLL, P., GEMÜND, C., CHABANIS-DAVIDSON, S., MICHAEL, S., SAYADI, A., BRYNE, J. C., CHICA, C., SEILER, M., DAVEY, N. E., HASLAM, N., WEATHERITT, R. J., BUDD, A., HUGHES, T., PAŚ, J., RYCHLEWSKI, L., TRAVÉ, G., AASLAND, R., HELMER-CITTERICH, M., LINDING, R. & GIBSON, T. J. ELM: the status of the 2010 eukaryotic linear motif resource. *Nucleic Acids Research.*

GRABNER, M., DIRKSEN, R. T., SUDA, N. & BEAM, K. G. 1999. The II-III loop of the skeletal muscle dihydropyridine receptor is responsible for the Bi-directional coupling with the ryanodine receptor. *J Biol Chem,* 274, 21913-9.

GREENFIELD, N. & FASMAN, G. D. 1969. Computed circular dichroism spectra for the evaluation of protein conformation. *Biochemistry,* 8, 4108-16.

GREENFIELD, N. J. 2006. Using circular dichroism spectra to estimate protein secondary structure. *Nat Protoc,* 1, 2876-90.

GREGG, R. G., MESSING, A., STRUBE, C., BEURG, M., MOSS, R., BEHAN, M., SUKHAREVA, M., HAYNES, S., POWELL, J. A., CORONADO, R. & POWERS, P. A. 1996. Absence of the beta subunit (cchb1) of the skeletal muscle dihydropyridine receptor alters expression of the alpha 1 subunit and eliminates excitation-contraction coupling. *Proc Natl Acad Sci U S A,* 93, 13961-6.

GROEMPING, Y. A. H., N 2005. Spectroscopic Methods for the Determination of protein interactions. *Current Protocols in Protein Science,* 20.8.1-20.8.27.

GURNETT, C. A., DE WAARD, M. & CAMPBELL, K. P. 1996. Dual function of the voltage-dependent Ca2+ channel alpha 2 delta subunit in current stimulation and subunit interaction. *Neuron,* 16, 431-40.

GURNETT, C. A., FELIX, R. & CAMPBELL, K. P. 1997. Extracellular interaction of the voltage-dependent Ca2+ channel alpha2delta and alpha1 subunits. *J Biol Chem,* 272, 18508-12.

HAGIWARA, S., OZAWA, S. & SAND, O. 1975. Voltage clamp analysis of two inward current mechanisms in the egg cell membrane of a starfish. *J Gen Physiol,* 65, 617-44.

HAKAMATA, Y., NAKAI, J., TAKESHIMA, H. & IMOTO, K. 1992. Primary structure and distribution of a novel ryanodine receptor/calcium release channel from rabbit brain. *FEBS Lett,* 312, 229-35.

HANKE, S., BUGERT, P., CHUDEK, J. & KOVACS, G. 2001. Cloning a calcium channel alpha2delta-3 subunit gene from a putative tumor suppressor gene region at chromosome 3p21.1 in conventional renal cell carcinoma. *Gene,* 264, 69-75.

HANLON, M. R., BERROW, N. S., DOLPHIN, A. C. & WALLACE, B. A. 1999. Modelling of a voltage-dependent Ca2+ channel beta subunit as a basis for understanding its functional properties. *FEBS Lett,* 445, 366-70.

HE, L. L., ZHANG, Y., CHEN, Y. H., YAMADA, Y. & YANG, J. 2007. Functional modularity of the beta-subunit of voltage-gated Ca2+ channels. *Biophys J,* 93, 834-45.

HELD, B., FREISE, D., FREICHEL, M., HOTH, M. & FLOCKERZI, V. 2002. Skeletal muscle L-type Ca(2+) current modulation in gamma1-deficient and wildtype murine myotubes by the gamma1 subunit and cAMP. *J Physiol,* 539, 459-68.

HOCHULI, E. 1990. Purification of recombinant proteins with metal chelate adsorbent. *Genetic Engineering, Principles and Practice,* 12 (J.Setlow,ed.), 87-98.

HULLIN, R., ASMUS, F., LUDWIG, A., HERSEL, J. & BOEKSTEGERS, P. 1999. Subunit expression of the cardiac L-type calcium channel is differentially regulated in diastolic heart failure of the cardiac allograft. *Circulation,* 100, 155-63.

HULLIN, R., KHAN, I. F., WIRTZ, S., MOHACSI, P., VARADI, G., SCHWARTZ, A. & HERZIG, S. 2003. Cardiac L-type calcium channel beta-subunits expressed in human heart have differential effects on single channel characteristics. *J Biol Chem,* 278, 21623-30.

HULLIN, R., SINGER-LAHAT, D., FREICHEL, M., BIEL, M., DASCAL, N., HOFMANN, F. & FLOCKERZI, V. 1992. Calcium channel beta subunit heterogeneity: functional expression of cloned cDNA from heart, aorta and brain. *Embo J,* 11, 885-90.

HULME, J. T., AHN, M., HAUSCHKA, S. D., SCHEUER, T. & CATTERALL, W. A. 2002. A novel leucine zipper targets AKAP15 and cyclic AMP-dependent protein kinase to the C terminus of the skeletal muscle Ca2+ channel and modulates its function. *J Biol Chem,* 277, 4079-87.

INUI, M., SAITO, A. & FLEISCHER, S. 1987. Purification of the ryanodine receptor and identity with feet structures of junctional terminal cisternae of sarcoplasmic reticulum from fast skeletal muscle. *J Biol Chem,* 262, 1740-7.

JAY, S. D., ELLIS, S. B., MCCUE, A. F., WILLIAMS, M. E., VEDVICK, T. S., HARPOLD, M. M. & CAMPBELL, K. P. 1990. Primary structure of the gamma subunit of the DHP-sensitive calcium channel from skeletal muscle. *Science,* 248, 490-2.

JAY, S. D., SHARP, A. H., KAHL, S. D., VEDVICK, T. S., HARPOLD, M. M. & CAMPBELL, K. P. 1991. Structural characterization of the dihydropyridine-sensitive calcium channel alpha 2-subunit and the associated delta peptides. *J*

Biol Chem, 266, 3287-93.

JONES, L. R., ZHANG, L., SANBORN, K., JORGENSEN, A. O. & KELLEY, J. 1995. Purification, primary structure, and immunological characterization of the 26-kDa calsequestrin binding protein (junctin) from cardiac junctional sarcoplasmic reticulum. *J Biol Chem,* 270, 30787-96.

KANEKO T, LI L & SS, L. 2008. The SH3 domain- a family of versatile peptide-and protein-recognition module. *Frontiers in Bioscience,* 13, 4938-52.

KAPOOR, K. N., BARRY, D. T., REES, R. C., ANTHONY DODI, I., MCARDLE, S. E. B., CREASER, C. S. & BONNER, P. L. R. 2009. Estimation of peptide concentration by a modified bicinchoninic acid assay. *Analytical Biochemistry,* 393, 138-140.

KARKKAINEN, S., HIIPAKKA, M., WANG, J. H., KLEINO, I., VAHA-JAAKKOLA, M., RENKEMA, G. H., LISS, M., WAGNER, R. & SAKSELA, K. 2006. Identification of preferred protein interactions by phage-display of the human Src homology-3 proteome. *EMBO Rep,* 7, 186-91.

KASIELKE, N., OBERMAIR, G. J., KUGLER, G., GRABNER, M. & FLUCHER, B. E. 2003. Cardiac-type EC-coupling in dysgenic myotubes restored with Ca2+ channel subunit isoforms alpha1C and alpha1D does not correlate with current density. *Biophys J,* 84, 3816-28.

KEELER, J. 2005. *Understanding NMR Spectroscopy*, John Wiley & Sons.

KELLY, R. C., JENSEN, D. E. & VON HIPPEL, P. H. 1976. DNA "melting" proteins. IV. Fluorescence measurements of binding parameters for bacteriophage T4 gene 32-protein to mono-, oligo-, and polynucleotides. *J Biol Chem,* 251, 7240-50.

KISTNER, U., GARNER, C. C. & LINIAL, M. 1995. Nucleotide binding by the synapse associated protein SAP90. *FEBS Lett,* 359, 159-63.

KUGLER, G., WEISS, R. G., FLUCHER, B. E. & GRABNER, M. 2004. Structural requirements of the dihydropyridine receptor alpha1S II-III loop for skeletal-type excitation-contraction coupling. *J Biol Chem,* 279, 4721-8.

KUMAR, B. V., ANAMIKA, D. & MANFRED, G. 2011. Regions of the DHPR beta1a sununit responsible for DHPR voltage sensing in skeletal muscle excitation-contraction coupling. *2011 Biophysical Society Meeting, Abstracts, Biophysical journal,* 100, 3199-pos.

LACINOVA, L. 2005. Voltage-dependent calcium channels. *Gen Physiol Biophys,* 24 Suppl 1, 1-78.

LAI, F. A., MISRA, M., XU, L., SMITH, H. A. & MEISSNER, G. 1989. The ryanodine receptor-Ca2+ release channel complex of skeletal muscle sarcoplasmic reticulum. Evidence for a cooperatively coupled, negatively charged homotetramer. *J Biol Chem,* 264, 16776-85.

LARSON, S. M. & DAVIDSON, A. R. 2000. The identification of conserved interactions within the SH3 domain by alignment of sequences and structures. *Protein Sci,* 9, 2170-80.

LAVER, D. 2001. The power of single channel recording and analysis: its application to ryanodine receptors in lipid bilayers. *Clinical and experimental pharmacology & physiology,* 28, 675-86.

LAVER, D. R., BAYNES, T. M. & DULHUNTY, A. F. 1997. Magnesium inhibition of ryanodine-receptor calcium channels: evidence for two independent mechanisms. *J Membr Biol,* 156, 213-29.

LAVER, D. R., LENZ, G. K. & LAMB, G. D. 2001. Regulation of the calcium release channel from rabbit skeletal muscle by the nucleotides ATP, AMP, IMP and adenosine. *J Physiol,* 537, 763-78.

LAVER, D. R., O'NEILL, E. R. & LAMB, G. D. 2004. Luminal Ca2+-regulated Mg2+ inhibition of skeletal RyRs reconstituted as isolated channels or coupled clusters. *J Gen Physiol,* 124, 741-58.

LEONG, P. & MACLENNAN, D. H. 1998. A 37-amino acid sequence in the skeletal muscle ryanodine receptor interacts with the cytoplasmic loop between domains II and III in the skeletal muscle dihydropyridine receptor. *J Biol Chem,* 273, 7791-4.

LEONG, P. & MACLENNAN, D. H. 1998. Complex interactions between skeletal muscle ryanodine receptor and dihydropyridine receptor proteins. *Biochemistry and cell biology = Biochimie et biologie cellulaire,* 76, 681-94.

LEONG, P. & MACLENNAN, D. H. 1998. The cytoplasmic loops between domains II and III and domains III and IV in the skeletal muscle dihydropyridine receptor bind to a contiguous site in the skeletal muscle ryanodine receptor. *J Biol Chem,* 273, 29958-64.

LEUNG, A. T., IMAGAWA, T., BLOCK, B., FRANZINI-ARMSTRONG, C. & CAMPBELL, K. P. 1988. Biochemical and ultrastructural characterization of the 1,4-dihydropyridine receptor from rabbit skeletal muscle. Evidence for a 52,000 Da subunit. *J Biol Chem,* 263, 994-1001.

LLINAS, R., SUGIMORI, M., LIN, J. W. & CHERKSEY, B. 1989. Blocking and isolation of a calcium channel from neurons in mammals and cephalopods utilizing a toxin fraction (FTX) from funnel-web spider poison. *Proc Natl Acad Sci U S A,* 86, 1689-93.

LLINAS, R. & YAROM, Y. 1981. Electrophysiology of mammalian inferior olivary neurones in vitro. Different types of voltage-dependent ionic conductances. *J Physiol,* 315, 549-67.

LORENZON, N. M., HAARMANN, C. S., NORRIS, E. E., PAPADOPOULOS, S. & BEAM, K. G. 2004. Metabolic biotinylation as a probe of supramolecular structure of the triad junction in skeletal muscle. *J Biol Chem,* 279, 44057-64.

LU, X., XU, L. & MEISSNER, G. 1994. Activation of the skeletal muscle calcium release channel by a cytoplasmic loop of the dihydropyridine receptor. *J Biol Chem,* 269, 6511-6.

MA, J. 1993. Block by ruthenium red of the ryanodine-activated calcium release channel of skeletal muscle. *J Gen Physiol,* 102, 1031-56.

MACKRILL, J. J., CHALLISS, R. A., O'CONNELL D, A., LAI, F. A. & NAHORSKI, S. R. 1997. Differential expression and regulation of ryanodine receptor and myo-inositol 1,4,5-trisphosphate receptor Ca2+ release channels in mammalian tissues and cell lines. *The Biochemical journal,* 327 (Pt 1), 251-8.

MARTIN, G. E. & ZEKTER, A. S. 1988. Two dimensional NMR Methods for Establishing Molecular Connectivity. New York: VCH Publishers.

MARTY, I., FAURE, J., FOUREST-LIEUVIN, A., VASSILOPOULOS, S., ODDOUX, S. & BROCARD, J. 2009. Triadin: what possible function 20 years later? *J Physiol,* 587, 3117-21.

MARX, S. O., ONDRIAS, K. & MARKS, A. R. 1998. Coupled gating between individual skeletal muscle Ca2+ release channels (ryanodine receptors). *Science,* 281, 818-21.

MAYER, B. J., HAMAGUCHI, M. & HANAFUSA, H. 1988. A novel viral oncogene with structural similarity to phospholipase C. *Nature,* 332, 272-5.

MCGEE, A. W., DAKOJI, S. R., OLSEN, O., BREDT, D. S., LIM, W. A. & PREHODA, K. E. 2001. Structure of the SH3-guanylate kinase module from PSD-95 suggests a mechanism for regulated assembly of MAGUK scaffolding proteins. *Mol Cell,* 8, 1291-301.

MCPHERSON, P. S. 1999. Regulatory role of SH3 domain-mediated protein-protein interactions in synaptic vesicle endocytosis. *Cell Signal,* 11, 229-38.

MEISSNER, G. 1984. Adenine nucleotide stimulation of Ca2+-induced Ca2+ release in sarcoplasmic reticulum. *J Biol Chem,* 259, 2365-74.

MEISSNER, G. 2002. Regulation of mammalian ryanodine receptors. *Front Biosci,* 7, d2072-80.

MEISSNER, G., DARLING, E. & EVELETH, J. 1986. Kinetics of rapid Ca2+ release by sarcoplasmic reticulum. Effects of Ca2+, Mg2+, and adenine nucleotides. *Biochemistry,* 25, 236-44.

MEISSNER, G., RIOS, E., TRIPATHY, A. & PASEK, D. A. 1997. Regulation of skeletal muscle Ca2+ release channel (ryanodine receptor) by Ca2+ and monovalent cations and anions. *J Biol Chem,* 272, 1628-38.

MILLER, J. H. 1978. The lacI gene: Its role in lac operon control and its uses as a genetic system. *In the operon (J.Miller, ed.) Cold Spring Harbor Laboratory, Cold Spring Harbor, N.Y,* 31-88.

MIRANDA-LAFERTE, E., GONZALEZ-GUTIERREZ, G., SCHMIDT, S., ZEUG, A., PONIMASKIN, E. G., NEELY, A. & HIDALGO, P. 2011. Homodimerization of the Src homology 3 domain of the calcium channel {beta}-subunit drives dynamin-dependent endocytosis. *The Journal of biological chemistry.*

MONNIER, N., PROCACCIO, V., STIEGLITZ, P. & LUNARDI, J. 1997. Malignant-hyperthermia susceptibility is associated with a mutation of the alpha 1-subunit of the human dihydropyridine-sensitive L-type voltage-dependent calcium-channel receptor in skeletal muscle. *Am J Hum Genet,* 60, 1316-25.

MURATA, K., NISHIMURA, S., KUNIYASU, A. & NAKAYAMA, H. 2010. Three-dimensional structure of the alpha1-beta complex in the skeletal muscle dihydropyridine receptor by single-particle electron microscopy. *J Electron Microsc (Tokyo),* 59, 215-26.

MURATA, K., ODAHARA, N., KUNIYASU, A., SATO, Y., NAKAYAMA, H. & NAGAYAMA, K. 2001. Asymmetric arrangement of auxiliary subunits of skeletal muscle voltage-gated l-type Ca(2+) channel. *Biochem Biophys Res Commun,* 282, 284-91.

MUSACCHIO, A., NOBLE, M., PAUPTIT, R., WIERENGA, R. & SARASTE, M. 1992. Crystal structure of a Src-homology 3 (SH3) domain. *Nature,* 359, 851-5.

NABAUER, M., CALLEWAERT, G., CLEEMANN, L. & MORAD, M. 1989. Regulation of calcium release is gated by calcium current, not gating charge, in cardiac myocytes. *Science,* 244, 800-3.

NAKAI, J., DIRKSEN, R. T., NGUYEN, H. T., PESSAH, I. N., BEAM, K. G. & ALLEN, P. D. 1996. Enhanced dihydropyridine receptor channel activity in the presence of ryanodine receptor. *Nature,* 380, 72-5.

NAKAI, J., IMAGAWA, T., HAKAMAT, Y., SHIGEKAWA, M., TAKESHIMA, H. & NUMA, S. 1990. Primary structure and functional expression from cDNA of the cardiac ryanodine receptor/calcium release channel. *FEBS Lett,* 271, 169-77.

NAKAI, J., SEKIGUCHI, N., RANDO, T. A., ALLEN, P. D. & BEAM, K. G. 1998. Two regions of the ryanodine receptor involved in coupling with L-type Ca2+ channels. *J Biol Chem,* 273, 13403-6.

NAKAI, J., TANABE, T., KONNO, T., ADAMS, B. & BEAM, K. G. 1998. Localization in the II-III loop of the dihydropyridine receptor of a sequence critical for excitation-contraction coupling. *J Biol Chem,* 273, 24983-6.

NEUHUBER, B., GERSTER, U., MITTERDORFER, J., GLOSSMANN, H. & FLUCHER, B. E. 1998. Differential effects of Ca2+ channel beta1a and beta2a subunits on complex formation with alpha1S and on current expression in tsA201 cells. *J Biol Chem,* 273, 9110-8.

NOWYCKY, M. C., FOX, A. P. & TSIEN, R. W. 1985. Three types of neuronal calcium channel with different calcium agonist sensitivity. *Nature,* 316, 440-3.

OBERMAIR, G. J., KUGLER, G., BAUMGARTNER, S., TULUC, P., GRABNER, M. & FLUCHER, B. E. 2005. The Ca2+ channel alpha2delta-1 subunit determines Ca2+ current kinetics in skeletal muscle but not targeting of alpha1S or excitation-contraction coupling. *J Biol Chem,* 280, 2229-37.

OBERMAIR, G. J., TULUC, P. & FLUCHER, B. E. 2008. Auxiliary Ca2+ channel subunits: lessons learned from muscle. *Current Opinion in Pharmacology,* 8, 311-318.

OHNISHI, M. & ORRY, D. W. 1969. Temperature dependance of amide proton chemical shifts: the secondary strutures of gramicidin S and valinomycin. *Biochemical and biophysical research communications,* 36, 194-202.

OPATOWSKY, Y., CHEN, C. C., CAMPBELL, K. P. & HIRSCH, J. A. 2004. Structural analysis of the voltage-dependent calcium channel beta subunit functional core and its complex with the alpha 1 interaction domain. *Neuron,* 42, 387-99.

OPATOWSKY, Y., CHOMSKY-HECHT, O., KANG, M. G., CAMPBELL, K. P. & HIRSCH, J. A. 2003. The voltage-dependent calcium channel beta subunit contains two stable interacting domains. *J Biol Chem,* 278, 52323-32.

ORLOVA, E. V., SERYSHEVA, II, VAN HEEL, M., HAMILTON, S. L. & CHIU, W. 1996. Two structural configurations of the skeletal muscle calcium release channel. *Nat Struct Biol,* 3, 547-52.

OTSU, K., WILLARD, H. F., KHANNA, V. K., ZORZATO, F., GREEN, N. M. & MACLENNAN, D. H. 1990. Molecular cloning of cDNA encoding the Ca2+ release channel (ryanodine receptor) of rabbit cardiac muscle sarcoplasmic reticulum. *J Biol Chem,* 265, 13472-83.

PACE, C. N. & SCHOLTZ, J. M. 1998. A helix propensity scale based on experimental studies of peptides and proteins. *Biophys J,* 75, 422-7.

PAOLINI, C., FESSENDEN, J. D., PESSAH, I. N. & FRANZINI-ARMSTRONG, C. 2004. Evidence for conformational coupling between two calcium channels. *Proc Natl Acad Sci U S A,* 101, 12748-52.

PAPADOPOULOS, S., LEURANGUER, V., BANNISTER, R. A. & BEAM, K. G. 2004. Mapping sites of potential proximity between the dihydropyridine receptor and RyR1 in muscle using a cyan fluorescent protein-yellow fluorescent protein tandem as a fluorescence resonance energy transfer probe. *J Biol Chem,* 279, 44046-56.

PATE, P., MOCHCA-MORALES, J., WU, Y., ZHANG, J. Z., RODNEY, G. G., SERYSHEVA, II, WILLIAMS, B. Y., ANDERSON, M. E. & HAMILTON, S. L. 2000. Determinants for calmodulin binding on voltage-dependent Ca2+ channels. *J Biol Chem,* 275, 39786-92.

PEREZ-IRATXETA, C. & ANDRADE-NAVARRO, M. A. 2008. K2D2: estimation of protein secondary structure from circular dichroism spectra. *BMC Struct Biol,* 8, 25.

PEREZ-REYES, E., CASTELLANO, A., KIM, H. S., BERTRAND, P., BAGGSTROM, E., LACERDA, A. E., WEI, X. Y. & BIRNBAUMER, L. 1992. Cloning and expression of a cardiac/brain beta subunit of the L-type calcium channel. *J Biol Chem,* 267, 1792-7.

PROENZA, C., O'BRIEN, J., NAKAI, J., MUKHERJEE, S., ALLEN, P. D. & BEAM, K. G. 2002. Identification of a region of RyR1 that participates in allosteric coupling with the alpha(1S) (Ca(V)1.1) II-III loop. *J Biol Chem,* 277, 6530-5.

PROENZA, C., WILKENS, C., LORENZON, N. M. & BEAM, K. G. 2000. A carboxyl-terminal region important for the expression and targeting of the skeletal muscle dihydropyridine receptor. *J Biol Chem,* 275, 23169-74.

QIN, N., PLATANO, D., OLCESE, R., STEFANI, E. & BIRNBAUMER, L. 1997. Direct interaction of gbetagamma with a C-terminal gbetagamma-binding domain of the Ca2+ channel alpha1 subunit is responsible for channel inhibition by G protein-coupled receptors. *Proc Natl Acad Sci U S A,* 94, 8866-71.

QIN, N., YAGEL, S., MOMPLAISIR, M. L., CODD, E. E. & D'ANDREA, M. R. 2002. Molecular cloning and characterization of the human voltage-gated calcium channel alpha(2)delta-4 subunit. *Mol Pharmacol,* 62, 485-96.

RAGHIB, A., BERTASO, F., DAVIES, A., PAGE, K. M., MEIR, A., BOGDANOV, Y. & DOLPHIN, A. C. 2001. Dominant-negative synthesis suppression of voltage-gated calcium channel Cav2.2 induced by truncated constructs. *J Neurosci,* 21, 8495-504.

REBBECK, R., KARUNASEKARA, Y., GALLANT, E., BOARD, P., BEARD, N., CASAROTTO, M. & DULHUNTY, A. In press. The b1a subunit of the skeletal DHPR binds to skeletal RyR1 and activates the channel via its 35 residue C-terminal tail. *Biochemical journal*.

REBBECK, R. T., KARUNASEKARA, Y., GALLANT, E. M., BOARD, P. G., BEARD, N. A., CASAROTTO, M. G. & DULHUNTY, A. F. 2011. The [beta]1a Subunit of the Skeletal DHPR Binds to Skeletal RyR1 and Activates the Channel via Its 35-Residue C-Terminal Tail. *Biophysical Journal,* 100, 922-930.

REED, J. & REED, T. A. 1997. A Set of Constructed Type Spectra for the Practical Estimation of Peptide Secondary Structure from Circular Dichroism. *Analytical Biochemistry,* 254, 36-40.

RICHARDS, M. W., BUTCHER, A. J. & DOLPHIN, A. C. 2004. Ca2+ channel beta-subunits: structural insights AID our understanding. *Trends Pharmacol Sci,* 25, 626-32.

RICHARDS, M. W., LEROY, J., PRATT, W. S. & DOLPHIN, A. C. 2007. The HOOK-domain between the SH3 and the GK domains of Cavbeta subunits contains key determinants controlling calcium channel inactivation. *Channels (Austin),* 1, 92-101.

RIOS, E. & BRUM, G. 1987. Involvement of dihydropyridine receptors in excitation-contraction coupling in skeletal muscle. *Nature,* 325, 717-20.

RIOS, E. & PIZARRO, G. 1991. Voltage sensor of excitation-contraction coupling in skeletal muscle. *Physiol Rev,* 71, 849-908.

RUTH, P., ROHRKASTEN, A., BIEL, M., BOSSE, E., REGULLA, S., MEYER, H. E., FLOCKERZI, V. & HOFMANN, F. 1989. Primary structure of the beta subunit of the DHP-sensitive calcium channel from skeletal muscle. *Science,* 245, 1115-8.

SAITO, A., SEILER, S., CHU, A. & FLEISCHER, S. 1984. Preparation and morphology of sarcoplasmic reticulum terminal cisternae from rabbit skeletal muscle. *The Journal of cell biology,* 99, 875-85.

SAMBROOK, J. & RUSSELL, D. W. 2001. Molecular cloning: a laboratory manual. *CSHL press.*

SAMSO, M., FENG, W., PESSAH, I. N. & ALLEN, P. D. 2009. Coordinated movement of cytoplasmic and transmembrane domains of RyR1 upon gating. *PLoS Biol,* 7, e85.

SCHREDELSEKER, J., DAYAL, A., SCHWERTE, T., FRANZINI-ARMSTRONG, C. & GRABNER, M. 2009. Proper restoration of excitation-contraction coupling in the dihydropyridine receptor beta1-null zebrafish relaxed is an exclusive function of the beta1a subunit. *J Biol Chem,* 284, 1242-51.

SCHREDELSEKER, J., DI BIASE, V., OBERMAIR, G. J., FELDER, E. T., FLUCHER, B. E., FRANZINI-ARMSTRONG, C. & GRABNER, M. 2005. The beta 1a subunit is essential for the assembly of dihydropyridine-receptor arrays in skeletal muscle. *Proc Natl Acad Sci U S A,* 102, 17219-24.

SENCER, S., PAPINENI, R. V., HALLING, D. B., PATE, P., KROL, J., ZHANG, J. Z. & HAMILTON, S. L. 2001. Coupling of RYR1 and L-type calcium channels via calmodulin binding domains. *J Biol Chem,* 276, 38237-41.

SERYSHEVA, II 2004. Structural insights into excitation-contraction coupling by electron cryomicroscopy. *Biochemistry (Mosc),* 69, 1226-32.

SERYSHEVA, II, LUDTKE, S. J., BAKER, M. R., CHIU, W. & HAMILTON, S. L. 2002. Structure of the voltage-gated L-type Ca2+ channel by electron cryomicroscopy. *Proc Natl Acad Sci U S A,* 99, 10370-5.

SHERIDAN, D. C., CHENG, W., CARBONNEAU, L., AHERN, C. A. & CORONADO, R. 2004. Involvement of a heptad repeat in the carboxyl terminus of the dihydropyridine receptor beta1a subunit in the mechanism of excitation-contraction coupling in skeletal muscle. *Biophys J,* 87, 929-42.

SHISTIK, E., IVANINA, T., PURI, T., HOSEY, M. & DASCAL, N. 1995. Ca2+ current enhancement by alpha 2/delta and beta subunits in Xenopus oocytes: contribution of changes in channel gating and alpha 1 protein level. *J Physiol,* 489 (Pt 1), 55-62.

SIPOS, I., PIKA-HARTLAUB, U., HOFMANN, F., FLUCHER, B. E. & MELZER, W. 2000. Effects of the dihydropyridine receptor subunits gamma and alpha2delta on the kinetics of heterologously expressed L-type Ca2+ channels. *Pflugers Arch,* 439, 691-9.

SKALICKY, J. J., SELSTED, M. E. & PARDI, A. 1994. Structure and dynamics of the neutrophil defensins NP-2, NP-5, and HNP-1: NMR studies of amide hydrogen exchange kinetics. *Proteins,* 20, 52-67.

SLAVIK, K. J., WANG, J. P., AGHDASI, B., ZHANG, J. Z., MANDEL, F., MALOUF, N. & HAMILTON, S. L. 1997. A carboxy-terminal peptide of the alpha 1-subunit of the dihydropyridine receptor inhibits Ca(2+)-release channels. *Am J Physiol,* 272, C1475-81.

SMITH, J. S., CORONADO, R. & MEISSNER, G. 1986. Single channel measurements of the calcium release channel from skeletal muscle sarcoplasmic reticulum. Activation by Ca2+ and ATP and modulation by Mg2+. *J Gen Physiol,* 88, 573-

88.

SMITH, J. S., IMAGAWA, T., MA, J., FILL, M., CAMPBELL, K. P. & CORONADO, R. 1988. Purified ryanodine receptor from rabbit skeletal muscle is the calcium-release channel of sarcoplasmic reticulum. *J Gen Physiol,* 92, 1-26.

SMITH, P. K., KROHN, R. I., HERMANSON, G. T., MALLIA, A. K., GARTNER, F. H., PROVENZANO, M. D., FUJIMOTO, E. K., GOEKE, N. M., OLSON, B. J. & KLENK, D. C. 1985. Measurment of protein using bicinchoninic acid. *Analytical Biochemistry,* 150, 76-85.

SONNLEITNER, A., CONTI, A., BERTOCCHINI, F., SCHINDLER, H. & SORRENTINO, V. 1998. Functional properties of the ryanodine receptor type 3 (RyR3) Ca2+ release channel. *EMBO J,* 17, 2790-8.

STEPHENS, G. J., PAGE, K. M., BOGDANOV, Y. & DOLPHIN, A. C. 2000. The alpha1B Ca2+ channel amino terminus contributes determinants for beta subunit-mediated voltage-dependent inactivation properties. *J Physiol,* 525 Pt 2, 377-90.

STRUBE, C., BEURG, M., POWERS, P. A., GREGG, R. G. & CORONADO, R. 1996. Reduced Ca2+ current, charge movement, and absence of Ca2+ transients in skeletal muscle deficient in dihydropyridine receptor beta 1 subunit. *Biophys J,* 71, 2531-43.

STUDIER, F. W. 2005. Protein production by auto-induction in high density shaking cultures. *Protein Expression and Purification,* 41, 207-234.

SUH-KIM, H., WEI, X., KLOS, A., PAN, S., RUTH, P., FLOCKERZI, V., HOFMANN, F., PEREZ-REYES, E. & BIRNBAUMER, L. 1996. Reconstitution of the skeletal muscle dihydropyridine receptor. Functional interaction among alpha 1, beta, gamma and alpha 2 delta subunits. *Receptors Channels,* 4, 217-25.

TAE, H. S., NORRIS, N. C., CUI, Y., KARUNASEKARA, Y., BOARD, P. G., DULHUNTY, A. F. & CASAROTTO, M. G. 2009. Molecular recognition of the disordered dihydropyridine receptor II-III loop by a conserved spry domain of the type 1 ryanodine receptor. *Clin Exp Pharmacol Physiol,* 36, 346-9.

TAKAHASHI, M., SEAGAR, M. J., JONES, J. F., REBER, B. F. & CATTERALL, W. A. 1987. Subunit structure of dihydropyridine-sensitive calcium channels from skeletal muscle. *Proc Natl Acad Sci U S A,* 84, 5478-82.

TAKEKURA, H., BENNETT, L., TANABE, T., BEAM, K. G. & FRANZINI-ARMSTRONG, C. 1994. Restoration of junctional tetrads in dysgenic myotubes by dihydropyridine receptor cDNA. *Biophysical journal,* 67, 793-803.

TAKEKURA, H., PAOLINI, C., FRANZINI-ARMSTRONG, C., KUGLER, G., GRABNER, M. & FLUCHER, B. E. 2004. Differential contribution of skeletal and cardiac II-III loop sequences to the assembly of dihydropyridine-receptor arrays in skeletal muscle. *Mol Biol Cell,* 15, 5408-19.

TAKESHIMA, H., IINO, M., TAKEKURA, H., NISHI, M., KUNO, J., MINOWA, O., TAKANO, H. & NODA, T. 1994. Excitation-contraction uncoupling and muscular degeneration in mice lacking functional skeletal muscle ryanodine-receptor gene. *Nature,* 369, 556-9.

TAKESHIMA, H., IKEMOTO, T., NISHI, M., NISHIYAMA, N., SHIMUTA, M., SUGITANI, Y., KUNO, J., SAITO, I., SAITO, H., ENDO, M., IINO, M. & NODA, T. 1996. Generation and characterization of mutant mice lacking ryanodine receptor type 3. *J Biol Chem,* 271, 19649-52.

TAKESHIMA, H., KOMAZAKI, S., HIROSE, K., NISHI, M., NODA, T. & IINO, M. 1998. Embryonic lethality and abnormal cardiac myocytes in mice lacking ryanodine receptor type 2. *EMBO J,* 17, 3309-16.

TAKESHIMA, H., NISHIMURA, S., MATSUMOTO, T., ISHIDA, H., KANGAWA, K., MINAMINO, N., MATSUO, H., UEDA, M., HANAOKA, M., HIROSE, T. & NUMA, S. 1989. Primary structure and expression from complementary DNA of skeletal muscle ryanodine receptor. *Nature,* 339, 439-445.

TANABE, T., BEAM, K. G., ADAMS, B. A., NIIDOME, T. & NUMA, S. 1990. Regions of the skeletal muscle dihydropyridine receptor critical for excitation-contraction coupling. *Nature,* 346, 567-9.

TANABE, T., BEAM, K. G., POWELL, J. A. & NUMA, S. 1988. Restoration of excitation-contraction coupling and slow calcium current in dysgenic muscle by dihydropyridine receptor complementary DNA. *Nature,* 336, 134-9.

TANABE, T., MIKAMI, A., NUMA, S. & BEAM, K. G. 1990. Cardiac-type excitation-contraction coupling in dysgenic skeletal muscle injected with cardiac dihydropyridine receptor cDNA. *Nature,* 344, 451-3.

TANABE, T., TAKESHIMA, H., MIKAMI, A., FLOCKERZI, V., TAKAHASHI, H., KANGAWA, K., KOJIMA, M., MATSUO, H., HIROSE, T. & NUMA, S. 1987. Primary structure of the receptor for calcium channel blockers from skeletal muscle. *Nature,* 328, 313-8.

TULUC, P., KERN, G., OBERMAIR, G. J. & FLUCHER, B. E. 2007. Computer modeling of siRNA knockdown effects indicates an essential role of the Ca2+ channel alpha2delta-1 subunit in cardiac excitation-contraction coupling. *Proc Natl Acad Sci U S A,* 104, 11091-6.

URSU, D., SCHUHMEIER, R. P., FREICHEL, M., FLOCKERZI, V. & MELZER, W. 2004. Altered inactivation of Ca2+ current and Ca2+ release in mouse muscle fibers deficient in the DHP receptor gamma1 subunit. *J Gen Physiol,* 124, 605-18.

VAN PETEGEM, F., CLARK, K. A., CHATELAIN, F. C. & MINOR, D. L., JR. 2004. Structure of a complex between a voltage-gated calcium channel beta-subunit and an alpha-subunit domain. *Nature,* 429, 671-5.

VAN PETEGEM, F., DUDERSTADT, K. E., CLARK, K. A., WANG, M. & MINOR, D. L., JR. 2008. Alanine-scanning mutagenesis defines a conserved energetic hotspot in the CaValpha1 AID-CaVbeta interaction site that is critical for channel modulation. *Structure,* 16, 280-94.

WAGENKNECHT, T., GRASSUCCI, R., FRANK, J., SAITO, A., INUI, M. & FLEISCHER, S. 1989. Three-dimensional architecture of the calcium channel/foot structure of sarcoplasmic reticulum. *Nature,* 338, 167-70.

WALKER, D., BICHET, D., GEIB, S., MORI, E., CORNET, V., SNUTCH, T. P., MORI, Y. & DE WAARD, M. 1999. A new beta subtype-specific interaction in alpha1A subunit controls P/Q-type Ca2+ channel activation. *J Biol Chem,* 274, 12383-90.

WEISS, R. G., O'CONNELL, K. M., FLUCHER, B. E., ALLEN, P. D., GRABNER, M. & DIRKSEN, R. T. 2004. Functional analysis of the R1086H malignant hyperthermia mutation in the DHPR reveals an unexpected influence of the III-IV loop on skeletal muscle EC coupling. *Am J Physiol Cell Physiol,* 287, C1094-102.

WILKENS, C. M. & BEAM, K. G. 2003. Insertion of alpha1S II-III loop and C terminal sequences into alpha1H fails to restore excitation-contraction coupling in dysgenic myotubes. *J Muscle Res Cell Motil,* 24, 99-109.

WILKENS, C. M., KASIELKE, N., FLUCHER, B. E., BEAM, K. G. & GRABNER, M. 2001. Excitation-contraction coupling is unaffected by drastic alteration of the sequence surrounding residues L720-L764 of the alpha 1S II-III loop. *Proc Natl Acad Sci U S A,* 98, 5892-7.

WISHART, D. S. & NIP, A. M. 1998. Protein chemical shift analysis: a practical guide. *Biochem Cell Biol,* 76, 153-63.

WISHART, D. S., SYKES, B. D. & RICHARDS, F. M. 1991. Relationship between nuclear magnetic resonance chemical shift and protein secondary structure. *J Mol Biol,* 222, 311-33.

WISHART, D. S., SYKES, B. D. & RICHARDS, F. M. 1992. The chemical shift index: a fast and simple method for the assignment of protein secondary structure through NMR spectroscopy. *Biochemistry,* 31, 1647-51.

WURTHRICH, K. 1986. *NMR of Proteins and Nucleic Acids,* New York (NY) USA, Wiley-Interscience.

XU, L., TRIPATHY, A., PASEK, D. A. & MEISSNER, G. 1999. Ruthenium red modifies the cardiac and skeletal muscle Ca(2+) release channels (ryanodine receptors) by multiple mechanisms. *J Biol Chem,* 274, 32680-91.

YU, H., CHEN, J. K., FENG, S., DALGARNO, D. C., BRAUER, A. W. & SCHREIBER, S. L. 1994. Structural basis for the binding of proline-rich peptides to SH3 domains. *Cell,* 76, 933-45.

ZARRINPAR, A., BHATTACHARYYA, R. P. & LIM, W. A. 2003. The structure and function of proline recognition domains. *Sci STKE,* 2003, RE8.

ZORZATO, F., FUJII, J., OTSU, K., PHILLIPS, M., GREEN, N. M., LAI, F. A., MEISSNER, G. & MACLENNAN, D. H. 1990. Molecular cloning of cDNA encoding human and rabbit forms of the Ca2+ release channel (ryanodine receptor) of skeletal muscle sarcoplasmic reticulum. *J Biol Chem,* 265, 2244-56.

ZUCCHI, R. & RONCA-TESTONI, S. 1997. The sarcoplasmic reticulum Ca2+ channel/ryanodine receptor: modulation by endogenous effectors, drugs and disease states. *Pharmacol Rev,* 49, 1-51.

Appendix

A.1 Buffers and Solutions

1. **LB/amp per litre**
   10 g Tryptone
   5 g Yeast extract
   5 g NaCl
   1 g Ampicillin

2. **LB/amp-agar 1.5 % per litre**
   10 g Tryptone
   5 g Yeast extract
   5 g NaCl
   1 g Ampicillin
   15 g Agar

3. **Buffer A**
   50 mM sodium phosphate pH 8.0
   300 mM NaCl

4. **Lysis Buffer A**
   50 mM sodium phosphate pH 8.0
   300 mM NaCl
   5 mM Imidazole
   10 % glycerol
   1 mM AEBSF (protease inhibitor)

5. **Wash Buffer A**
   50 mM sodium phosphate pH 8.0
   300 mM NaCl
   5 mM Imidazole
   10 % glycerol

6. **Elution Buffer A**
   50 mM sodium phosphate pH 8.0
   300 mM NaCl
   250 mM Imidazole
   10 % glycerol

7. **Buffer B**
   8 M Urea
   50 mM sodium phosphate pH 8.0
   300 mM NaCl
   5 mM Imidazole
   12 mM β- Mercaptoethanol
   10 % glycerol

8. **Elution Buffer B**
   8 M Urea
   50 mM sodium phosphate pH 8.0
   300 mM NaCl
   500 mM Imidazole
   12 mM β- Mercapto-ethanol
   10 % glycerol

9. **Resolving Gel Buffer**
   25 % Tris-HCl (v:v)1.5 M Tris-HCl pH 8.8 stock
   7 – 12 % (v:v) Acrylamide/Bis solution 30% (37.5:1)
   0.05% (v:v) 10 % APS stock
   0.125% (v:v) TEMED

10. **Stacking Gel Buffer**
    25 % (v:v) 0.5 M Tris-HCl pH 6.8 stock
    6 % (v:v) Acrylamide/Bis solution 30% (37.5:1)
    0.05% (v:v) 10 % APS stock
    0.125% (v:v) TEMED

11. **Electrophoresis Buffer**
    0.025 M Tris pH 8.3
    0.192 M Glycine
    0.1 % (v:v) SDS

12. **Sample buffer (SDS-reducing buffer)**
    0.06 M Tris-HCl pH 6.8
    2 % (v:v) 10 % SDS stock
    5 % (v:v) β-mercapto-ethanol
    10 % (v:v)Glycerol
    0.025 % (v:v)Bromophenol blue

13. **De-staining solution**
    30% (v:v) methanol
    10% (v:v) acetic acid

14. **Transfer buffer**
    129 mM Glycine
    25 mM Tris
    10 % Methanol

15. **Blocking buffer**
    150 mM NaCl
    50 mM TrisHCl pH 7.5
    5 % (w:v) skimmed milk

A.2 Chemicals and Reagents

No.	Name	Manufacturer
1.	1,2-bis(o-aminophenoxy)ethane-N,N,N',N'-tetraacetic acid (BAPTA)	Sigma-Aldrich
2.	$^{15}NH_4Cl$, 99.80%	Novachem
3.	Acetic acid glacial, 99.80%	Scharlau
4.	Acetone, 99.50%	LabScan Asia
5.	Acrylamide/Bis solution 30% (37.5:1)	National Diagnostics
6.	AEBSF (4-(2-Aminoethyll)Benzenesulfonyl Fluoride Hydrochloride	MP Biomedicals
7.	Agar	Difco laboratories
8.	Ammonium persulfate (APS)	WWR International
9.	Ampicillin	Sigma-Aldrich
10.	BCA (Bicinchoninic Acid) ™ Protein Assay Kit	Pierce
11.	Benzamadine	Sigma-Aldrich
12.	beta-mercaptoethanol, 99.00%	BDH Chemicals
13.	Bromophenol blue	Sigma-Aldrich

14.	$CaCl_2$	Mallinckrodt
15.	$CsCH_3O_3S$	Sigma-Aldrich
16.	CsCl	Merck
17.	Deuterium (D_2O), 99.96%	Cambridge Isotope Laboratories
18.	D-Glucose, 99.00%	Sigma-Aldrich
19.	Dialysis tubing cellulose membrane, 25mm	Sigma-Aldrich
20.	Dithiothreitol (DTT)	MP Biomedicals
21.	Ethanol, 99.50%	Ajax Finechem
22.	Ethylene diamine tetraacetic acid (EDTA), 99.50%	Merck
23.	Glycerol, 99.50%	Ajax Finechem
24.	Glycine, 98.50%	Chem-Supply
25.	Imidazole	Sigma-Aldrich
26.	Isopropyl β-D-1-thiogalactopyranoside (IPTG), 99.00%	Sigma-Aldrich
27.	K_2HPO_4	Mallinckrodt

28.	KCl	Ajax Finechem
29.	KH_2PO_4	Mallinckrodt
30.	Mannitol	Scharlau
31.	Methanol, 99.90%	Ajax Finchem
32.	$MgSO_4$	BDH Chemicals
33.	Na_2HPO_4	Ajax Finechem
34.	NaCl	Merck
35.	NaH_2PO_4	Ajax Finechem
36.	n-Decane, 99.00%	Sigma-Aldrich
37.	PhastGel™ Blue R (Coomassie Blue Stain)	Amersham Pharmacia Biotech
38.	Ruthenium red	Sigma-Aldrich
39.	Silver Stain Plus™ Kit	Bio-Rad Laboratories
40.	Skimmed milk powder	Diploma brand
41.	Sodium dodecyl sulfate (SDS)	Sigma-Aldrich

42.	Sucrose	Sigma-Aldrich
43.	TES	Sigma-Aldrich
44.	Tetramethylethylenediamine (TEMED), 99.00%	Sigma-Aldrich
45.	Tris, 99.80%	BioRad Laboratories
46.	Tryptone	Difco laboratories
47.	Urea, 99.50%	Amresco
48.	Yeast Extract	Difco laboratories